STUDYING CHIRALITY IN A ~ 100, 130 AND 190 MASS REGIONS

by

Obed Shirinda

A thesis submitted in the partial fulfillment of the requirements for the degree of Doctor of Philosophy in the Department of Physics, University of the Western Cape

Supervisor: Dr. E. A. Lawrie
Department of Nuclear Physics
iThemba LABS

Co-supervisor: Prof. R. Lindsay
Department of Physics
University of the Western Cape

February 2011

UNIVERSITY of the
WESTERN CAPE

UNIVERSITY of the
WESTERN CAPE

DECLARATION

I declare that *studying chirality in A ~ 100, 130 and 190 mass regions* is my own work, that it has not been submitted for any degree or examination in any other university, and that all the sources I have used or quoted have been indicated and acknowledged by complete references.

Full name: ……. OBED SHIRINDA ….……..

Signed: ……..  ..…… **Date:** ……04 JULY 2011……

KEYWORDS

- Quasiparticle-hole configuration
- Degenerate $\Delta I = 1$ rotational band
- Excitation energies
- Alignment
- Angular momenta
- Electromagnetic transitions
- $B(M1)$ staggering
- Aplanar rotation
- Chirality
- Two-quasiparticle-plus-triaxial-rotor model

ABSTRACT

STUDYING CHIRALITY IN A ~ 100, 130 AND 190 MASS REGIONS

Obed Shirinda

iThemba LABS, P. O. Box 722, Somerset West, 7129, South Africa

PhD Thesis, Department of Physics, University of the Western Cape, Private Bag X17,

Bellville 7535, South Africa

Chirality is a nuclear symmetry which is suggested to occur in nuclei when the total angular momentum of the system has an aplanar orientation [Fra97, Fra01]. It can occur for nuclei with triaxial shape, which have valence protons and neutrons with predominantly particle and hole nature. It is expected that the angular momenta of an odd particle and an odd hole (both occupying high-j orbitals) are aligned predominantly along the short and the long axes of the nucleus respectively, whereas the collective rotation occurs predominantly around the intermediate axis of a triaxially deformed nucleus in order to minimize the total energy of the system. Such symmetry is expected to be exhibited by a pair of degenerate $\Delta I = 1$ rotational bands, i.e. all properties of the partner bands should be identical. Up to now several odd-odd, even-even and odd-A nuclei were suggested as chiral candidates in the mass regions of A ~ 100, 130 and 190 [Bal04, Bar01, Har01, Hec01, Hec03, Jos04, Jos05a-b, Jos07, Koi01, Koi03a, Law08, Law10b, Luo09, Mas09, Mer02, Moo00a-b, Pet02, Pet96, Rai03a-b, Sim05, Sta02, Tim04, Tim06, Tim07, Vam04 , Wan06, Yon05, Zhu03, Zhu05]. However, no perfect degeneracy has been found so far for any nucleus and none of the experimentally observed partner bands show all of the suggested fingerprints of chirality [Fra97, Fra01, Vam04, Koi3b, Koi04, Koi05]. The conditions that should be met for two-quasiparticle chiral bands (i.e. $\pi g_{9/2}^{-1} \otimes \nu h_{11/2}$, $\pi h_{11/2} \otimes \nu h_{11/2}^{-1}$ and $\pi h_{9/2} \otimes \nu i_{13/2}^{-1}$ configurations in the A ~ 100, 130 and 190 mass regions respectively) to reach degeneracy and their characteristic features, were examined in this study using two-quasiparticle-plus-triaxial-rotor model (TQPRM) [Sem92]. The results showed that degeneracy occurs simultaneously in all properties of the partner bands if the calculations are performed with a restricted configuration (i.e. the odd proton and the odd neutron are restricted to one orbital each located at the lowest- and highest-energy orbitals or vice versa of a high-j shells) in all three mass regions. Furthermore, perfect alignment of the angular momenta of the two odd particles and the core along the three nuclear axes is needed, i.e. three mutually orthogonal angular momenta are required. Even

small contributions with lower alignments of the particle angular momenta lead to a loss of the degeneracy in all properties of the partner bands. The requirement for such perfect alignment seems to be unreachable for real nuclei, where components with vanishing rotation along the intermediate axis at low spins, and Coriolis effects at high spins destroy the degeneracy in the chiral bands. This might explain why no degenerate chiral bands are found so far in nuclei.

Allowing a larger configuration space i.e. non-restricted configurations (the odd proton and the odd neutron span for instance five orbitals each, while the Fermi surfaces are located at the lowest- and highest-energy orbitals or vice versa of the high-j shells) has much larger effect in destroying the degeneracy than many others, (for example a change in non-axiality parameter γ to 20^0, a move of the Fermi levels of either nucleon or for both the proton and neutron to the second lowest-energy and second highest-energy orbitals in the high-j shell, etc). The calculations also showed that optimal conditions for chirality may require γ slightly different from 30^0 particularly for asymmetric configurations.

The results suggested that spin independence of the energy staggering parameter $S(I)$ within two-quasiparticle chiral bands (previously suggested a fingerprint of chirality) is found only if the Coriolis interaction can be completely neglected. However, if the configuration is non-restricted, the Coriolis interaction is often strong enough to create considerable energy staggering. It was also found that staggering in the intra- and inter-band $B(M1)$ reduced transition probabilities (proposed as another fingerprint of chirality) may be a result of effects other than strongly broken chirality. Therefore, the use of the $B(M1)$ staggering as a fingerprint of strongly broken chiral symmetry seems rather risky, in particular if the phase of the staggering is not checked.

February 2011

UNIVERSITY of the
WESTERN CAPE

ACKNOWLEDGEMENTS

I wish to express my sincere gratitude to the following for making the realization of this thesis possible:

- Dr E. A. Lawrie[1] for the supervision, support, guidance, encouragement and for being patient with me throughout the duration of this project,
- Prof R. Lindsay[2] for the guidance and support throughout the duration of this project,
- Prof J. F. Sharpey-Schafer[2] and Prof A. A. Pasternak[3] for reading this entire thesis,
- Dr R. T. Newman[1] for allowing me to pursue this research in the nuclear physics department,
- All staff members within the nuclear physics department at iThemba LABS,
- My parents and family members, for their love, guidance, moral support and so many things, just being there for me in time I needed them most and for inspiring me in my studies,
- The postgraduate students past and present, male and female at iThemba LABS for their friendship and supporting me,
- My wife (Mrs Lindelwa Shirinda), for giving me a strong courage especially when I am hopeless,
- The National Institute of Theoretical Physics (NITheP), National Research Foundation (NRF), University of the Western Cape (UWC) and iThemba LABS for the funding I received,
- The Almighty and all my ancestors.

This work is dedicated to my parents (Mr P. W. Shirinda and Mrs K. A. Shirinda).

Obed Shirinda **February 2011**

---

1. *iThemba LABS, P. O. Box 722, Somerset West, 7129, South Africa*
2. *Dept. of Physics, University of the Western Cape, Private Bag X17, Bellville 7535, South Africa*
3. *Cyclotron Laboratory, A.F loffe Physical-Technical Institute, 194021, ul. Polytechnitscheskaya 26, St.- Petersburg, Russia*

CONTENTS

LIST OF FIGURES

LIST OF TABLES

CHAPTER 1 Introduction

One of the hot topics in nuclear structure today is the suggested chirality in nuclei. Chirality is a symmetry which is present in nuclei when the total angular momentum of the system has an aplanar orientation forming either a left- or right-handed system [Fra97, Fra01]. The simplest chiral system is built on a two-quasiparticle configuration, (where one quasiparticle has predominantly particle nature, while the other one has predominantly hole nature), coupled to the rotation of the triaxial core. It is expected that the angular momenta of the odd particle and odd hole (both occupying orbitals of a high-j shell) point predominantly along the short and the long axes of the nucleus respectively, whereas the collective rotation occurs predominantly around the intermediate axis of a triaxially deformed nucleus in order to minimize the total energy of the system. Up to now candidates for chirality have been observed in the A ~ 100, 130 and 190 mass regions [Bal04, Bar01, Har01, Hec01, Hec03, Jos04, Jos05a-b, Jos07, Koi01, Koi03a, Law08, Law10b, Luo09, Mas09, Mer02, Moo00a-b, Pet02, Pet96, Rai03a-b, Sim05, Sta02, Tim04, Tim06, Tim07, Vam04 , Wan06, Yon05, Zhu03, Zhu05]. In these mass regions candidate chiral partner bands are associated with $\pi g_{9/2}^{-1} \otimes \nu h_{11/2}$, $\pi g_{9/2}^{-1} \otimes \nu h_{11/2}^{2}$, $\pi g_{9/2}^{-1} \otimes \nu h_{11/2}(d_{5/2}g_{9/2})$, $\nu h_{11/2} \otimes \nu(d_{5/2}g_{7/2})^{-1}$; $\pi h_{11/2} \otimes \nu h_{11/2}^{-1}$, $\pi h_{11/2}^{2} \otimes \nu h_{11/2}^{-1}$, $\pi h_{11/2}(d_{5/2}g_{7/2}) \otimes \nu h_{11/2}^{-2}$; and $\pi h_{9/2} \otimes \nu i_{13/2}^{-1}$ configurations respectively. When the chiral symmetry is strongly broken, a pair of degenerate $\Delta I = 1$ rotational bands should appear, i.e. two rotational bands with the same excitation energies, single-particle properties (such as alignments, Routhians, etc), collective properties (such as moments of inertia) and intra- and inter-band $B(M1)$ and $B(E2)$ reduced transition probabilities. Such degeneracy in a pair of $\Delta I = 1$ rotational bands is the most revealing feature of a strongly broken chiral system. Although chiral degeneracy is theoretically predicted by various models in A ~ 100, 130 and 190 mass regions, experimental confirmation of their existence has proved challenging, in particular no chiral partner bands were observed that show perfect degeneracy. Proposed fingerprints of chirality as of writing of this thesis are as follow: degeneracy in all measurable physical properties of the partner bands (i.e. the same excitation energies, the same intra- and inter-band $B(M1)$ and $B(E2)$ reduced transition probabilities, the same moment of inertia, the same quasiparticle alignments, etc) [Fra97, Fra01]; smooth dependence of the energy staggering parameter $S(I)$ with spin [Vam04]; and the staggering in opposite phase in the intra- and inter-band $B(M1)$ reduced transition probabilities

[Koi03b, Koi04, Koi05]. Note that none of the experimentally observed chiral partner bands fulfill all proposed fingerprints of chirality.

In order to try to explain the lack of perfect degeneracy in the chiral candidates, several phenomena which may affect it were investigated. For instance, it has been suggested that if the nuclear potential has a shallow minimum with respect to the γ deformation and the nuclear shape undergoes vibrations, the rotational angular momentum may be able to oscillate between the left- and right-handed systems [Sta01a]. Such chiral vibrations may create energy displacement between the chiral partners. Other phenomena which are suggested to destroy degeneracy are as follows: Coriolis effects at high spins and vanishing rotational angular momentum of the core along the intermediate nuclear axis [Fra97, Fra01]; deviation of the core shape from maximum triaxiality with $\gamma = 30^0$ [Sta01a, Zha07]; dynamical fluctuations of the nuclear shape [Ton07]; position of the Fermi level for the valence odd nucleons away from top/bottom of a high-j shell [Zha07]. Thus, it seems that degeneracy can occur in chiral nuclei with stable deformation and with suitable nucleon configuration. In this study we want to examine whether perfect degeneracy indeed occurs for such nuclei, and what may cause its disappearance. So the two-quasiparticle-plus-triaxial-rotor model (TQPRM) [Sem92] calculations were performed for the $\pi g_{9/2}^{-1} \otimes \nu h_{11/2}$, $\pi h_{11/2} \otimes \nu h_{11/2}^{-1}$ and $\pi h_{9/2} \otimes \nu i_{13/2}^{-1}$ chiral bands in A ~ 100, 130 and 190 mass regions respectively. The aims of doing this investigation are as follows: (i) to examine if there is a possibility that a strongly broken chirality exhibited by perfect degeneracy in the partner bands may exist in nuclei with large and stable triaxiality and with suitable two-quasiparticle configurations, (ii) to have a systematic study of the conditions for reaching degeneracy in the chiral partner bands built on two-quasiparticle configurations in A ~ 100, 130 and 190 mass regions, and (iii) to study further the characteristic features (more especially the energy staggering $S(I)$ parameter and the staggering in the reduced $B(M1)$ electromagnetic transition probabilities) of chiral partner bands.

The relevant nuclear models are discussed in chapter 2. The theoretical calculations and some previous studies in A ~ 100, 130 and 190 mass regions are presented in chapters 3 and 4. Discussion of the theoretical predictions is made in chapter 5. A summary of this work is given in chapter 6. Some results from theoretical calculations in A ~ 100, 130 and 190 mass regions are given in appendix A.

CHAPTER 2 Nuclear models

Nuclear models are developed to interpret specific features observed in nuclei in different mass regions. A good model is the one that could predict most of the features that nuclei exhibit. Usually in order to describe all features exhibited by all nuclei, more than one nuclear model is needed. The reason for this is that every nuclear model has its own limitations or shortcomings. For example the spherical shell model is only applicable to magic nuclei or nuclei near closed shell (i.e. near-spherical nuclei) and fails for nuclei whose particle number of protons Z and neutrons N are located far away from magic numbers. To predict features observed for nuclei located far away from shell gaps other models are needed (for example, Nilsson model). Up to the present there are varieties of nuclear models that one can use, but the applicability of the model rests on how the model relates to the physical properties of the nucleus. The nuclear models of interest to us are classified as microscopic or collective or a combination of the two. In this chapter nuclear models that will be reviewed include the shell model, the Nilsson model, and the particle-plus-rotor model (PRM).

To find the proper theoretical starting point some more formal estimates of the relevant physical quantities have to be introduced. The radii of nuclei follow the empirical law

$$R(A) = r_0 A^{1/3} \tag{2.1}$$

with $r_0 \sim 1.2$ fm. Nuclear radii thus range up to ~ 7.5 fm. The formula implies that the volume of the nucleus is proportional to the number of particles in the nucleus, indicating the near incompressibility of the nuclear matter. The least bound nucleon has a binding energy of the order of 8 MeV and kinetic energy close to 40 MeV. Since a nucleon has a mass of $mc^2 = 938$ MeV, the kinetic energy is quite negligible by comparison, so that a non-relativistic approach appears quite sufficient, and this assumption is made in the vast majority of nuclear structure models. The velocity of a nucleon with kinetic energy of 40 MeV is $\sim 0.3c$ and the associated de Broglie wavelength is $\lambda \sim 4.5$ fm. This result shows that quantum effects are certainly not negligible, as λ is small when compared to the nuclear radii. This is even more pronounced for the more tightly bound nucleons, which have a bigger kinetic energy.

Taking these considerations into account, the starting point for a theory of nuclear eigenstates should be a stationary Schrödinger equation very generally given by

$$H|\psi\rangle = E|\psi\rangle \tag{2.2}$$

The rest of the models are about what to write for Hamiltonian H and which degrees of freedom to use in the wave functions $|\psi\rangle$.

2.1 Microscopic versus collective models

Microscopic models are those in which the degrees of freedom are those of the constituent particles of the nucleus. The most natural selection for the degrees of freedom is to use nucleonic ones. The total Hamiltonian of the system consists of the Hamiltonians for the individual particles and the nucleon-nucleon interaction which may depend on all degrees of freedom of a pair of nucleons. It is one of the important features of nuclear theory that there is no a priori theory for the nucleon-nucleon interaction. Instead, various parameterizations are employed which are good for different purposes. Thus a typical microscopic model depends on a nucleon-nucleon interaction which necessarily contains parameters fitted to reproduce some experimental data. The lack of knowledge about the fundamental interaction is replaced by the proposal of a reasonable functional form with limited number of parameters, which can be determined from underlying theory. The proposal of suitable functional forms for the nucleon-nucleon interaction depends to a large extent on symmetry arguments.

A complementary and important role is also played by collective models. These are based on degrees of freedom that do not refer to individual nucleons, but instead indicate some bulk property of the whole nucleus. Note that in these cases it is possible to express the collective coordinates in terms of the microscopic ones, so that at least theoretically one should be able to go back and forth between both descriptions.

2.2 The shell model

The shell model forms the basis for various theoretical models. This model was first developed in the 1940s and many unsuccessful attempts were made in constructing a nuclear potential that will fit the observed properties of the nuclei.

Mayer [May49], Haxel, Jensen and Suess [Hax49] further developed this model in 1949 by introducing a spin-orbit interaction in the nuclear potential. It now accounts very well for the observed nuclear properties such as nuclear transitions, spins and parities of the states. It is also called a single-particle model because it treats the nucleons individually. The occurrence

of so-called magic numbers (N or Z is equal to 2, 8, 20, 28, 50, 82 and N = 126) has, from the experimental point of view, been one of the strongest motivations for the formulation of the nuclear shell model. Magic numbers correspond to filled major nuclear shells.

The shell model proposes that a valence nucleon moves in an attractive potential well created by the other nucleons in the nucleus. The most often discussed potential wells are an isotropic harmonic oscillator, infinite or finite square well and Woods-Saxon potential, which are shown in Figure 2.1. The infinite or finite square well potentials are an oversimplification of the nuclear potential as they have sharp edges which do not approximate the shape of the nuclear matter. The nuclear matter requires uniform charge distribution within the nuclear radius and to be zero outside the nucleus. For spherical nuclei, the potential must, in addition be spherically symmetric and depend only on the distance r from the centre of the nucleus. Another reasonable possibility is the harmonic oscillator potential, but it tends to infinity for large r. This potential therefore also gives an unrealistic shape of the nucleus. It is though, a good first approximation of the nuclear potential and can be represented by

$$V_{HO}(r) = -V_0 + \frac{1}{2} M \omega_0^2 r^2 \tag{2.3}$$

where V_0 is the well depth, M is the mass of the nucleon, and ω_0 is the oscillator frequency of a harmonic motion of the particle in a spherical potential.

The Woods-Saxon potential V_{WS} [Woo54] is an intermediate between the harmonic oscillator and square well potentials and represents a more realistic shape of the nucleus:

$$V_{WS}(r) = \frac{-V_0}{1 + e^{\left(\frac{r-R}{\alpha}\right)}} \tag{2.4}$$

where V_0, R and α are the potential depth, the mean nuclear radius and the surface thickness (≈ 0.524 fm) respectively.

The Hamiltonian H_{sph} of a single-particle moving in spherically symmetric potential of equation (2.3) is given by

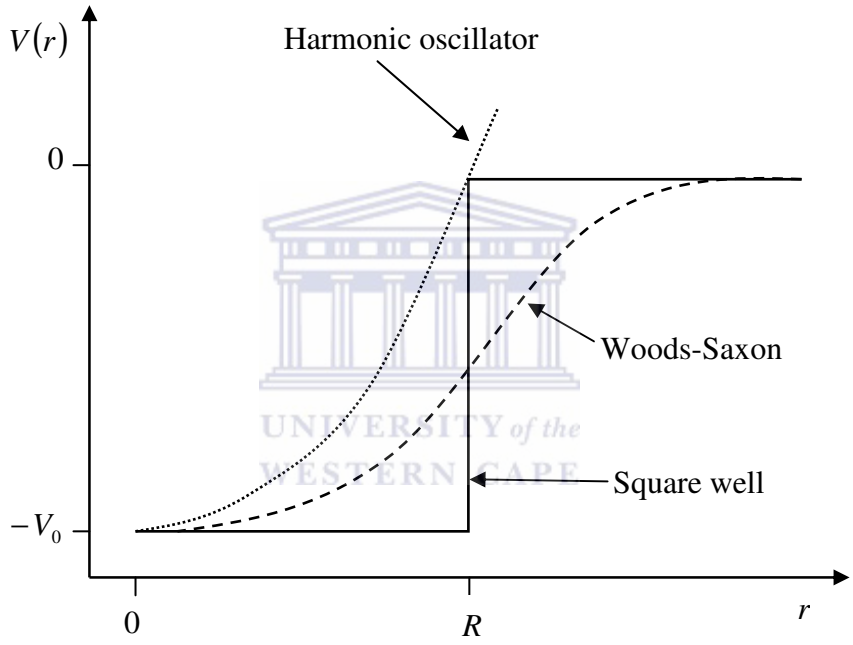

Figure 2.1: *A comparison of one-dimensional harmonic oscillator potential, square well potential and Woods-Saxon potential.*

$$H_{sph} = \frac{-\hbar^2}{2M}\nabla^2 + V_{HO}(r) \tag{2.5}$$

where ∇^2 is the Laplacian.

When the potential of equation (2.3) is included in the three-dimensional time independent Schrödinger equation, eigenvalues of the Hamiltonian H_{sph} with equally spaced energy levels are obtained,

$$E_N = \left(N + \frac{3}{2}\right)\hbar\omega_0 - V_0 \tag{2.6}$$

where E_N are the energy eigenvalues corresponding to the major oscillator quantum number N and $N = n_x + n_y + n_z$. In terms of n and l, the integer N is given by

$$N = 2(n-1) + l \tag{2.7}$$

where n, l are the radial quantum number and orbital angular momentum, respectively.

Note that n takes values 1, 2, 3, ... and l takes even values 0, 2, 4, ..., N if N is even and odd values 1, 3, 5, ..., N if N is odd. The l values are labelled using spectroscopic notation shown in Table 2.1.

Table 2.1: *Spectroscopic notations for l values.*

l **value**	0	1	2	3	4	5	6
Symbol	s	p	d	f	g	h	i

In Figure 2.2, each energy level is degenerate and is called a shell and it is labelled by integer values of N, where $N = 0, 1, 2, ...$ represents the number of the energy shell. Each shell can be occupied by $(N+1)(N+2)$ identical nucleons and this is shown in Table 2.2. The degeneracy $D(N)$ of each oscillator shell is calculated by

$$D(N) = \frac{1}{2}(N+1)(N+2) \tag{2.8}$$

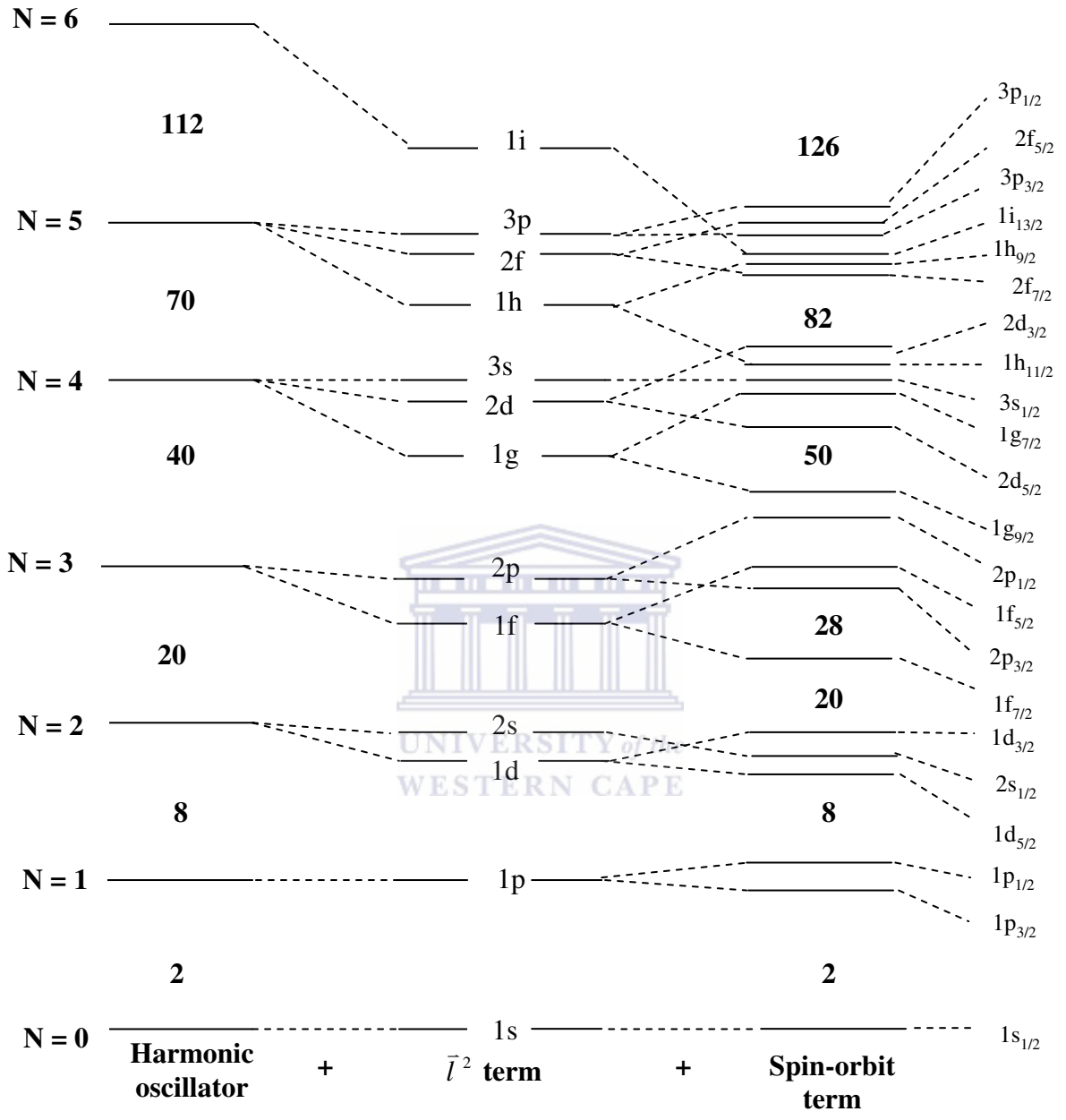

Figure 2.2: *Energy levels in a modified oscillator potential. The levels on the left are those for the harmonic oscillator potential. These are split by the $\vec{l}^{\,2}$ term to produce the second set of levels, and then again by the spin-orbit $(\vec{l}\,.\,\vec{s})$ term to produce the experimentally observed shells on the right [Cas00].*

The parity of each level is determined from

$$\pi = (-1)^{l} = (-1)^{N} \tag{2.9}$$

Table 2.2: *Allowed values of l, level label, oscillator energy E_N, maximum number of identical nucleons in each oscillator shell, and the total number of nucleons.*

N	Allowed l	Level label	$E_N(\hbar\omega_0)$	Occupation	Total
0	0	$1s$	3/2	2	2
1	1	$1p$	5/2	6	8
2	2, 0	$1d, 2s$	7/2	12	20
3	3, 1	$1f, 2p$	9/2	20	40
4	4, 2, 0	$1g, 2d, 3s$	11/2	30	70
5	5, 3, 1	$1h, 2f, 3p$	13/2	42	112

The shells corresponding to $N \geq 2$ consist of more than one degenerate levels called subshells. For example, for the shell corresponding to $N = 2$, $2s$ and $1d$ levels are subshells. Note that the shells are separated from each other by large gaps. The following magic numbers 2, 8, 20, 40, 70, 112 are obtained by the shell model calculations when a harmonic oscillator potential is used and this is shown in Figure 2.2. The first three magic numbers meet experimental observation but the model fails in predicting the higher ones. The next section presents the needed correction in the harmonic oscillator potential so that it can reproduce the correct experimental shell gaps. This correction was introduced in 1949 by Mayer [May49] following a suggestion by Fermi, and independently by Haxel, Jensen and Suess [Hax49].

2.2.1 Modification of the harmonic oscillator potential

2.2.1.1 Addition of $\vec{l}^{\,2}$ term

Inclusion of a term proportional to $\vec{l}^{\,2}$ leads to the following harmonic oscillator potential

$$V_{HO}(r) = -V_0 + \frac{1}{2}M\omega_0^2 r^2 - A\,\vec{l}^{\,2} \tag{2.10}$$

where A is an empirically determined constant. The actual correction is $A\left(\vec{l}^{\,2} - \left\langle \vec{l}^{\,2} \right\rangle_N\right)$, where $\left\langle \vec{l}^{\,2} \right\rangle_N = \frac{1}{2}N(N+3)$ is the expectation value of $\vec{l}^{\,2}$ averaged over one major shell with quantum number N. With this correction, only states within the shell are shifted and the

centre of gravity between different major shells remains unaffected. This provides a more realistic shape of the nuclear potential. The last term in equation (2.10) has an effect in splitting the degenerate oscillator levels into levels with different energies, particularly oscillator levels with $N \geq 2$. This shifts levels with higher l-values downward. The effect of this splitting is shown in Figure 2.2. But even when this term is added to the harmonic oscillator potential, the calculated magic numbers are not correct except the first three, which are 2, 8 and 20.

2.2.1.2 Addition of spin-orbit interaction term $(\vec{l} \,.\, \vec{s})$

The second correction that was done to the harmonic oscillator potential so that it produces the observed higher magic numbers is the addition of a term due to spin-orbit coupling. Mayer [May49], Haxel, Jensen and Suess [Hax49] proposed this correction. The mathematical form of the spin-orbit potential is

$$V_{SO}(r) = f(r)\,\vec{l}\,.\vec{s} \tag{2.11}$$

where $f(r)$ is the strength of the spin-orbit coupling which is peaked at the nuclear surface. One chooses $f(r)$ related to the spin independent part of the average potential in the following way:

$$f(r) = \lambda \frac{1}{r}\frac{\partial V(r)}{\partial r} \tag{2.12}$$

Hence the modified harmonic oscillator potential takes the form

$$V(r) = V_{HO}(r) + V_{SO}(r) \tag{2.13}$$

The spin-orbit interaction is proportional to the inner product of the orbital angular momentum $\vec{l}$ and spin angular momentum $\vec{s}$ of the nucleon. The spin-orbit coupling causes further splitting of the p, d, f, g, h, ... levels into two levels. The energy splitting of the levels increases with orbital angular momentum l. Choosing $V_{SO}(r)$ to be negative, the state with total angular momentum $j = l + s$ will be pushed down and the state with total angular

momentum $j = l - s$ will be raised up. Figure 2.2 shows the effect of this splitting. The $1f_{7/2}$ level now appears in the gap between the second and the third oscillator shells, and by adding a capacity of 8 more nucleons the magic number 28 is obtained. The p and d level splitting do not result in any major regrouping of the levels. The $1g_{9/2}$ level is pushed down to lower major shell and taking into account its capacity of 10 nucleons a magic number of 50 is calculated. A similar effect is observed at other higher major shells. The states with opposite parity from high-j N shell penetrating major oscillator shell below (i.e. $N-1$) are called intruder states. Note that the capacity of each level (with spin-orbit interaction included) is given by $2j+1$ with j being a good quantum number, and the states are therefore labeled by $n\,l\,j$ (e.g. $1f_{7/2}$). The magic numbers produced with the modified harmonic oscillator potential are 2, 8, 20, 28, 50, 82, 126 in agreement with experiment. The neutron or proton number 40 is sometimes called a semi-magic number.

2.3 Nuclear surface deformations

The excitation spectra of even-even nuclei in the energy range ≤ 2 MeV show characteristic band structures that are interpreted as vibrations and rotations of the nuclear surface in the geometrical collective model first proposed by Bohr and Mottelson [Bo52, Bo53] and elaborated by Faessler and Greiner [Fae62, Fae64a-b, Fae65a-c]. The moving nuclear surface may be described quite generally by an expansion in spherical harmonics:

$$R(\theta,\phi) = R_0\left[1 + \alpha_{00} + \sum_{\lambda=1}^{\infty}\sum_{\mu=-\lambda}^{\lambda}\alpha_{\lambda\mu}Y_{\lambda\mu}(\theta,\phi)\right] \tag{2.14}$$

where $R(\theta,\phi)$ denotes the nuclear radius in the direction (θ,ϕ), R_0 is the radius of the spherical nucleus, which is realized when all the $\alpha_{\lambda\mu}$ vanish, and $Y_{\lambda\mu}(\theta,\phi)$ are the spherical harmonics. The parameter λ gives the deformation type of the nucleus and μ is an integer taking its values from $-\lambda$ to $+\lambda$. The deformation parameter α_{00} with $\lambda = 0$ corresponds to monopole mode of deformation. This term (α_{00}) may be ignored because such deformation corresponds to the changes of the volume of the nucleus and is not expected to be seen except at high excitation energy. The next higher order terms, $\lambda = 1, 2, 3$ and 4 correspond to dipole, quadrupole, octupole and hexadecupole deformations respectively.

Shapes of nuclei associated with these kinds of deformations are shown in Figure 2.3. Most of the coming discussion of collective models will be based on quadrupole nuclear deformation (i.e $\lambda = 2$ mode of deformation).

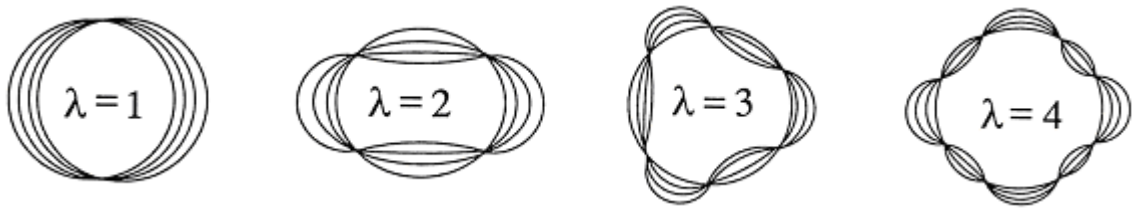

Figure 2.3: *Schematic representation of dipole, quadrupole, octupole and hexadecupole deformations* [Mar96].

Constraint on $R(\theta,\phi)$ and therefore on the parameters $\alpha_{\lambda\mu}$ is that $R(\theta,\phi)$ should be invariant under a reflection and a rotation of the coordinate system. In order for this to be the case, the parameters $\alpha_{\lambda\mu}$ must be multiplied by a factor $(-1)^{\lambda}$ under a parity transformation, and must behave like $Y_{\lambda\mu}(\theta,\phi)$ under a rotation of the coordinate system characterized by the Euler angles $\Omega = (\Omega_1, \Omega_2, \Omega_3)$ [Edm57].

In the case of quadrupole deformations ($\lambda = 2$), we have five coefficients for $\alpha_{2\mu}$. Not all of them describe the shape of the nucleus. Three determine only the orientation of the nucleus in space, and correspond to the three Euler angles $\Omega = (\Omega_1, \Omega_2, \Omega_3)$. By a suitable rotation we can transform to the body fixed system characterized by three axes 1, 2, 3, which coincide with the major axes of the nucleus. Then the five coefficients $\alpha_{\lambda\mu}$ reduce to two really independent variables α_{20} and $\alpha_{22} = \alpha_{2-2}$ $(\alpha_{21} = \alpha_{2-1} = 0)$, which together with the three Euler angles $\Omega = (\Omega_1, \Omega_2, \Omega_3)$ give a complete description of the system. The coefficients α_{20} and α_{22} are related to the Hill-Wheeler [Hil53] coordinates β_2, γ $(\beta_2 > 0)$ through the following equations:

$$\alpha_{20} = \beta_2 \cos\gamma \tag{2.15}$$

$$\alpha_{22} = \frac{1}{\sqrt{2}} \beta_2 \sin\gamma \tag{2.16}$$

The factor $\frac{1}{\sqrt{2}}$ was chosen such that

$$\sum_{\mu}\left|\alpha_{2\mu}\right|^2 = \alpha_{20}^2 + 2\alpha_{22}^2 = \beta_2^2 \tag{2.17}$$

The nuclear shape is then determined only in terms of β_2 and γ, where β_2 represents the extent of quadrupole deformation and γ gives the degree of axial asymmetry.

The increments of the three semi-axes in the body-fixed frame as a function of β_2 and γ are

$$\delta R_k(\theta,\phi) = \sqrt{\frac{5}{4\pi}}\beta_2 \cos\left(\gamma - \frac{2\pi}{3}k\right) \qquad k = 1, 2, 3 \tag{2.18}$$

where k refers to the three principal axes of the nucleus.

In Figure 2.4 the quadrupole shapes $(\lambda = 2)$ are represented in the polar coordinates β_2, γ. We see that γ values of 0^0 and -120^0 correspond to prolate spheroids which rotate collectively and non-collectively respectively, while $\gamma = -60^0$ and 60^0 correspond to oblate nuclei which rotate collectively and non-collectively respectively. Non-collective rotation occurs when the nucleus rotates around its symmetry axis. This mode of motion represents single-particle excitations. Within the sector $-60^0 < \gamma < 0^0$, we have maximum collective rotation of the nucleus. When γ is not a multiple of 60^0 (i.e. $0^0 < \gamma < 60^0$, $-60^0 < \gamma < 0^0$, and $-120^0 < \gamma < -60^0$) it corresponds to a triaxial shape. Within these three sectors i.e. $-120^0 < \gamma < -60^0$, $-60^0 < \gamma < 0^0$ and $0^0 < \gamma < 60^0$ the nucleus rotates around the longest, the medium and the shortest axis respectively [And76]. The cranked shell model (CSM) and total Routhian surface (TRS) calculations use this parameterization called the Lund parameterization. The parameterization using the quadrupole parameters of β_2 and γ is suitable when the nuclear potential is of the Woods-Saxon type.

There is another parameterization of the nuclear shape in terms of the quadrupole deformation parameters ε_2 and γ, which is often referred to as the Nilsson parameterization. It is used when the deformed harmonic oscillator potential is involved in the description of the nuclear potential. More details about this description of the nuclear potential are given in section 2.4. The parameters of deformation are included in the expression of the three harmonic oscillator frequencies, which correspond to the motion of the nucleon along the three principal axes [Boh52] (labelled 1, 2 and 3):

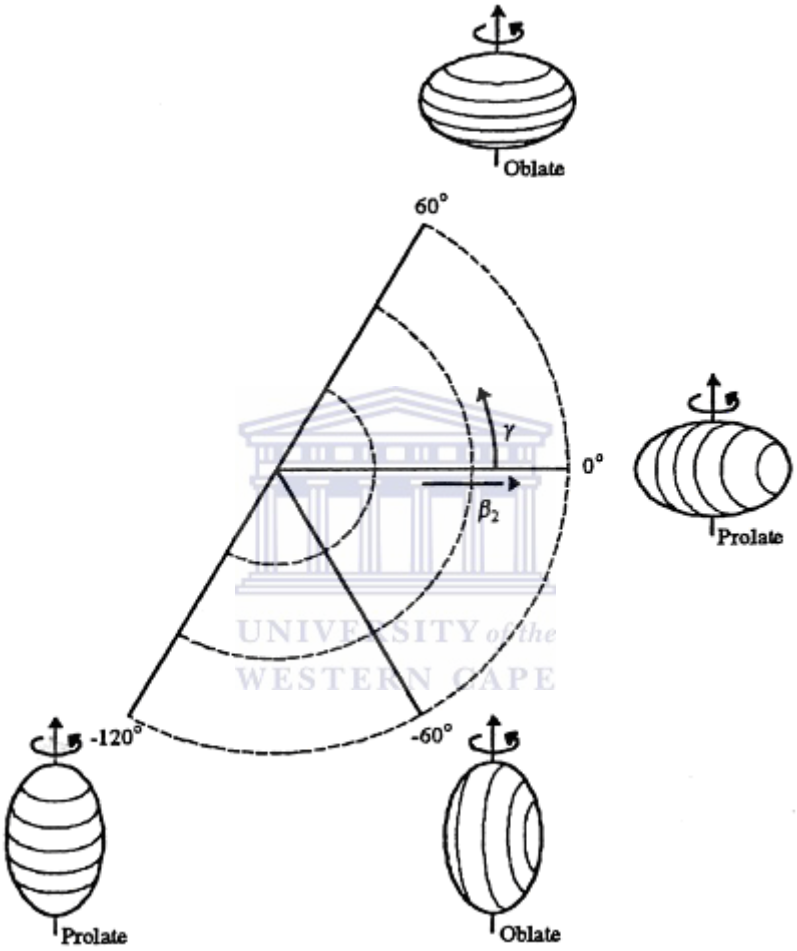

Figure 2.4: *Diagrammatic representation of the nuclear shape* $(\lambda = 2)$ *in the* β_2 *,*γ *plane [And76].*

$$\omega_1(\varepsilon_2,\gamma)=\omega_0\left\{1+\frac{1}{3}\varepsilon_2\cos\gamma+\frac{1}{\sqrt{3}}\varepsilon_2\sin\gamma\right\} \tag{2.19}$$

$$\omega_2(\varepsilon_2,\gamma)=\omega_0\left\{1+\frac{1}{3}\varepsilon_2\cos\gamma-\frac{1}{\sqrt{3}}\varepsilon_2\sin\gamma\right\} \tag{2.20}$$

$$\omega_3(\varepsilon_2,\gamma)=\omega_0\left\{1-\frac{2}{3}\varepsilon_2\cos\gamma\right\} \tag{2.21}$$

where ω_0 is the oscillator frequency of a harmonic motion of the particle in a spherical potential. The parameter ε_2 indicates the elongation of the nuclear potential, and the parameter γ describes its non-axiality. If $\gamma=0^0$ or 60^0, two of the axes will have the same length and therefore the nucleus is axially symmetric. For $\gamma=0^0$ the nucleus has a prolate ellipsoidal shape with the major axis being the axis of symmetry. For $\gamma=60^0$ the nucleus has an oblate shape with the axis of symmetry being the minor axis. The range $0^0<\gamma<60^0$ is sufficient to describe all the nuclear shapes, the three axes having different length.

The shape parameters (ε_2,γ) are used in the rigid triaxial rotor (RTR) calculations with the Nilsson nuclear potential. An alternative convention is that γ ranges from 0^0 (axially symmetric) to 30^0 (maximum axial asymmetric) and that the prolate nuclei have $\beta_2,\varepsilon_2>0$, while oblate nuclei have $\beta_2,\varepsilon_2<0$.

Both (ε_2,γ) and (β_2,γ) parameterizations of nuclear shape are equivalent. The γ parameter has the same value in both parameterizations, while the elongation parameters are not exactly the same. For not very large deformation $\varepsilon_2\approx 0.946\beta_2$.

2.4 The Nilsson model

If the nuclear shape is not spherical, the average nuclear potential created by the nucleons within the nucleus will no longer be spherically symmetric. Therefore the average nuclear potential proposed for the shell model discussed in section 2.2 needs to be modified in order to predict experimental observations for deformed nuclei. In this section two cases of a deformed potential well that approximate an axially symmetric ellipsoidal shape of the nucleus are used. The two ellipsoidal shapes are prolate and oblate. A parameterization in which the prolate nucleus has positive values of the deformation parameter ε_2 or β_2, whereas an oblate nucleus has negative values of ε_2 or β_2 is used.

Assuming that the nuclear shape is ellipsoidal, the average harmonic oscillator potential takes the form

$$V_{HO}(r) = \frac{M}{2}\left(\omega_x^2 x^2 + \omega_y^2 y^2 + \omega_z^2 z^2\right) \tag{2.22}$$

$$\frac{1}{2}M\overline{\omega}_0^2 R^2 = \frac{M}{2}\left(\omega_x^2 x^2 + \omega_y^2 y^2 + \omega_z^2 z^2\right) \tag{2.23}$$

where $\hbar\overline{\omega}_0 = 41A^{-1/3}$ MeV is the oscillator constant for the equivalent spherical nucleus. The axes X, Y, Z of an ellipsoid are given by

$$\overline{\omega}_0 R = \omega_x X = \omega_y Y = \omega_z Z \tag{2.24}$$

The condition of incompressibility of the nuclear matter requires that the volume of the ellipsoid be the same as that of the sphere, implying $R^3 = XYZ$, and this imposes a condition on the oscillator frequencies:

$$\overline{\omega}_0^3 = \omega_x \omega_y \omega_z \tag{2.25}$$

For spherical nuclei, the three frequencies $\omega_x, \omega_y, \omega_z$ are the same. Considering an axially symmetric deformed nuclei with the z-axis as the symmetry axis (i.e. $\omega_x = \omega_y \neq \omega_z$). The single-particle Hamiltonian can be written in the form

$$H_{def} = -\frac{\hbar^2}{2M}\nabla^2 + \frac{M}{2}\left[\omega_x^2\left(x^2 + y^2\right) + \omega_z^2 z^2\right] \tag{2.26}$$

It is convenient to introduce a deformation parameter δ (the eccentricity of the ellipsoid defined by $\Delta R / R_{rms}$ where ΔR is the difference between the semi-major and semi-minor axes of the ellipsoid and R_{rms} is the root mean square nuclear radius) [Nil55] using the following prescription

$$\omega_{\perp}^2 = \omega_x^2 = \omega_y^2 = \omega_0^2(\delta)\left(1+\frac{2}{3}\delta\right) \qquad \omega_z^2 = \omega_0^2(\delta)\left(1-\frac{4}{3}\delta\right) \tag{2.27}$$

which clearly fulfills the volume conservation condition of (2.25) to the first order with $\omega_0(\delta) = \overline{\omega}_0$. Volume conservation can be fulfilled to the second order using

$$\overline{\omega}_0^6 = \left(1-\frac{4}{3}\delta\right)\left(1+\frac{2}{3}\delta\right)^2 \omega_0^6(\delta) \tag{2.28}$$

leading in second order to

$$\omega_0(\delta) \approx \overline{\omega}_0\left(1+\frac{2}{9}\delta^2\right) \tag{2.29}$$

According to Nilsson [Nil55] one can introduce a deformation that depends on the length of the oscillator $b(\delta) = \left[\hbar / M\omega_0(\delta)\right]^{1/2}$ so that dimensionless coordinates expressed by prime $r', \theta', \phi', \ldots$ (i.e. $r' = r/b(\delta)$) can be used. Under these conditions the Hamiltonian of equation (2.26) becomes

$$H_{def} = -\frac{\hbar^2}{2M}\nabla'^2 + \frac{1}{2}M\omega_0^2(\delta)r'^2 - M\omega_0^2(\delta)r'^2\delta\frac{4}{3}\sqrt{\frac{\pi}{5}}Y_{20}(\theta',\phi') \tag{2.30}$$

where we have utilized the spherical harmonic $Y_{20}(\theta',\phi')$. For ellipsoids with small deformation, the deformation parameters δ and ε_2 are both approximately equal to β_2 since

$$\varepsilon_2 = \delta + \frac{1}{6}\delta^2 + \ldots \cong \delta \qquad \beta_2 = \frac{4}{3}\sqrt{\frac{\pi}{5}}\varepsilon_2 + \frac{4}{9}\sqrt{\frac{\pi}{5}}\varepsilon_2^2 + \ldots \cong 1.057\varepsilon_2 \tag{2.31}$$

Since spherical symmetry is broken but axial symmetry remains, the solutions of Nilsson Hamiltonian of equation (2.30) can be obtained using cylindrical coordinates [Flü71]. In cylindrical coordinates eigenstates of this Hamiltonian are characterized by quantum numbers n_z, n_ρ, m_l, (where m_l is the projection of the orbital angular momentum on the symmetry

axis), also called $\Lambda = m_l$. With the relations $N = n_z + 2n_\rho + m_l = n_x + n_y + n_z$ and assuming small deformation, the eigenvalues become

$$\begin{aligned} E(n_z, n_\rho, m_l) &= \hbar\omega_z\left(n_z + \frac{1}{2}\right) + \hbar\omega_\rho\left(2n_\rho + m_l + 1\right) \\ &\cong \hbar\overline{\omega}_0\left[\left(N + \frac{3}{2}\right) + \delta\left(\frac{N}{3} - n_z\right)\right] \end{aligned} \tag{2.32}$$

which implies a splitting, linear in the number of oscillator quanta in the z direction, as a function of the deformation variable δ. In this case m_l, the spin component s_z and the j-component j_z (where j_z is the total angular momentum along the z-axis) are good quantum numbers. The eigenvalues Ω of j_z are given by

$$\Omega = m_l + m_s = m_l \pm \frac{1}{2} \tag{2.33}$$

Two terms similar to the ones included in the case of spherical potential were also added in the Nilsson deformed harmonic oscillator potential in order to give realistic single-particle energies [Nil55]. So, the Nilsson Hamiltonian of equation (2.30) becomes

$$\begin{aligned} H_{def} = &-\frac{\hbar^2}{2M}\nabla^{'2} + \frac{1}{2}M\omega_0^2(\delta)r^{'2} - M\omega_0^2(\delta)r^{'2}\delta\frac{4}{3}\sqrt{\frac{\pi}{5}}Y_{20}(\theta^{'},\phi^{'}) \\ &- \kappa\hbar\overline{\omega}_0\left\{2\vec{l}.\vec{s} + \mu\left(\vec{l}^{\,2} - \left\langle\vec{l}^{\,2}\right\rangle_N\right)\right\} \end{aligned} \tag{2.34}$$

where

$$\mu^{'} = \kappa\mu \tag{2.35}$$

The Nilsson Hamiltonian of equation (2.34) does not contain a Coulomb term, the effect of that term is contained in the appropriate choice of the constants κ and μ. To get a good fit of the experimental data, different values of κ and μ for different shells are used. κ typically takes values around 0.06 and μ varies from 0 to ~ 0.7 for different shells.

For small deformations, j_z is approximately a good quantum number. The eigenstates of the Hamiltonian of equation (2.34) can be labeled by the quantum numbers $N\,l\,j\,m$ of the spherical single-particle sates. The expression for the energy eigenvalues is given by

$$\begin{aligned} E(n_z, n_\rho, m_l) &= \hbar\overline{\omega}_0\left[\left(N+\frac{3}{2}\right)+\delta\left(\frac{N}{3}-n_z\right)\right]-2\kappa\hbar\overline{\omega}_0 m_l m_s \\ &= -\mu'\hbar\overline{\omega}_0\left[m_l^2+2n_\rho n_z+n_\rho-\frac{N(N+3)}{2}\right] \end{aligned} \tag{2.36}$$

In the opposite limit of large deformations, the $\vec{l}.\vec{s}$ and $\vec{l}^{\,2}$ terms are negligible and the Hamiltonian of equation (2.34) simply reduces to an anisotropic harmonic oscillator. In this limit, the cylindrical quantum numbers $\Omega^{\pi}[N\ n_z\ m_l]$ can be used to label single-particle orbitals. The quantum numbers in the square bracket are called asymptotic quantum numbers. The only quantum numbers that remain conserved are the parity π and Ω, while N, n_z and m_l are only approximate and may be determined for a given level only by looking at its behavior near the spherical state. In this case energy eigenvalues are calculated using expression given in equation (2.32).

2.4.1 Nilsson diagrams

Even though these diagrams seem to be very complicated, many properties of the Nilsson orbitals can be understood in simple terms. For the deformed modified harmonic oscillator potential, the single-particle levels are split according to the projection Ω of the total angular momentum j along the symmetry axis of the nucleus. The splitting of the levels depends on the total angular momentum j of the orbital and the deformation δ. Due to the reflection symmetry of the nucleus, Ω has two-fold degeneracy, i.e. $\pm\Omega$ and the corresponding single-particle levels have the same energy. An odd particle in a particular j shell will orbit the nucleus with specific Ω value ranging from,

$$-j \le \Omega \le j \tag{2.37}$$

For example, the $2f_{7/2}$ orbital will have eight possible orientation of j ranging from -7/2 to 7/2. Therefore $f_{7/2}$ level will split into four states labeled $\Omega = 1/2, 3/2, 5/2, 7/2$ and with

negative parity, since the parity is determined from $(-1)^l$ and each orbital can be occupied by a maximum of two nucleons. At $\varepsilon_2 = 0$ the nucleus is spherical and the Nilsson diagram in Figure 2.5 shows degenerate levels, with each holding the maximum of $2j+1$ nucleons. Figure 2.5 also shows how the levels would split as the deformation increases. When the deformation increases the spherical states mix with each other resulting into new smaller gaps, hence new magic numbers are produced. Figure 2.5 shows this kind of situation. According to Pauli exclusion principle, it is not allowed in quantum mechanics for any two levels with same quantum numbers to cross. Since Ω and π are good quantum numbers in Nilsson model, we can expect that as orbits with the same Ω and π approach each other, they must repel each other. The repulsive interaction between two energy levels is commonly referred to as mixing. Even though the levels may not cross, this interaction between them implies that the wave function properties are exchanged near the turning point. Nilsson diagram shows single-particle levels for prolate and oblate deformed nuclei. In order to see which state has lowest energy among the states originating from j shell, let us first consider an odd particle orbiting a prolate deformed nucleus. We may define the classical orbit angle θ by

$$\theta = \sin^{-1}\left(\frac{\Omega}{j}\right) \tag{2.38}$$

From equation (2.38) we can see that for low Ω values, the orbiting odd particle is closer to the bulk of the nuclear matter. In addition to this, it is evident from equation (2.38) that θ changes slowly for low Ω values and more rapidly for high Ω ones. Therefore the difference in energy between successive Ω values increases with increasing Ω. Therefore for prolate deformation ($\varepsilon_2 > 0$), the state with smallest possible value of Ω (equal to 1/2) interacts more strongly with the core (bulk of the nuclear matter) and is thus strongly bound and lowest in energy (see left panel of Figure 2.6). The situation is opposite for oblate deformation ($\varepsilon_2 < 0$), in which the state with maximum Ω (equal to j) has the strongest interaction with the core and thus is lowest in energy (see right panel of Figure 2.6). Figure 2.7 shows schematically the Ω-splitting effect for an odd particle placed in an orbital with $j = 7/2$.

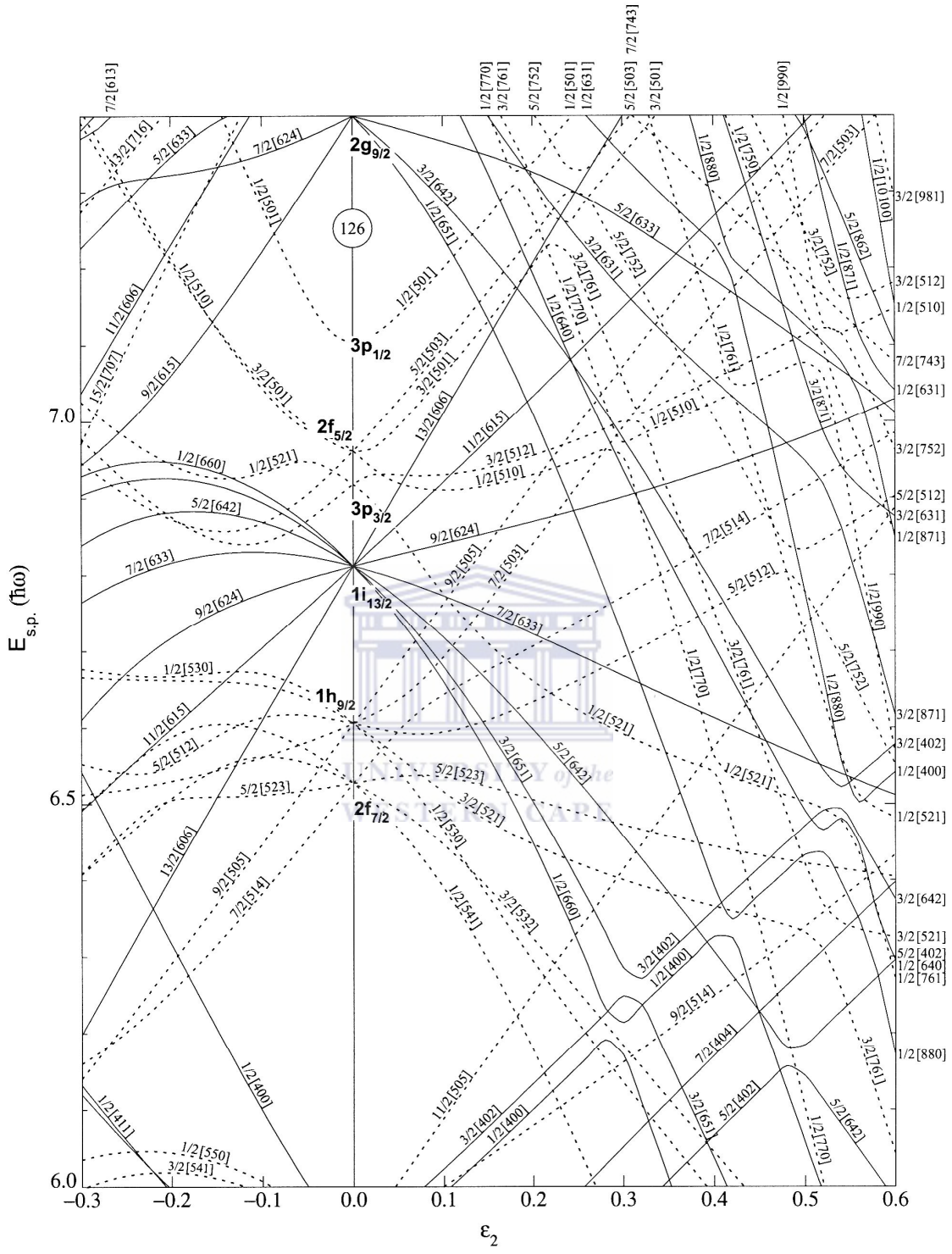

Figure 2.5: *Energy levels for neutrons ($82 \le N \le 126$) in a prolate ($\varepsilon_2 > 0$) and oblate ($\varepsilon_2 < 0$) deformed potential as a function of ε_2 ($\varepsilon_4 = \varepsilon_2^2 / 6$). The quantum numbers $\Omega[N\ n_z\ m_l]$ label the states. Solid and dashed lines show states with positive and negative parity respectively [Fir96a].*

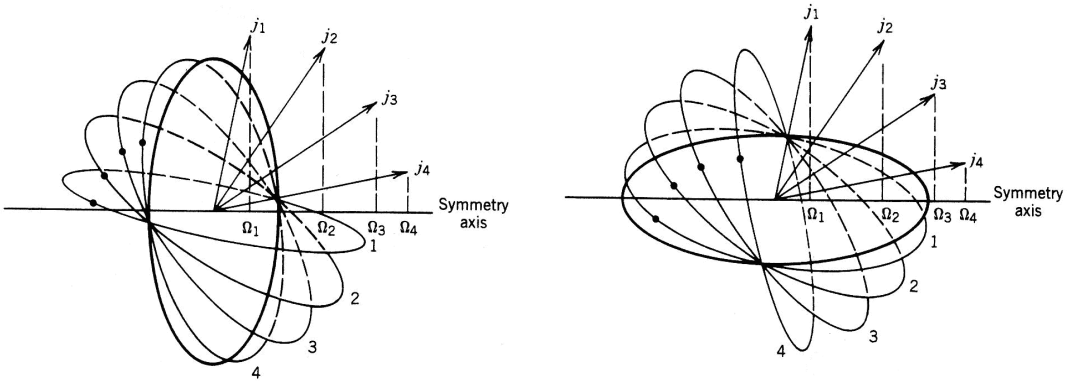

Figure 2.6: *Single-particle orbits with* $j = 7/2$ *and the possible projections of* j *along the symmetry axis, for prolate (left panel) and oblate (right panel) deformations. The possible projections are* $\Omega = 1/2, 3/2, 5/2, 7/2$ *(for clarity only the positive projections are shown). Note that in the prolate case, orbit 1 lies closest (on the average) to the core and will interact most strongly with the core while in the oblate case, it is orbit 4 that has the strongest interaction with the core [Kra98].*

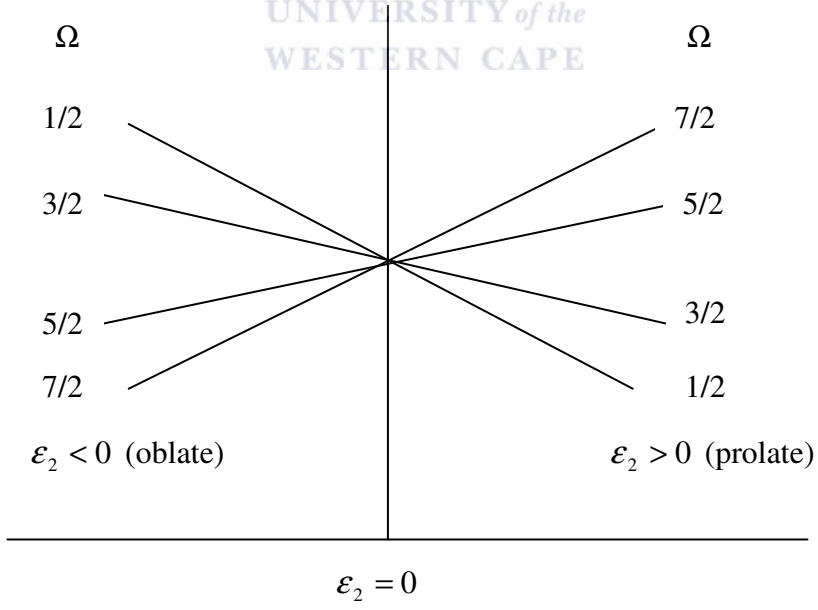

Figure 2.7: *Schematic representation of* Ω *splitting effect of the* $j = 7/2$ *orbital.*

2.5 Nuclear rotation

An important consequence of deformation is the fact that rotational motion is a possible mode of excitation. In the spherical case shown in Figure 2.8 (a), it is not possible to observe collective rotation about an axis of symmetry, since the different orientations of the nucleus are quantum-mechanically indistinguishable. In the case of an axially symmetric nucleus shown in Figure 2.8 (b) and (c), there is a set of axes of rotation, perpendicular to the symmetry axis. The collective motion of many nucleons around this rotation axis generates the rotational angular momentum $\vec{R}$.

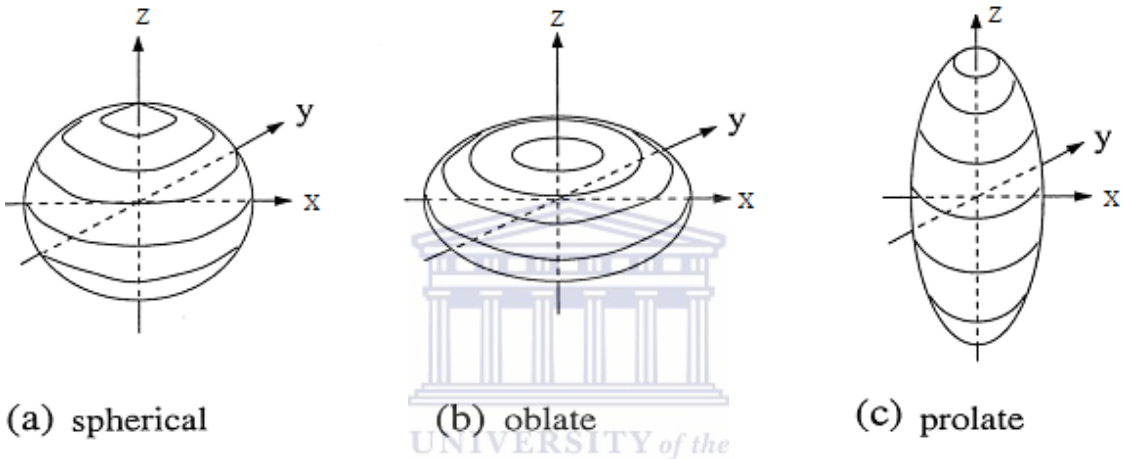

Figure 2.8: *Schematic representation of the spherical (a), oblate (b) and prolate (c) nuclear shapes. The z-axis represents the symmetry axis for these nuclear shapes [Mab03].*

2.5.1 Non-collective (single-particle) motion

Non-collective motion is mainly observed in spherical or weakly deformed nuclei. The total angular momentum is generated by the alignment of the individual nucleon spins. The bulk of the nucleons from the rest of the nuclear matter (the core) make no contribution due to pair correlations. The resulting level scheme shows irregular sequences of states connected by γ-transitions with different energies and multipolarities.

2.5.2 Collective motion

Well-deformed nuclei characterized by non-spherical mass distribution are known to show collective motion. The well-deformed nuclei give rise to regular sequences of states with consecutively increasing angular momentum known as rotational bands. The total angular momentum comes from the coherent motion of the whole nucleus. For an ellipsoidal nucleus (prolate or oblate) rotation takes place around the axis perpendicular to the symmetry axis of

the nucleus, while for a triaxial nucleus rotation takes place around any one of the three axes. The relation between the excitation energy E_{exc} and spin I for the states in the rotational bands can be approximated by

$$E_{exc} \propto I(I+1) \tag{2.39}$$

The lowest level of the rotational band is called the bandhead.

2.5.3 Nuclear angular momentum

To describe the interplay between the motion of the particles and the collective rotation, consider an axially symmetric deformed nucleus rotating around the x-axis, with orbiting valence nucleon as shown in Figure 2.9. The total angular momentum, $\vec{I}$, of the nucleus is given by

$$\vec{I} = \vec{R} + \vec{J} \tag{2.40}$$

where $\vec{R}$ is the angular momentum generated by the collective rotation of many nucleons (core) around the x-axis, and $\vec{J}$ is the intrinsic angular momentum that is generated by the valence nucleon.

If there are more than one valence nucleons, the intrinsic angular momentum of the valence nucleons $\vec{J}$ is represented as the sum of the angular momenta of the individual valence nucleons, i.e.

$$\vec{J} = \sum_{i=1}^{A} \vec{j}_i \tag{2.41}$$

The projection of the total angular momentum $\vec{I}$ on to the symmetry axis is K, and is the same as the projection of $\vec{J}$. The projection of the angular momentum $\vec{j}_i$, of a valence nucleon is Ω_i, thus

$$K = \sum_{i=1}^{A} \Omega_i \tag{2.42}$$

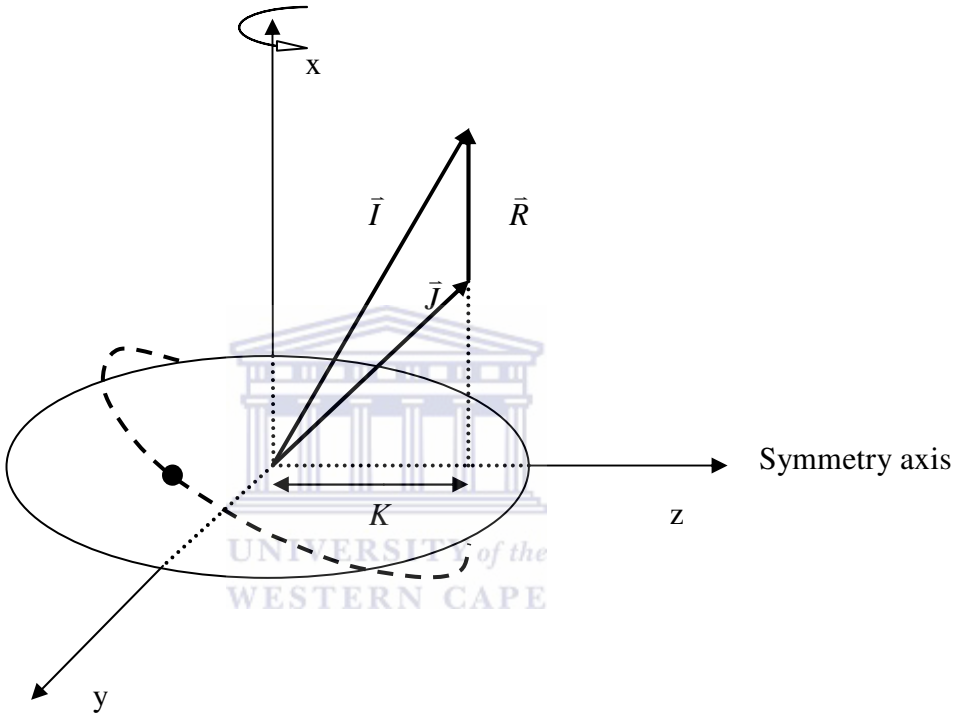

Figure 2.9: *Schematic of the coupling of the collective angular momentum* $\vec{R}$*, and the intrinsic angular momentum of valence nucleons* $\vec{J}$*. The projection of the total angular momentum* $\vec{I}$*, on to the symmetry axis is* K*.*

The projection of the total angular momentum on to the rotational axis is given by

$$I_x = \left\{\sqrt{I(I+1)-K^2}\right\}\hbar \tag{2.43}$$

and it is known as the aligned angular momentum.

In the ground state rotational band of an even-even nucleus, the valence particles are paired such that $\vec{J}=0$, and the total angular momentum is $\vec{I}=\vec{R}$. Therefore the collective rotational energy can be determined through analogy with a classical rotating rigid body. The classical kinetic energy of the rotating body is given by

$$E = \frac{1}{2\Im}\vec{R}^2 = \frac{1}{2\Im}\vec{I}^2 \tag{2.44}$$

where $\Im$ is the classical moment of inertia. Quantum mechanically, the length of $\vec{I}^2$ is $I(I+1)\hbar^2$. Using this relation, equation (2.44) becomes

$$E = \frac{\hbar^2}{2\Im} I(I+1) \tag{2.45}$$

Thus the rotational motion of the nucleus leads to a sequence of states with energies given by equation (2.45). It is a simple expression for the energies of a collective rotating nucleus, when there are no single-particle excitations. One can calculate from equation (2.45) that a restricted rigid rotor would have $E(I=4^+)/E(I=2^+)=3.33$, and in fact most of the N = 92, 94 and 96 nuclei have ratios near this value [Hey99]. However, real nuclei deviate from the $I(I+1)$ law. This deviation may be expressed by an expansion in powers of the quantity $I(I+1)$ as follows:

$$E(I) = E_0 + AI(I+1) + B[I(I+1)]^2 + C[I(I+1)]^3 + \ldots \tag{2.46}$$

It turns out that this expansion is poorly convergent for higher values of the angular momentum I, and an expansion in the angular frequency ω is more appropriate. In principle, ω is not a measurable quantity. We can define it classically as

$$\omega = \frac{dE}{dI} \tag{2.47}$$

The quantum-mechanical analogue (where I is replaced by I_x) of this is given by

$$\hbar\omega = \frac{dE(I)}{d\sqrt{I(I+1)-K^2}} \tag{2.48}$$

where $\sqrt{I(I+1)-K^2}$ is the projection of the total angular momentum on the rotational axis. For $K=0$, a rotational band of stretched $E2$ transitions is formed. Thus a transition from an initial state with spin I to a final state with spin $I-2$ has γ-ray energy

$$E_\gamma = E(I) - E(I-2) \tag{2.49}$$

If the rotational frequency ω is expanded along the average value of the angular momentum between I and $I-2$, we obtain

$$\hbar\omega(I-1) = \frac{E(I)-E(I-2)}{\sqrt{I(I+1)}-\sqrt{(I-2)(I-1)}} \approx \frac{E_\gamma}{2} \quad when \;\; I >> 1 \tag{2.50}$$

Thus the rotational frequency is directly related to the γ-ray energy.

Another energy expansion in powers of angular velocity ω of rotation introduced by Harris [Har65] is as follows:

$$E(I) = \alpha\omega^2 + \beta\omega^4 + \gamma\omega^6 + \ldots \tag{2.51}$$

Odd powers of ω do not occur, since $E(I)$ cannot change by reversing the angular velocity. The series in equation (2.51) is often taken up to the second term only.

Further attempts to explain the deviation from the $I(I+1)$ law for low lying second 2^+ sates in many nuclei have been undertaken by Davydov *et al.* using the picture of a pure triaxial rotor model [Dav58, Dav59a-b, Dav65]. This will be explained in more detail in section 2.6.2.

2.5.4 Moment of inertia

It should be noted that the nucleus is not a rigid body, and measured moments of inertia are less than rigid body values at low spins [Bar57]. This is due to the effects of the pairing interactions, which make the nucleus behave like a superfluid. Experimental moments of inertia are larger than those of the corresponding irrotational flow of a superfluid, showing that the nucleus is somewhere between these two extremes. As the nucleus rotates, it is found that the moment of inertia changes as a function of spin.

Rotational energy spectra can be discussed in terms of three spin-dependent moments of inertia, which are related to the zero-, first- and second-order derivatives of the excitation energy with respect to the aligned angular momentum I_x.

An expression for the static moment of inertia $\Im = \Im^{(0)}$, which is related to the excitation energy E, and spin I, in the $K = 0$ rotational band is shown in equation (2.44). By substituting an expression of the total aligned angular momentum $I_x^2 = I(I+1)\hbar^2$ into equation (2.44), one obtains an expression which can be used to calculate the static moment of inertia.

$$\Im^{(0)} = \frac{\hbar^2}{2}\left(\frac{E}{I_x^2}\right)^{-1} = \frac{\hbar^2}{2}\frac{I_x^2}{E} \tag{2.52}$$

The first derivative of equation (2.45) is the kinematical moment of inertia, $\Im^{(1)}$, which is related to the total angular momentum of the nucleus [Boh81]. The kinematical moment of inertia is given by:

$$\Im^{(1)} = I_x\left(\frac{dE}{dI_x}\right)^{-1}\hbar^2 = \hbar\frac{I_x}{\omega} \tag{2.53}$$

The kinematical moment of inertia can be related to the transition energy E_γ, through equation (2.50). Thus, for $K = 0$ rotational band

$$E_\gamma = \frac{\hbar^2}{\Im^{(1)}}(2I - 1) \tag{2.54}$$

The second derivative of equation (2.45) is the dynamical moment of inertia $\Im^{(2)}$, which carries information about the response of the nucleus if it is subjected to an applied torque [Boh81]. This dynamical moment of inertia is given by:

$$\Im^{(2)} = \left(\frac{d^2 E}{dI_x^2} \right)^{-1} \hbar^2 = \hbar \frac{dI_x}{d\omega} \tag{2.55}$$

For a rotational band consisting of $E2$ γ-ray transitions, the dynamical moment of inertia can be related to the difference in the transition energy of two consecutive γ-rays,

$$\Delta E_\gamma = \frac{4\hbar^2}{\Im^{(2)}} \tag{2.56}$$

For a dipole band consisting of $M1$ γ-ray transitions, the dynamical moment of inertia is also related to the difference of the energy of the consecutive γ-rays as

$$\Delta E_\gamma = \frac{\hbar^2}{\Im^{(2)}} \tag{2.57}$$

If the dynamical moment of inertia was constant, the transition energy difference would be the same for all values of spin. Often $\Im^{(2)}$ is found to vary with increasing spin. The two moments of inertia $\Im^{(1)}$ and $\Im^{(2)}$ can be related as follows:

$$\Im^{(2)} = \frac{dI_x}{d\omega} = \frac{d}{d\omega}\left(\omega \Im^{(1)}\right) = \Im^{(1)} + \omega \frac{d\Im^{(1)}}{d\omega} \tag{2.58}$$

In the limit of rigid rotation, $\Im^{(2)} = \Im^{(1)}$. Starting from the explicit definition of the rotational frequency ω in equation (2.47), the following relation can be derived

$$\frac{dE}{d\omega} = \omega \frac{dI}{d\omega} \tag{2.59}$$

which leads to the expansion for $\Im^{(2)}$, which is similar to the Harris expansion in equation (2.51):

$$\Im^{(2)} = 2\alpha + 4\beta\omega^2 + 6\gamma\omega^4 + \ldots \tag{2.60}$$

The integration of equation (2.58) yields the expansion for $\Im^{(1)}$:

$$\Im^{(1)} = 2\alpha + \frac{4}{3}\beta\omega^2 + \frac{6}{5}\gamma\omega^4 + \ldots \tag{2.61}$$

In practice, instead of $\alpha, \beta, \gamma, \ldots$, the parameters $J_0, J_1, J_2, \ldots$ (called the Harris parameters), are commonly used, where

$$J_0 = 2\alpha, \quad J_1 = \frac{4}{3}\beta, \quad J_2 = \frac{6}{5}\gamma \tag{2.62}$$

Then equations (2.60) and (2.61) become:

$$\Im^{(1)} = J_0 + J_1\omega^2 + J_2\omega^4 + \ldots \tag{2.63}$$

$$\Im^{(2)} = J_0 + 3J_1\omega^2 + 5J_2\omega^4 + \ldots \tag{2.64}$$

The Harris expansion equations (2.63) and (2.64), even if they are taken up to the first two terms, give very good agreement with the experimental data in the spin regions comprise of pure particle configuration (i.e. the spin region without particle excitations or band crossings) of even-even deformed nuclei. The shortened expansions are used to fit the moment of inertia of a band structure, which can serve later as a reference for other rotational bands in the nucleus, e.g. the reference rotor.

2.6 The particle-plus-rotor model (PRM)

This model developed by Bohr [Boh52], and by Bohr and Mottelson [Boh53] and elaborated by Faessler and Greiner [Fae62, Fae64a-b, Fae65a-c] describes the interplay between the motion of the particles and the collective rotation. Bohr and Mottelson described microscopically only a few so-called valence particles, which move more or less independently in the deformed well of the core. These valence particles are coupled to a

collective rotor, which stands for the rest of the particles. In an odd mass nucleus the unpaired nucleon is treated as a valence nucleon coupled to an even-even core. One can also attribute the particle-hole excitations in this nucleus to the excitations of the valence particles.

The nuclear Hamiltonian is divided into two parts: an intrinsic part H_{int}, which describes microscopically one or more valence particles near the Fermi surface, and a phenomelogical part H_{core} which describes the collective nuclear rotation, $\frac{\hbar^2}{2\Im_k}\vec{R}^2$, where $k = 1, 2, 3$ defines the three principal axes of the nucleus. The expression for the total Hamiltonian is

$$H = H_{\text{int}} + H_{core} \tag{2.65}$$

The intrinsic part has the form:

$$H_{\text{int}} = \sum_k \varepsilon_k a_k^+ a_k + \frac{1}{4}\sum_{klmn} \overline{\upsilon}_{klmn} a_k^+ a_l^+ a_n a_m \tag{2.66}$$

where ε_k are single-particle energies in the deformed potential (e.g. Nilsson energies), a_k^+, a_k, a_n, a_m are quasiparticle operators, and $\overline{\upsilon}$ is the interaction between the valence particles which is neglected in many cases.

The collective part has the form:

$$H_{core} = \frac{\vec{R}_1^2}{2\Im_1} + \frac{\vec{R}_2^2}{2\Im_2} + \frac{\vec{R}_3^2}{2\Im_3} \tag{2.67}$$

where $\vec{R}_i$ are the body fixed components of the collective angular momentum of the core. The sum of the collective angular momentum $\vec{R}$ of the core and the intrinsic angular momentum of the valence particles $\vec{j}$ give the total angular momentum of the system (see section 2.5.3).

$$\vec{I} = \vec{R} + \vec{j} \tag{2.68}$$

Substituting equation (2.68) into equation (2.67), H_{core} can be decomposed into three parts:

$$H_{core} = H_{rot} + H_{rec} + H_{cor} \tag{2.69}$$

where

$$H_{rot} = \frac{\vec{I}_1^{\,2}}{2\Im_1} + \frac{\vec{I}_2^{\,2}}{2\Im_2} + \frac{\vec{I}_3^{\,2}}{2\Im_3} \tag{2.70}$$

$$H_{rec} = \sum_{i=1}^{3} \frac{\vec{j}_i^{\,2}}{2\Im_i} \tag{2.71}$$

$$H_{cor} = -\sum_{i=1}^{3} \frac{\vec{I}_i \cdot \vec{j}_i}{\Im_i} \tag{2.72}$$

The expression in equation (2.70) is the pure rotational operator of the core which acts only on the degrees of freedom of the rotor, i.e. the Euler angles. The term in equation (2.71) is called the recoil term which represents the recoil energy of the rotor. The Coriolis interaction term in equation (2.72) couples the degree of freedom of the valence particles to the degree of freedom of the rotor.

This model is effective in describing slow nuclear rotation. Using it, a large number of the experimental spectra of odd nuclei have been reproduced very accurately. Nowadays, with some modifications this model has become the best tool of studying chirality in nuclei (this nuclear symmetry will be explained in more detail in chapter 3).

Some of the most commonly used particle-plus-core coupling models are:

(i) the axially symmetric particle-plus-rotor model (for example see reference [Rin80])

(ii) the asymmetric particle-plus-rotor model commonly known as particle-plus-triaxial-rotor model (example see references [Dav58, Dav59a-b, Dav65, Mey75, Lar78])

(iii) the core-quasiparticle coupling model (CQCM) and the interacting boson-fermion model (IBFM) which are applicable to a broader variety of collective cores (i.e. the core has greater flexibility). With an appropriate choice of the core description, the CQCM contains the particle-plus-vibrator and particle-plus-rotor models listed above. The IBFM uses the interacting boson model (IBM) for its core description.

More discussion will be given for the particle-plus-core coupling models (i) and (ii), because we have used a version of them in our work.

2.6.1 The axially symmetric particle-plus-rotor model

Assuming that the 3-axis is the axis of symmetry of the rotor, i.e. $\Im_1 = \Im_2 = \Im$, there can be no collective rotation around this axis and the 3-component of $\vec{R}$ has to vanish. From equation (2.67) it follows immediately that K, the 3-component of the total angular momentum $\vec{I}$, has to be equal to Ω, the 3-component of $\vec{j}$:

$$K = \Omega \tag{2.73}$$

For the different terms of the Hamiltonian (2.65, 2.69), we obtain in this case

$$H_{\text{int}} = \sum_{i,\Omega} \varepsilon^i_\Omega a^+_{i,\Omega} a_{i,\Omega} \tag{2.74}$$

$$H_{rot} = \frac{\vec{I}^2 - I_3^2}{2\Im} \tag{2.75}$$

$$H_{rec} = \frac{1}{2\Im}\left(j_1^2 + j_2^2\right) \tag{2.76}$$

$$H_{cor} = -\frac{1}{\Im}\left(I_1 j_1 + I_2 j_2\right) = -\frac{1}{2\Im}\left(I_+ j_- + I_- j_+\right) \tag{2.77}$$

where I_+, I_- and j_+, j_- are the raising and lowering operators of total angular momentum and particle angular momentum respectively (i.e. $I_\pm = I_1 \pm iI_2$ and $j_\pm = j_1 \pm ij_2$). The selection rule for $j_\pm$ and $I_\pm$ is $\Delta\Omega = \pm 1$. This leads to an admixture of states with different Ω values. It is only for $\Omega = 1/2$ that the diagonal matrix elements of the $(I_+ j_- + I_- j_+)$ expression are different from zero, and therefore give an additional contribution to the energy.

In equation (2.74) we have neglected the residual interaction. The single-particle levels in the axially symmetric well are labelled by (i, Ω), and the corresponding eigenfunctions are denoted by Φ^i_Ω, where i stands for all other Nilsson quantum numbers (see sections 2.4 and 2.4.1) associated with that eigenfunction. The recoil term in equation (2.76) only acts in the intrinsic coordinate system. It is often neglected because the intrinsic single-particle energies ε^i_Ω are adjusted to experimental data. In the following discussion we will omit H_{rec}. However, the different terms in equation (2.74-2.77) are of different importance, depending on the physical situation. Therefore, it is useful to consider two limits in which one of the

terms becomes predominant and which as a consequence can be solved analytically (see [Ste75]):

(i) the strong coupling limit (deformation alignment),

(ii) the decoupling limit (rotational alignment).

2.6.1.1 The strong coupling limit (deformation alignment)

The strong coupling limit is realized when the Coriolis term is small compared with the level splitting of the single-particle energies in the deformed shell model for different values of Ω. The deformation alignment takes place in a nucleus with large deformations ε_2 or β_2, and at low spins I, or when nucleons occupy orbitals with small angular momentum j. It is called strong coupling or deformation alignment limit because in this case K is a good quantum number. The angular momentum j of the valence particles is strongly coupled to the motion of the core as shown in the top panel of Figure 2.10. In this case, the rotational band has spins increasing with $\Delta I = 1$ and its moment of inertia is that of a rotor. The expression for the total energy of the levels of the band is given by

$$E_K(I) = \left|\varepsilon^i_\Omega - \lambda\right| + \frac{\hbar^2}{2\Im}\left[I(I+1) - K^2\right] \quad for \quad K \neq \frac{1}{2} \tag{2.78}$$

where the single-particle energy is counted relative to the Fermi level energy λ. For $I \geq K$, the spins $I = K, K+1, K+2, \ldots$ are observed.

For $K = 1/2$, the general expression for the energies of the rotational bands in the strong coupling approximation is given by

$$E_K(I) = \left|\varepsilon^i_\Omega - \lambda\right| + \frac{\hbar^2}{2\Im}\left[I(I+1) - K^2 + \delta_{K\frac{1}{2}} a(-1)^{I+\frac{1}{2}}\left(I + \frac{1}{2}\right)\right] \tag{2.79}$$

where a is called decoupling parameter, which has a fixed value for each $K = 1/2$ orbital. It is calculated as

$$a = \sum_{Nj}(-1)^{j-\frac{1}{2}}\left(j + \frac{1}{2}\right)\left|a^{\Omega}_{Nlj\frac{1}{2}}\right|^2 \tag{2.80}$$

where the last expression is independent of phase conventions. For $|a| = 1$, equation (2.80) shows that the levels occur in degenerate pairs. If $a = -1$, the 3/2 state coincides with the 1/2 state. Similarly, the (5/2, 7/2) and (9/2, 11/2) pairs are degenerate. If $a = +1$, the degenerate pairs are (3/2, 5/2); (7/2, 9/2); etc. For $|a| > 1$, the level order within the rotational band is no longer monotonic in spin.

2.6.1.2 The decoupling limit (rotational alignment)

In the case of intermediate deformation, the energy splitting in the intrinsic part of the Hamiltonian is not neglected. In this case, the orientation of the valence high-j particle with low Ω is independent of the motion of the core as shown in the bottom panel of Figure 2.10. The Coriolis force is so strong that the coupling to the deformation core may be neglected. The total angular momentum I and the single-particle angular momentum j are aligned along the rotational axis. The energies for the $I = 13/2, 17/2, 21/2, \cdots$ states are calculated as

$$E(I, j = \alpha) = \sum_{\Omega} 2|C_{\Omega}|^2 \left(\varepsilon_{\Omega} - \varepsilon_{\frac{1}{2}}\right) + \frac{\hbar^2}{2\Im}\left[I(I+1) + j(j+1) - 2I\alpha\right] \tag{2.81}$$

where C_{Ω} is the expansion coefficient and $j = \alpha = 13/2$ in the present case. The first term is the single-particle contribution, which gets larger when deformation increases. This term will thus make the rotational aligned coupling scheme disadvantageous at large deformations. The dependence of the energy splitting on the deformation can be extracted from Nilsson diagrams. The second term represents rotational energy of the rotor, and for this rotational aligned case can be expressed as

$$\begin{aligned} E_{rot}(I, j = \alpha) &= \frac{\hbar^2}{2\Im}\left[I(I+1) + j(j+1) - 2I\alpha\right] \\ &= \frac{\hbar^2}{2\Im}\left[(I-\alpha)(I-\alpha+1) + 2\alpha\right] \\ &= \frac{\hbar^2}{2\Im}\left[R(R+1) + 2\alpha\right] \end{aligned} \tag{2.82}$$

where $R = I - \alpha = 0, 2, 4, \ldots$ describes the collective rotation and α is the projection of the single-particle angular momentum j along the rotational axis.

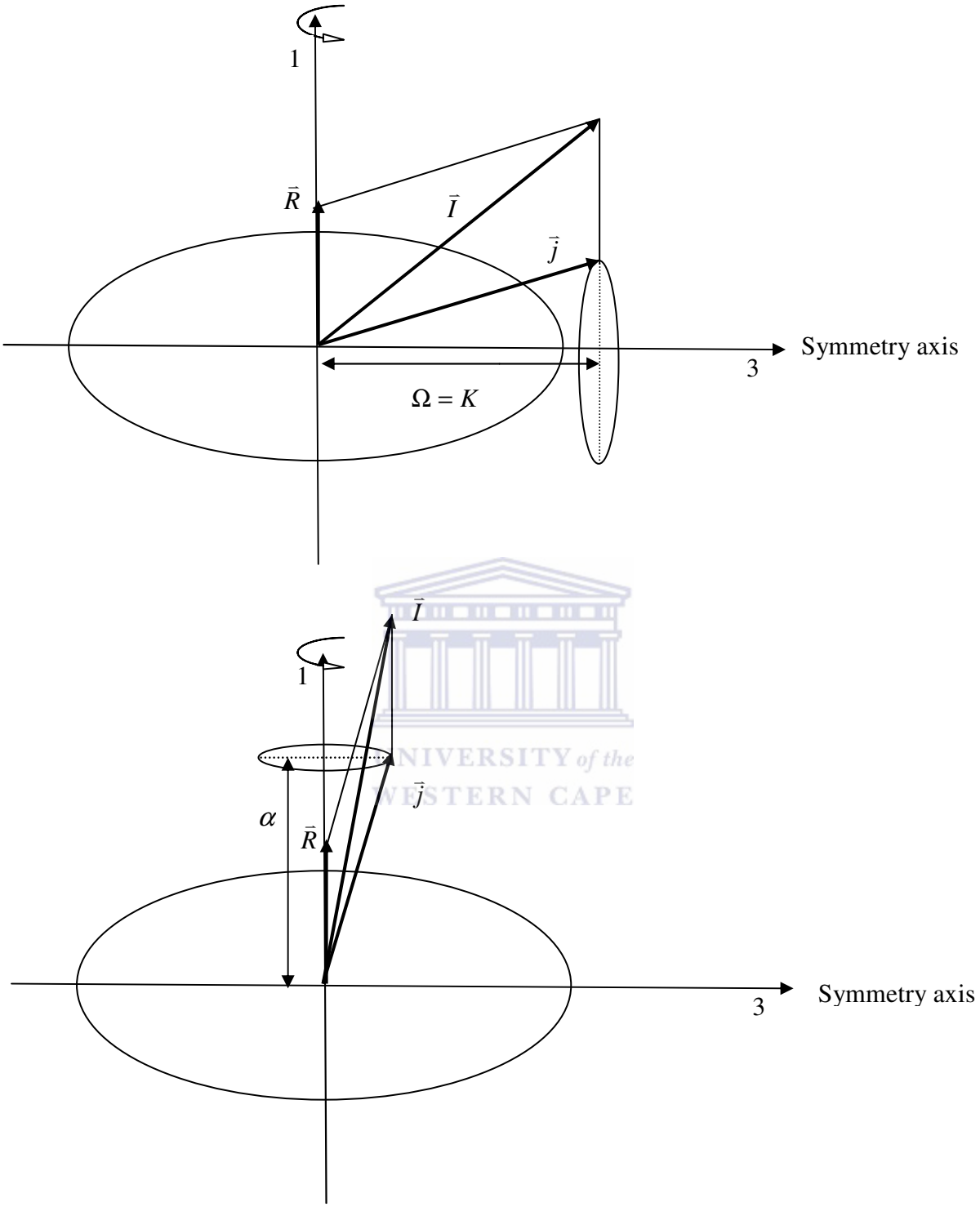

Figure 2.10: *Coupling schemes in the particle-plus-rotor model: strong coupling (top panel) and rotational alignment (bottom panel) [Rin80].*

Generally $\alpha = j - n$, where $n = 0, 1, 2, 3, \ldots$ The spectrum of the Hamiltonian is

$$\begin{aligned} E_{rot}(I, j = \alpha + n) &= \frac{1}{2\Im}\left[(I-\alpha)(I-\alpha+1)+(2\alpha+n)(n+1)\right] \\ &= \frac{1}{2\Im}\left[R(R+1)+(2\alpha+n)(n+1)\right] \end{aligned} \tag{2.83}$$

In this case the values of n correspond to different bands. For $n = 0$ we have maximally aligned band with a band-head spin of $\alpha = j$ and this is a favored band. For the values of n different from zero we have lesser-aligned unfavored bands with band head spins of $\alpha = j-1,\ j-2, \ldots$

2.6.2 The asymmetric particle-plus-rotor model

In this model, Davydov *et al.,* [Dav58, Dav59a-b, Dav65] diagonalized only the rotational energy operator shown in equation (2.70). The energy eigenvalues for the deformed asymmetric rotor were calculated with irrotational moment of inertia defined by

$$\Im_k = \frac{4}{3}\Im_0 \sin^2\left(\gamma - \frac{2\pi}{3}k\right) \qquad k = 1, 2, 3 \tag{2.84}$$

where k represents the three principal axes of the nucleus. 1-, 2- and 3-axes correspond to an intermediate, the short and the long axes of the nucleus respectively.

Diagrammatic representation of equation (2.84) is shown in Figure 2.11. The asymmetric rotor energy spectrum is symmetric about $\gamma = 30^0$. This symmetry says that a particle coupled to a core with parameters $\varepsilon_2, \gamma, \lambda_F, \Delta$ has the same energy spectrum as a hole coupled to a core with parameters $\varepsilon_2, 60^0 - \gamma, -\lambda_F, -\Delta$. The permutations of the intrinsic axes and the sign change of pairing gap Δ under transformation have no effect on the energy spectrum.

The energies of the first 2_1^+ and second 2_2^+ states are given by

$$E_{2_{1,2}^+} = \frac{6\hbar^2}{2\Im_0}\frac{9 \mp \sqrt{81 - 72\sin^2(3\gamma)}}{4\sin^2(3\gamma)} \tag{2.85}$$

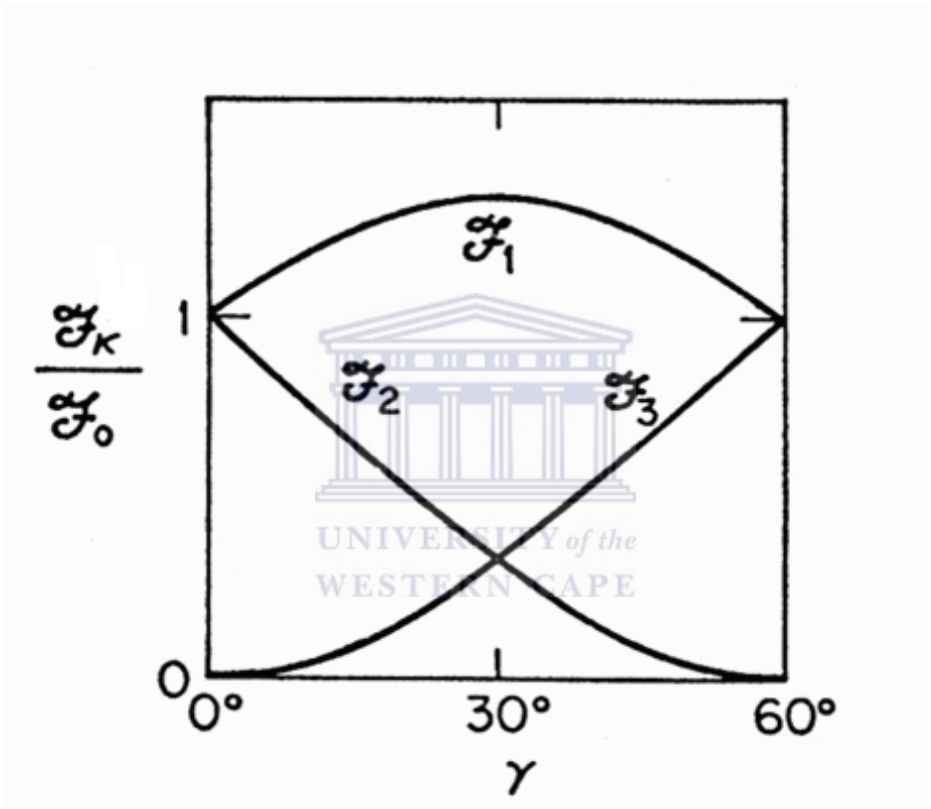

Figure 2.11: *Irrotational moment of inertia as a function of* γ *[Mey75].*

where the inertial parameter is often taken as $6\hbar^2/2\Im_0 \cong 1225/(\beta_2^2 A^{7/3})$ MeV according to an empirical rule [Gro62].

Figure 2.12 shows the energy eigenvalues of equation (2.70). For $\gamma = 0^0$ and $\gamma = 60^0$ one gets an $I(I+1)$ dependence for the excitation energy E_I. Even for strong triaxial deformations, one gets only slight deviations of this form. However additional $2_2^+, 3_1^+, 4_2^+, \ldots$ levels come down in energy. It is a characteristic feature of a non-axial shape to have a low-lying second 2_2^+ state. The $0_1^+, 2_1^+, 4_1^+, \ldots$ and $2_2^+, 3_1^+, 4_2^+, \ldots$ states belong to the ground band and the γ-band respectively. In the case of maximal triaxiality ($\gamma = 30^0$), $\Im_2 = \Im_3 = \frac{1}{4}\Im_1 = \frac{1}{3}\Im_0$, where $\Im_0$ is the moment of inertia at $\gamma = 0^0$ (see Figure 2.11).

This model can be extended to odd mass nuclei by coupling an external particle to an asymmetric rotor. It has been applied to cases where the external particle is placed in a high-j shell, and has turned out to be very powerful as a description of energy levels and decay scheme of many transitional nuclei. Restricting the considerations to one external particle in a high-j shell, the model Hamiltonian has the form [Mey74]:

$$H = \sum_{i=1}^{3} \frac{(I_k - j_k)^2}{2\Im_k} + k(r)\left\{(\cos\gamma)Y_{20} + \left(\frac{1}{\sqrt{2}}\sin\gamma\right)(Y_{22} - Y_{2-2})\right\} \qquad (2.86)$$

where I_k and j_k are the components of the total and the single-particle angular momentum respectively. $k(r)$ is the potential energy strength and depends on the quadrupole deformation. This potential energy strength is taken as $k(r) = (16\pi/5)^{1/2} 206 A^{-1/3}\beta_2$ MeV which is consistent with empirical single-particle spacing at $\gamma = 0^0$ for a nucleus with mass A.

Figure 2.13 shows the spectrum of the Hamiltonian of equation (2.86) as a function of γ at a deformation of $\beta_2 = 5A^{-2/3}$. It shows calculated levels of the yrast band up to spin $I = 23/2$ built on a $j = 11/2$ single-particle state. At $\gamma = 0^0$ we have decoupled structure with the favored $11/2, 15/2, 19/2, 23/2$ and unfavored $13/2, 17/2, 21/2$ states respectively, relative to the $11/2$ bandhead. These states are also clearly seen for strongly coupled limit at $\gamma = 60^0$. The unfavored $13/2, 17/2, 21/2$ states lie relatively high at $\gamma = 0^0$, but come down sharply around $\gamma = 25^0$. The strongly coupled level order persists over the whole region

$30^0 \leq \gamma \leq 60^0$. In this region, the particle angular momentum mainly points along the 2-axis which becomes the oblate symmetry axis at $\gamma = 60^0$, whereas the core angular momentum is perpendicular to it, since the irrotational moment of inertia about the 2-axis is small and vanishes for $\gamma = 60^0$. The low spin levels correspond to opposite directions of the core and particle angular momentum and may also be grouped into favored $7/2, 3/2$ and unfavored $9/2, 5/2, 1/2$ states.

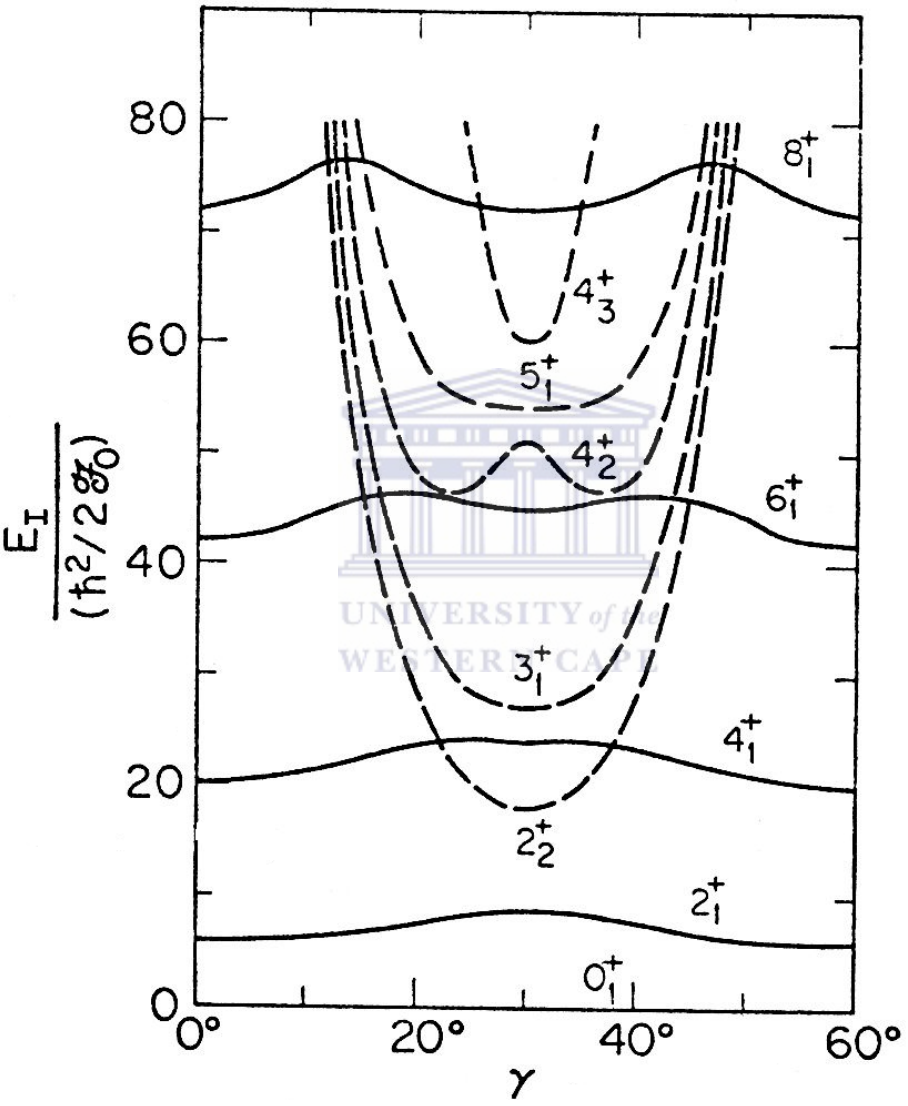

Figure 2.12: *The low-energy spectrum of a deformed asymmetric rotor as a function of* γ *[Mey75].*

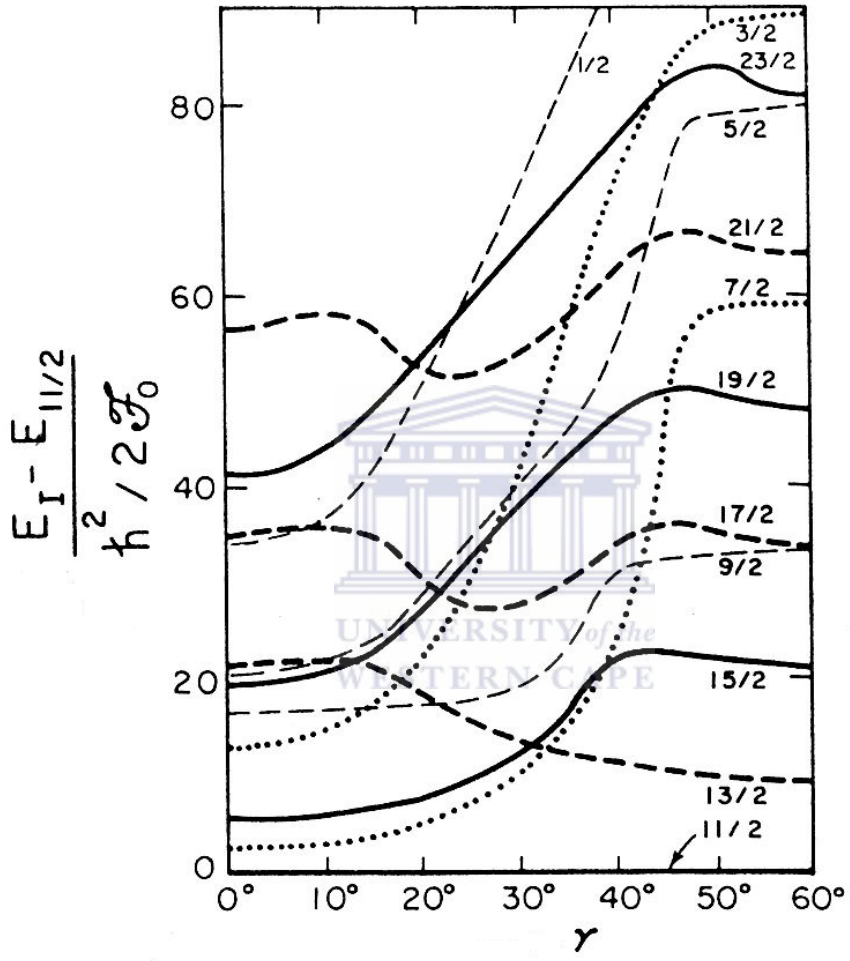

Figure 2.13: *Spectrum of a j = 11/2 particle coupled to an asymmetric rotor as a function of γ, for the Fermi surface at the bottom of the j = 11/2 shell. The states with (π, α) = (+, +1/2) are represented with bold-dashed and faint-dashed lines, while (+, -1/2) with solid and dotted lines [Mey74].*

CHAPTER 3 Chiral symmetry in nuclei

3.1 Chiral rotation

If the total angular momentum does not lie in one of the three principal planes of a triaxial nucleus the coupling of three angular momenta form a chiral system as shown in Figure 3.1. In this symmetry, the left- and right-handed mean field solutions are related to each other by

$$|L\rangle = TR_y(\pi)|R\rangle \tag{3.1}$$

$$|R\rangle = TR_y(\pi)|L\rangle \tag{3.2}$$

where $TR_y(\pi)$ is the chiral operator which is the product of the operators of a rotation around 180^0 ($R_y(\pi)$) and a time reversal (T).

In general these wave functions obey the following relations

$$\langle L|L\rangle = \langle R|R\rangle = 1 \tag{3.3}$$

$$\langle L|R\rangle = \langle R|L\rangle = \varepsilon \tag{3.4}$$

$$\langle L|H|L\rangle = \langle R|H|R\rangle = E \tag{3.5}$$

$$\langle L|H|R\rangle = \langle R|H|L\rangle = \Delta E \tag{3.6}$$

That is, they are normalized, but not necessarily orthogonal, the expectation values of the Hamiltonian are real and the same for both systems, but the Hamiltonian might not be diagonal in the $|R\rangle$, $|L\rangle$ basis. Wave functions which restore the chiral symmetry can be defined as

$$|+\rangle = \frac{1}{\sqrt{2(1+\varepsilon)}}\{|L\rangle + |R\rangle\} \tag{3.7}$$

$$|-\rangle = \frac{i}{\sqrt{2(1-\varepsilon)}}\{|L\rangle - |R\rangle\} \tag{3.8}$$

These wave functions are normalized and orthogonal, and $TR_y(\pi)|\pm\rangle = \pm|\pm\rangle$. Then

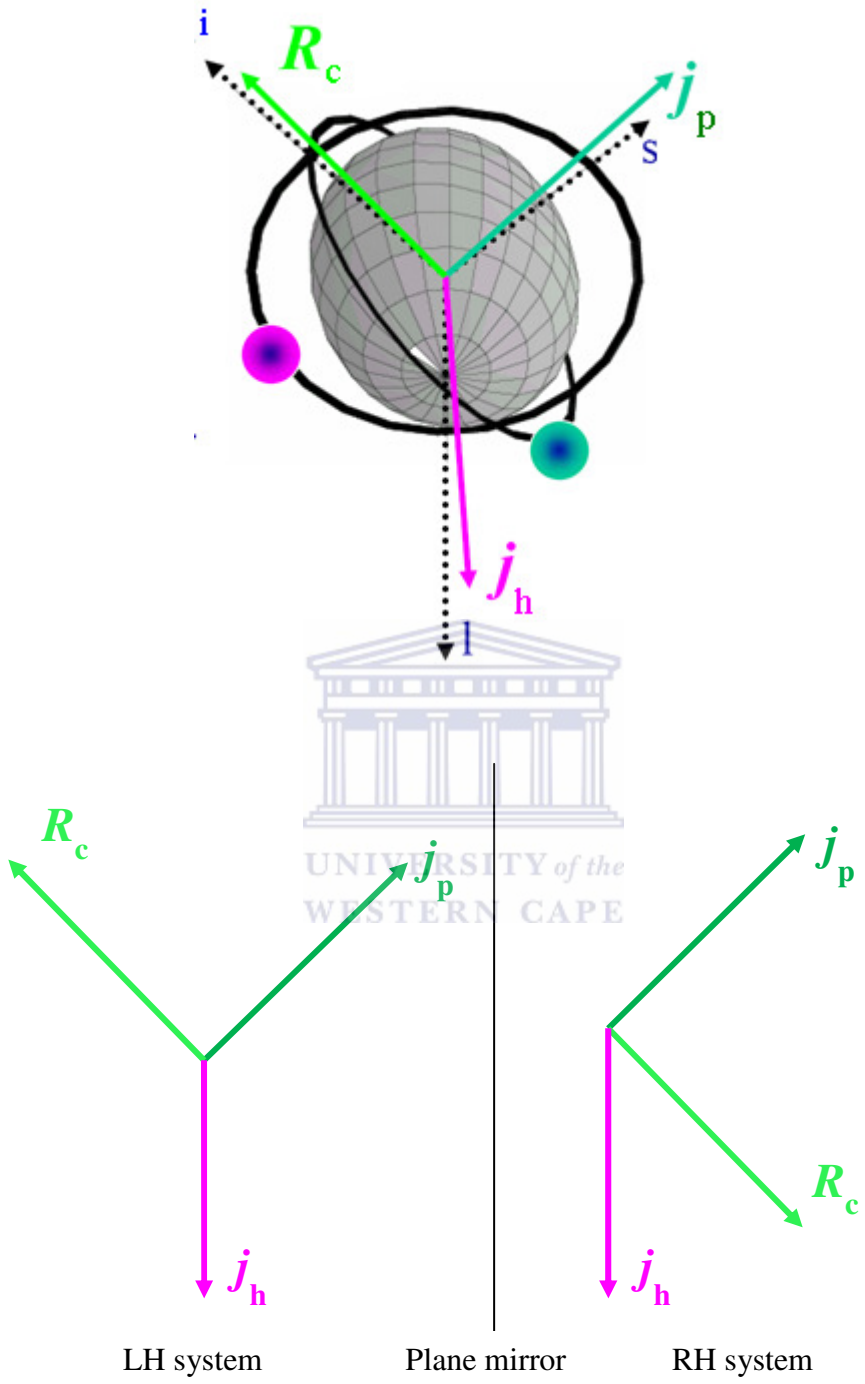

Figure 3.1: *Sketch of the idealized chiral geometry. The core, proton and neutron angular momenta denoted by R_c, j_p and j_n respectively are aligned along the principal axes of the triaxial nucleus, which are labeled by s (short), i (intermediate) and l (long). The right- and left-handed systems are denoted by RH and LH respectively.*

$$\left\langle \pm \middle| H \middle| \pm \right\rangle = \frac{E \pm \Delta E}{1 \pm \varepsilon} \tag{3.9}$$

Therefore the excitation energy in the partner bands can be degenerate only if

(i) $\Delta E = \varepsilon E$ or

(ii) both $\Delta E = \varepsilon = 0$

The first case can occur if $\langle L|H|R\rangle = \langle L|R\rangle\langle R|H|R\rangle$, $\langle L| = \langle L|R\rangle\langle R|$, which means that $|L\rangle$ and $|R\rangle$ are identical and planar, i.e. this is a trivial solution corresponding to one band only ($|-\rangle$ vanishes). In the second case, (ii), there is no mixture between the wave functions $|L\rangle$ and $|R\rangle$ and also the Hamiltonian is diagonal in the $|L\rangle$, $|R\rangle$ basis. This is the chiral solution. It was suggested in reference [Law10a] that since the same argument can be carried out not only for the Hamiltonian, but for all other operators, which are invariant with respect to the chiral operator $R_y(\pi)$ (for which an equation equivalent to equation (3.5) holds true), the degeneracy in the chiral partner bands appears and disappears simultaneously in many properties of the bands. Such operators are for instance the squared projections of all angular momenta along the three principal axes, the operator including scalar products of two angular momenta, the operators of the reduced transition probabilities, etc. Thus, the degeneracy associated with strongly broken chiral symmetry appears simultaneously in the excitation energies, squared projections of the total and individual (particle and collective rotation) angular momenta, reduced transition probabilities, etc. It is interesting to note, that if there is an overlap between the wave functions $|L\rangle$ and $|R\rangle$, (i.e. $\varepsilon \neq 0$) there will be a loss of the degeneracy simultaneously in all properties of the bands, irrespective of whether the operators are diagonal in the $|L\rangle$, $|R\rangle$ basis.

Frauendorf and Meng [Fra97] showed how to form a chiral system. For instance consider a high-j $h_{11/2}$ proton particle coupled to a $h_{11/2}$ neutron hole within the PRM or TAC with $\gamma = -30^0$. The angular momentum of the hole tends to align along the long nuclear axis. If a proton particle and a neutron hole are coupled to a triaxial rotor, the angular momentum of a high-j proton particle tends to align along the short nuclear axis, and that of a high-j neutron hole tends to align along the long nuclear axis, while the rotational angular momentum of the triaxial deformed core is mainly oriented along the intermediate axis. The moment of inertia of a triaxial nucleus is largest for a rotation around the intermediate axis (see Figure 2.11 and

equation (2.84)). Thus such rotation will correspond to minimum rotational energy for a given spin I. Therefore, the simplest chiral system is built by a coupling of the angular momenta of a particle, a hole and the collective rotation. This means that chiral bands require particle(s)-hole(s) configuration and a deformed nucleus with large stable triaxiality.

3.1.1 Theoretical fingerprints of chiral partner bands

Frauendorf and Meng [Fra97], and Frauendorf [Fra01] suggested the following criteria (known as fingerprints) that should be exhibited by chiral bands: all measurable properties of the partner bands should be degenerate (i.e. the same excitation energies, the same intra- and inter-band $B(M1)$ and $B(E2)$ reduced transition probabilities, the same moment of inertia, the same quasiparticle alignments, etc). Other fingerprints of chirality were suggested too. For instance it was pointed out that the energy staggering parameter $S(I)$ defined as

$$S(I) = \frac{E(I) - E(I-1)}{2I} \tag{3.10}$$

should possess smooth dependence with spin if the particle and the hole orbital angular momenta are both perpendicular to the core rotation [Koi3b, Vam04]. Staggering in this parameter is caused by Coriolis effects, which should vanish when the particle and rotational angular momenta are orthogonal (see equation (3.11)).

$$E_{cor} = \frac{1}{2\Im}\vec{I}.\vec{j} = \frac{1}{2\Im}\left(\vec{R}.\vec{j} + \vec{j}.\vec{j}\right) \tag{3.11}$$

This however is clearly not a necessary requirement for all chiral bands. Indeed, an aplanar orientation of the total angular momentum is needed in order to form a chiral system [Fra97, Fra01] but the individual angular momenta of the particles and rotational core may not necessary be orthogonal.

Another fingerprint proposed by Koike *et al.* [Koi04] for a symmetric particle-hole configuration (i.e. $\pi h_{11/2} \otimes \nu h_{11/2}^{-1}$) in the A ~ 130 mass region, is that there should be staggering in opposite phase in the intra- and inter-band $B(M1)$ reduced transition probabilities. The $B(M1)$ reduced transition probabilities should have the same phase of staggering for both chiral partner bands. Furthermore, the intra-band $B(M1)$ transition probabilities should be high for even values of I, and low for odd values of I, whereas the

inter-band $B(M1)$ transition probabilities should be low for even values of I, and high for odd values of I. The simple PRM (where the odd proton particle and odd neutron hole lie in the lowest- and highest-energy $h_{11/2}$ orbitals respectively) which describes a specific symmetric $\pi h_{11/2} \otimes \nu h_{11/2}^{-1}$ configuration for a triaxial odd-odd nucleus was utilized to propose this fingerprint. The model consists of a triaxially deformed core with $\gamma = 90^0$ coupled to one odd proton particle and one odd neutron hole in the same single-j $h_{11/2}$ shell. Note that rotation with $\gamma = 90^0$ is equivalent to $\gamma = -30^0$ rotation in Lund convention [And76], except that the intermediate axis is the quantization axis (3-axis). In this model pairing correlation and proton-neutron interaction (V_{pn}) were not considered, and only one oscillator shell was used. In this special case, an additional symmetry exists, such that the total Hamiltonian is invariant under the rotation by 90^0 or 270^0 about the 3-axis combined with an exchange of the valence proton and neutron. The presence of this new symmetry leads to the additional selection rule for the electromagnetic transitions. Note that the new symmetry holds only for symmetric configurations (i.e. when the angular momentum of the odd particle and odd hole are equal, and when the projection of the particle angular momentum along the short axis is equal to the projection of the hole angular momentum along the long axis).

3.1.2 Some factors suggested to cause a loss of degeneracy in the chiral partner bands

(i) Coriolis effects at high spins and vanishing rotational angular momentum of the core $\vec{R}$ along the intermediate axis at low spin [Fra97, Fra01], i.e. at low spin, $\vec{R}$ and the angular momentum $\vec{I}$ may lie in the 1-3 plane, because this orientation minimizes the Coriolis interaction.

(ii) oscillation of the rotational angular momentum of the core between the left- and right-handed systems due to γ-vibration of nuclear shape at low spin [Sta01a], i.e. the rotational angular momentum vector does not remain out of the plane all the times but spends some time within the plane as well. For nuclei with smaller barriers and large γ-softness the excited band may easily undergo a shape transformation such as that predicted by TRS in ^{106}Ag [Jos07].

(iii) deviation of the core shape from maximum triaxiality with $\gamma = 30^0$ [Sta01a, Zha07].

(iv) dynamical fluctuations of the nuclear shape [Ton07].

(v) position of the Fermi level for the valence odd nucleons away from top/bottom of a high-j shell [Zha07].

3.2 Suggested chiral candidates in A ~ 100, 130 and 190 mass regions and theoretical interpretation

Strongly broken chiral symmetry is associated with the observation of degenerate $\Delta I = 1$ partner bands which have the same parity. However, truly degenerate partner bands have not been found so far in nuclei. Pairs of $\Delta I = 1$ rotational bands with similar properties have been observed in A ~ 100, 130 and 190 nuclear mass regions [Bal04, Bar01, Har01, Hec01, Hec03, Jos04, Jos05a-b, Jos07, Koi01, Koi03a, Law08, Law10b, Luo09, Mas09, Mer02, Moo00a-b, Pet02, Pet96, Rai03a-b, Sim05, Sta02, Tim04, Tim06, Tim07, Vam04 , Wan06, Yon05, Zhu03, Zhu05] and have been suggested as candidate chiral bands. These bands are built on two- or three-quasiparticle configurations. Most of the side bands are linked with the yrast bands via mixed $M1/E2$ and $E2$ transitions. These bands share common characteristics and fulfill approximately some of the fingerprints suggested for chirality by Koike *et al.* [Koi03b, Koi04, Koi05], Frauendorf *et al.* [Fra97, Fra01] and Vaman *et al.* [Vam04]. The majority of chiral candidates belong to the A ~ 130 and 100 mass regions. The least studied mass region is A ~ 190. Suggested chiral candidates, as of writing of this thesis, and their corresponding single-particle configurations of their $\Delta I = 1$ partner bands are summarized in Tables 3.1-3.3. Though the observation of degeneracy of the partner bands is a primary indication of strongly broken chiral symmetry, the presence of this symmetry can be supported in a more definitive way if the electromagnetic transition probabilities measured for the chiral bands are the same too. The reduced electromagnetic transition probabilities carry important information on the nuclear intrinsic structure. However, experimental lifetime measurements needed in order to deduce the electromagnetic transition rates have been measured for eight nuclei only among these chiral candidates (i.e. ^{103,104}Rh [Suz08], ^{128}Cs [Gro05], ^{130}Cs [Wan09], ^{132}La [Gro05, Gro06], ^{134}Pr [Ton06, Ton07], ^{135}Nd [Muk07] and ^{136}Nd [Muk08]). In the 100 mass region, ^{104}Rh nucleus is suggested as the best chiral candidate due to small energy displacement between the partner bands. The $B(M1)$ and $B(E2)$ reduced electromagnetic transition probabilities were measured only for a few levels in the yrast band [Suz08]. In the 130 mass region, ^{128}Cs nucleus is suggested as the best chiral candidate so far due to similar values of the excitation energies and measured $B(M1)$ and $B(E2)$ reduced transition probabilities in the partner bands [Gro05].

Several theoretical models defined in a rotating (intrinsic) or laboratory frames were applied to account for this newly identified nuclear phenomenon. The models using a rotating frame are the three-dimensional tilted axis cranking (3D TAC) [Dim00] and Skyrme-Hatree-Fock (SHF) cranking [Olb04], whereas the models based on the laboratory frame were the core-quasiparticle-coupling (CQPC) model using Kerman-Kleintra-Dönau-Frauendorf (KKDF) method [Sta02], core-particle-hole-coupling (CPHC) model [Dro09], variations of particle-plus triaxial rotor model (PRM) with different complexity [Law08, Law10b, Qi09a-b, Koi04, Zha07], pair-truncated shell model (PTSM) [Hig05], quadrupole coupling model (QCM) [Yos06, Hig07], interacting boson fermion-fermion model (IBFFM) [Bra04] and interacting vector boson model (IVBM) [Gan09]. Theoretical models such as the relativistic mean field (RMF) [Pen08], total Routhian surface (TRS), etc were used to predict the nuclear deformation parameters. All of these models support the chiral interpretation proposed for the partner bands observed in various nuclei in A ~ 100, 130 and 190 mass regions. Alternatively, the pair-truncated shell model (PTSM) [Hig05] and quadrupole coupling model (QCM) [Yos06, Hig07] give an interpretation of the partner bands which is different from the chiral interpretation.

An existence of multiple chiral partner bands in one single nucleus ($M\chi D$) was suggested to occur in ^{102,106,108,110}Rh, ^{108,110,112}Ag and ^{112}In nuclei by RMF model [Men06, Pen08, Yao09]. One should note that for the observed chiral partner bands in these mass regions (i.e. A ~ 100, 130 and 190), the separation energies between the partner bands were found to be too small for the side bands to be interpreted as bands built either on the unfavored signature of the proton j_π or on a γ-phonon excitation. Indeed, the γ-vibrational energies in these regions are $\geq$ 600 keV [Ser87].

3.3 Theoretical models used to study chirality in nuclei

3.3.1 The particle-rotor model (PRM)

In section 3.1.1 we have briefly described a simple PRM (without pairing, proton-neutron interaction and considering only one shell) which was used for the identification of selection rules in the electromagnetic transitions in chiral bands [Koi04]. In this section we will briefly describe other important studies dedicated to the same chiral system using other versions of PRM.

In the work of Zhang *et al*. [Zha07], the PRM with a quasi-proton and a quasi-neutron coupled with a triaxial rotor was applied to study chiral partner bands with configuration of

Table 3.1: *Experimentally suggested chiral candidates and corresponding single-particle configurations of their* $\Delta I = 1$ *partner bands in A ~ 100 mass region. E.M denotes reduced electromagnetic transition probabilities.*

A ~ 100 mass region			
Nucleus	**Single-particle configuration**	**Type of nucleus**	**E.M measurement**
$^{106}_{42}Mo_{64}$ [Zhu05]	$\nu h_{11/2} \otimes \nu(d_{5/2}g_{7/2})^{-1}$	even-even	no
$^{100}_{43}Tc_{57}$ [Jos05b]	$\pi g_{9/2}^{-1} \otimes \nu h_{11/2}$	doubly-odd	no
$^{108}_{44}Ru_{64}$ [Luo09]	$\nu h_{11/2} \otimes \nu(d_{5/2}g_{7/2})^{-1}$	even-even	no
$^{110}_{44}Ru_{66}$ [Luo09]	$\nu h_{11/2} \otimes \nu(d_{5/2}g_{7/2})^{-1}$	even-even	no
$^{112}_{44}Ru_{68}$ [Luo09]	$\nu h_{11/2} \otimes \nu(d_{5/2}g_{7/2})^{-1}$	even-even	no
$^{102}_{45}Rh_{57}$ [Tim06]	$\pi g_{9/2}^{-1} \otimes \nu h_{11/2}$	doubly-odd	no
$^{103}_{45}Rh_{58}$ [Tim06]	$\pi g_{9/2}^{-1} \otimes \nu h_{11/2}^{2}$	odd-mass	yes [Suz08]
$^{104}_{45}Rh_{59}$ [Vam04]	$\pi g_{9/2}^{-1} \otimes \nu h_{11/2}$	doubly-odd	yes [Suz08]
$^{105}_{45}Rh_{60}$ [Tim04]	$\pi g_{9/2}^{-1} \otimes \nu h_{11/2}^{2}$	odd-mass	no
$^{106}_{45}Rh_{61}$ [Jos04]	$\pi g_{9/2}^{-1} \otimes \nu h_{11/2}$	doubly-odd	no
$^{105}_{47}Ag_{58}$ [Tim07]	$\pi g_{9/2}^{-1} \otimes \nu h_{11/2}(d_{5/2}g_{9/2})$	odd-mass	no
$^{106}_{47}Ag_{59}$ [Jos05a, Jos07]	$\pi g_{9/2}^{-1} \otimes \nu h_{11/2}$	doubly-odd	no

Table 3.2: *Experimentally suggested chiral candidates and corresponding single-particle configurations of their* $\Delta I = 1$ *partner bands in A ~ 130 mass region. E.M denotes reduced electromagnetic transition probabilities.*

A ~ 130 mass region			
Nucleus	**Single-particle configuration**	**Type of nucleus**	**E.M measurement**
$^{122}_{55}Cs_{67}$ [Yon05]	$\pi h_{11/2} \otimes \nu h_{11/2}^{-1}$	doubly-odd	no
$^{124}_{55}Cs_{69}$ [Moo00a, Moo00b]	$\pi h_{11/2} \otimes \nu h_{11/2}^{-1}$	doubly-odd	no
$^{126}_{55}Cs_{71}$ [Wan06]	$\pi h_{11/2} \otimes \nu h_{11/2}^{-1}$	doubly-odd	no
$^{128}_{55}Cs_{73}$ [Koi03a]	$\pi h_{11/2} \otimes \nu h_{11/2}^{-1}$	doubly-odd	yes [Gro05, Gro06]
$^{130}_{55}Cs_{75}$ [Sim05]	$\pi h_{11/2} \otimes \nu h_{11/2}^{-1}$	doubly-odd	yes [Wan09]
$^{132}_{55}Cs_{77}$ [Rai03a, Rai03b]	$\pi h_{11/2} \otimes \nu h_{11/2}^{-1}$	doubly-odd	no
$^{130}_{57}La_{73}$ [Koi01]	$\pi h_{11/2} \otimes \nu h_{11/2}^{-1}$	doubly-odd	no
$^{132}_{57}La_{75}$ [Sta02]	$\pi h_{11/2} \otimes \nu h_{11/2}^{-1}$	doubly-odd	yes [Gro05, Gro06]
$^{134}_{57}La_{77}$ [Bar01]	$\pi h_{11/2} \otimes \nu h_{11/2}^{-1}$	doubly-odd	no
$^{128}_{59}\mathrm{Pr}_{69}$ [Pet02]	$\pi h_{11/2} \otimes \nu h_{11/2}^{-1}$	doubly-odd	no
$^{132}_{59}\mathrm{Pr}_{73}$ [Koi01]	$\pi h_{11/2} \otimes \nu h_{11/2}^{-1}$	doubly-odd	no
$^{134}_{59}\mathrm{Pr}_{75}$ [Pet96]	$\pi h_{11/2} \otimes \nu h_{11/2}^{-1}$	doubly-odd	yes [Ton06, Ton07]
$^{135}_{60}Nd_{75}$ [Zhu03]	$\pi h_{11/2}^{2} \otimes \nu h_{11/2}^{-1}$	odd-mass	yes [Muk07]
$^{136}_{60}Nd_{76}$ [Mer02]	$\pi h_{11/2}(d_{5/2}g_{7/2}) \otimes \nu h_{11/2}^{-2}$	even-even	yes [Muk08]
$^{136}_{61}Pm_{75}$ [Har01]	$\pi h_{11/2} \otimes \nu h_{11/2}^{-1}$	doubly-odd	no
$^{138}_{63}Eu_{75}$ [Hec01]	$\pi h_{11/2} \otimes \nu h_{11/2}^{-1}$	doubly-odd	no
$^{140}_{63}Eu_{77}$ [Hec03]	$\pi h_{11/2} \otimes \nu h_{11/2}^{-1}$	doubly-odd	no

Table 3.3: *Experimentally suggested chiral candidates and corresponding single-particle configurations of their* $\Delta I = 1$ *partner bands in A ~ 190 mass region. E.M denotes reduced electromagnetic transition probabilities .* denotes that the level scheme was revised and the suggested chirality was found unlikely [Jun08].*

A ~ 190 mass region			
Nucleus	**Single-particle configuration**	**Type of nucleus**	**E.M measurement**
$^{188}_{77}Ir^{*}_{111}$ [Bal04]	$\pi h_{9/2} \otimes \nu i_{13/2}^{-1}$	doubly-odd	no
$^{194}_{81}Tl_{113}$ [Mas09]	$\pi h_{9/2} \otimes \nu i_{13/2}^{-1}$	doubly-odd	no
$^{198}_{81}Tl_{117}$ [Law08, Law10b]	$\pi h_{9/2} \otimes \nu i_{13/2}^{-1}$	doubly-odd	no

$h_{11/2}$ quasi-proton and $h_{11/2}$ quasi-neutron. With pairing correlations taken into account by the BCS method, a proton-quasiparticle and a neutron-quasiparticle were coupled with a triaxial rotor. Calculations were done when changing the neutron Fermi level λ_F from the top $h_{11/2}$ orbital to the lowest $h_{11/2}$ orbital. Note that in this model the proton-neutron interaction V_{pn} was not taken into account. The energy spectra, electromagnetic properties, as well as the orientations of the angular momenta of the partner bands have been investigated in detail. Large staggering in the intra- and inter-band $B(M1)$ reduced transition probabilities was also reported, but with opposite phase compared to the one reported in reference [Koi04]. It was also found that the odd-even staggering of $B(M1)/B(E2)$ values is strongly influenced by the deformation γ as well as the Fermi surface λ_F, which suggests that the odd-even staggering of $B(M1)/B(E2)$ values may not be a general feature/fingerprint for chiral bands.

The work of Qi *et al*. [Qi09b], reports on the study of the electromagnetic transitions of the $\pi h_{11/2} \otimes \nu h_{11/2}^{-1}$ partner bands with different triaxiality parameter γ using the particle rotor model (PRM) similar to the one used in reference [Koi04]. The model also predicted that the $B(M1)/B(E2)$ and $B(M1)_{in}/B(M1)_{out}$ staggering are sensitive to the triaxiality parameter γ. This kind of behaviour of $B(M1)/B(E2)$ was also pointed out in reference [Zha07]. Their work further suggested that for the partner bands with near degenerate energy spectra and similar $B(E2)$ and $B(M1)$ transitions, a large amplitude of the $B(M1)$ staggering can be regarded as an indication for strongly broken chirality (i.e. the staggering is weak for weakly broken chirality, while it is strong for strongly broken chirality). The phase of staggering in the $B(M1)$ reduced transition probabilities was opposite compared to the one reported in reference [Koi04].

3.3.2 The tilted axis cranking (TAC) model

The basic assumption of this model is that one considers a coordinate system which rotates with fixed angular frequency ω about an axis that is tilted, i.e. out side of the major planes defined by the major nuclear axes. The nucleons are assumed to be moving independently in this rotating potential.

In the TAC model the rotational axis is tilted with respect to the principal axes of the nuclear density distribution. The orientation of the rotational axis with respect to the principal axes is described by two polar angles. An additional constrains to the TAC case is that, the total

angular momentum $\vec{I}$ and angular frequency $\vec{\omega}$ vectors must be parallel, because for that geometry the rotational energy is minimum. Note that parallel orientation between the total angular momentum $\vec{I}$ and angular frequency $\vec{\omega}$ vectors may occur in three different situations:

(i) the total angular momentum $\vec{I}$ has the direction of one of the principal axes. This is called the principal axis cranking (PAC) and the corresponding cranking term is one-dimensional.

(ii) the total angular momentum $\vec{I}$ is tilted away from the principal axes but still lies within one of the three principal planes. This is called the tilted axis cranking (TAC) or planar tilted axis cranking and the corresponding cranking term is two-dimensional.

(iii) the total angular momentum $\vec{I}$ does not lie in one of the principal planes. This is called aplanar tilted axis cranking or three dimensional tilted axis cranking (3D TAC) and the corresponding cranking term is three-dimensional.

The PAC is known to be associated with a $\Delta I = 2$ rotational bands composed of one or two signature partner sequences of $E2$ transitions [Fra93, Fra97, Fra01]. The TAC is associated with a $\Delta I = 1$ rotational band of parity π, whose states are directly connected by strong $M1$ and weak or missing $E2$ cross over transitions [Fra93, Fra97, Fra01].

The TAC model has been used extensively in the description of shears bands (also called magnetic rotation, for example see reference [Bal94]), while the 3D-TAC model was applied to describe chirality in nuclei (for example see references [Hec01, Muk07, Rai03a, Tim04, Zhu05, Luo09]).

3.3.3 Core-quasiparticle-coupling (CQPC) model and Kerman-Klein-Dönau-Frauendorf (KKDF) method

In general in the frame of CQPC model an odd-odd nucleus is treated as a system of two quasiparticles coupled to four even-even cores. The procedure of this model follows that of Kerman-Klein-Dönau-Frauendorf (KKDF) method [Don77, Don79]. For KKDF method, the first step is to couple a valence proton to an even-even core, and energies and matrix elements of the electromagnetic operators are calculated for the resulting odd-proton nucleus. This odd-proton nucleus is then treated as a core in an odd-neutron coupling scheme which results in predicted energies and electromagnetic properties for the corresponding odd-odd nucleus. In addition the neutron can be coupled directly to the even-even core which results in the calculated properties of the corresponding odd-neutron nucleus. Comparison between the calculated and experimental observables for odd-mass nuclei provides a test for the

correctness of the coupling scheme as well as the applied model parameters. This model was used to support proposed chirality within the partner bands in ^{128}Cs [Kio03a] and of ^{130}Cs [Sim05] nuclei.

The simplified version of CQPC model is called core-particle-hole coupling (CPHC) model [Sta02]. In CPHC model the odd proton is assumed to be a pure particle whereas the odd neutron is assumed to be a pure hole. There is no need to apply CQPC model twice (first to the proton and the even-even core, and next to the neutron hole and the odd-even core). States of the odd-odd nucleus can be found through diagonalizing the three body Hamiltonian within the three body basis.

In the work of Droste *et al.* [Dro09], the properties of chiral bands associated with $\pi h_{11/2} \otimes \nu h_{11/2}^{-1}$ configuration in A ~ 130 were studied using CPHC [Sta02] model with either a rigid or a soft core. Large staggering in the intra- and inter-band $B(M1, I \rightarrow I-1)$ reduced transition probabilities was again found, and its phase was similar to the one reported in reference [Koi04]. A staggering was also found in the $B(E2, I \rightarrow I-2)$ reduced transition probabilities and its phase was similar to the one in the $B(M1, I \rightarrow I-1)$ transitions. The CPHC model was also used to support chirality in ^{132}Cs [Rai03a] (complemented with the 3D-TAC model) and ^{132}La [Sta02].

3.3.4 The interacting boson fermion-fermion model (IBFFM)

The IBFFM is based on the interacting boson model (IBM) [Ari76] for even-even nuclei and the interacting boson-fermion model (IBFM) [Iac79] for odd-A nuclei. This model is similar to other particle-plus-core coupling models (e.g. PRM, CPHC, etc) except that it uses bosons for its core description. The core is composed of s and d bosons, with angular momenta of $0\hbar$ and $2\hbar$ respectively. Valence quasiparticles in the IBFFM are coupled to all structures of the boson core (for example, ground state band, gamma-band, etc) that are present in the basis limited by the total boson number. Due to the general form of the IBM and its successful phenomenological description of a wide range of quadrupole collective structures (rotational, vibrational and transitional) the IBFFM also claims wide phenomenological applicability.

Within the IBFM [Bra09] and IBFFM [Bra04, Bra08, Ton07] near degeneracy in the partner bands is obtained too. In the studies of [Bra04, Bra08, Ton07], the IBFFM was applied to interpret partner bands in ^{134}Pr nucleus. A detailed analysis of the wave function in IBFFM showed that the angular momenta of the odd proton, the odd neutron and the core couple in

an aplanar configuration, for which almost orthogonal geometry is possible but far from being dominant. It was found that there are large fluctuations of the deformation parameters β_2 and γ around the triaxial equilibrium shape which are not the same for both bands. This could cause discrepancy in the properties of the partner bands. Hence the structure of the partner bands in ^{134}Pr is characterized by an aplanar orientation of the total angular momentum and β_2 and γ fluctuations. This was called dynamical chirality. Similarly, the IBFM calculations performed for the partner bands in ^{135}Nd suggested that the structure of these bands is strongly influenced by shape fluctuations [Bra09].

3.3.5 The pair-truncated shell model (PTSM)

This model is the version of shell model, where the collective core is made of collective S and D pairs. Similar to IBM the collective S and D pairs have angular momenta of $0\hbar$ and $2\hbar$ respectively. These pairs form the building blocks of this model (PTSM). In this model the effective interactions consist of spherical single-particle energies, monopole paring interaction, quadrupole pairing interaction and quadrupole-quadrupole interaction, whose strength are determined so as to describe the level scheme of even-even nuclei. Like the IBM, the PTSM was extended for the description of odd-mass and odd-odd nuclei. The detailed description for PTSM is given in references [Yos04, Hig05].

Within the PTSM it was found that the band structure of the partner bands in ^{130,132}Cs and ^{132,134}La nuclei can be also explained by the chopsticks-like coupling of the two angular momenta of the odd proton and the odd neutron [Hig05, Yos05]. It was found that the level scheme of the partner bands arises in this case not from a chiral picture (the angular momenta of the odd neutron and the odd proton are strongly coupled with an even-even core), but from different angular momentum configurations of the unpaired neutron and unpaired proton in the $h_{11/2}$ orbitals, weakly coupled with the collective excitations of the even-even core. It was also found that the staggering in the $B(M1)/B(E2)$ ratios occurs when the coupling of the core and the odd particles are weak and that the staggering is caused by a chopsticks-like coupling of the neutron and proton angular momenta.

3.3.6 The quadrupole coupling model (QCM)

This model is regarded as the simplified version of PTSM, where the collective core is made up of even number of protons and neutrons. The two valence nucleons couple with the even-even collective core through a quadrupole-quadrupole interaction. The model Hamiltonian consists of a Hamiltonian of the collective core, and in addition the quadrupole-quadrupole

interaction between the core and the neutron, the core and the proton, and the neutron and the proton. The quadrupole-quadrupole interactions are determined from experimental energy levels of odd-odd nuclei, and assumed to be smooth functions of the proton number Z and the neutron number N. This model is described in more details in references [Yos06] and [Hig07]. The QCM has been used for a description of partner bands built on the $\pi h_{11/2} \otimes \nu h_{11/2}^{-1}$ configuration in several odd-odd nuclei in the mass 130 (^{128,130,132,134}La, ^{128,130,132}Cs, ^{130,132,134,136}Pr [Yos06, Hig07]), but it gives an interpretation of the partner bands similar to that of PTSM [Hig05, Yos05].

3.4 Problem identification and objectives

The pioneering work of Frauendorf *et al*. [Fra97, Fra01] showed that in order for a chiral system to form, an aplanar orientation (i.e. pointing outside of the planes defined by the major nuclear axes) of the total angular momentum is needed. Furthermore, ideal chiral systems (i.e. system with strongly broken chiral symmetry) should exhibit a pair of $\Delta I = 1$ rotational bands, which are degenerate within a certain spin range. Perfect degeneracy within a spin range was not found experimentally. Thus it was suggested that perfect degeneracy corresponding to strongly broken chirality occurs at the crossing point between the partner bands. Alternatively, it was also thought that a strongly broken chirality may in practice correspond not to degeneracy, but to similarity in the partner bands [Pet06]. Thus, it seems some open questions remain concerning how exactly strongly broken chiral symmetry should be exhibited.

Another interesting question concerns the necessary conditions for a chiral system to form. Indeed, it was originally suggested [Fra97, Fra01], that in order for a chiral symmetry to occur the system should have an aplanar orientation of the total angular momentum. This however seems to be not quite sufficient to reach degeneracy in the partner bands. Calculations were published, in which the total angular momentum of the system is found to be aplanar, but the calculated excitation energies of the partner bands are not degenerate. This seems to indicate that the requirement for forming a strongly broken system might be stronger that the suggested aplanar orientation of the total angular momentum. Thus the first task of this work is to investigate whether a strongly broken chiral system exhibits degeneracy in the partner bands, and what is the necessary condition for reaching such degeneracy.

A previous study of a chiral system in 130 mass region showed the presence of an additional symmetry which requires different $B(M1, I \rightarrow I-1)$ intra-band reduced transition probabilities for consecutive levels in the chiral bands, i.e. the $B(M1)$ transition probabilities should be high for even values of I, and low for odd values of I [Koi04]. Other studies of the same chiral system also suggested the presence of a staggering in the $B(M1)$ values [Zha07, Qi09b, Dro09]. However the phase of the $B(M1)$ staggering obtained in all these works [Koi04, Zha07, Qi09b, Dro09] is not the same. This shows that open questions remain, for example whether the staggering in the $B(M1)$ values is a reliable indication for a strongly broken chiral symmetry. Furthermore it remains unclear what should be expected for a chiral system built on an asymmetric configuration (like those in the 100 and 190 mass regions) for which the symmetry responsible for the $B(M1)$ staggering [Koi04] is not present. Thus the next task of this work is to investigate other characteristics of chiral bands.

In summary, the objectives of these investigations are as follows:

(i) to examine if there is a possibility that a strongly broken chirality and thus perfect degeneracy in the chiral partner bands may exist in nuclei with large and stable triaxiality, and with a suitable two-quasiparticle configurations.

(ii) to have a systematic study on the conditions for reaching degeneracy in the chiral partner bands built on two-quasiparticle configurations in the A ~ 100, 130 and 190 mass regions.

(iii) to study further the characteristic features of chiral bands, such as the energy staggering $S(I)$ parameter and the staggering in the reduced $B(M1)$ electromagnetic transition probabilities.

CHAPTER 4 TQPRM calculations performed for the chiral partner bands in A ~ 100, 130 and 190 mass regions

4.1 Why are TQPRM calculations suitable for this study?

In section 3.1.2 we have mentioned some of the phenomena which are suggested as able to destroy the degeneracy in chiral partner bands. Thus it seems that degeneracy can occur in chiral nuclei with stable triaxial deformation and with suitable nucleon configuration. Thus in order to exclude those effects mentioned in section 3.1.2 we chose for our calculations the two-quasiparticle-plus-triaxial-rotor model (TQPRM) [Sem92], in which the nuclear shape is stable. Such calculations were performed for the chiral partner bands associated with $\pi g_{9/2}^{-1} \otimes \nu h_{11/2}$, $\pi h_{11/2} \otimes \nu h_{11/2}^{-1}$ and $\pi h_{9/2} \otimes \nu i_{13/2}^{-1}$ configurations in A ~ 100, 130 and 190 mass regions respectively. The collective core in these calculations is described by a rotor with stable deformation, thus γ-vibrations in the nuclear shape are excluded. It describes the coupling of odd particles (occupying fixed single-particle configurations) to a core (which can be parameterized by its deformation ε_2 and non-axiality γ). The total angular momentum is a good quantum number. Furthermore, the calculations within this model are carried out in the laboratory frame, where the wave functions of the chiral partner bands are different. Thus a different solution is obtained for each partner band, which allows us to study the conditions at which the partner bands become degenerate. We can also extract information on the orientation of the angular momenta and determine whether the total angular momentum is aplanar. The calculated yrast states form the yrast band, while the second lowest lying states for a given spin form the side or the partner band. This model was further developed to calculate the distributions of the angular momenta too [Rag08]. However, the deformation parameters ε_2 and γ are not calculated, but given as input parameters. Different variations of particle-rotor models have been used extensively to study chirality in nuclei before [Koi03a, Har01, Bar01, Wan07, Jos05b, Law08, Law10b, Sta01b, Koi01, Sta02, Pen03, Ton06, Gro06, Ton07, Zha07, Wan08, Qi09a-b]. It should be noted that in none of these cases a perfect degeneracy was calculated for the partner bands.

4.2 The formalism of two-quasiparticle-plus-triaxial-rotor model (TQPRM)

A brief introduction of a particle-core coupling model first developed by Bohr and Mottelson [Boh52, Boh53] was given in section 2.6. Some improvements of the model performed by

Meyer-ter-Vehn *et al*. [Mey74, Mey75] were also briefly discussed in section 2.6.2. In this section we shall briefly discuss some recent developments of the PRM where two odd particles in odd-odd nuclei and also the residual proton-neutron interaction between them may be treated. This development was performed by Ragnarsson and Semmes [Rag88]. Note that this model was first presented in Reference [Lar78] based on formalism introduced by Hecht and Satchler [Hec62]. In reference [Lar78] only one odd particle was considered.
The Hamiltonian for one valence odd particle coupled to the triaxial rotor core can be written

$$H = H_{core} + \left(H_{sph} + H_{\text{int}} + H_{pair}\right) \tag{4.1}$$

where H_{core} describes the collective even-even core, H_{sph} is the spherical shell model Hamiltonian for the odd particle, H_{int} describes the interaction between the odd particle and the core, and H_{pair} represents the pairing force between like particles.

In the case of two odd valence particles (i.e. a proton and neutron), the Hamiltonian of equation (4.1) becomes

$$H = H_{core} + \left(H_{sph} + H_{\text{int}} + H_{pair}\right)^{p,n} + V_{pn} \tag{4.2}$$

where the terms inside the brackets are taken twice, one for the odd proton and the other one for the odd neutron. The term V_{pn} represents the interaction between the two odd particles.

With restriction to the rigid triaxial rotor core, the sum $H_{sph} + H_{\text{int}}$ can be transformed to the intrinsic frame of reference, where it takes the form of a one-body deformed shell model Hamiltonian. The eigenstates of this static deformed potential form a convenient basis for subsequent calculations. The pairing term is included by a standard BCS calculation on these adiabatic single-particle states. In the strong coupling basis these single-particle terms are diagonal.

4.2.1 The single-particle Hamiltonian

With the introduction of stretched coordinates (i.e. redefining the unit lengths of the deformed nucleus in real space such that it is spherical in the new stretched coordinate system) [Nil55], the modified oscillator Hamiltonian can be written

$$H = H_{def}(\varepsilon_2, \gamma) + 2\hbar\omega_0 r'^2 \varepsilon_4 V_4(\gamma) + V' \tag{4.3}$$

where r' represents the radius in the stretched coordinate system, i.e. $r' = r(M\omega_0/\hbar)^{1/2}$.

The deformed harmonic oscillator Hamiltonian $H_{def}(\varepsilon_2, \gamma)$ is written similarly to equation (2.26)

$$H_{def}(\varepsilon_2, \gamma) = \frac{p^2}{2M} + \frac{M}{2}\left(\omega_x^2 x^2 + \omega_y^2 y^2 + \omega_z^2 z^2\right) \tag{4.4}$$

where oscillator frequencies ω_x, ω_y and ω_z are expressed by equations (2.19), (2.20) and (2.21) in terms of quadrupole deformation parameters ε_2, γ.

The hexadecupole deformation potential $V_4(\gamma)$ is made dependent on γ in such a way that axial symmetry is not broken for prolate ($\gamma = 0^0$) or oblate ($\gamma = 60^0$) shape, and so that the same shape is obtained in all six 60^0 sectors. This is achieved by choosing

$$V_4(\gamma) = \alpha_{40} Y_{40} + \alpha_{42}\left(Y_{42} + Y_{4-2}\right) + \alpha_{44}\left(Y_{44} + Y_{4-4}\right) \tag{4.5}$$

where the α_{4i} parameters have transformation properties of a hexadecupole tensor

$$\alpha_{40} = \frac{1}{6}\left(5\cos^2\gamma + 1\right) \tag{4.6}$$

$$\alpha_{42} = -\frac{1}{12}\sqrt{30}\sin 2\gamma \tag{4.7}$$

$$\alpha_{44} = \frac{1}{12}\sqrt{30}\sin^2\gamma \tag{4.8}$$

The potential term V' takes the form of the sum of the two correction terms included in the Nilsson model (see equation (2.34) in section 2.4). The stretched basis has the advantage that the couplings between different oscillator shells N are generally small. Therefore, a good numerical accuracy is obtained even if the number of the oscillator shells is small.

The diagonalisation of the Hamiltonian of equation (4.3) leads to adiabatic single-particle states defined by

$$|\upsilon\rangle = \sum_{Nj\Omega} C^{(\upsilon)}_{Nlj\Omega} |Nlj\Omega\rangle \tag{4.9}$$

with Ω chosen as $\ldots, -7/2, -3/2, +1/2, +5/2, \ldots$. The conjugate orbitals are defined as

$$|\tilde{\upsilon}\rangle = \sum_{Nj\Omega} (-1)^{(j-\Omega)} C^{(\upsilon)}_{Nlj\Omega} |Nlj-\Omega\rangle \tag{4.10}$$

To include pairing effects quasiparticle operators are introduced. The quasiproton operators a^+_υ are defined by

$$a^+_\upsilon = U_\upsilon \alpha^+_\upsilon - V_\upsilon \alpha_{\tilde{\upsilon}} \qquad a^+_{\tilde{\upsilon}} = U_\upsilon \alpha^+_{\tilde{\upsilon}} - V_\upsilon \alpha_{\tilde{\upsilon}} \tag{4.11}$$

where $U^2_\upsilon + V^2_\upsilon = 1$ and α^+_υ is the creation operator for a proton in the orbital $|\upsilon\rangle$. The quasineutron operators are defined in a similar way and they are denoted by β^+_μ where μ refers to neutron orbitals. The quasiparticle destruction operators are obtained from the hermitian conjugates of creation operators.

The intrinsic state of an odd mass nucleus in which the unpaired nucleon occupies the orbital $|\upsilon\rangle$ can be written as

$$|\upsilon\rangle = a^+_\upsilon |\tilde{0}\rangle \tag{4.12}$$

where $|\tilde{0}\rangle$ denotes the BCS vacuum states. The U^2_υ and V^2_υ factors are the non-occupation and occupation probabilities respectively, and given by the usual equations

$$U^2_\upsilon = \frac{1}{2}\left(1 + \frac{e_\upsilon - \lambda_F}{\sqrt{(e_\upsilon - \lambda_F)^2 + \Delta^2}}\right) \qquad V^2_\upsilon = \frac{1}{2}\left(1 - \frac{e_\upsilon - \lambda_F}{\sqrt{(e_\upsilon - \lambda_F)^2 + \Delta^2}}\right) \tag{4.13}$$

where e_υ is the adiabatic single-particle energy, λ_F is the Fermi level of the particles and Δ is the pairing gap. Similarly, the quasiparticle energy is given by

$$E_\upsilon = \sqrt{(e_\upsilon - \lambda_F)^2 + \Delta^2} \tag{4.14}$$

The blocking effect is roughly taken into account if the BCS vacuum corresponds to the odd number of particles [Sem92].

4.2.2 The core Hamiltonian and basis states for odd nuclei

The basis states should be symmetrized under the point group D_2 (associated with rotations of 180^0 about each of the intrinsic axes). When written in terms of quasiparticle operators and with the conjugate state defined in equation (4.10), they take the form

$$\left|IMK\upsilon\right\rangle = \sqrt{\frac{2I+1}{16\pi^2}}\left\{D^I_{MK}a^+_\upsilon\left|\tilde{0}\right\rangle + (-1)^{I-K}D^I_{M-K}a^+_{\bar{\upsilon}}\left|\tilde{0}\right\rangle\right\} \tag{4.15}$$

Where D^I_{MK} is a matrix corresponding to total angular momentum I and projections M and K on the lab quantization axis and the intrinsic quantization axis respectively.

Since the D function does not depend explicitly on the core angular momentum $\vec{R}$, but on the total angular momentum $\vec{I}$, the core Hamiltonian of a triaxial rotor takes the form

$$H_{core} = \frac{\hbar^2}{2\Im_k}R^2 = \frac{\hbar^2}{2\Im_k}(I_k - j_k)^2 \tag{4.16}$$

where $k = 1, 2, 3$ define the three principal axes of the nucleus.

For one odd particle, equation (4.16) can be expanded as follows

$$\begin{aligned} H_{core} = {} & \frac{1}{2}\left(\frac{\hbar^2}{2\Im_1} + \frac{\hbar^2}{2\Im_2}\right)\left\{I^2 - I_3^2 + j^2 - j_3^2 - (I_+ j_- + I_- j_+)\right\} \\ & + \frac{1}{4}\left(\frac{\hbar^2}{2\Im_1} - \frac{\hbar^2}{2\Im_2}\right)\left\{I_+^2 + I_-^2 + j_+^2 + j_-^2 - 2(I_+ j_+ + I_- j_-)\right\} + \frac{\hbar^2}{2\Im_3}(I_3 - j_3)^2 \end{aligned} \tag{4.17}$$

which is the appropriate form if the intrinsic 3-axis is taken as the quantization axis. One should note that often the moments of inertia $\Im_1, \Im_2$ and $\Im_3$ are assumed to vary with γ according to the hydrodynamical relation (see equation 2.84).

4.2.3 The core Hamiltonian and basis states for odd-odd nuclei

If one ignores pairing, an unsymmetrized strong coupling basis states for odd-odd nuclei has the form

$$\left|IMK\upsilon\mu\right\rangle \sim D^{I}_{MK}\phi_{pn} \tag{4.18}$$

where ϕ_{pn} is the product of a proton state $\left|\upsilon\right\rangle$ and a neutron state $\left|\mu\right\rangle$. Note that for a proton orbital $\left|\upsilon\right\rangle$, neutron orbital $\left|\mu\right\rangle$ and their conjugates, two different product states can be formed

$$\phi_{pn} = \left|\upsilon\right\rangle\left|\mu\right\rangle \text{ or } \phi_{pn} = \left|\upsilon\right\rangle\left|\tilde{\mu}\right\rangle \tag{4.19}$$

In the case of axial symmetry, $\left\langle j_z \right\rangle = \Omega$ is conserved for adiabatic orbitals, and these two product states correspond to

$$K = \Omega_p + \Omega_n \text{ and } K = \Omega_p - \Omega_n \tag{4.20}$$

With the restrictions on Ω as noted with equation (4.9), K is even (odd) if the product states do (do not) involve conjugate neutron orbitals. Therefore, for axially symmetric case, a given proton and neutron intrinsic states give rise to two strong coupling Nilsson basis states for a given I (with $I \geq K$). For axially asymmetric shapes more Nilsson states are generated from each intrinsic product state, but the total projection quantum number K remains even (odd) if the product state does (does not) contain a neutron conjugate orbital. When symmetrized, these states are

$$\left|IMK\upsilon\mu\right\rangle = \sqrt{\frac{2I+1}{16\pi^2}}\left\{D^{I}_{MK}a^{+}_{\upsilon}\beta^{+}_{\mu}\left|\tilde{0}\right\rangle + (-1)^{I+1}D^{I}_{M-K}a^{+}_{\tilde{\upsilon}}\beta^{+}_{\tilde{\mu}}\left|\tilde{0}\right\rangle\right\} \tag{4.21}$$

for $K = \pm 1, \pm 3, \pm 5, \ldots, \pm(I-1)$ or $\pm I$ and

$$\left|IMK\upsilon\tilde{\mu}\right\rangle = \sqrt{\frac{2I+1}{16\pi^2}}\left\{D^{I}_{MK}a^{+}_{\upsilon}\beta^{+}_{\tilde{\mu}}\left|\tilde{0}\right\rangle + (-1)^{I+1}D^{I}_{M-K}a^{+}_{\tilde{\upsilon}}\beta^{+}_{\mu}\left|\tilde{0}\right\rangle\right\} \tag{4.22}$$

for $K = 0, \pm 2, \pm 4, \ldots, \pm(I-1)$ or $\pm I$.

In the core Hamiltonian of equation (4.16), the core rotational angular momentum $\vec{R}$ is now expressed in terms of the total angular momentum $\vec{I}$, the intrinsic angular momenta of the proton and neutron $\vec{j}_p$, $\vec{j}_n$ as

$$\vec{R} = \vec{I} - \vec{j}_p - \vec{j}_n \tag{4.23}$$

Then the core Hamiltonian becomes

$$\begin{aligned} H_{core} = {} & \frac{1}{2}\left(\frac{\hbar^2}{2\Im_1} + \frac{\hbar^2}{2\Im_2}\right)\{I^2 - I_3^2 + j_p^2 - j_{p3}^2 + j_n^2 - j_{n3}^2 + j_{p+}j_{n-} + j_{p-}j_{n+} - I_+(j_{p-} + j_{n-}) \\ & - I_-(j_{p+} + j_{n+})\} + \frac{1}{4}\left(\frac{\hbar^2}{2\Im_1} - \frac{\hbar^2}{2\Im_2}\right)\{I_+^2 + I_-^2 + j_{p+}^2 + j_{p-}^2 + j_{n+}^2 + j_{n-}^2 + 2(j_{p+}j_{n+} + j_{p-}j_{n-}) \\ & - 2I_+(j_{p+} + j_{n+}) - 2I_-(j_{p-} + j_{n-})\} + \frac{\hbar^2}{2\Im_3}\{I_3^2 - 2I_3(j_{p3} + j_{n3}) + j_{p3}^2 + j_{n3}^2 + 2j_{p3}j_{n3}\} \end{aligned} \tag{4.24}$$

Note that the proton matrix elements which are the same as for the case of one odd particle are multiplied by proton pairing factors $UU' + VV'$ and similarly for neutrons.

Sometimes the mixing between the intrinsic states induced by the Coriolis terms seems too large compared with experimental data, especially when high-j orbitals are considered. The relative strength of the Coriolis interaction can be reduced by decreasing the pairing factor (i.e. by small adjustments in the pairing parameters), by decreasing the single-particle matrix elements of j_+ (i.e. by adjusting the deformation, and thus changing the Nilsson orbitals), or by increasing the quasiparticle energy separation (perhaps by adjusting the pairing and/or the deformation parameters). These adjustments are possible within particle-plus-rotor model. The attenuation can also be achieved by introducing an attenuation factor ξ that multiplies the Coriolis matrix elements, or by raising the pairing factors $UU' + VV'$ to some power η. Both options are available in the two-quasiparticle-plus-triaxial-rotor model [Sem92].

4.2.4 The residual proton-neutron interaction

For the residual interaction, a phenomenological finite range force is used

$$V_{pn} = \sqrt{8\pi^3} b^3 \delta(\vec{r}_p - \vec{r}_n)\left(u_0 + u_1 \sigma_p . \sigma_n\right) \tag{4.25}$$

where b is the oscillator length, u_0 and u_1 are strength parameters and σ is a Pauli spin matrix. When this residual interaction is calculated in the strong coupling basis we obtain for odd K

$$\begin{aligned}\left\langle IK'\upsilon'\mu' \left| V_{pn} \right| IK\upsilon\mu \right\rangle = \delta_{K'K} \left\{ A\left\langle \upsilon'\mu' \left| V_{pn} \right| \upsilon\mu \right\rangle - B\left\langle \upsilon'\tilde{\mu} \left| V_{pn} \right| \upsilon\tilde{\mu}' \right\rangle \right\} \\ + (-1)^{I+1} \delta_{K'-K} \left\{ A\left\langle \tilde{\upsilon}'\tilde{\mu}' \left| V_{pn} \right| \upsilon\mu \right\rangle + B\left\langle \tilde{\upsilon}\tilde{\mu}' \left| V_{pn} \right| \upsilon'\mu \right\rangle \right\}\end{aligned} \tag{4.26}$$

and for even K

$$\begin{aligned}\left\langle IK'\upsilon'\tilde{\mu}' \left| V_{pn} \right| IK\upsilon\tilde{\mu} \right\rangle = \delta_{K'K} \left\{ A\left\langle \upsilon'\tilde{\mu}' \left| V_{pn} \right| \upsilon\tilde{\mu} \right\rangle - B\left\langle \upsilon'\mu \left| V_{pn} \right| \upsilon\mu' \right\rangle \right\} \\ + (-1)^{I+1} \delta_{K'-K} \left\{ A\left\langle \tilde{\upsilon}'\mu' \left| V_{pn} \right| \upsilon\tilde{\mu} \right\rangle + B\left\langle \tilde{\upsilon}\mu' \left| V_{pn} \right| \upsilon'\tilde{\mu} \right\rangle \right\}\end{aligned} \tag{4.27}$$

where A and B are pairing factors

$$A = U_{\upsilon'} U_{\upsilon} U_{\mu'} U_{\mu} + V_{\upsilon'} V_{\upsilon} V_{\mu'} V_{\mu} \qquad B = U_{\upsilon'} U_{\upsilon} V_{\mu'} V_{\mu} + V_{\upsilon'} V_{\upsilon} U_{\mu'} U_{\mu} \tag{4.28}$$

and the matrix elements like $\left\langle \upsilon'\mu' \left| V_{pn} \right| \upsilon\mu \right\rangle$ involve the proton and neutron adiabatic single-particle sates $\left| \upsilon \right\rangle$, $\left| \mu \right\rangle$, etc. Additional terms involving sums over all occupied proton and neutron states; these terms must represent part of the core contribution and have been discarded. Note that off-diagonal as well as diagonal matrix elements are included in the calculation.

4.2.5 Electromagnetic transition probabilities

With the standard definitions of Bohr and Mottelson [Boh69], electromagnetic transition rates are proportional to the reduced transition probability $B(E\lambda)$ or $B(M\lambda)$ with

$$B(O\lambda; I_i \to I_f) = \frac{1}{2I_i + 1} \left| \left\langle I_f \left\| T(O\lambda) \right\| I_i \right\rangle \right|^2 \tag{4.29}$$

where O denotes E or M, λ indicates the multipolarity of electromagnetic transition and T is the transition operator. The $M1$ operator can be written

$$T(M1,\mu) = g_R \vec{R}_\mu + \sum \left(g_l \vec{l}_\mu + g_s \vec{s}_\mu \right) \tag{4.30}$$

where the sum is performed over the valence particles. The orbital and spin g-factors for the valence particle are denoted by g_l and g_s, and g_R is the core g-factor. μ is the magnetic dipole moment. The general expression for the $E2$ operator

$$T(E2,\mu) = \int \rho_{chg}(r) r^2 Y_{2\mu} d^3 r + e_{eff} r^2 Y_{2\mu} \tag{4.31}$$

splits into one core part which is generally dominating and one term for the odd particle(s). In reference [Lar78], the explicit formulae for the $M1$ and $E2$ matrix elements are given for odd mass nuclei. Equivalent formulae are straightforward to derive in the odd-odd case. The mixing ratio is given by

$$\delta = \sqrt{0.7} E_\gamma \frac{\langle I \| T(E2) \| I-1 \rangle}{\langle I \| T(M1) \| I-1 \rangle} \tag{4.32}$$

Magnetic dipole moments μ and electric quadrupole moments Q_s are obtained as

$$\mu = \sqrt{\frac{4\pi}{3}} \frac{\langle II10 | II \rangle}{\sqrt{2I+1}} \langle I \| T(M1) \| I \rangle \tag{4.33}$$

$$Q_s = \sqrt{\frac{16\pi}{5}} \frac{\langle II20 | II \rangle}{\sqrt{2I+1}} \langle I \| T(E2) \| I \rangle \tag{4.34}$$

4.3 The two-quasiparticle-plus-triaxial-rotor model (TQPRM) calculations

The TQPRM [Sem92] which uses a modified oscillator potential was used to perform the calculations for the chiral partner bands in A ~ 100, 130 and 190 mass regions. These calculations were run using the codes called GAMPN, VPNDELTA, ASYRMO and PROBAMO [Sem92]. These programs are run one after the other in the sequence as listed

above. The calculations can be performed with or without residual proton-neutron (V_{pn}) interaction.

The input parameters for GAMPN are nuclear deformation parameters ε_2, γ, ε_4; the number of protons Z and the mass A of a nucleus; and the Nilsson's strength parameters κ and μ of the $\vec{l}.\vec{s}$ and $\vec{l}^2$ terms. The code GAMPN calculates the single-particle energies and eigenfunctions (Nilsson states) for either the odd proton, the odd neutron or both proton and neutron at a fixed nuclear deformation. Note that for an asymmetric nuclear shape, the single-particle state is composed of a mixture of Nilsson states with same parity and different occupation probabilities, whereas for a symmetric nuclear shape, the single-particle state is a pure Nilsson state. From the single-particle states generated from GAMPN, one selects a set of orbitals lying close to the Fermi level λ_F from which the particle-plus-rotor states will be constructed. Note that these single-particle states are labeled with a certain natural number which is referred to as the orbital number.

The input parameters for VPNDELTA are the pairing strength parameters u_0 and u_1. From selected single-particle states corresponding to the band of interest, the VPNDELTA calculates the two-body residual proton-neutron (V_{pn}) interaction using the single-particle energies calculated by GAMPN. Note that for calculations without a residual proton-neutron interaction $u_0 = u_1 = 0$.

Within the selected set of single-particle states, the code ASYRMO couples the rotation of the core with the single-particle eigenvectors (matrix elements). The calculation can be performed with a maximum of 15 single-particle states (or some subset of these) above and below the Fermi level λ_F. This code treats even multipoles only in the deformed field (i.e. no octupole deformation), so there is no mixing between positive and negative parity orbitals. Therefore one must specify the parity of the orbitals to be retained for later use. There is no restriction to unique parity states (high-j shells) in these codes.

From the single-particle energies calculated by ASYRMO, the residual pairing interaction is treated within the BCS approximation. This implies that for each deformed single-particle state, the quasiparticle energy and the pairing factors U and V are calculated, from the single-particle energy, the Fermi level λ_F and the pairing gap Δ. If the calculation is made by adopting a standard value for the pairing strength parameter G, then the Fermi level λ_F and the pairing gap Δ are derived quantities, and not input parameters. Alternatively, λ_F

and Δ can be input directly in the calculation. The blocking effect is roughly included by requiring that λ_F corresponds to the odd number of particles, Z or N. It is well known from the axially symmetric case (for nuclei in A ~ 150 mass region) that agreement with experiments can generally be improved by introducing a Coriolis attenuation parameter. In this work it is denoted by ξ and the paring U and V occupational probabilities can be multiplied by it. Then, the particle-plus-rotor Hamiltonian matrix is constructed and diagonalized for a selected range of values for the total spin I, either in the one- or two-quasiparticle strong coupling basis. Various angular momentum expectation values are calculated from the energy eigenvectors. One has to provide some information about the moment of inertia for the even-even core. The moment of inertia can be approximated either by using Harris parameters (see section 2.5.4) or by specifying the energy of the first 2_1^+ state in the even-even core. The energy of the first 2_1^+ state of the core can also be estimated from the deformation using Grodzins's relation (see section 2.6.2)

$$E_{2_1^+} \cong \frac{1225}{\beta_2^2 A^{7/2}} MeV \tag{4.35}$$

For the triaxial case, the three moments of inertia are assumed to be related by the hydrodynamical expression shown in equation (2.84). The final test of the parameters lies in the comparison of the calculated and experimental properties of the nucleus

The code PROBAMO calculates the electromagnetic matrix elements, both diagonal and off-diagonal, from the eigenvectors of the particle-plus-rotor Hamiltonian generated by ASYRMO. The diagonal matrix elements are displayed as the static moments (electric quadrupole moment Q_s and the magnetic dipole moment μ), in units of e-barn (eb) and nuclear magnetons (μ_N) respectively. Note that the electric quadrupole moment Q_s is the spectroscopic moment, which is directly observable in experiments, and not the intrinsic moment Q_0. The off-diagonal matrix elements are displayed as $B(E2)$s and $B(M1)$s (in units of e^2b^2 and μ_N^2 respectively), and as γ-ray partial transition rates $T(E2)$ and $T(M1)$. Furthermore, for mixed $E2/M1$ transitions, the mixing ratio $\delta(E2/M1)$ is calculated. All the transition rate calculations use the computed γ-ray energies when needed.

Note that for particle-plus-triaxial-rotor model applications, only one 60^0 sector (i.e. $0^0 \le \gamma \le 60^0$) in the ε_2, γ plane is necessary. The other sectors (i.e. $-60^0 \le \gamma \le 0^0$ and

$-120^0 \le \gamma \le -60^0$) simply correspond to permutations of the labels on the nuclear axes. Table 4.1 shows three equivalent ways of labelling the nuclear axes which correspond to different quantization axis. The TQPRM codes that we have employed in our work use the intrinsic z-axis (i.e. 3-axis) as the quantization axis. For $\varepsilon_2 > 0$, $0^0 < \gamma < 30^0$ we have prolatish triaxial shapes while for $\varepsilon_2 > 0$, $30^0 < \gamma < 60^0$ we have obtalish triaxial shapes. For $\varepsilon_2 > 0$, $\gamma = 0^0$; $\varepsilon_2 > 0$, $\gamma = 60^0$ and $\varepsilon_2 > 0$, $\gamma = 30^0$ we have axially symmetric prolate, axially symmetric oblate and triaxial shapes respectively. It is possible to define all nuclear shapes within a 30^0 sector (i.e. $0^0 \le \gamma \le 30^0$) if one uses negative values of ε_2 too. Then for $0^0 \le \gamma \le 30^0$, the obtalish triaxial shapes will correspond to $\varepsilon_2 < 0$, while the prolatish shapes will correspond to $\varepsilon_2 > 0$.

Table 4.1: *Three equivalent ways of labelling the nuclear axes in ε_2, γ plane.*

Quadrupole deformation ε_2	Non-axiality parameter γ	Nuclear axes length	Quantization axis
$\varepsilon_2 > 0$	$0^0 < \gamma < 60^0$	z -long, x -short, y -intermediate	z (long)
$\varepsilon_2^{'} = -\varepsilon_2$	$\gamma^{'} = 60^0 - \gamma$	$x^{'} \equiv z$, $z^{'} \equiv x$, $y^{'} \equiv y$	$z^{'} \equiv x$ (short)
$\varepsilon_2^{'} = +\varepsilon_2$	$\gamma^{'} = -120^0 + \gamma$	$x^{'} \equiv z$, $z^{'} \equiv y$, $y^{'} \equiv x$	$z^{'} \equiv y$ (intermediate)

4.4 Parameters employed in the calculations for chiral partner bands in A ~ 100, 130 and 190 mass regions

In the 100 and 130 mass regions, the chiral symmetry was associated with bands built on $\pi g_{9/2}^{-1} \otimes \nu h_{11/2}$ and $\pi h_{11/2} \otimes \nu h_{11/2}^{-1}$ configurations respectively. From Nilsson diagrams (see Figures 4.1 and 4.2), the odd proton (neutron) occupying the highest-energy (lowest-energy) orbital in $g_{9/2}$ ($h_{11/2}$) shell at quadrupole deformation of $\varepsilon_2 = 0.15$ correspond to $Z = 49, (N = 57)$ nucleons for 100 mass region. In the 130 mass region, the odd proton (neutron) occupying the lowest-energy (highest-energy) orbital in the $h_{11/2}$ shell at quadrupole deformation of $\varepsilon_2 = 0.15$ corresponds to $Z = 57, (N = 81)$ nucleons (see Figures 4.1 and 4.2). Thus our calculations were performed for $\pi g_{9/2}^{-1} \otimes \nu h_{11/2}$ and $\pi h_{11/2} \otimes \nu h_{11/2}^{-1}$ bands A ~ 100 and 130 mass regions using the following nuclear deformation parameters of the core: $\varepsilon_2 = 0.15$ which has been previously used for ^{134}La [Bar01], $\varepsilon_4 = 0$, the value of non-axiality parameter γ close/equal to 30^0 and with no variable moment of inertia (VMI).

We have used standard parameters for the Nilsson potential [Ben85, Nil69] and the pairing gap Δ (corresponding to $\Delta_p = 0.525$ MeV and $\Delta_n = 0.759$ MeV in the 130 mass region). These calculations were carried out with residual proton-neutron interaction (V_{pn}) and also with both Coriolis attenuation and pairing strength factor of $\xi = \eta = 1$. The strength parameters for the residual proton-neutron (V_{pn}) interaction were set to $u_0 = -7.20$ MeV and $u_1 = -0.80$ MeV as previously used in 130 mass region [Taj94] and as proposed by Semmes and Ragnarsson [Sem90]. Since no direct comparison with the experimental data was intended the moment of inertia was calculated with a fixed energy of the first 2_1^+ state of the even-even core. Concerning the recoil term, operators $\vec{j}_p^{\,2}$, $\vec{j}_n^{\,2}$, $j_{p+} j_{n-}$, etc were treated as two-body operators with appropriate pairing factors. Stretched coordinates were used.

In the 190 mass regions, chiral symmetry was associated with bands built on $\pi h_{9/2} \otimes \nu i_{13/2}^{-1}$ configuration. From Nilsson diagrams (see Figures 2.5 and 4.3), the odd proton (neutron) occupying the lowest-energy (highest-energy) orbital in $h_{9/2}$ ($i_{13/2}$) shell at quadrupole deformation of $\varepsilon_2 = -0.15$ corresponds to $Z = 81, (N = 117)$ nucleons. We have used $\varepsilon_2 < 0$ because the shape of ^{198}Tl nucleus is expected to be oblatish. The calculations in the 190 mass region were performed similarly to those in A ~ 100 and 130 mass regions, but the parameters for the residual proton-neutron (V_{pn}) interaction were set to $u_0 = -4.95$ MeV and $u_1 = -0.55$ MeV as previously used [Bar97].

At $\varepsilon_2 = 0.15$ and -0.15, the protons $\pi g_{9/2}$, $\pi h_{11/2}$, $\pi h_{9/2}$ and the neutrons $\nu h_{11/2}$, $\nu i_{13/2}$ configurations involve intruder and extruder orbitals and do not have large mixing with orbitals from other sub-shells. In all three mass regions (i.e. A ~ 100, 130 and 190), five proton and neutron states close to the Fermi level were included in the calculations. Examples of such proton and neutrons states are shown in Tables 4.2 and 4.3.

In the calculations of electromagnetic transition probabilities, the effective spin g-factor g_s was taken as 60% of the free nucleon value for both protons and neutrons. The core g-factor g_R was chosen approximately equal to Z/A while the core quadrupole moment was calculated microscopically.

In these calculations no attempt was made to adjust the input parameters in order to obtain best agreement with experimental data. The aim was rather to investigate in general the behaviour of the partner bands associated with chiral symmetry in the three mass regions.

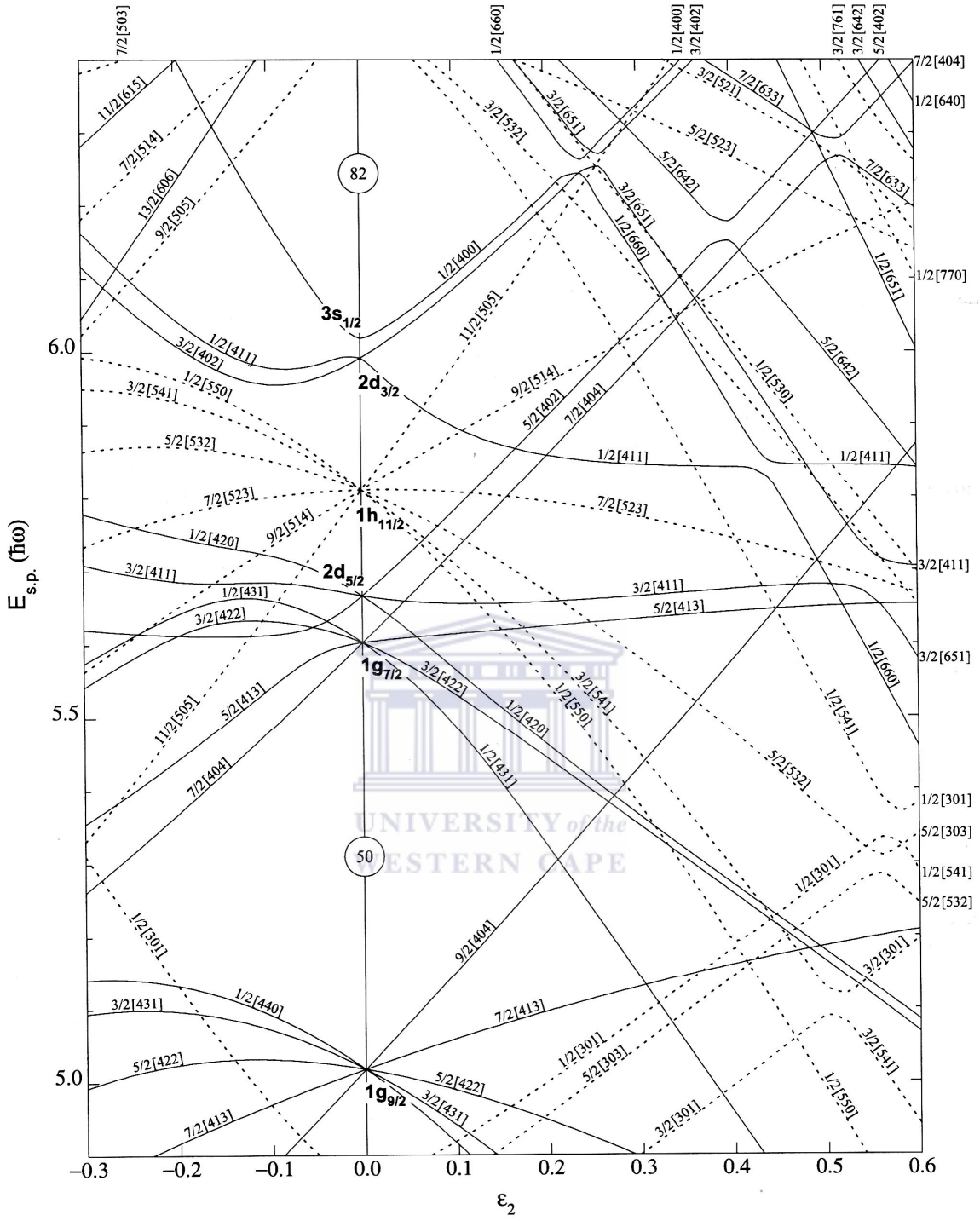

Figure 4.1: *Energy levels for protons ($50 \le Z \le 82$) in a prolate ($\varepsilon_2 > 0$) and oblate ($\varepsilon_2 < 0$) deformed potential as a function of ε_2 ($\varepsilon_4 = \varepsilon_2^2/6$). The quantum numbers $\Omega[N\ n_z\ m_l]$, label the states. Solid and dashed lines show states with positive and negative parity respectively [Fir96b].*

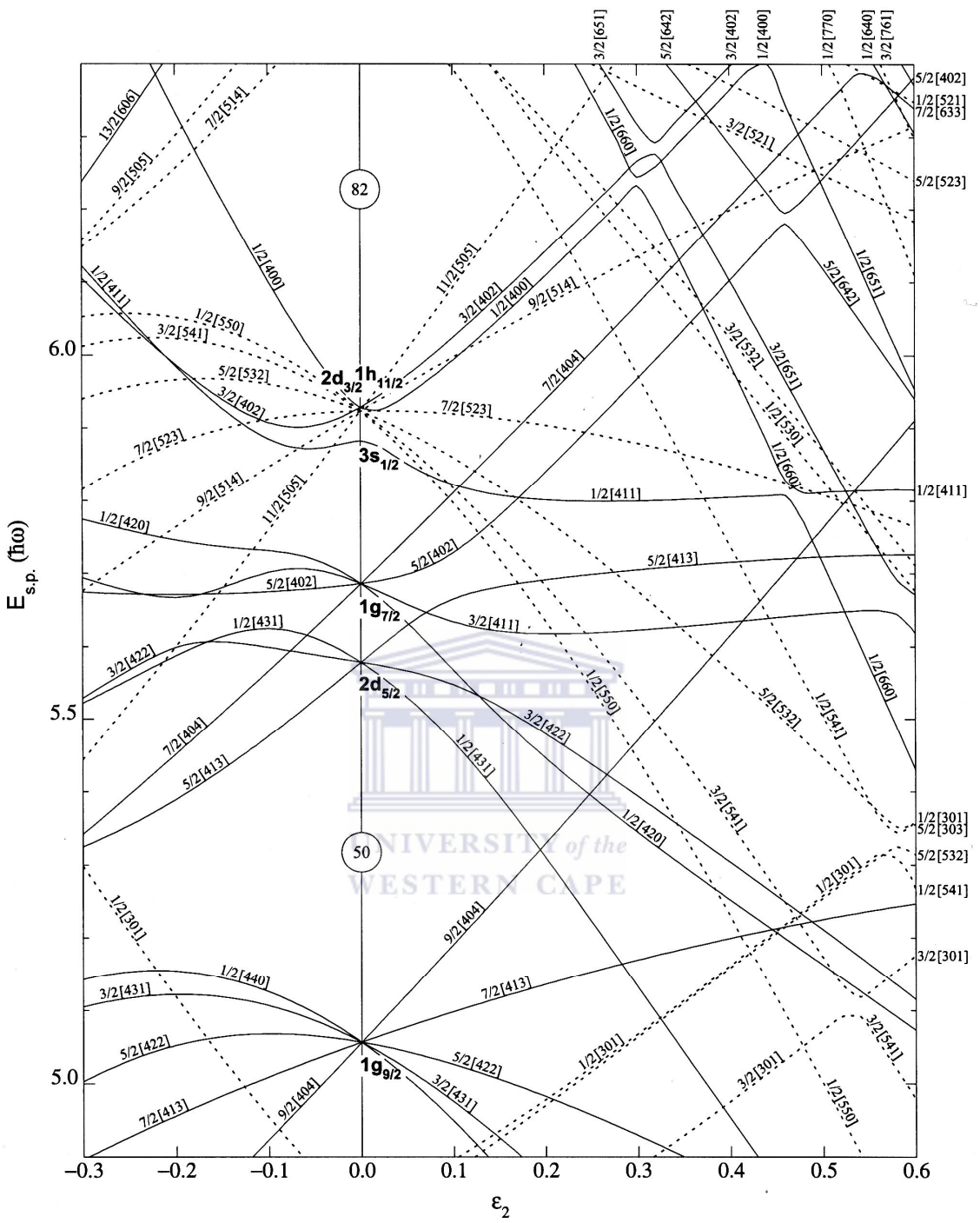

Figure 4.2: *Energy levels for neutrons ($50 \le N \le 82$) in a prolate ($\varepsilon_2 > 0$) and oblate ($\varepsilon_2 < 0$) deformed potential as a function of ε_2 ($\varepsilon_4 = \varepsilon_2^2/6$). The quantum numbers $\Omega[N\ n_z\ m_l]$, label the states. Solid and dashed lines show states with positive and negative parity respectively [Fir96c].*

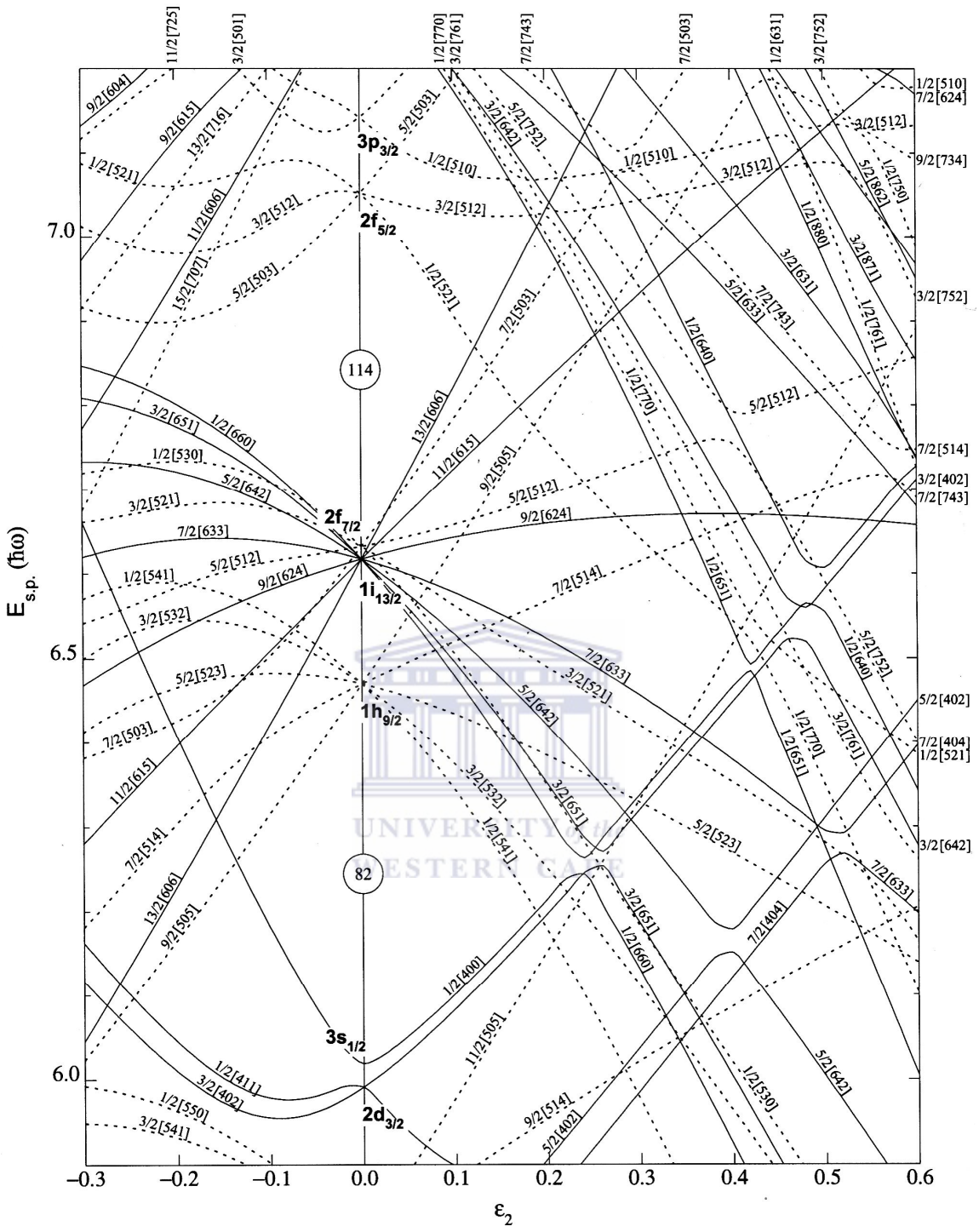

Figure 4.3: *Energy levels for protons ($Z \geq 82$) in a prolate ($\varepsilon_2 > 0$) and oblate ($\varepsilon_2 < 0$) deformed potential as a function of ε_2 ($\varepsilon_4 = \varepsilon_2^2/6$). The quantum numbers $\Omega[N\ n_z\ m_l]$, label the states. Solid and dashed lines show states with positive and negative parity respectively [Fir96d].*

Table 4.2: *Proton orbitals for ^{106}In ($g_{9/2}$), ^{138}La ($h_{11/2}$) and ^{198}Tl ($h_{9/2}$) nuclei calculated at* ε_2 = 0.15 *and* $\gamma = 30^0$.

^{106}In				
Single-particle level (proton orbital number)	**Single-particle energy (MeV)**	**Average projection along the quantization axis $\langle j_z \rangle$ ($\hbar$)**	**Nilsson basis state ($\lvert Nlj\Omega \rangle$) with large occupation probability**	**Parity (π)**
8	4.8283	0.04	$\lvert 4\,4\,\frac{9}{2}\,\frac{1}{2}\rangle$	+
9	4.9281	0.62	$\lvert 4\,4\,\frac{9}{2}\,\frac{3}{2}\rangle$	+
10	4.9923	1.98	$\lvert 4\,4\,\frac{9}{2}\,\frac{5}{2}\rangle$	+
11	5.0741	3.36	$\lvert 4\,4\,\frac{9}{2}\,\frac{7}{2}\rangle$	+
12	5.1832	4.44	$\lvert 4\,4\,\frac{9}{2}\,\frac{9}{2}\rangle$	+
^{138}La				
14	5.5784	0.01	$\lvert 5\,5\,\frac{11}{2}\,\frac{1}{2}\rangle$	–
15	5.6840	0.26	$\lvert 5\,5\,\frac{11}{2}\,\frac{3}{2}\rangle$	–
16	5.7548	1.46	$\lvert 5\,5\,\frac{11}{2}\,\frac{5}{2}\rangle$	–
17	5.8187	3.13	$\lvert 5\,5\,\frac{11}{2}\,\frac{7}{2}\rangle$	–
18	5.9082	4.38	$\lvert 5\,5\,\frac{11}{2}\,\frac{9}{2}\rangle$	–
19	6.0197	5.45	$\lvert 5\,5\,\frac{11}{2}\,\frac{11}{2}\rangle$	–
^{198}Tl				
20	6.2446	0.05	$\lvert 5\,5\,\frac{9}{2}\,\frac{1}{2}\rangle$	–
21	6.3649	0.56	$\lvert 5\,5\,\frac{9}{2}\,\frac{3}{2}\rangle$	–
22	6.4309	1.42	$\lvert 5\,5\,\frac{9}{2}\,\frac{5}{2}\rangle$	–
23	6.4457	0.67	$\lvert 5\,5\,\frac{9}{2}\,\frac{7}{2}\rangle$	–
24	6.5323	3.23	$\lvert 5\,5\,\frac{9}{2}\,\frac{9}{2}\rangle$	–

Table 4.3: *Neutron orbitals for ^{106}In ($h_{11/2}$), ^{138}La ($h_{11/2}$) and ^{198}Tl ($i_{13/2}$) nuclei calculated at* ε_2 = 0.15 *and* γ = 30^0.

^{106}In and ^{138}La				
Single-particle level (neutron orbital number)	**Single-particle energy (MeV)**	**Average projection along the quantization axis $\langle j_z \rangle$ ($\hbar$)**	**Nilsson basis state ($\lvert Nlj\Omega \rangle$) with large occupation probability**	**Parity (π)**
14	5.6870	0.01	$\lvert 5\,5\,\frac{11}{2}\,\frac{1}{2} \rangle$	–
15	5.7920	0.34	$\lvert 5\,5\,\frac{11}{2}\,\frac{3}{2} \rangle$	–
16	5.8586	1.61	$\lvert 5\,5\,\frac{11}{2}\,\frac{5}{2} \rangle$	–
17	5.9250	3.20	$\lvert 5\,5\,\frac{11}{2}\,\frac{7}{2} \rangle$	–
18	6.0167	4.38	$\lvert 5\,5\,\frac{11}{2}\,\frac{9}{2} \rangle$	–
19	6.1283	5.43	$\lvert 5\,5\,\frac{11}{2}\,\frac{11}{2} \rangle$	–
^{198}Tl				
23	6.5288	0.01	$\lvert 6\,6\,\frac{13}{2}\,\frac{1}{2} \rangle$	+
24	6.6372	0.16	$\lvert 6\,6\,\frac{13}{2}\,\frac{3}{2} \rangle$	+
25	6.7106	1.18	$\lvert 6\,6\,\frac{13}{2}\,\frac{5}{2} \rangle$	+
26	6.7687	2.88	$\lvert 6\,6\,\frac{13}{2}\,\frac{7}{2} \rangle$	+
27	6.8459	4.28	$\lvert 6\,6\,\frac{13}{2}\,\frac{9}{2} \rangle$	+
28	6.9433	5.38	$\lvert 6\,6\,\frac{13}{2}\,\frac{11}{2} \rangle$	+
29	7.0650	6.42	$\lvert 6\,6\,\frac{13}{2}\,\frac{13}{2} \rangle$	+

CHAPTER 5 Results and discussion

This chapter discusses features of the partner bands built on configurations suitable for chiral symmetry as predicted by the TQPRM calculations. Such calculations were performed with non-restricted and restricted configurations at various values of the non-axiality parameter γ in the A ~ 100, 130 and 190 mass regions. We shall also discuss the impact on the degeneracy of the partner bands due to a change in the non-axiality parameter γ, in the quadrupole deformation ε_2, in the Coriolis attenuation factor ξ, and in the Fermi surface λ_F of the proton and the neutron. Furthermore, we shall also discuss other fingerprints of chirality such as the staggering in the intra- and inter-band $B(M1)$ reduced transition probabilities, and the energy staggering parameter $S(I)$.

Four cases will be discussed in which the triaxiality of the nuclear shape and the nucleon configuration space differ:

(i) $\gamma = 20^0$ in A ~ 100 and 130; $\gamma = 36^0$ in A ~ 190, and both the odd proton and neutron span a configuration space of five orbitals close to the Fermi surface with dominant contributions from $\pi g_{9/2}$ and $\nu h_{11/2}$ sub-shells in A ~ 100, $\pi h_{11/2}$ and $\nu h_{11/2}$ sub-shell in A ~ 130, and $\pi h_{9/2}$ and $\nu i_{13/2}$ sub-shells in A ~ 190.

(ii) $\gamma = 30^0$ in A ~ 100, 130 and 190, and the odd proton and neutron span the same configuration space as in case (i) in all three mass regions

(iii) $\gamma = 20^0$ in A ~ 100 and 130; $\gamma = 30^0$ in A ~ 190, and the odd proton and neutron are restricted to one orbital each (i.e. the highest- and lowest-energy orbitals with predominant $\pi g_{9/2}$ and $\nu h_{11/2}$ nature respectively in A ~ 100, lowest- and highest-energy orbitals with predominant $\pi h_{11/2}$ and $\nu h_{11/2}$ nature respectively in A ~ 130, and the lowest- and highest-energy orbitals with predominant $\pi h_{9/2}$ and $\nu i_{13/2}$ nature respectively in A ~ 190).

(iv) $\gamma = 30^0$ in A ~ 100 and 130; $\gamma = 36^0$ in A ~ 190, and the odd proton and neutron are restricted to one orbital each as in case (iii) in all three mass regions

In all these cases the proton and neutron Fermi levels are fixed at the lowest-energy and highest-energy orbitals of the corresponding high-j shell. Note that we shall call “non-restricted”, a configuration as described in cases (i) and (ii), and “restricted”, a configuration as described in cases (iii) and (iv). The results of these calculations for all four cases are

shown in Figures 5.1-5.9 and Tables A.1-29, A.45-72. The calculations of the distributions of the projections of the angular momenta of the odd proton and neutron were performed for both the non-restricted and restricted configurations. The results for all four cases are shown in Figures 5.10-5.15 and Tables A.30-44.

The calculations were also performed for both non-restricted and restricted configurations at various values of non-axiality parameter γ (i.e. $\gamma = 17^0, 20^0, 24^0, 27^0, 30^0, 33^0, 36^0, 40^0$) and $\varepsilon_2 = 0.15$ to see for what optimal value(s) of γ the partner bands are closest to degeneracy. The results of such calculations are shown in Figure 5.16 and Tables A.1-3.

We have also investigated whether a change in the value of the quadrupole deformation and the Coriolis attenuation factor have a significant impact on the degeneracy between the partner bands. Thus the calculations were performed for both non-restricted and restricted configurations by changing the value of the quadrupole deformation ε_2 from 0.15 to 0.25. In another set of calculations, the Coriolis attenuation factor ξ was changed from 1 to 0.8. Since changing the quadrupole deformation parameter has an impact on the position of the Fermi surface λ_F of the nucleons at $\varepsilon_2 = 0.25$, the calculations were performed for the $\pi h_{11/2} \otimes \nu h_{11/2}^{-1}$ configuration corresponding to $Z = 57$, $N = 87$ in A ~ 130 mass regions (see Figures 2.5 and 4.1). It should be noted that for larger deformation the protons $\pi h_{11/2}$ and the neutrons $\nu h_{11/2}$ configurations have larger mixing with orbitals from other sub-shells (see Figures 2.5 and 4.1). Results from these calculations are shown in Figures 5.33-5.40 and Tables A.73-80.

Chirality was also investigated for restricted configurations when either the Fermi surface of the proton or the neutron changes (i.e. when either the odd particle or the odd hole occupies the second lowest- or second highest-energy orbital in a high-j shell for the $\pi h_{11/2} \otimes \nu h_{11/2}^{-1}$ configuration). These calculations were also performed when both Fermi surfaces of the proton and the neutron change (i.e. when both the odd particle and the odd hole occupy the second lowest- and the second highest-energy orbitals in the high-j shell respectively). The results from these calculations are shown in Figures 5.41-5.50 and Tables A.81-96.

5.1 Calculations for cases (i), (ii), (iii) and (iv) in A ~ 100, 130 and 190 mass regions

To investigate whether the system has chiral geometry, the values of the angular momentum components for the valence proton $j_{pk} = \sqrt{\langle j_{pk}^2 \rangle}$, the valence neutron $j_{nk} = \sqrt{\langle j_{nk}^2 \rangle}$, and the core $j_{Rk} = \sqrt{\langle j_{Rk}^2 \rangle}$, (where $k = x, y, z$) for the partner bands in all mass regions were calculated and are shown in Figures 5.1-5.3 and Tables A.10-21, in which $k = x, y, z$ represent the short, intermediate and long nuclear axes respectively. In all four cases the calculated total angular momentum is aplanar, having large projections on all three nuclear axes (see Figures 5.1-5.3). In these aplanar systems we have major contributions from the proton angular momentum along the z-axis (long axis), and from the neutron angular momentum along the x-axis (short axis) in A ~ 100 mass region (see Figure 5.1). While for A ~ 130, 190 mass regions we have major contributions from the proton angular momentum along the x-axis (short axis), and from the neutron angular momentum along the z-axis (long axis) (see Figures 5.2 and 5.3). In all three mass regions the angular momentum of the core is predominant along the y-axis (intermediate axis) (see Figures 5.1-5.3). Thus the requirement for the formation of chiral system is fulfilled for all four cases in the three mass regions.

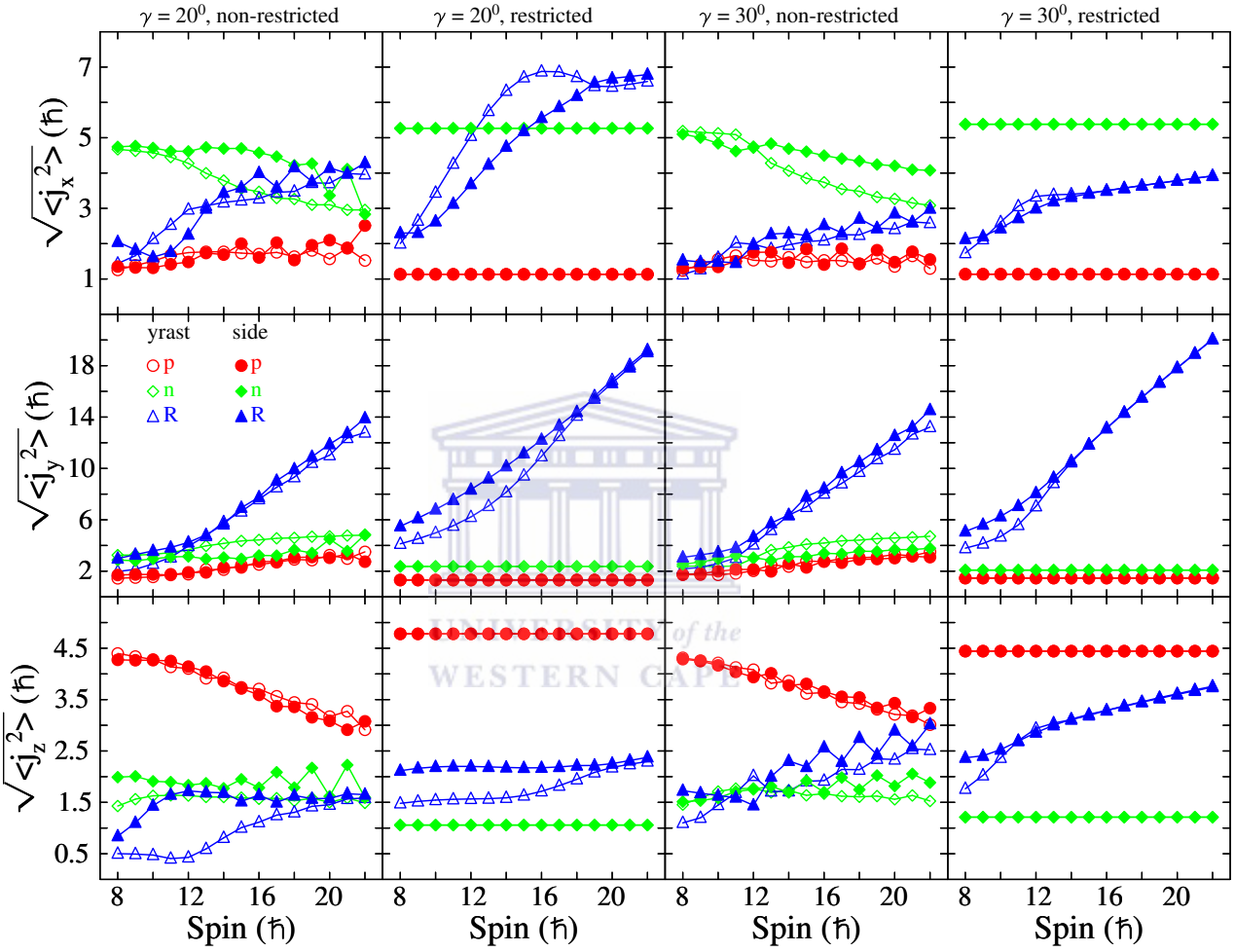

Figure 5.1: *Calculated projections of the angular momenta of the proton, neutron and the rotational core for the partner bands in A ~ 100 mass region at* $\varepsilon_2 = 0.15$ *and* $\gamma = 20^0, 30^0$. *Open and filled symbols denote the yrast and side bands respectively.*

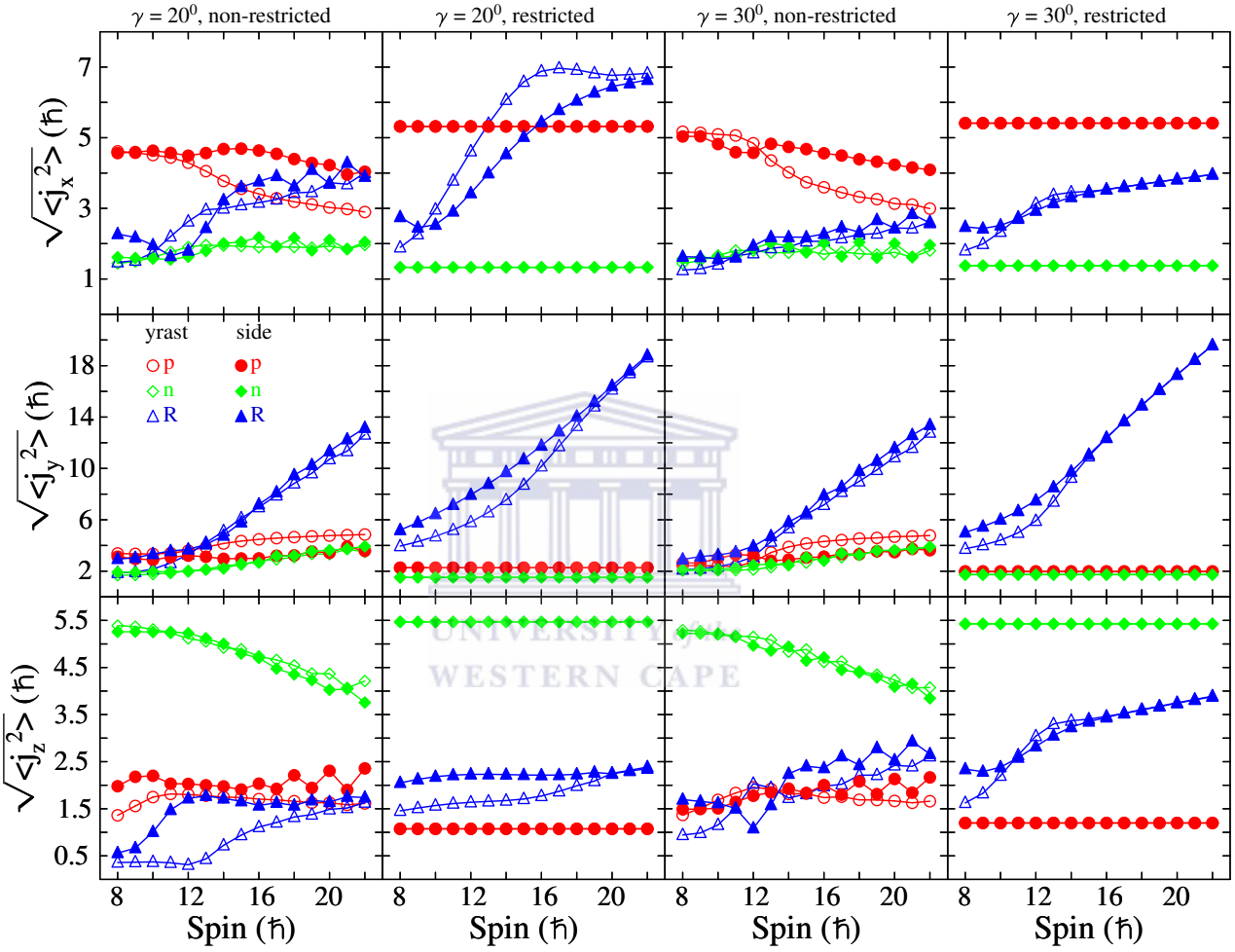

Figure 5.2: *Calculated projections of the angular momenta of the proton, neutron and the rotational core for the partner bands in A ~ 130 mass region at* $\varepsilon_2 = 0.15$ *and* $\gamma = 20^0, 30^0$. *Open and filled symbols denote the yrast and side bands respectively.*

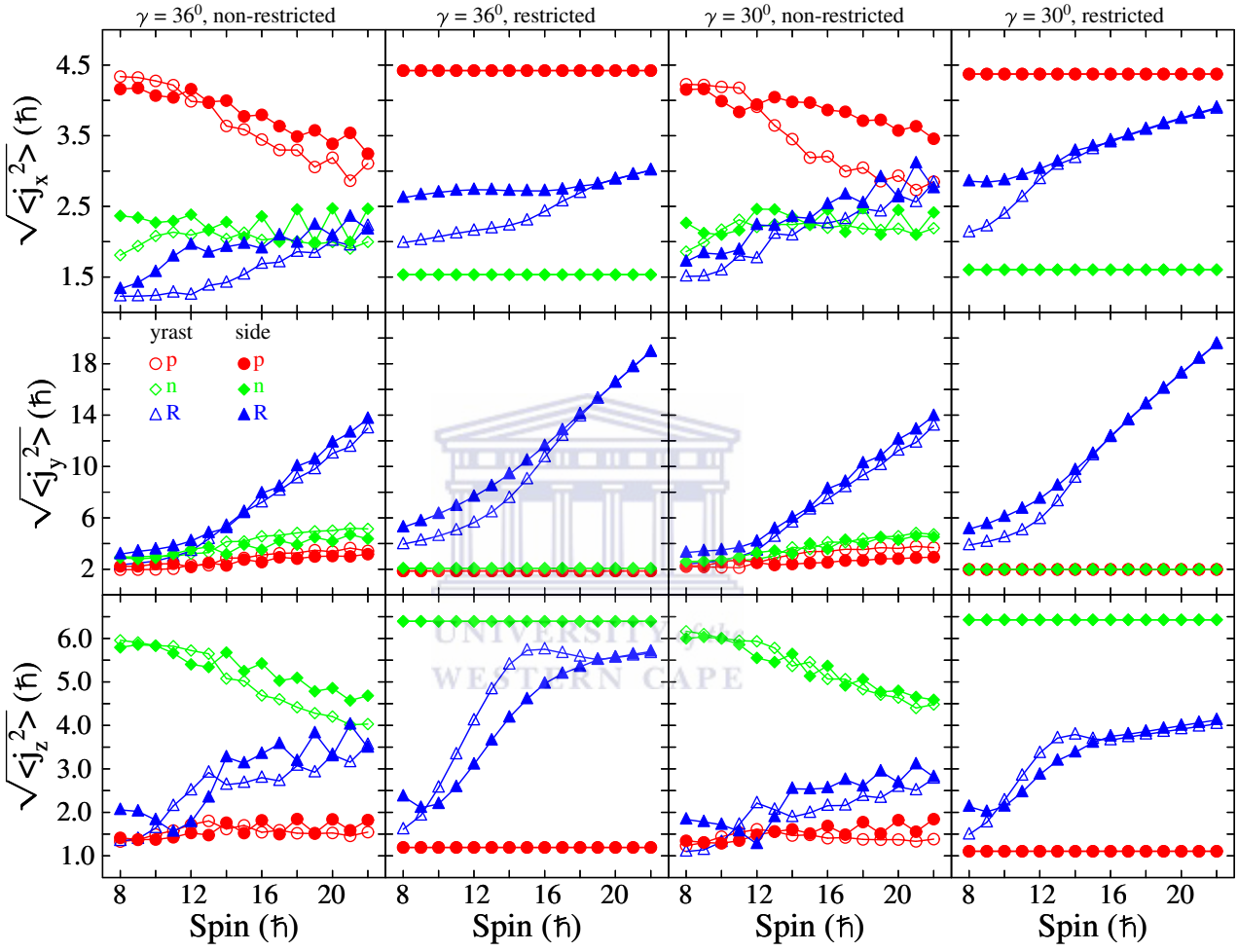

Figure 5.3: *Calculated projections of the angular momenta of the proton, neutron and the rotational core for the partner bands in A ~ 190 mass region at* $\varepsilon_2 = 0.15$ *and* $\gamma = 30^0, 36^0$. *Open and filled symbols denote the yrast and side bands respectively.*

In order to examine how close to degenerate the partner bands are, we have compared the differences in the features of the partner bands, i.e. the difference in the excitation energies ($\Delta E = E_{side} - E_{yrast}$), the differences in the average projections of the particle, hole and core angular momenta (e.g. $\Delta j_{p,s} = \sqrt{\langle j_{p,s}^2 \rangle_{side}} - \sqrt{\langle j_{p,s}^2 \rangle_{yrast}}$ for the projection of the proton angular momentum along the short axis), the differences in the average projections of the total angular momentum along the three nuclear axes (e.g. $\Delta I_s = \sqrt{\langle I_s \rangle_{side}^2} - \sqrt{\langle I_s \rangle_{yrast}^2}$, for the projection of the total angular momentum along the short axis), the differences between the reduced $B(M1)$ and $B(E2)$ transition probabilities (e.g. $\Delta B(M1)_{in} = B(M1)_{yrast} - B(M1)_{side}$ and $\Delta B(M1)_{out} = B(M1)_{side \to yrast} - B(M1)_{yrast \to side}$ for the intra- and inter-band reduced $B(M1)$ transition probabilities respectively). The properties of the partner bands are shown in Figures 5.4-5.8 and Tables A.1-3, A.22-26, A.69-72. The calculations for non-restricted configurations i.e. cases (i) and (ii), show clear divergence from degeneracy in all features of the partner bands in all mass regions. Such discrepancies in the properties of the partner bands were calculated previously for other chiral candidates before [Ton06, Ton07, Har01, Sta01b, Bar01, Sta02, Koi03a, Pen03, Jos05b, Gro06, Zha07, Wan07, Wan08, Law08, Law10b, Qi09a-b]. The calculations for restricted configuration and $\gamma = 30^0$ or 36^0 i.e. case (iv), show almost perfect degeneracy, which occurs simultaneous in all properties of the partner bands at high spin in all mass regions. Large discrepancy in the properties of partner bands is found for the other cases. Note that better near-degeneracy in 190 mass region occurs for $\gamma = 36^0$ rather than $\gamma = 30^0$.

5.1.1 Degeneracy in the features of the partner bands for case (iv)

5.1.1.1 Degeneracy in the excitation energies

The smallest values of ΔE are predicted to occur at $I \geq 15\,\hbar$, $I \geq 16\,\hbar$ and $I \geq 19\,\hbar$ in the 100, 130 and 190 mass regions respectively (see Figure 5.4 and Tables A.1-3). At high spins the values of ΔE for the partner bands in the 100 and 130 mass regions lie between 1 keV and 5 keV, whereas in 190 mass region the values of ΔE for the partner bands lie between 9 keV and 14 keV.

5.1.1.2 Degeneracy in the angular momenta

Since the two valence odd nucleons (i.e. the odd proton and the odd neutron) were restricted to only one orbital each, perfect degeneracy was predicted in the angular momenta of the odd

proton and the odd neutron between the partner bands in all mass regions in the whole calculated spin range. Comparison for the difference in the angular momenta of the rotational core (Δj_R) along the intermediate axis and the difference in the total angular momentum of the system I along three nuclear axes (i.e. $\Delta I_l, \Delta I_i, \Delta I_s$) between the partner bands is shown in Figures 5.5-5.6 and Tables A.22-26. The values of Δj_R and ΔI are almost zero (less than $0.04\,\hbar$) in the spin region where near degeneracy occurs for the excitation energies of the partner bands in all three mass regions (see Figures 5.5-5.6 and Tables A.22-26).

5.1.1.3 Degeneracy in the reduced electromagnetic (EM) transition probabilities

Figures 5.7-5.8 and Tables A.69-72 show the calculated relative intra- and inter-band $B(M1)$ and $B(E2)$ reduced transition probabilities of the partner bands in all three mass regions. Degenerate values of the intra-band $B(M1)$ transitions (corresponding to $\Delta B(M1)_{in} \leq 0.0036\,\mu_N^2$) for the partner bands were found at $I > 15\,\hbar$, $I > 16\,\hbar$ and $I \geq 19\,\hbar$ in 100, 130 and 190 mass regions respectively (the same spin region for which the bands show near degeneracy in the excitation energies). For the inter-band $B(M1)$ transitions degenerate values between the partner bands (i.e. $\Delta B(M1)_{out} \leq 0.0044\,\mu_N^2$), were found at $I \geq 11\,\hbar$, $I \geq 12\,\hbar$ and $I \geq 19\,\hbar$ in 100, 130 and 190 mass regions respectively. Degenerate values for the intra-band $B(E2)$ transitions (i.e. $\Delta B(E2)_{in} \leq 0.0020\,e^2b^2$) for the partner bands were found for $I \geq 10\,\hbar$ in both 100, 130 mass regions and at $I \geq 21\,\hbar$ in 190 mass region. Degenerate values for the inter-band $B(E2)$ transitions (i.e. $\Delta B(E2)_{out} \leq 0.0041\,e^2b^2$) for the partner bands were found at $I = 12\,\hbar, I \geq 15\,\hbar$ in A ~ 100, $I \geq 18\,\hbar$ in A ~ 130, and at $I \geq 13\,\hbar$ except at $I = 15\,\hbar, 19\,\hbar$ in A ~ 190.

5.1.2 Degeneracy for cases (i), (ii) and (iii)

For cases (i), (ii) and (iii) the features of the partner bands are not degenerate. For case (i), the smallest values of ΔE are around 550 keV at $I = 12\,\hbar$ in A ~ 100, 130; and 126 keV at $I = 13\,\hbar$ in A ~ 190 (see Tables A.1-3). For case (ii), the smallest values of ΔE are around 55 keV at $I = 12\,\hbar$ in A ~ 100, 101 keV at $I = 12\,\hbar$ in A ~ 130, and 98 keV at $I = 12\,\hbar$ in A ~ 190 (see Tables A.1-3). For case (iii), the smallest absolute values of ΔE are between 23-59 keV at $I \geq 17\,\hbar$ in A ~ 100, 10-75 keV at $I \geq 17\,\hbar$ in A ~ 130, and 20-59 keV at $I \geq 14\,\hbar$ in A ~ 190 (see Tables A.1-3). At high spins, the average values of Δj_R along the intermediate

axis is greater than $0.3\,\hbar$ for both cases (i) and (ii) in all three mass regions, while for case (iii) they are above $0.2\,\hbar$ in A ~ 100, 130 mass regions and greater than $0.04\,\hbar$ for A ~ 190 (see Table A.23). Similarly one can see that the values of ΔI_s, ΔI_i and ΔI_l are large for cases (i), (ii) and (iii) as compared to the ones for case (iv) (see Tables A.24-26). The same applies for the values of $\Delta B(M1)_{in}$, $\Delta B(M1)_{out}$ and $\Delta B(E2)_{in}$. The values for $\Delta B(E2)_{out}$ are comparable and close to zero in all four cases (i.e. cases (i), (ii), (iii) and (iv)), (see Tables A. 69-72).

5.1.3 Conclusions

Thus, the previously suggested necessary condition for forming a chiral system, i.e. an aplanar orientation of the total angular momentum is not sufficient to ensure degeneracy in the chiral partner bands, even for the most favorable nucleon configuration with Fermi levels placed at the lowest- and highest-energy orbitals of the high-j shell and $\gamma = 30^0$. We have shown that in addition one has to restrict the nucleon configuration, i.e. the mixing with neighbouring single-particle orbitals should be forbidden. Such restriction is rather unrealistic showing that most likely perfect degeneracy (and therefore strongly broken chiral symmetry) is unlikely to be observed in real nuclei. Further investigations of the properties of the restricted and non-restricted chiral configurations are carried out in the following sections.

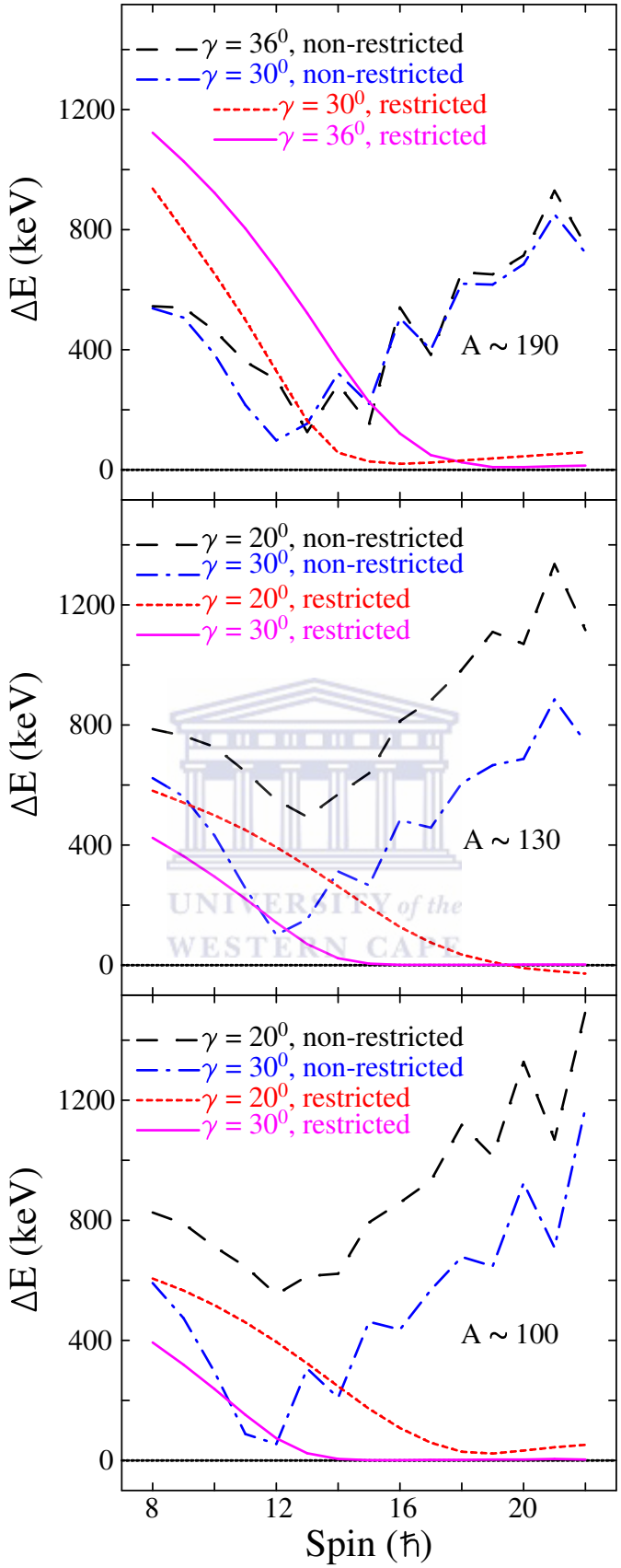

Figure 5.4: *Calculated relative excitation energy (ΔE), in A ~ 100, 130 and 190 mass regions for the four sets of parameters as described in the text. The dashed, dashed-dotted, dotted and solid lines correspond to cases (i), (ii), (iii) and (iv) respectively.*

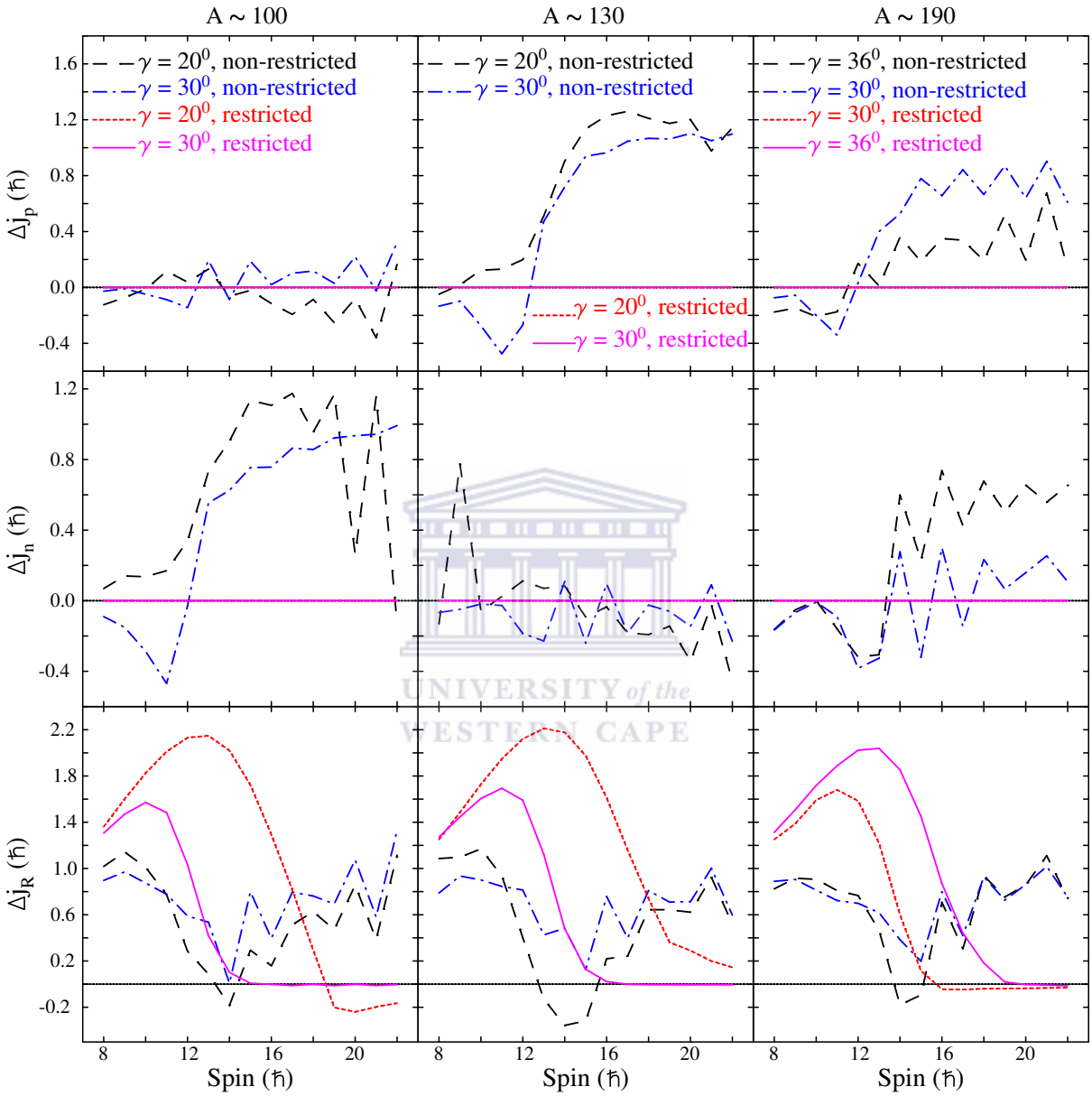

Figure 5.5: *Calculated relative angular momenta of the proton (along the short axis in A ~ 130, 190 and along the long axis in A ~ 100), neutron (along the long axis in A ~ 130, 190 and along the short axis in A ~ 100) and the core (along the intermediate axis in A ~ 100, 130 and 190). Notation is the same in Figure 5.4.*

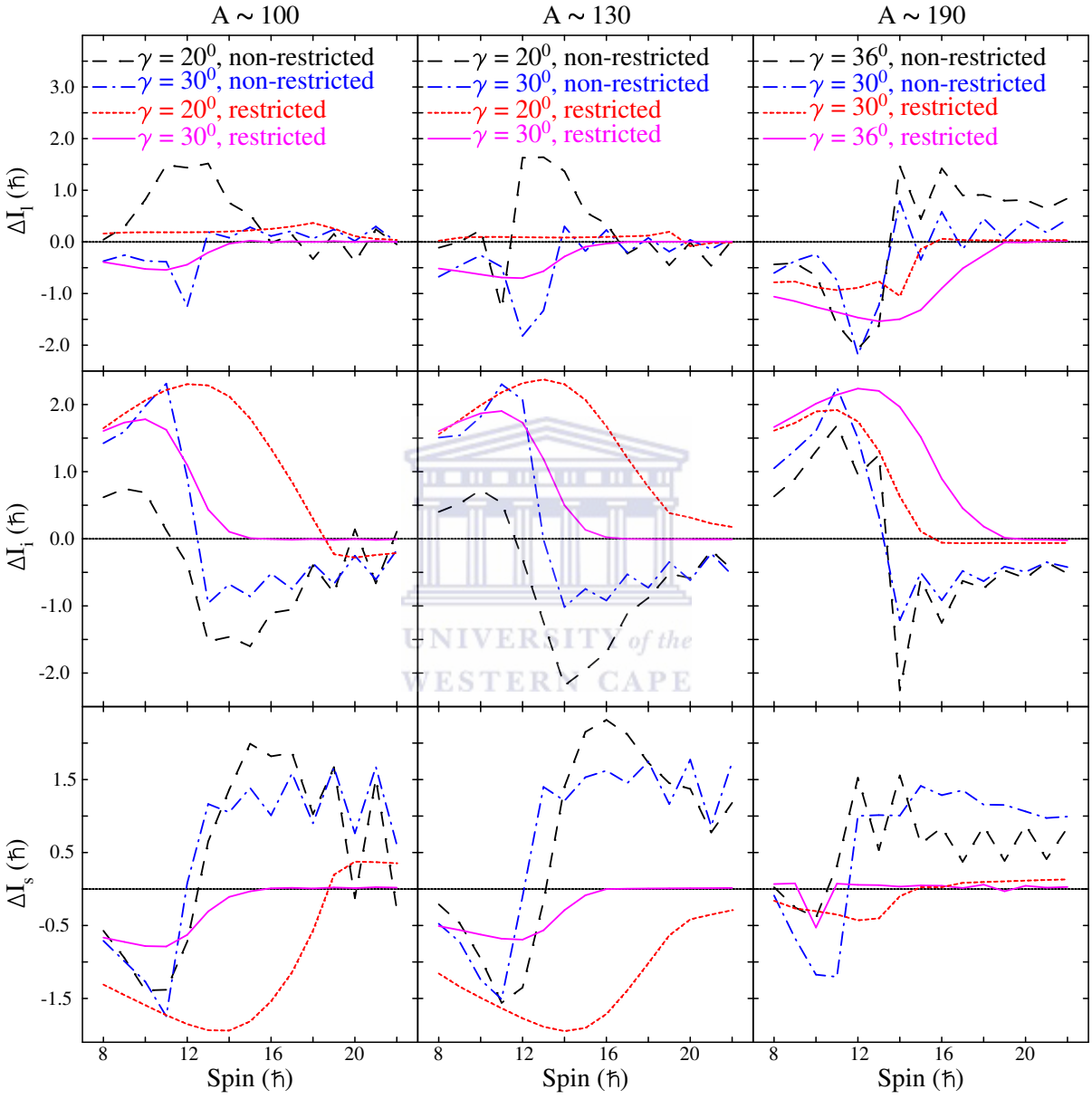

Figure 5.6: *Calculated relative projections of the total angular momentum I along the short, long and intermediate axes in A ~ 100, 130 and 190 mass regions. Notation is the same in Figure 5.4.*

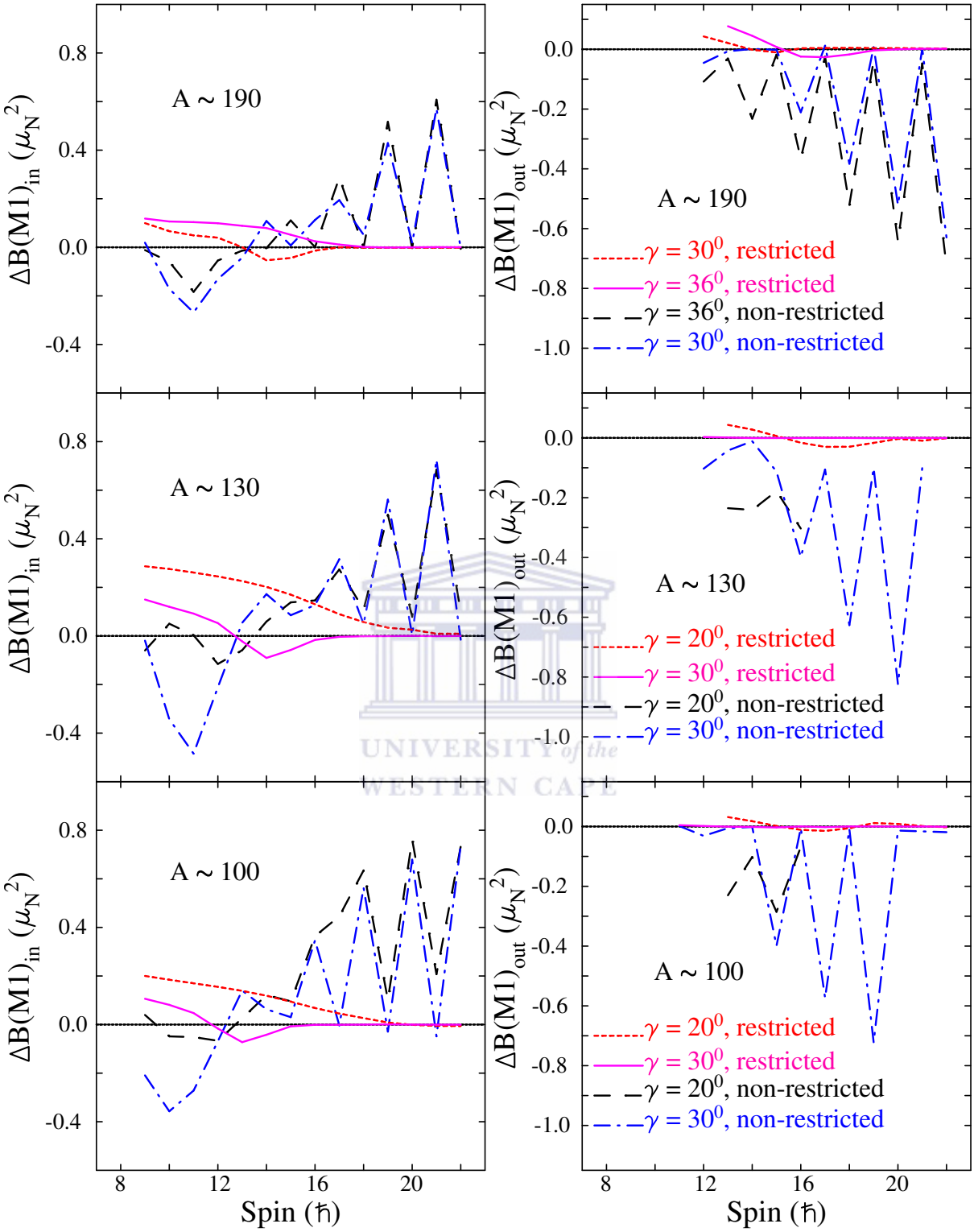

Figure 5.7: *Calculated relative* $B(M1)_{in}$ *and* $B(M1)_{out}$ *reduced transition probabilities in A ~ 100, 130 and 190 mass regions. Notation is the same in Figure 5.4.*

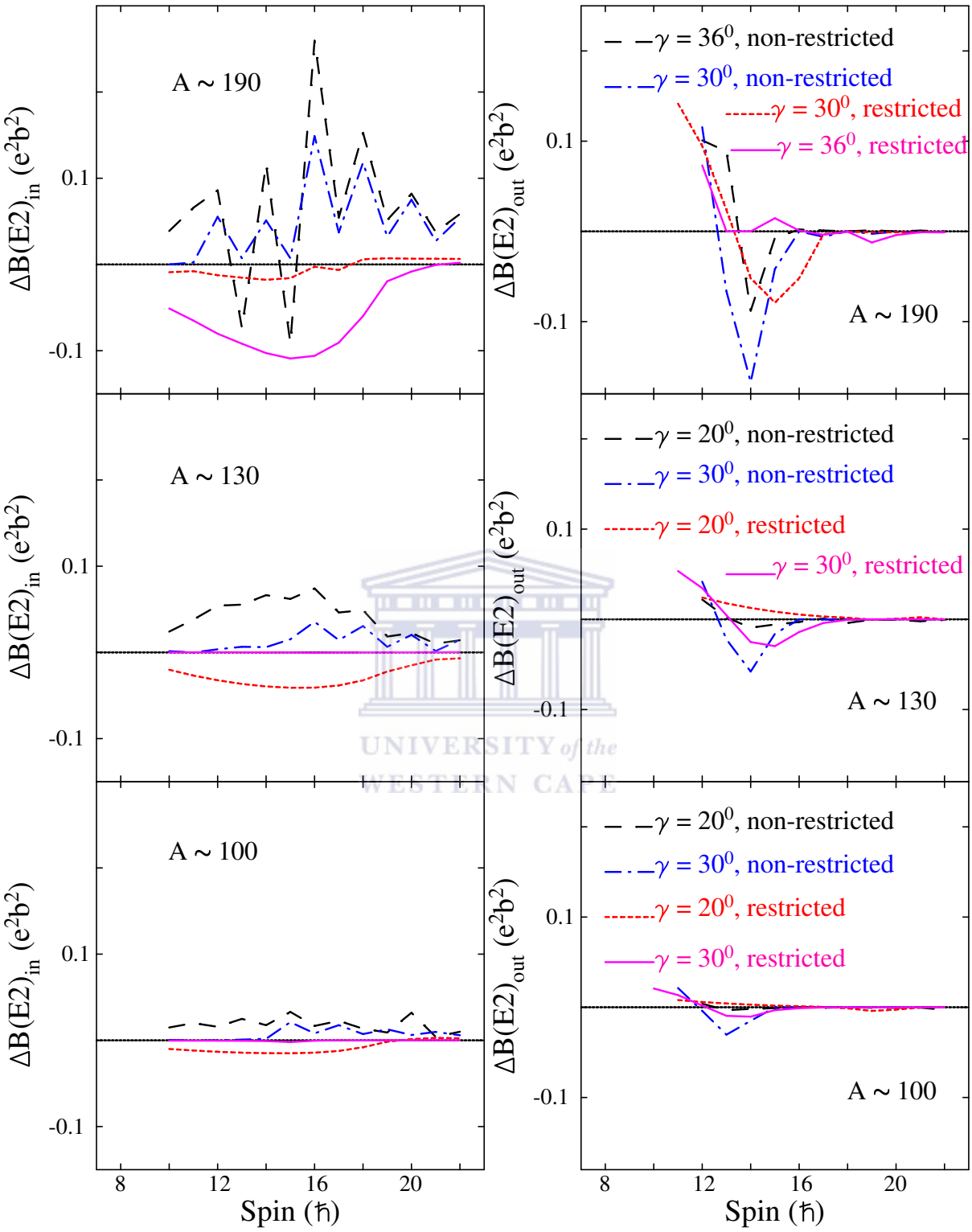

Figure 5.8: *Calculated relative* $B(E2)_{in}$ *and* $B(E2)_{out}$ *reduced transition probabilities in A ~ 100, 130 and 190 mass regions. Notation is the same in Figure 5.4.*

5.1.4 Possible causes for the loss of degeneracy within the partner bands

It had been suggested before that chiral partner bands may show divergence from degeneracy at the lowest and highest ends of the spin range of interest. At low spins the rotational angular momentum could be oriented in the plane of the short-long axes, due to Coriolis effects [Fra97, Fra01]. Alternatively the rotational angular momentum could oscillate between the left- and right-handed systems due to chiral vibrations [Sta01a]. At very high spins Coriolis effects may change the orientation of the particle angular momenta, and align them along the intermediate axis. In order to check the spin ranges where these effects might occur we have examined the relative orientation of the angular momenta of the odd nucleons and the core by investigating the average angles between these three angular momenta.

The average angles between the angular momenta of the proton, the neutron and the core, defined in the usual manner are shown in Figure 5.9 and Tables A.27-29. For example the angle between the angular momenta of the proton and the neutron were calculated as follows

$$\alpha(p,n) = \cos^{-1}\left(\frac{\langle j_p \cdot j_n \rangle}{|j_p||j_n|}\right) \tag{5.1}$$

where j_p and j_n are the angular momenta of the proton and the neutron respectively. Similarly, one can define the effective angle $\alpha(R,p)$ (i.e. orientation between the angular momenta of the core and the odd proton) and $\alpha(R,n)$ (i.e. orientation between the angular momenta of the core and the odd neutron). For cases (i) and (ii) these angles are close to 90^0 at low spins, showing no signs of an orientation of the rotational angular momentum in the plane of the short-long axes. These angles start to decrease as the spin increases indicating that the angular momenta start to deviate from their initial alignments along the nuclear axes already at low spins. It should be noted that these angles remain considerably larger than zero at high spins ($\alpha > 30^0$), confirming that the total angular momentum remains aplanar through the whole calculated spin range. Therefore the chiral symmetry should persist through the whole band. However, the large discrepancies in the properties of the partner bands for cases (i) and (ii) (shown in Figures 5.4-5.8 and Tables A.1-3, A.22-26, A.69-72) indicate that although the geometry is on average chiral, degeneracy in the partner bands is not reached.

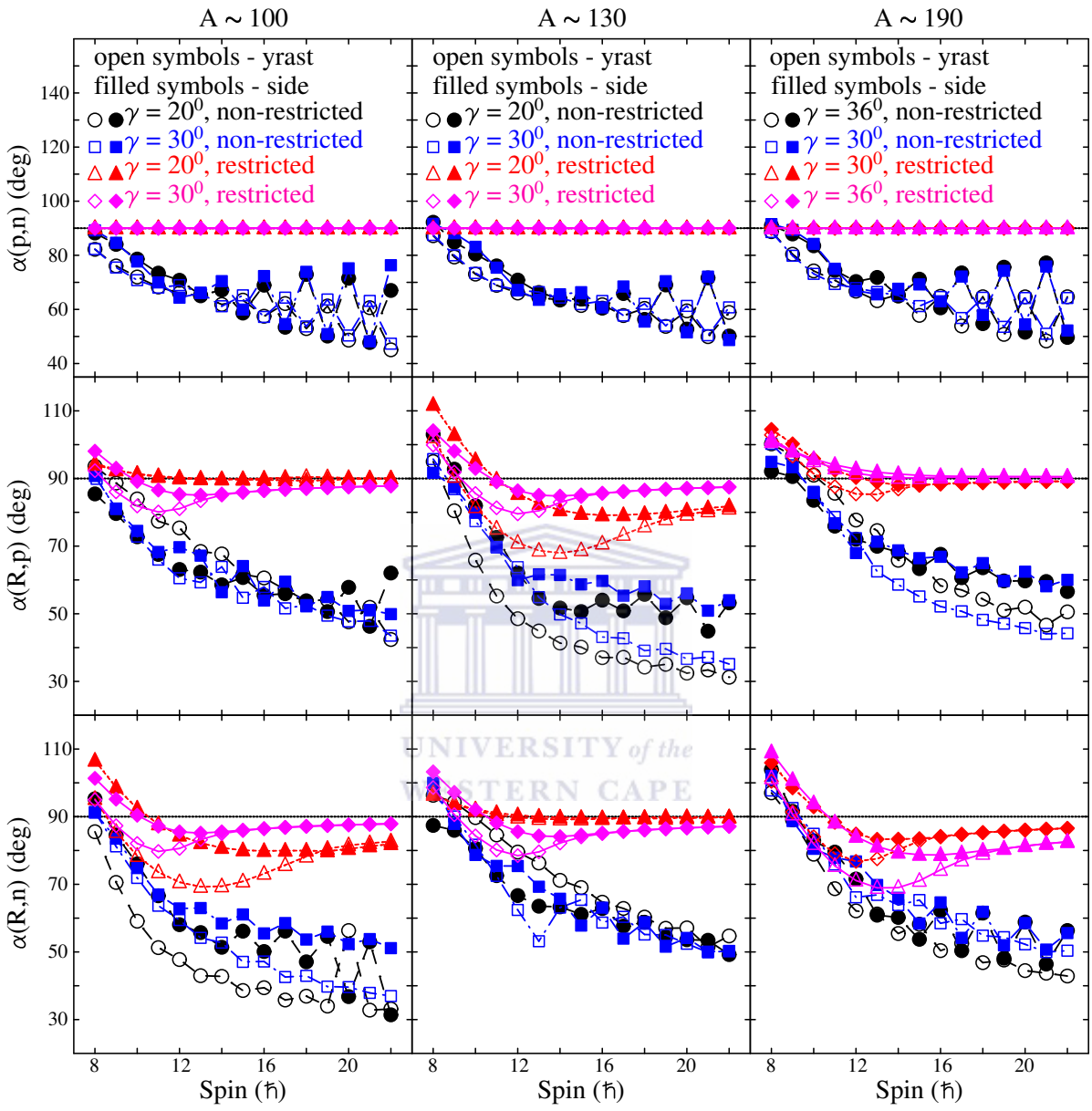

Figure 5.9: *Calculated average angles (in degrees) between the angular momenta of the proton (j_p), neutron (j_n) and the collective rotation (j_R), for the yrast (open symbols) and side (filled symbols) bands in A ~ 100, 130 and 190 mass regions. The circles, squares, triangles and diamonds correspond to cases (i), (ii), (iii) and (iv) respectively.*

Let us now examine the calculations for cases (iii) and (iv), where the configuration space is restricted to only one orbital for the proton and one for the neutron. Such restriction leads to fixing all projections of the angular momentum of the proton and the neutron to the same values for both partner bands, which correspond to nearly maximum alignment along the short and long nuclear axes or vice versa in all three mass regions. It also excludes any de-alignments of these angular momenta at higher spins, where in normal conditions the proton and the neutron angular momenta gradually move away from the short and long axes under the influence of the Coriolis effects. As a result in the whole calculated spin region the average angles between the angular momenta of the proton and neutron ($\alpha(p,n)$) are equal to 90^0 for both cases (iii) and (iv) in all three mass regions. At high spins the expected values of the angles between the angular momenta of the proton and the collective rotation (i.e. $\alpha(R,p)$), and the neutron and the collective rotation (i.e. $\alpha(R,n)$) become equal and are almost equal to 90^0 for case (iv) in all three mass regions. For case (iii), the average angles $\alpha(R,n)$ in A ~ 130, 190 and $\alpha(R,p)$ in A ~ 100 become equal and are smaller as compared to the ones calculated for case (iv) at higher spins in all three mass regions. This suggests that in order to obtain degeneracy in the chiral bands the three individual angular momenta should be mutually orthogonal to each other.

One can examine how strong the alignment of the particle angular momenta is in the four calculated cases. The two-quasiparticle-plus-triaxial rotor model codes were further developed to calculate the distributions of the angular momenta [Rag08]. Figures 5.10-5.15 and Tables A.30-44 show the distributions of the projections of the proton and neutron angular momentum for $I = 8\,\hbar, 16\,\hbar$ and $20\,\hbar$. It is remarkable how strong the alignment of the proton and the neutron angular momenta are in the case of restricted nucleon configuration, with $>93\%$ of the wave function corresponding to the maximum possible alignment of the proton and neutron angular momenta. This result is consistent with previous calculations [Lar78], where it had been shown that the projection of the angular momentum of $h_{11/2}$ particle remains almost pure and very close to its maximum value of $11/2\,\hbar$ when the triaxiality parameter γ changes between 0^0 and 30^0. One can note that such good alignment cannot be achieved for the calculations with a larger configuration space (cases (i) and (ii)) even at low spins, due to mixtures with orbitals with lower angular momentum projections. At higher spins the Coriolis effects cause even larger mixing with such orbitals. It should be noted, that even at the highest spins the proton and the neutron angular momenta

remain approximately aligned along the short and long nuclear axes, thus conserving the chiral configuration on average (for instance, see Figures 5.1-5.3). The components with lower projections of the angular momenta however cause the loss of the degeneracy in the partner bands.

At low spins there is no degeneracy in the partner bands for all four calculated cases. That can be associated with a relatively large probability for a vanishing projection of the rotational angular momentum along the intermediate axis. It had been previously suggested that a vanishing projection of the rotational angular momentum implies chiral vibrations of this angular momentum between the left- and right-handed systems [Qi09b]. An alternative interpretations, e.g. wave functions involving components with opposite orientations of the rotational angular momentum, and/or components with vanishing magnitudes of the rotational angular momentum, is also possible.

These results show that, in principle, degeneracy in chiral bands might be possible if there is a spin range, where the components with vanishing projection of the rotational angular momentum along the intermediate axis become negligible, but the particle angular momenta still have full alignment along the short and long axes. Such spin range could not be found in all mass regions as shown by the calculations for cases (i) and (ii). Thus, it seems that degeneracy in two-quasiparticle chiral partner bands is unlikely to be reached in real cases, where the nucleon configuration is unrestricted.

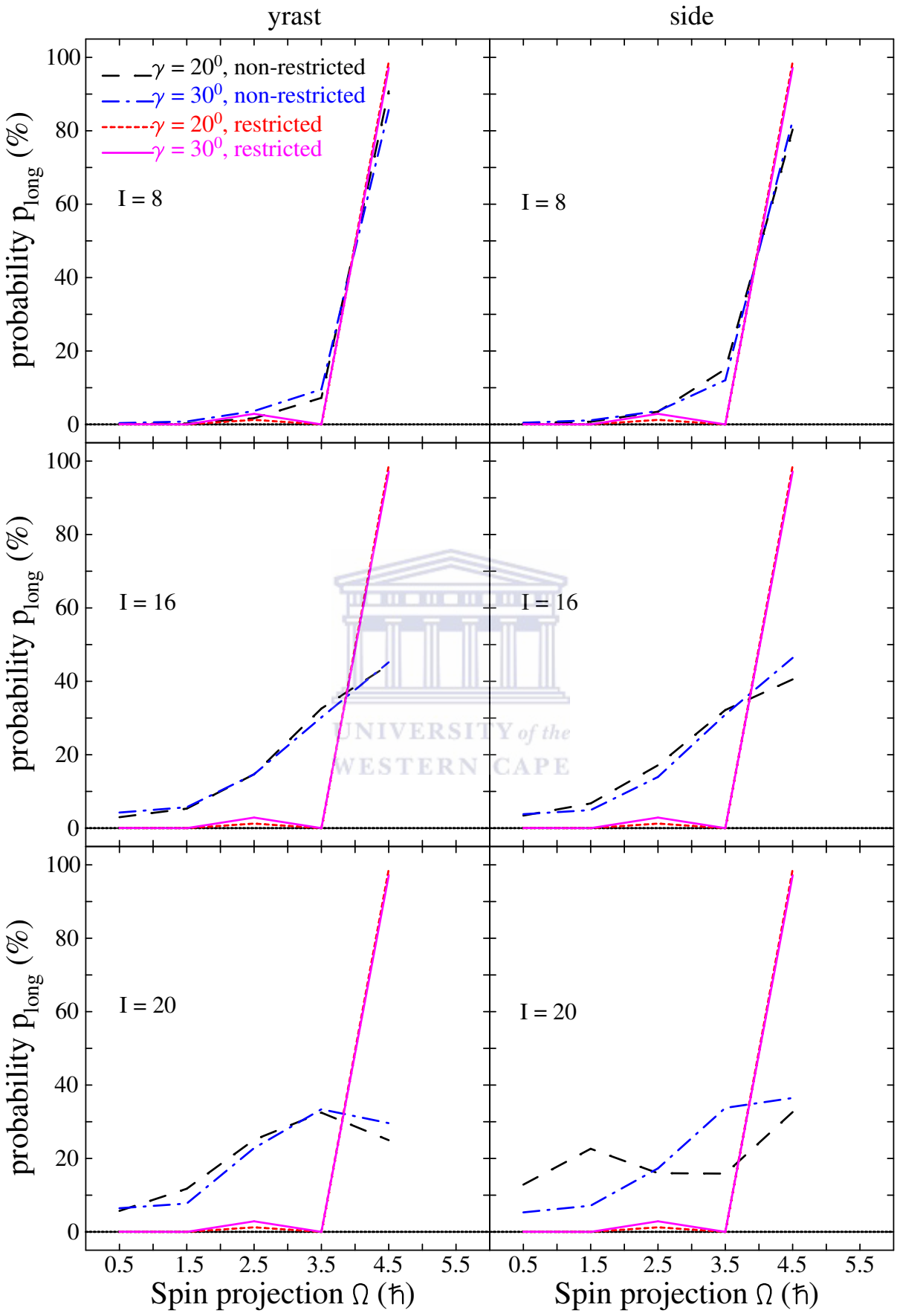

Figure 5.10: *Distributions of the projection of the angular momentum of the proton calculated for the yrast and side bands in A ~ 100 mass region. Notation is the same in Figure 5.4.*

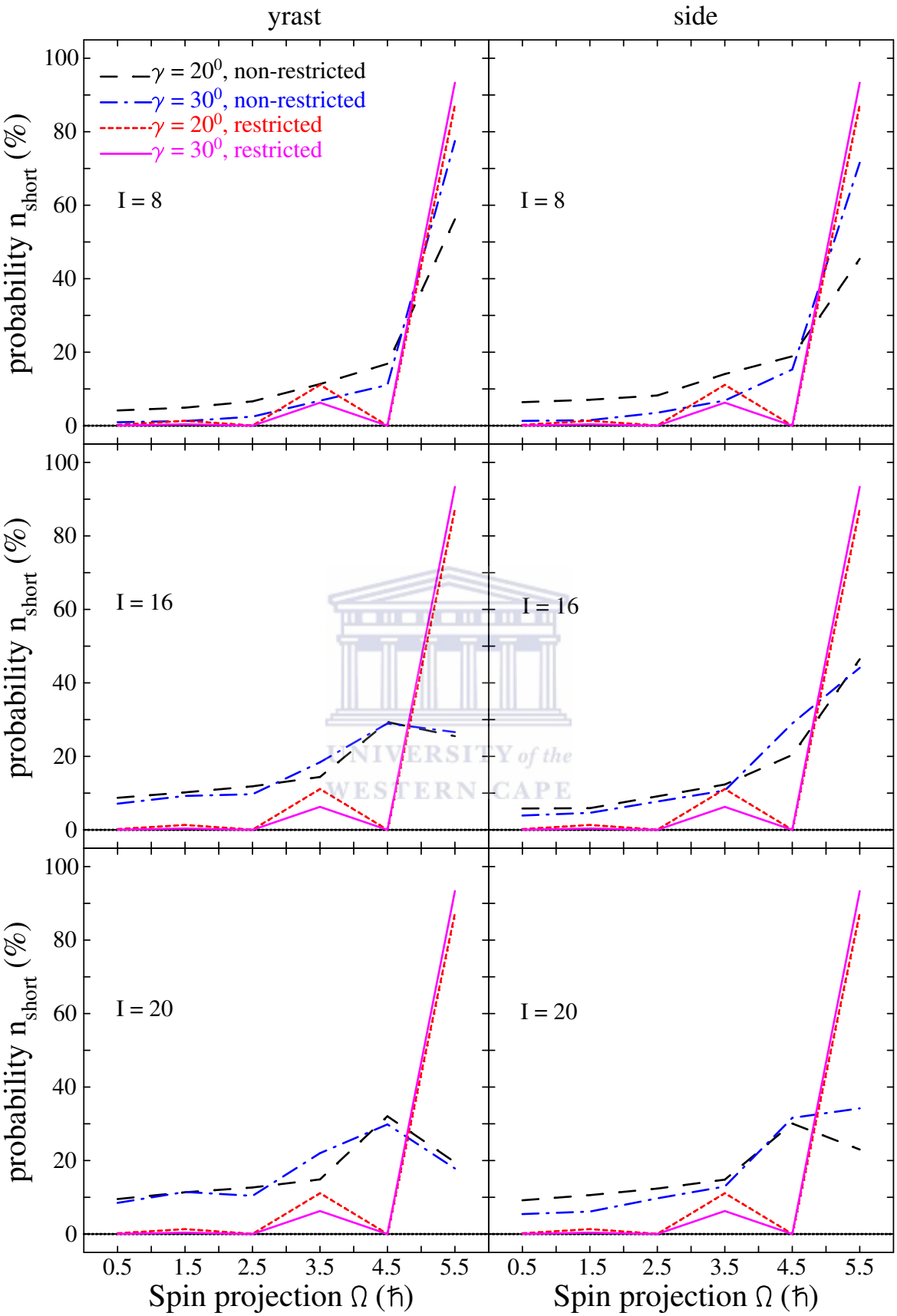

Figure 5.11: *Distributions of the projection of the angular momentum of the neutron calculated for the yrast and side bands in A ~ 100 mass region. Notation is the same in Figure 5.4.*

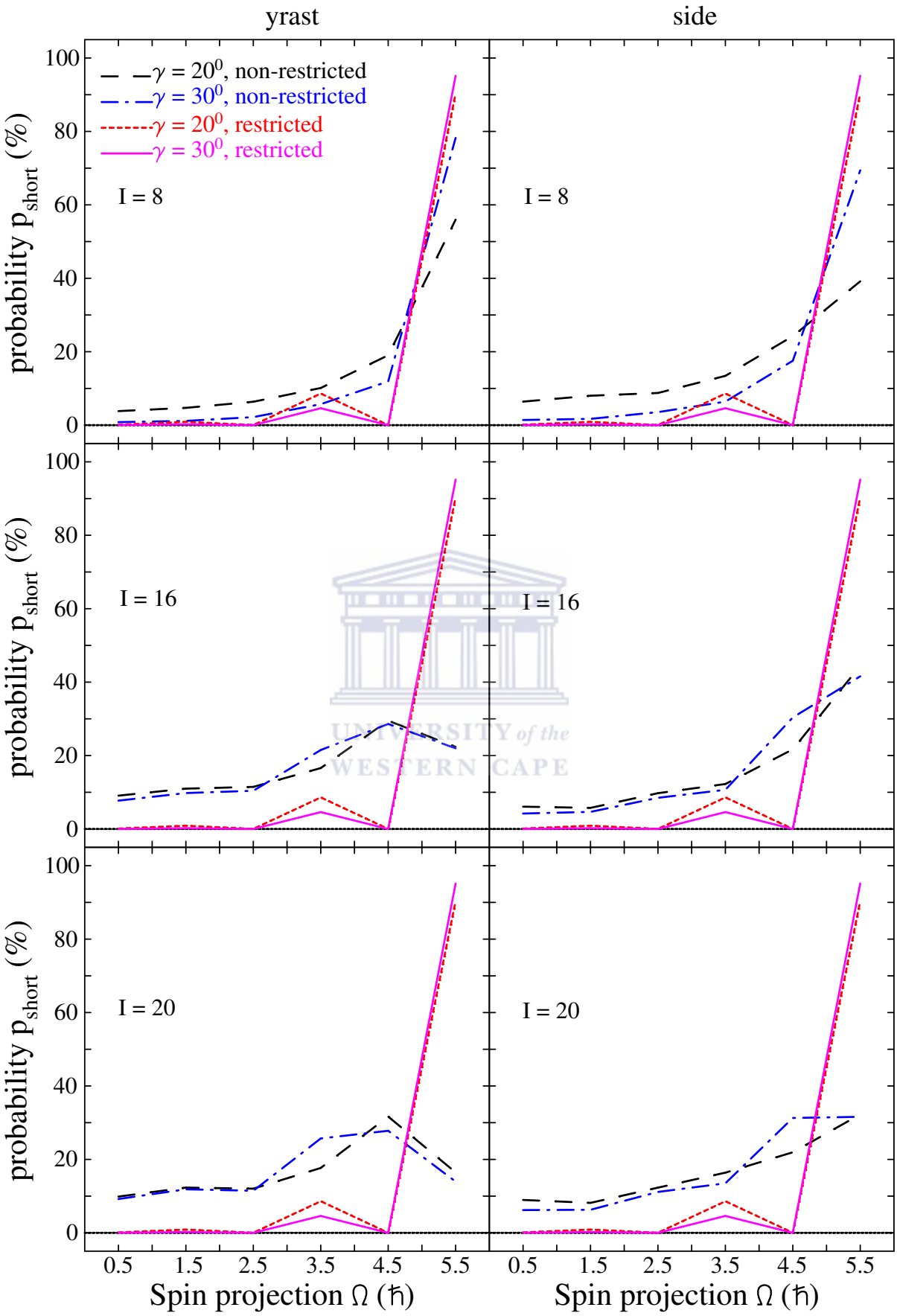

Figure 5.12: *Distributions of the projection of the angular momentum of the proton calculated for the yrast and side bands in A ~ 130 mass region. Notation is the same in Figure 5.4.*

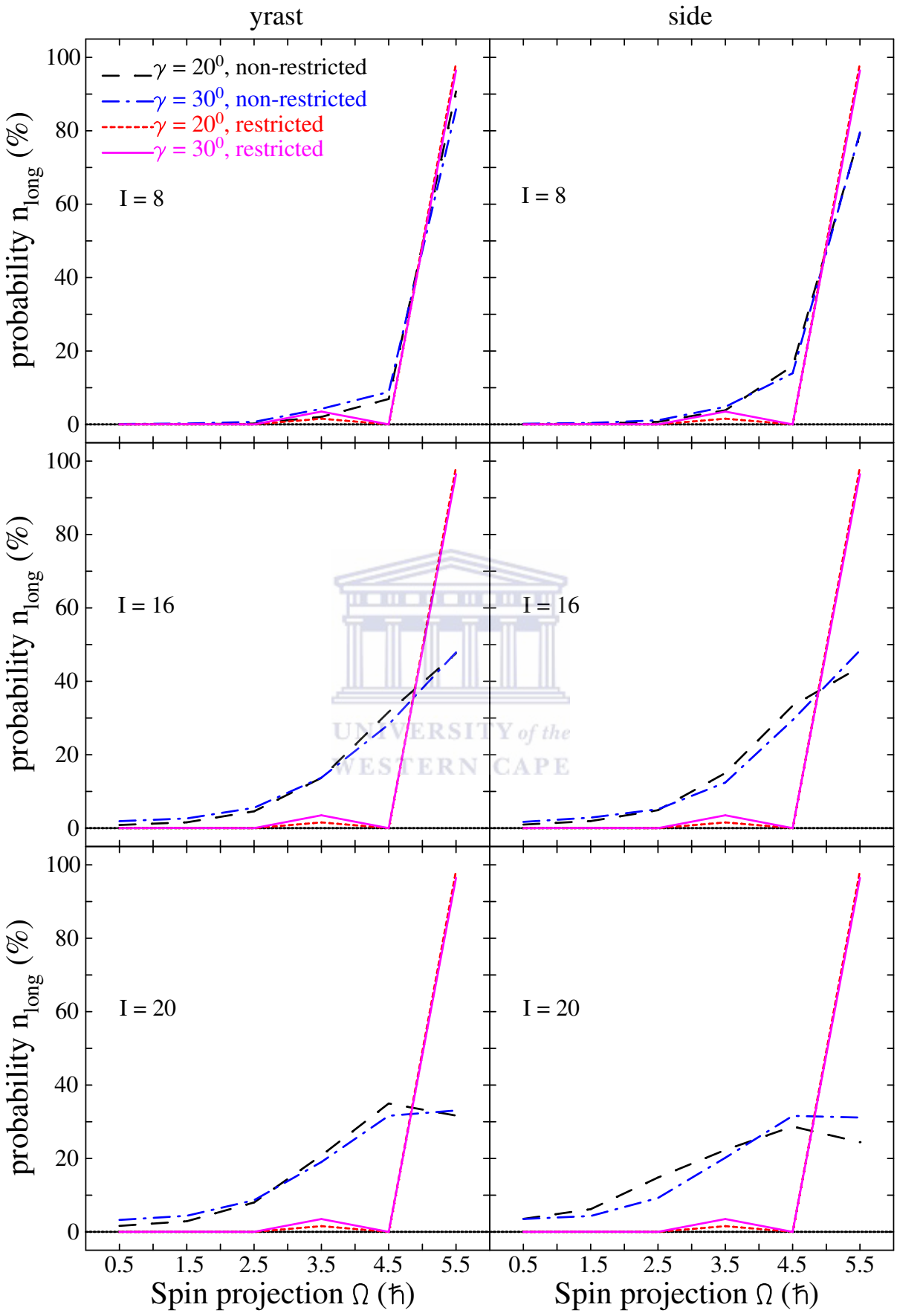

Figure 5.13: *Distributions of the projection of the angular momentum of the neutron calculated for the yrast and side bands in A ~ 130 mass region. Notation is the same in Figure 5.4.*

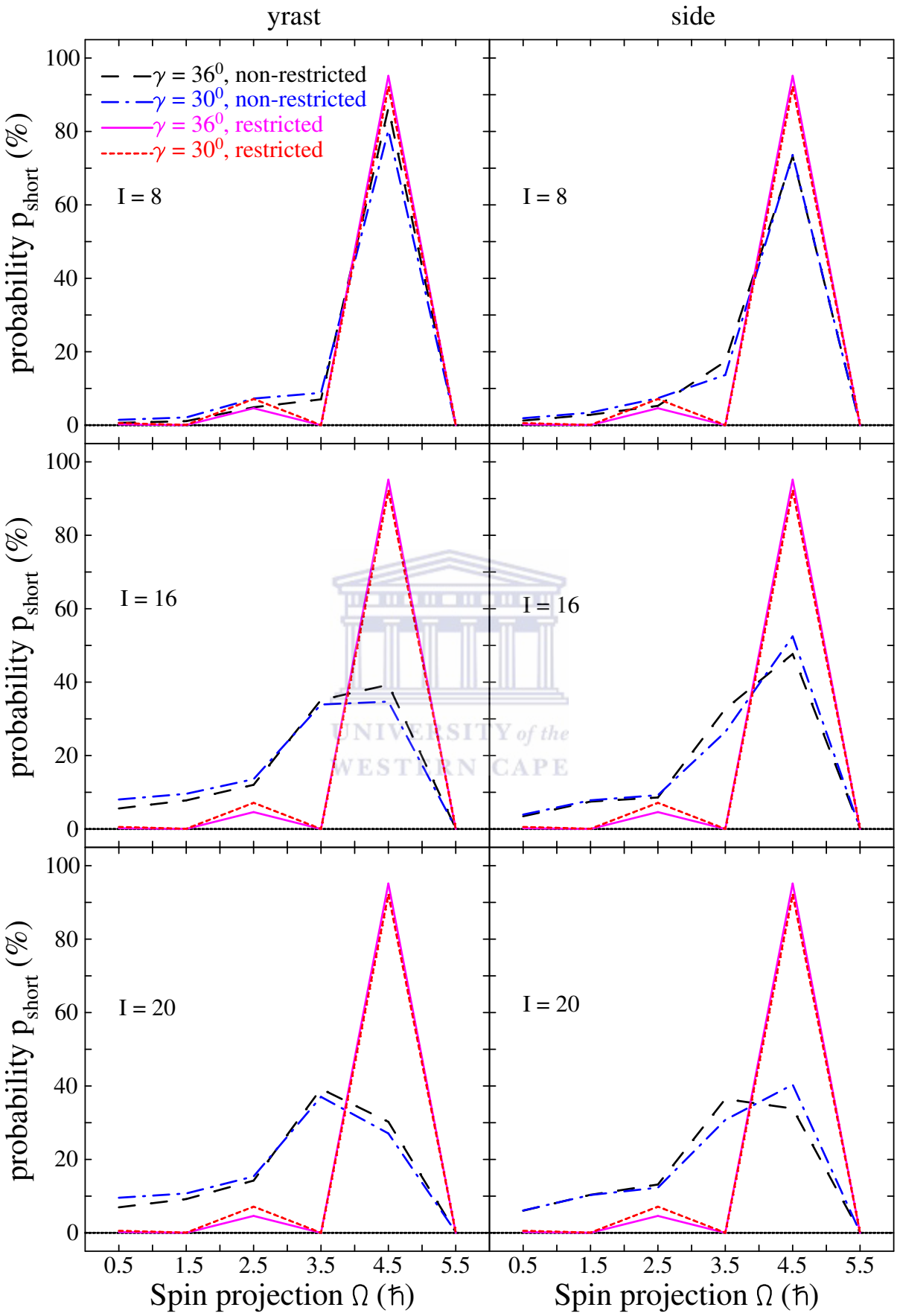

Figure 5.14: *Distributions of the projection of the angular momentum of the proton calculated for the yrast and side bands in A ~ 190 mass region. Notation is the same in Figure 5.4.*

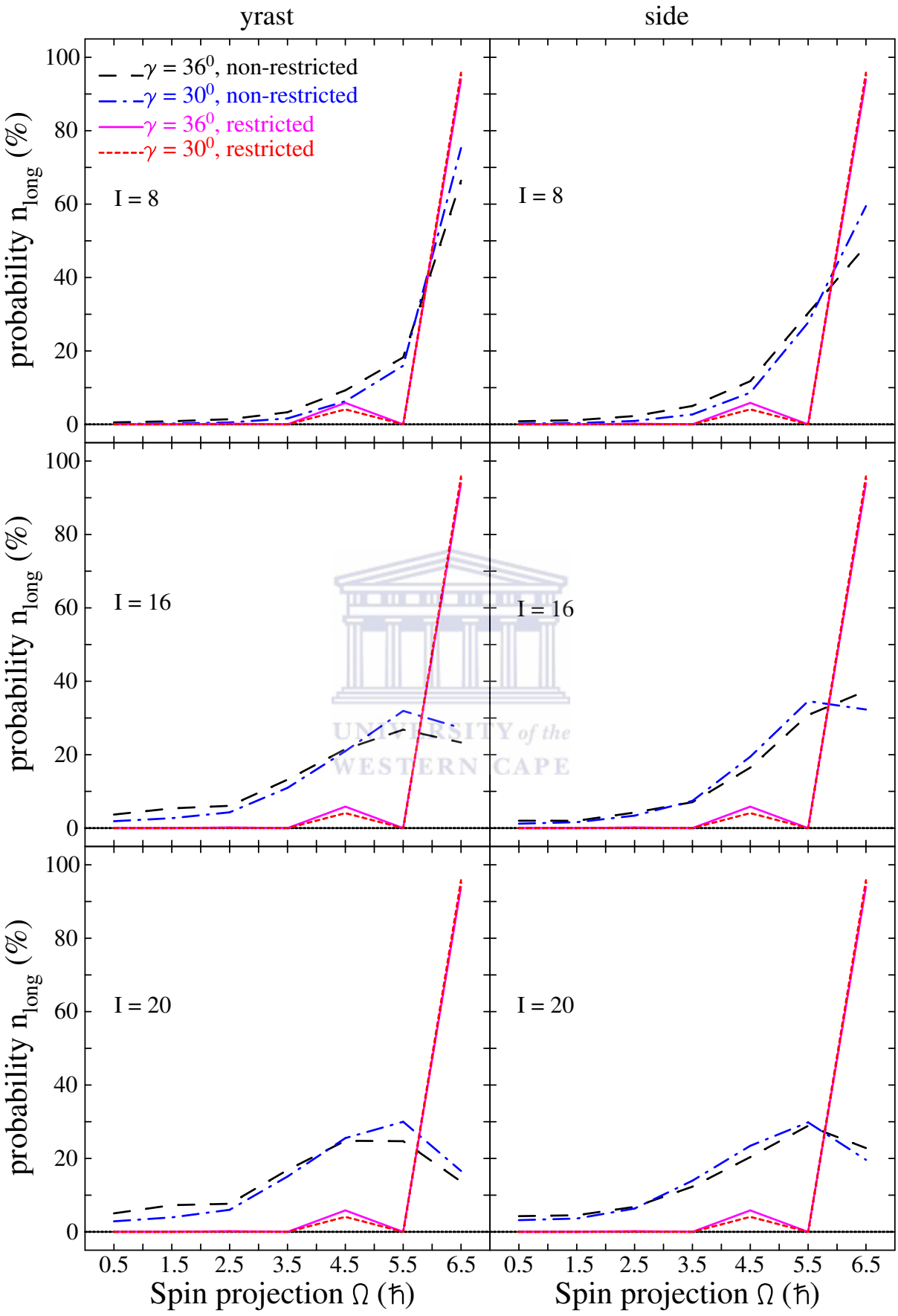

Figure 5.15: *Distributions of the projection of the angular momentum of the neutron calculated for the yrast and side bands in A ~ 190 mass region. Notation is the same in Figure 5.4.*

5.1.5 Optimal conditions for strongly broken chirality in A ~ 100, 130 and 190 mass regions

It has been suggested before that strongly broken chirality is favored for a particle-hole configuration and for stable maximum triaxiality of the deformed nuclear shape (i.e. $\gamma = 30^0$) [Fra97, Fra01]. To investigate this condition, we have performed calculations for the partner bands associated with non-restricted and restricted configurations in all three mass regions using different values of the non-axiality parameter γ. The calculations were performed with $\varepsilon_2 = 0.15$ and $\gamma = 17^0, 20^0, 24^0, 27^0, 30^0, 33^0, 36^0, 40^0$. Figure 5.16 and Tables A.1-3 show calculated values of ΔE for different values of γ in A ~ 100, 130 and 190 mass regions. The calculated values of ΔE for restricted configurations in 100, 130 and 190 mass regions reach values closest to zero keV for $30^0 \le \gamma \le 33^0$, $30^0 \le \gamma \le 36^0$ and $\gamma \sim 36^0$ respectively. For non-restricted configurations the optimal values of γ are $27^0 \le \gamma \le 33^0$ for the 100 mass region, $27^0 \le \gamma \le 33^0$ for the 130 mass region, and $27^0 \le \gamma \le 36^0$ for the 190 mass region. Therefore, these calculations show that optimal conditions for chirality may require γ slightly different from 30^0.

Note that negative values of ΔE are due to crossing between the partner bands. This happens when the partner bands come very close in excitation energy, and then interact with each other. Sometimes the partner bands may interact but never cross each other. If crossing occurs between them, the wave function properties are exchanged at the turning point (i.e. the wave function properties of the side band become that of the yrast band, and that of the yrast band become that of the side band). Even though the partner bands may not cross, this interaction between them implies that the wave function properties are mixed near the turning point. Crossing between the partner bands is associated with a sudden decrease (increase) on two consecutive values of the intra-band (inter-band) $B(E2)$ transition probabilities, making the values of inter-band $B(E2)$ transition probabilities higher than these of the intra-band $B(E2)$ transition probabilities. In some other cases the strength of the intra-band $E2$ transition is shared between the two transitions (i.e. the intra-band $E2$ and the inter-band $E2$ transitions). This happens in both partner bands at the same spin. Figure 5.17 shows the calculated excitation energies and $B(E2)$ transition probabilities for the partner bands in A ~ 190 mass region. Suppose we have two bands (i.e. the yrast and side bands) which have been identified as follows. The yrast band contains all yrast levels, while the side band includes the levels at higher energy. Using this definition the two bands do not cross as shown in

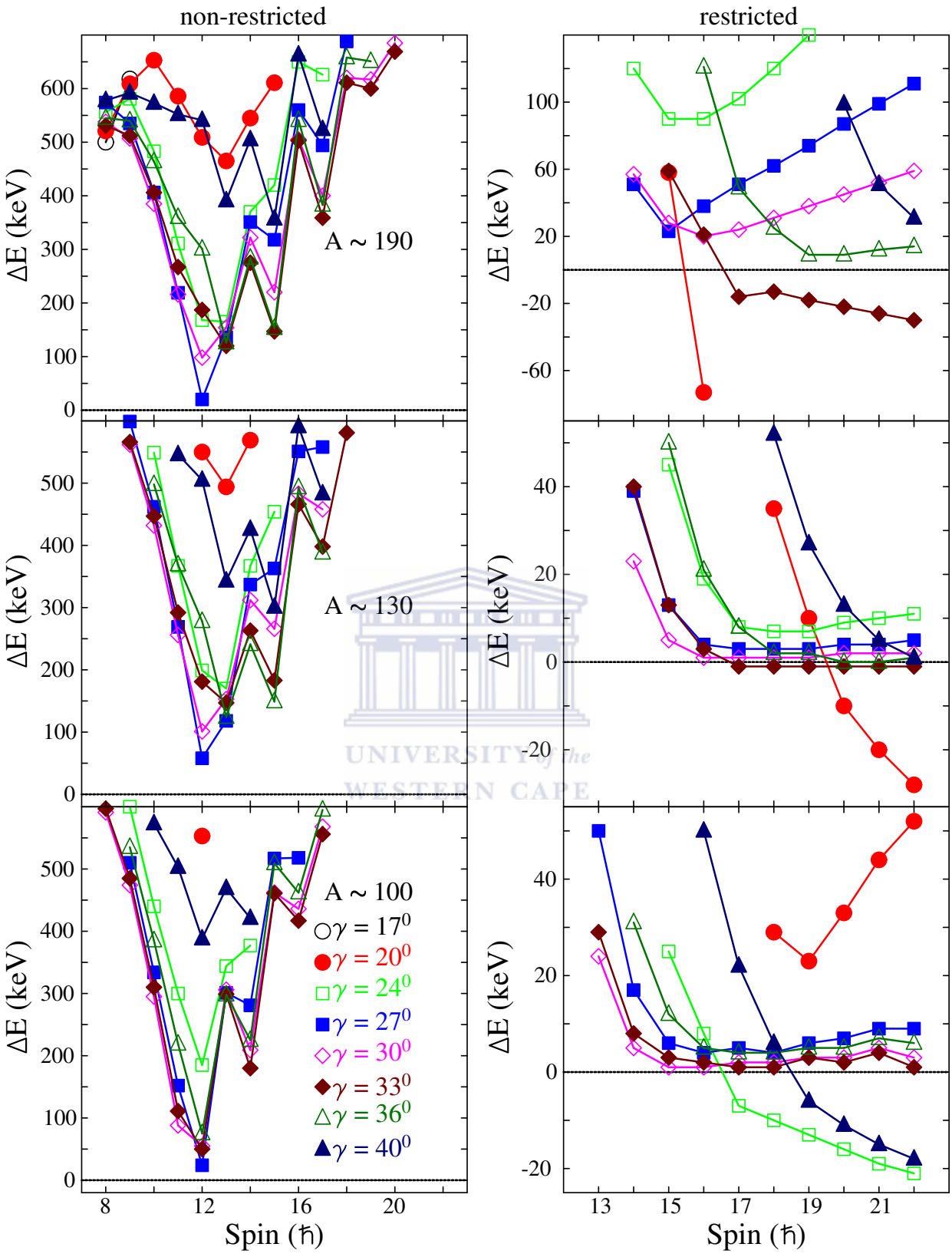

Figure 5.16: *Calculated relative excitation energy (ΔE) for the partner bands in A ~ 100, 130 and 190 mass regions. The right (left) panels correspond to calculations performed with a restricted (non-restricted) configuration. The calculations were performed with* $\varepsilon_2 = 0.15$ *and* $\gamma = 17^0, 20^0, 24^0, 27^0, 30^0, 33^0, 36^0, 40^0$.

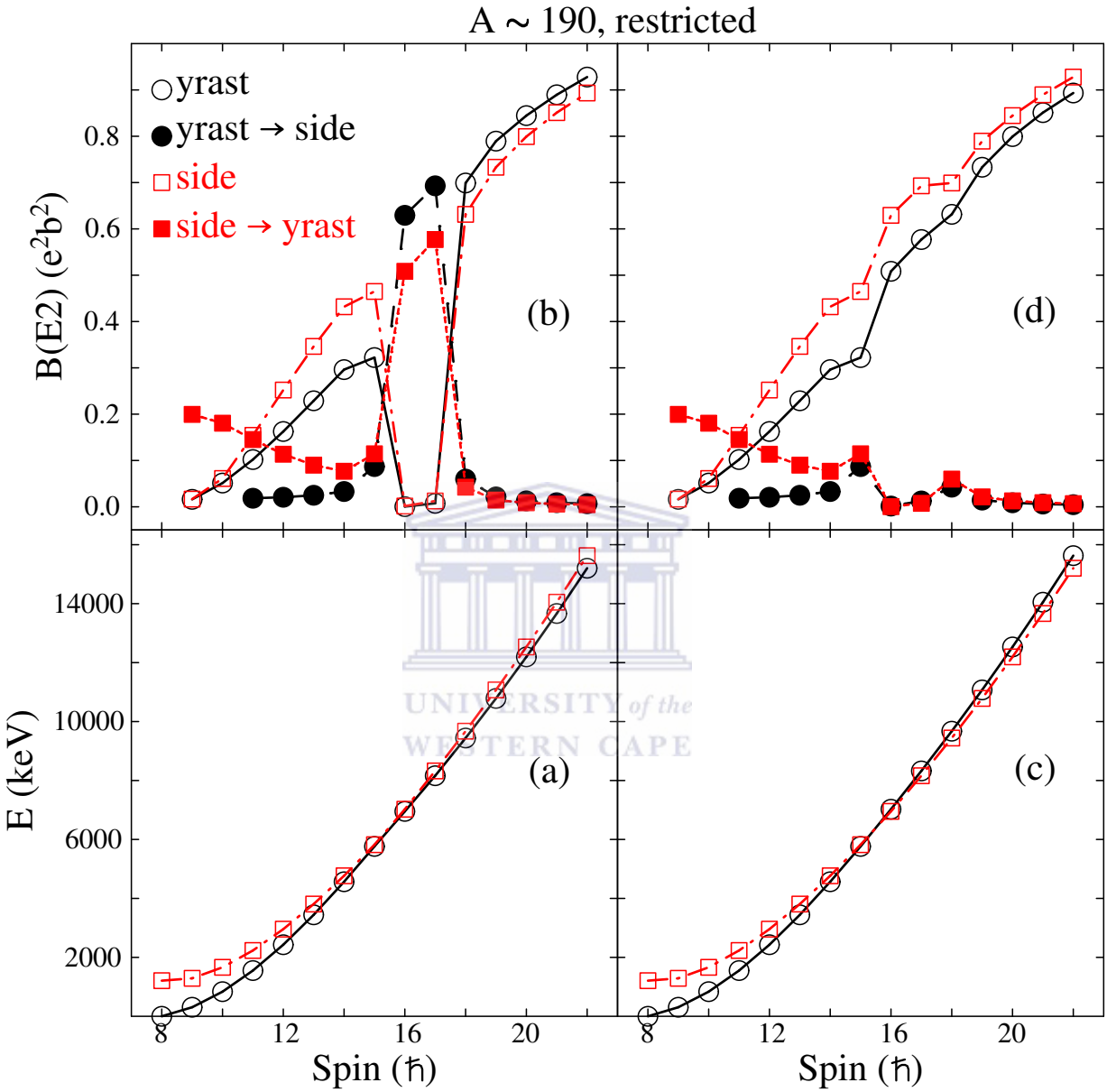

Figure 5.17: *Calculated intra- and inter-band $B(E2)$ reduced transition probabilities, and excitation energies for the partner bands in A ~ 190 mass region. Open and filled symbols denote the intra- and inter-band $B(E2)$ transitions respectively, in panels (b) and (d). Open circle and open square symbols denote the yrast and side bands respectively, in panels (a) and (c). The calculations were performed with $\varepsilon_2 = 0.15$ and $\gamma = 20^0$.*

Figure 5.17 (a). However the corresponding $B(E2)$ s do not behave as expected in this case (see Figure 5.17 (b)). For instance, it is not very likely to have a sudden large drop in the intra-band $B(E2)$ transition probabilities for two levels only as shown in Figure 5.17 (b) at $16\,\hbar \le I \le 17\,\hbar$. But if one assumes that the two bands cross each other, then the excitation energies and the $B(E2)$ transitions will look like the ones shown in Figure 5.17 (c) and (d) respectively, which is much more reasonable behaviour.

5.1.6 Further examination of other fingerprints of chirality

5.1.6.1 Energy staggering parameter $S(I)$

The energy staggering parameter $S(I)$ is an indication of the strength of the Coriolis interaction in the nuclei. Small Coriolis interaction, and therefore smooth variation of $S(I)$ as a function of spin can be caused among other things, by a perpendicular coupling of the single-particle and rotational angular momenta. Thus it was suggested that for such orthogonal coupling the chiral bands should show no energy staggering [Koi3b, Vam04]. Figures 5.18-5.20 and Tables A.4-9 show the calculated energy staggering parameter $S(I)$ for the partner bands in all three mass regions. For all values of triaxiality γ considered in all three mass regions, the values of $S(I)$ for both bands increase smoothly with increasing spin at low spins. For non-restricted nucleon configuration, the values of $S(I)$ show large staggering in opposite phase for both bands at high spins. This staggering is caused mainly by the Coriolis effects at high spins and also by the proton-neutron interaction. The phase of the $S(I)$ staggering is the same in A ~ 130, 190, while opposite in A ~ 100. Staggering was also found in the relative orientation of the angular momenta of the proton and neutron, as observed in the expected value of the angle $\alpha(p,n)$ between them, in all three mass regions (see Figure 5.9). This shows that the energy staggering is most likely a result of the orientation of the proton and neutron angular momenta.

For the restricted configuration, on average the values of $S(I)$ show a smooth dependence with spin for both bands at high spins for all values of triaxiality γ considered in all three mass regions. For all restricted configurations both the Coriolis effects and the proton-neutron interaction vanish, which causes the lack of energy staggering also for configurations without orthogonal coupling of single-particle and rotational angular momenta.

In summary these results suggested that spin independence of the energy staggering $S(I)$ within two-quasiparticle chiral bands is found when both the proton-neutron interaction and the Coriolis interaction can be completely neglected, which is rather unlikely in real nuclei. Therefore, it is rather risky to rule out a chirality interpretation in nuclei due to absence of spin independence of $S(I)$ within the partner bands.

5.1.6.2 Electromagnetic (EM) transitions

Electromagnetic transition probabilities are critical observables that carry important information on the nuclear intrinsic structure. The electromagnetic transitions that are observed in chiral partner bands are the dipole ($M1$) and quadrupole ($E2$) transitions. Thus for chiral bands the $B(M1)$ and $B(E2)$ transitions probabilities are most important.

Using a simple model (where the odd proton and the odd neutron lie in the lowest- and highest-energy $h_{11/2}$ orbitlas respectively) for a symmetric $\pi h_{11/2} \otimes \nu h_{11/2}^{-1}$ configuration with maximal triaxiality ($\gamma = 30^0$) in an odd-odd nucleus, Koike *et al*. [Koi04] suggested specific selection rules for electromagnetic transitions in a chiral geometry. These selection rules are due to the specific symmetry of the system considered (see section 3.1.1). The selection rules require staggering of the reduced $B(M1)$ intra- and inter-band transition probabilities. The $B(M1)_{in}$ and $B(M1)_{out}$ should stagger in opposite phase. The $B(M1)_{in}$ values stagger high for even spins and low for odd spins, while it is opposite for the values of $B(M1)_{out}$. As a result staggering of $B(M1)/B(E2)$ and $B(M1)_{in}/B(M1)_{out}$ ratios for the partner bands occur, and should be in the same phase [Koi04]. Such staggering behavior has been regarded as a fingerprint of chirality in odd-odd triaxial nuclei and has been used to support the existence of chiral partner bands (for example see Ref. [Vam04]).

In two recent publications dedicated to the same chiral system [Zha07, Qi09b], (which employed the two-quasiparticle-plus-triaxial-rotor model, and the particle-rotor model respectively), staggering in the $B(M1)$ values was reported too, however with an opposite phase compared to the one reported in reference [Koi04]. In another work [Dro09], large staggering was again reported for this $\pi h_{11/2} \otimes \nu h_{11/2}^{-1}$ configuration, but its phase was similar to the one reported in reference [Koi04].

The differences in the phase of the $B(M1)$ staggering obtained in these calculations [Koi04, Zha07, Qi09b, Dro09] were not pointed out or discussed previously. This raises the questions whether the $B(M1)$ staggering can be used as a reliable indication for a chiral system.

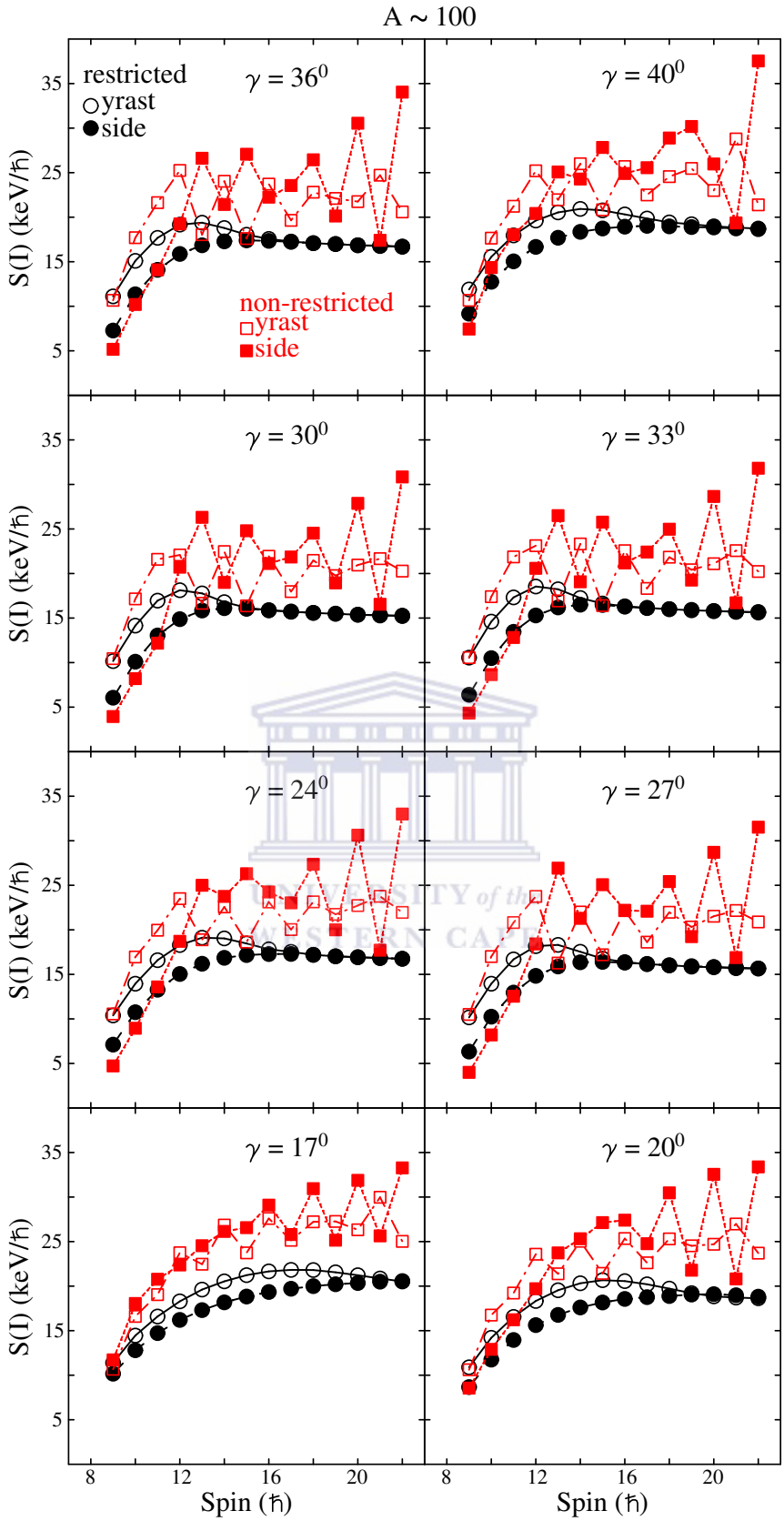

Figure 5.18: *Calculated energy staggering parameter $S(I)$ for the partner bands in A ~ 100 mass region. Open and filled symbols denote the yrast and side bands respectively. The calculations were performed with ε_2 = 0.15 and γ = 17⁰, 20⁰, 24⁰, 27⁰, 30⁰, 33⁰, 36⁰, 40⁰.*

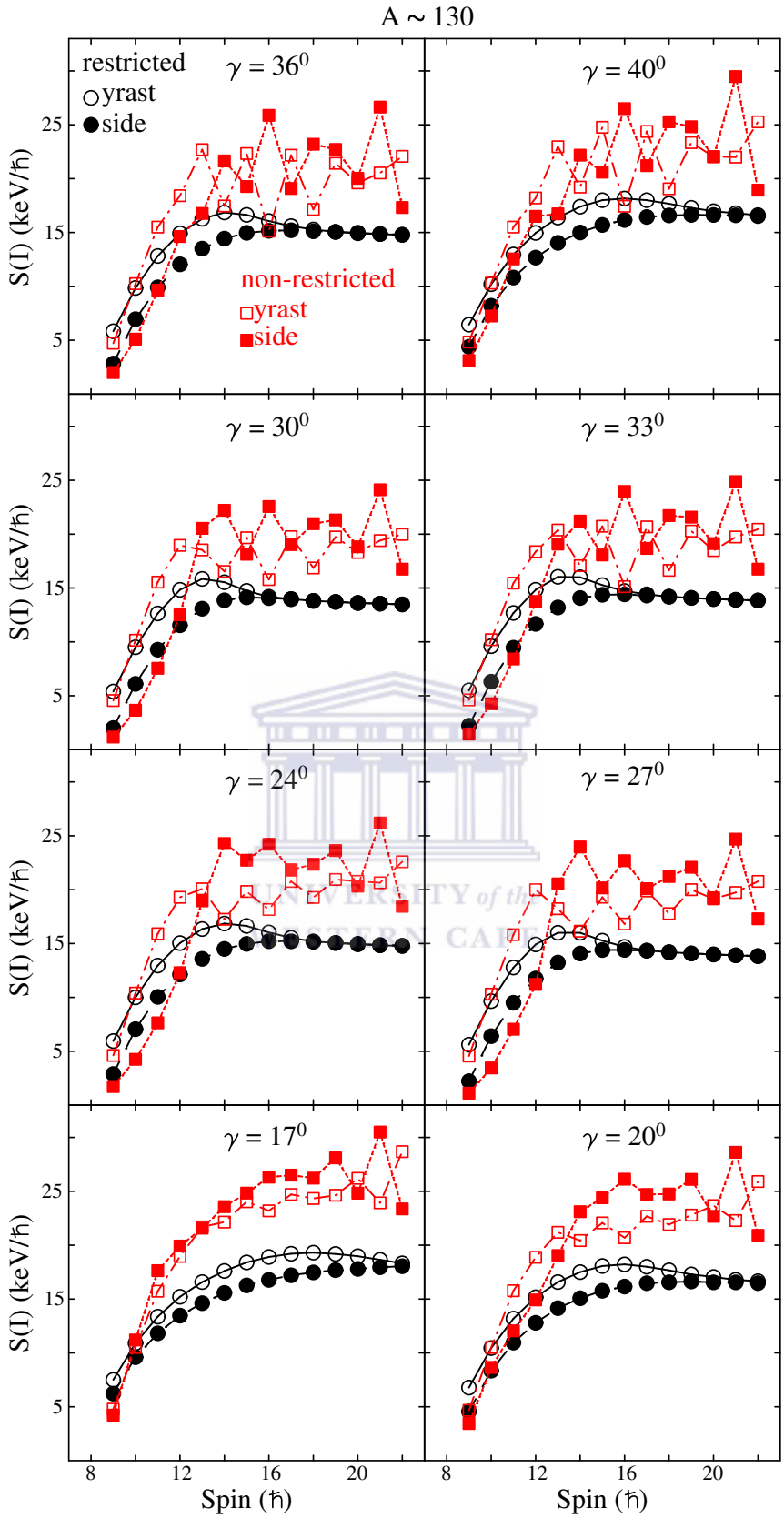

Figure 5.19: *Calculated energy staggering parameter $S(I)$ for the partner bands in A ~ 130 mass region. Open and filled symbols denote the yrast and side bands respectively. The calculations were performed with ε_2 = 0.15 and γ = 17⁰, 20⁰, 24⁰, 27⁰, 30⁰, 33⁰, 36⁰, 40⁰.*

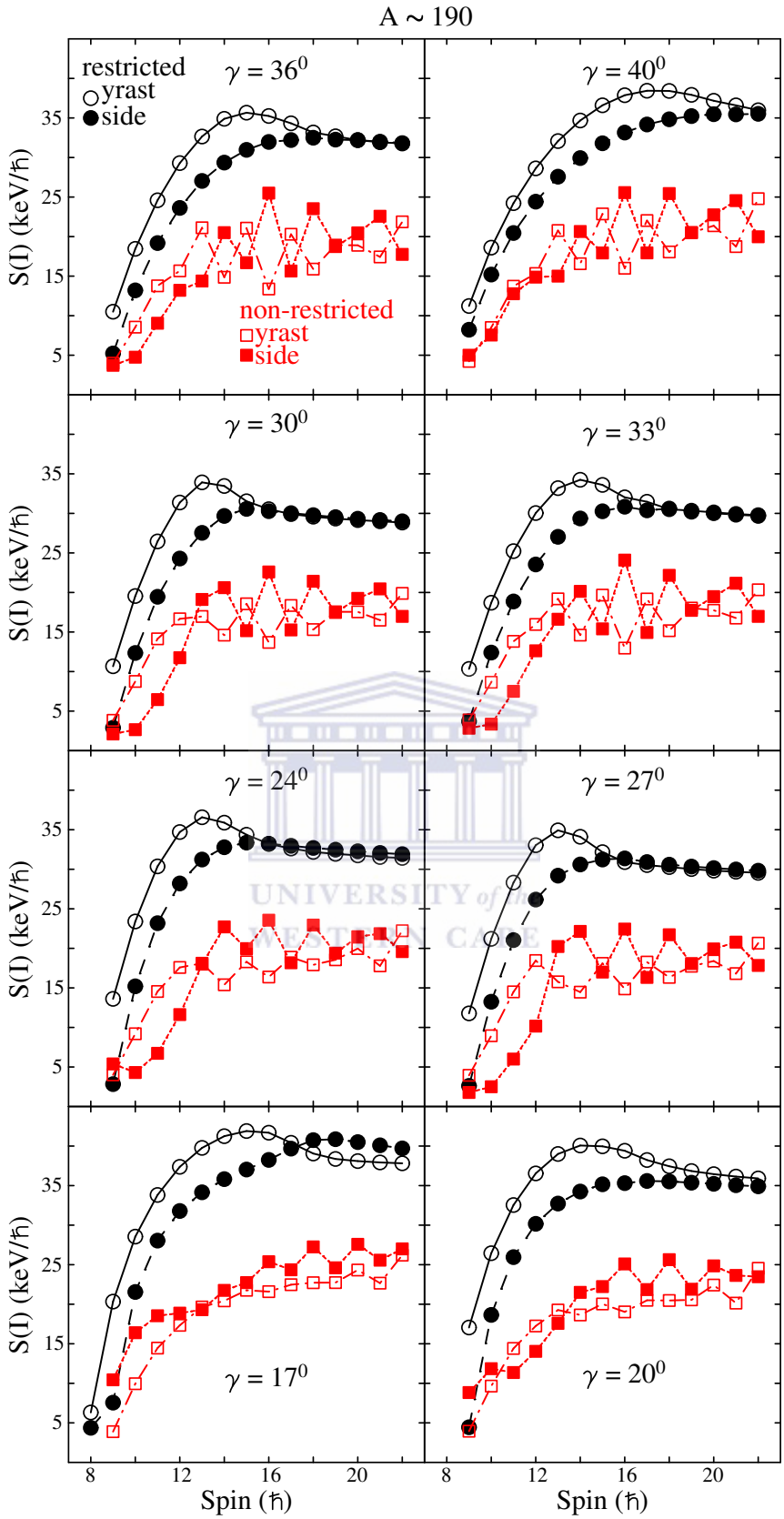

Figure 5.20: *Calculated energy staggering parameter* $S(I)$ *for the partner bands in A ~ 190 mass region. Open and filled symbols denote the yrast and side bands respectively. The calculations were performed with* ε_2 *= 0.15 and* γ *=* 17^0, 20^0, 24^0, 27^0, 30^0, 33^0, 36^0, 40^0.

Furthermore it remains unclear whether it will be present for chiral structures built on asymmetric particle-hole configurations. In this work, the electromagnetic transition probabilities of the chiral partner bands are investigated further. We study whether such behavior of $B(M1)$ transition probabilities is present in our TQPRM calculations performed for symmetric (i.e. $\pi h_{11/2} \otimes \nu h_{11/2}^{-1}$) and asymmetric (i.e. $\pi g_{9/2}^{-1} \otimes \nu h_{11/2}$ and $\pi h_{9/2} \otimes \nu i_{13/2}^{-1}$) nucleon configurations and also what is the phase of the $B(M1)$ staggering.

The calculated intra- and inter-band $B(M1)$ reduced electromagnetic transition probabilities for the partner bands for restricted and non-restricted configurations in 100, 130 and 190 mass regions are shown in Figures 5.21, 5.23, 5.25, 5.27, 5.29, 5.31 and Tables A.45-46, A.49-50, A.53-54, A.57-58, A.61-62, A.65-66. For the calculations performed with $\gamma = 17^0, 20^0, 24^0, 27^0, 30^0, 33^0, 36^0, 40^0$ and restricted configurations in all three mass regions at low spin, the intra-band $B(M1)$ transitions for the partner bands are strong, while the inter-band $B(M1)$ transitions are weak. At high spins, the values of intra- and inter-band $B(M1)$ transitions may show staggering in opposite phase for certain values of γ. In the 100 mass region, the largest staggering in the $B(M1)$ rates is found for $\gamma = 30^0, 33^0$. In the 130 mass region, the largest staggering occurs for $\gamma = 33^0$, whereas in 190 mass region it is found for $\gamma = 36^0$. It is worth noting that large $B(M1)$ staggering is always found for such values of γ for which the chiral partner bands are nearly degenerate. It is important to note the phase of the $B(M1)$ staggering. For a symmetric configuration (i.e. $\pi h_{11/2} \otimes \nu h_{11/2}^{-1}$ in A ~ 130), the intra-band $B(M1)$ rates stagger high and low for even and odd spins respectively as was initially suggested by Koike *et al.* [Koi04]. The phase is opposite for the inter-band $B(M1)$ transitions rates. For both asymmetric configurations (i.e. $\pi g_{9/2}^{-1} \otimes \nu h_{11/2}$ in A ~ 100 and $\pi h_{9/2} \otimes \nu i_{13/2}^{-1}$ in A ~ 190), the intra-band $B(M1)$ transitions rates stagger low and high for even and odd spins respectively, and the phase is opposite for the inter-band $B(M1)$ transitions rates.

For the calculations performed with non-restricted configurations in all three mass regions, the intra-band $B(M1)$ transitions for the partner bands decrease fast at low spins, while the inter-band $B(M1)$ transitions are weak. At high spins, staggering in opposite phase is found for the intra-band and inter-band $B(M1)$ transition probabilities for some values of γ. In general it seems that the $B(M1)$ staggering occurs for a larger interval of γ for non-restricted

configuration. It is important to note that the phase of the $B(M1)$ staggering for non-restricted configurations in A ~ 100, 130 mass regions is opposite to that for the restricted configurations. However, in 190 mass region the same phase in the $B(M1)$ staggering is found for both restricted and non-restricted configurations.

The calculated intra- and inter-band $B(E2)$ electromagnetic transition probabilities of the partner bands in 100, 130 and 190 mass regions are shown in Figures 5.22, 5.24, 5.26, 5.28, 5.30, 5.32 and Tables A.47-48, A.51-52, A.55-56, A.59-60, A.63-64, A.67-68. For the calculations performed with both restricted and non-restricted configuration in all three mass regions, for values of γ close to 30^0, the intra-band $B(E2)$ transition probabilities for the partner bands are weak, while the inter-band ones are strong at low spins. This is more pronounced for $\gamma = 30^0$ in A ~ 100, 130 and $\gamma = 27^0, 30^0$ in A ~ 190 mass regions. For values of γ away from 30^0, the intra-band $B(E2)$ transition probabilities at low spins increase gradually, while the inter-band $B(E2)$ transition probabilities are suppressed gradually. Often in certain spin region the two partner bands interact strongly with each other, which is exhibited by irregularities in the smooth behavior of $B(E2)$, (for example see calculations with restricted configurations for $\gamma = 24^0, 40^0$ in Figures 5.22, and $\gamma = 20^0, 33^0$ in Figures 5.26, 5.30). At high spins, the intra-band $B(E2)$s increase smoothly with spin, while the inter-band $B(E2)$ transition probabilities become negligible, (except for the spin region where the two bands interact with each other).

In summary these results suggest that staggering in the $B(M1)$ reduced transition probabilities occur when near perfect degeneracy of the chiral partner bands is exhibited. Furthermore, the phase of the $B(M1)$ staggering is specific for the strongly broken chiral systems, i.e. the values are high for even spins and low for odd spins for symmetric configurations in nuclei with A ~ 130, and opposite for asymmetric configurations in A ~ 100, 190 nuclei. It is should be noted that $B(M1)$ staggering may occur for non-restricted configurations too, when the partner bands do not show near degeneracy. In that case the phase of the $B(M1)$ staggering in A ~ 100, 130 is opposite to that observed for the restricted configuration. However, in A ~ 190, the same phase of the $B(M1)$ staggering is found for both the restricted and non-restricted configurations. The amplitude of the $B(M1)$ staggering may not be straight forward related to how good the chirality is. The staggering may disappear completely for partner bands which are almost degenerate (for example for

restricted configuration, but not optimal value of γ), and be large for bands which do not have close excitation energies (for example non-restricted configurations). Therefore staggering in the $B(M1)$ values while linked to chiral symmetry may be a result of other effects too. Thus it is risky to consider it as a reliable indication of a strongly broken chiral symmetry. An examination of the phase of the $B(M1)$ staggering is of particular importance, since the phase is sensitive to the intrinsic structure.

5.2 Calculations performed with different parameters in the A ~ 130 mass region

Three sets of additional two-quasiparticle-plus-triaxial-rotor model calculations were performed in A ~ 130 mass region. These calculations are as follows:

(i) calculations for partner bands associated with $\pi h_{11/2} \otimes \nu h_{11/2}^{-1}$ configuration in A ~ 130 mass region with larger quadrupole nuclear deformation of $\varepsilon_2 = 0.25$. These calculations were done in order to check whether at larger deformation the Coriolis effects will be sufficiently small, such that the chiral partner bands built on non-restricted configuration will show degeneracy.

(ii) calculations for the partner bands associated with $\pi h_{11/2} \otimes \nu h_{11/2}^{-1}$ configuration in A ~ 130 mass region with Coriolis attenuation factor of $\xi = 0.8$. These calculations were done in order to check whether by decreasing the Coriolis effects when using an attenuation factor the chiral partner bands built on non-restricted configuration will show degeneracy.

(iii) calculations for a restricted $\pi h_{11/2} \otimes \nu h_{11/2}^{-1}$ configuration in A ~ 130 region when either the Fermi surface of the proton or that of the neutron is moved inside the $h_{11/2}$ shell. The conditions for reaching degeneracy in such partner bands were studied too.

Note that in the following discussion (i.e. discussion in sections 5.2.1-5.2.3) we shall call "standard", the previous calculations performed for the partner bands in A ~ 130 mass region with $\varepsilon_2 = 0.15$ and $\xi = 1$.

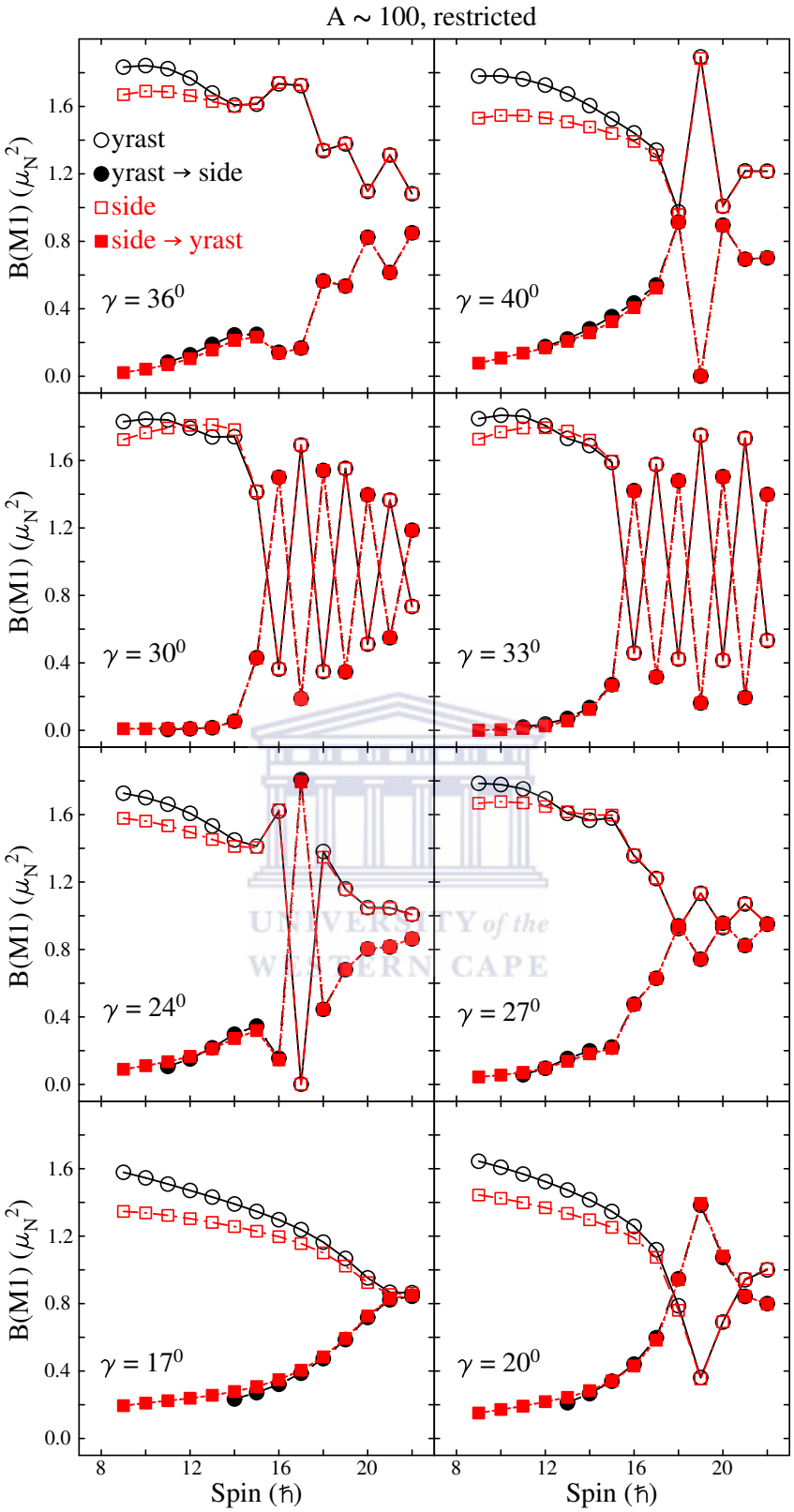

Figure 5.21: *Calculated intra- and inter-band $B(M1)$ reduced transition probabilities for the partner bands in A ~ 100 mass region. Open and filled symbols denote intra- and inter-band $B(M1)$ transitions respectively. The calculations were performed with ε_2 = 0.15 and γ = 17^0, 20^0, 24^0, 27^0, 30^0, 33^0, 36^0, 40^0.*

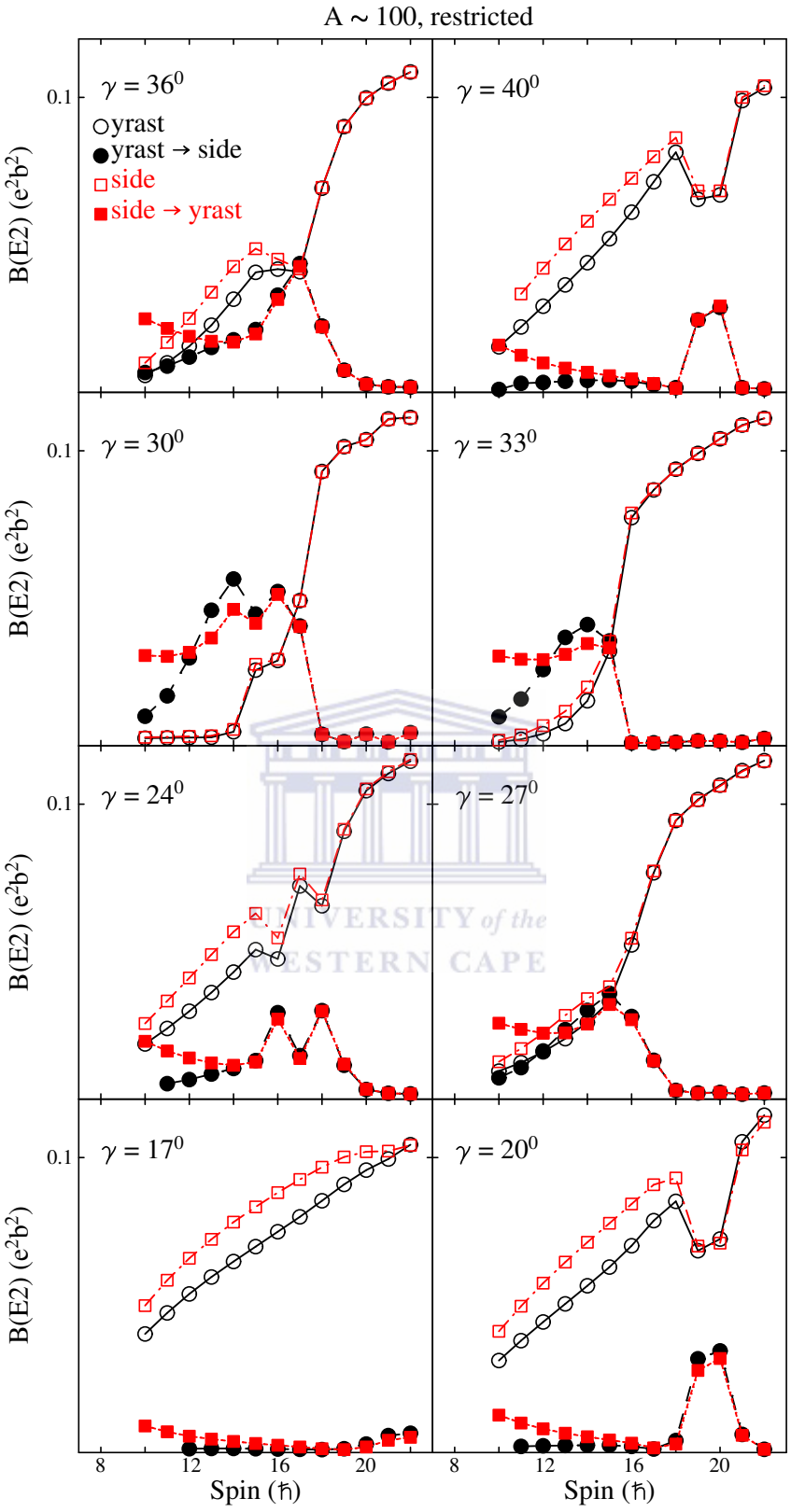

Figure 5.22: *Calculated intra- and inter-band $B(E2)$ reduced transition probabilities for the partner bands in A ~ 100 mass region. Open and filled symbols denote intra- and inter-band $B(E2)$ transitions respectively. The calculations were performed with ε_2 = 0.15 and γ = 17^0, 20^0, 24^0, 27^0, 30^0, 33^0, 36^0, 40^0.*

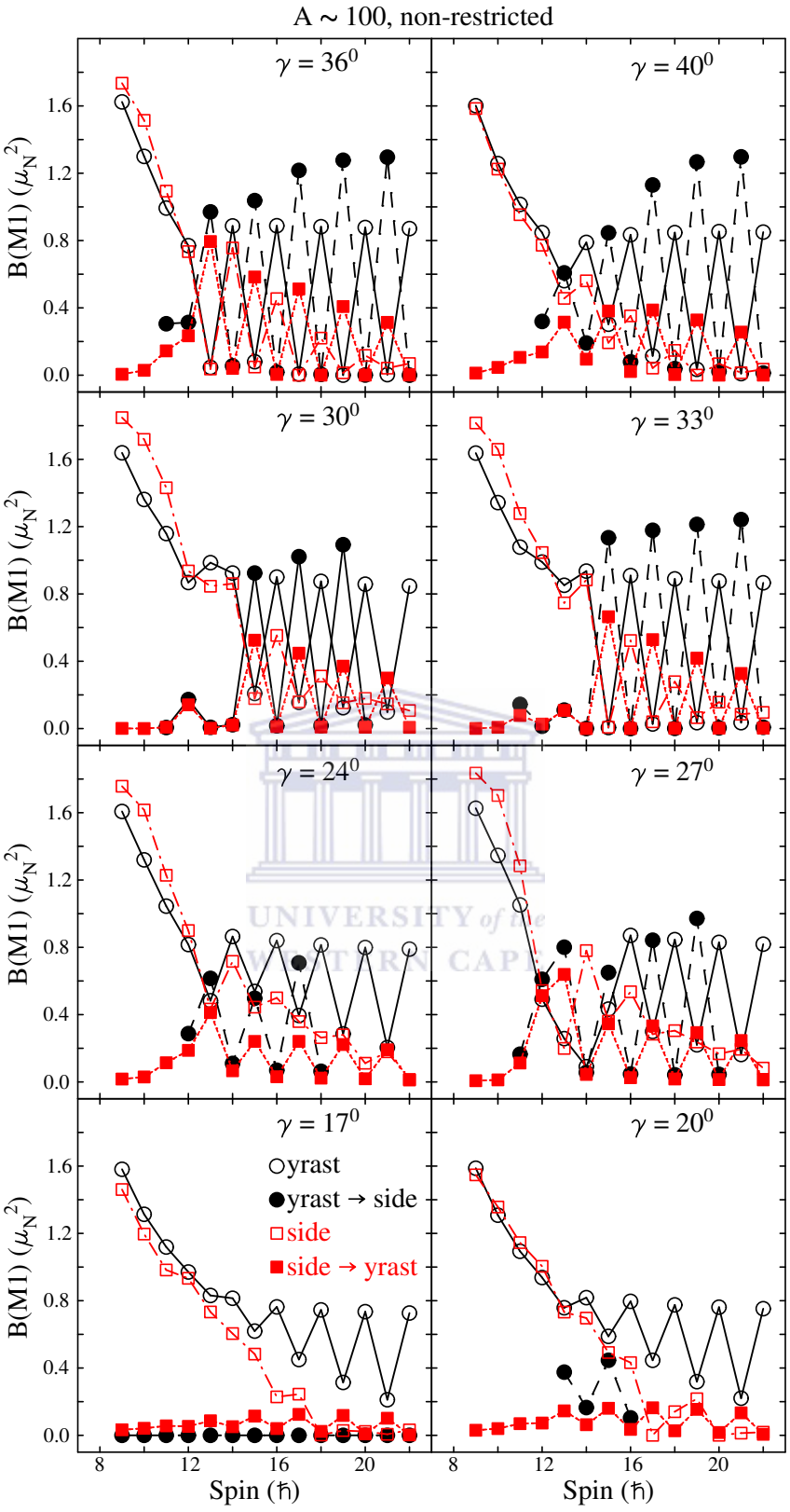

Figure 5.23: *Calculated intra- and inter-band $B(M1)$ reduced transition probabilities for the partner bands in A ~ 100 mass region. Open and filled symbols denote intra- and inter-band $B(M1)$ transitions respectively. The calculations were performed with ε_2 = 0.15 and γ = 17^0, 20^0, 24^0, 27^0, 30^0, 33^0, 36^0, 40^0.*

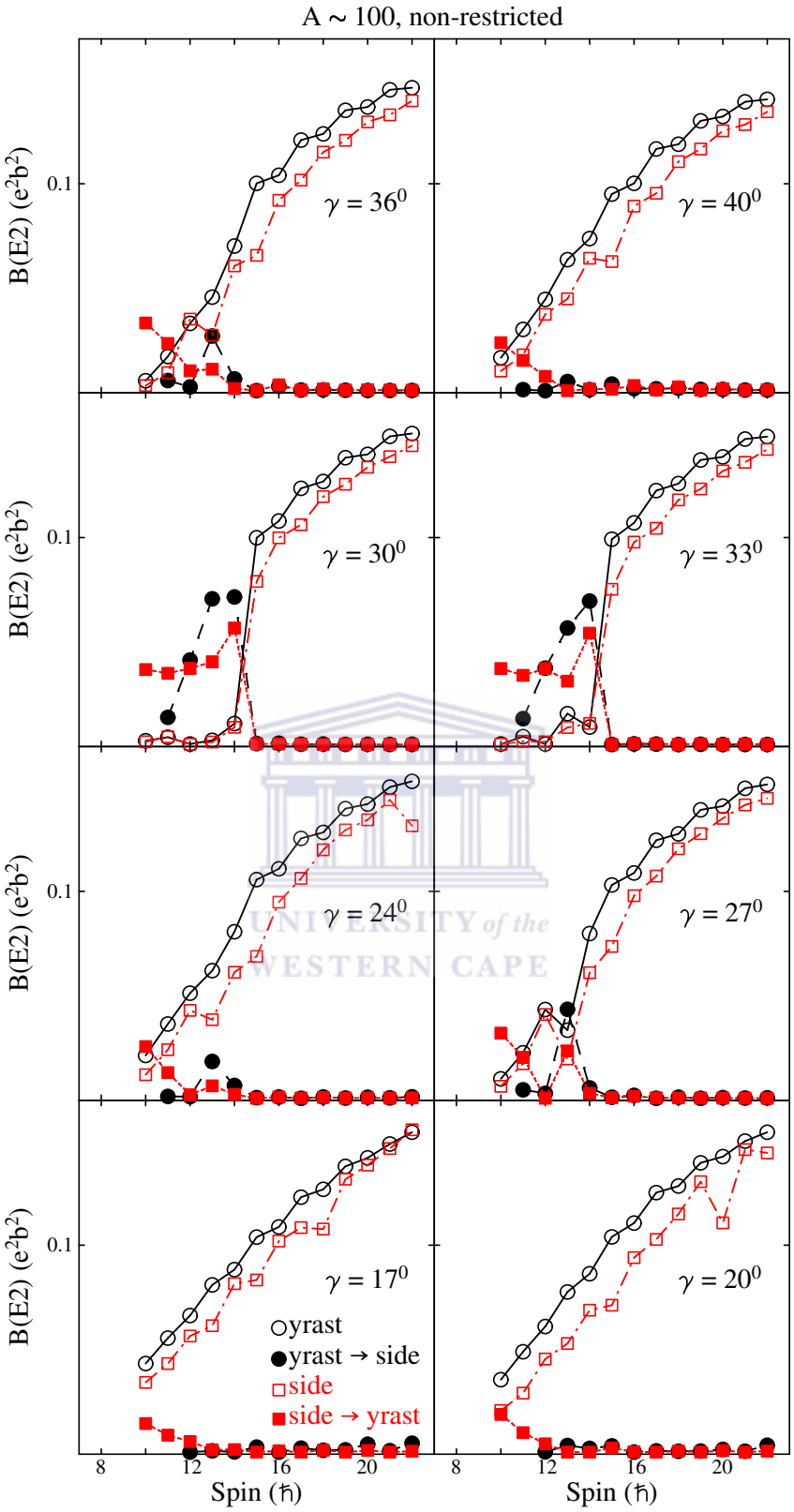

Figure 5.24: *Calculated intra- and inter-band $B(E2)$ reduced transition probabilities for the partner bands in A ~ 100 mass region. Open and filled symbols denote intra- and inter-band $B(E2)$ transitions respectively. The calculations were performed with ε_2 = 0.15 and γ = 17⁰, 20⁰, 24⁰, 27⁰, 30⁰, 33⁰, 36⁰, 40⁰.*

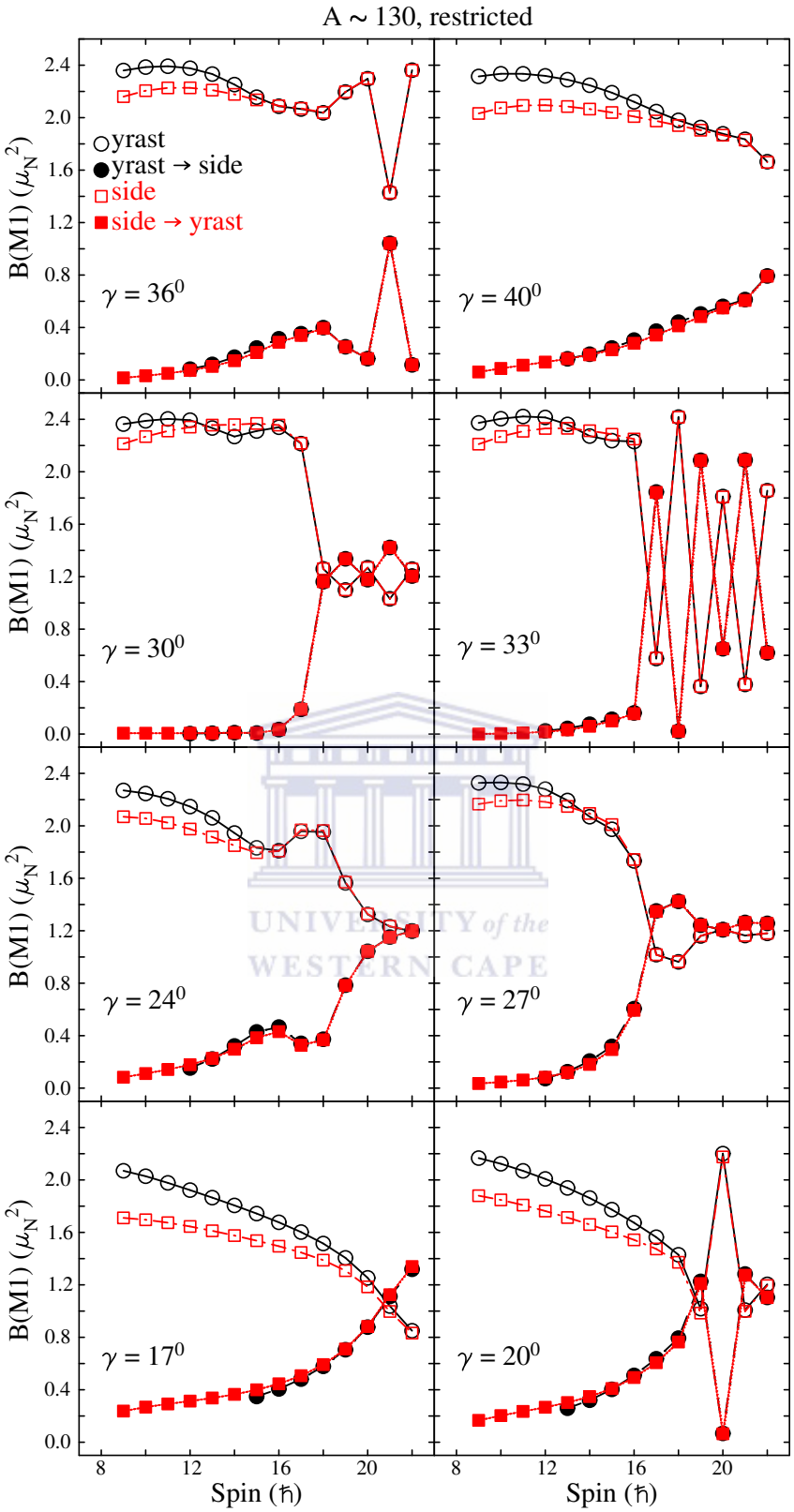

Figure 5.25: *Calculated intra- and inter-band $B(M1)$ reduced transition probabilities for the partner bands in A ~ 130 mass region. Open and filled symbols denote intra- and inter-band $B(M1)$ transitions respectively. The calculations were performed with ε_2 = 0.15 and γ = 17⁰, 20⁰, 24⁰, 27⁰, 30⁰, 33⁰, 36⁰, 40⁰.*

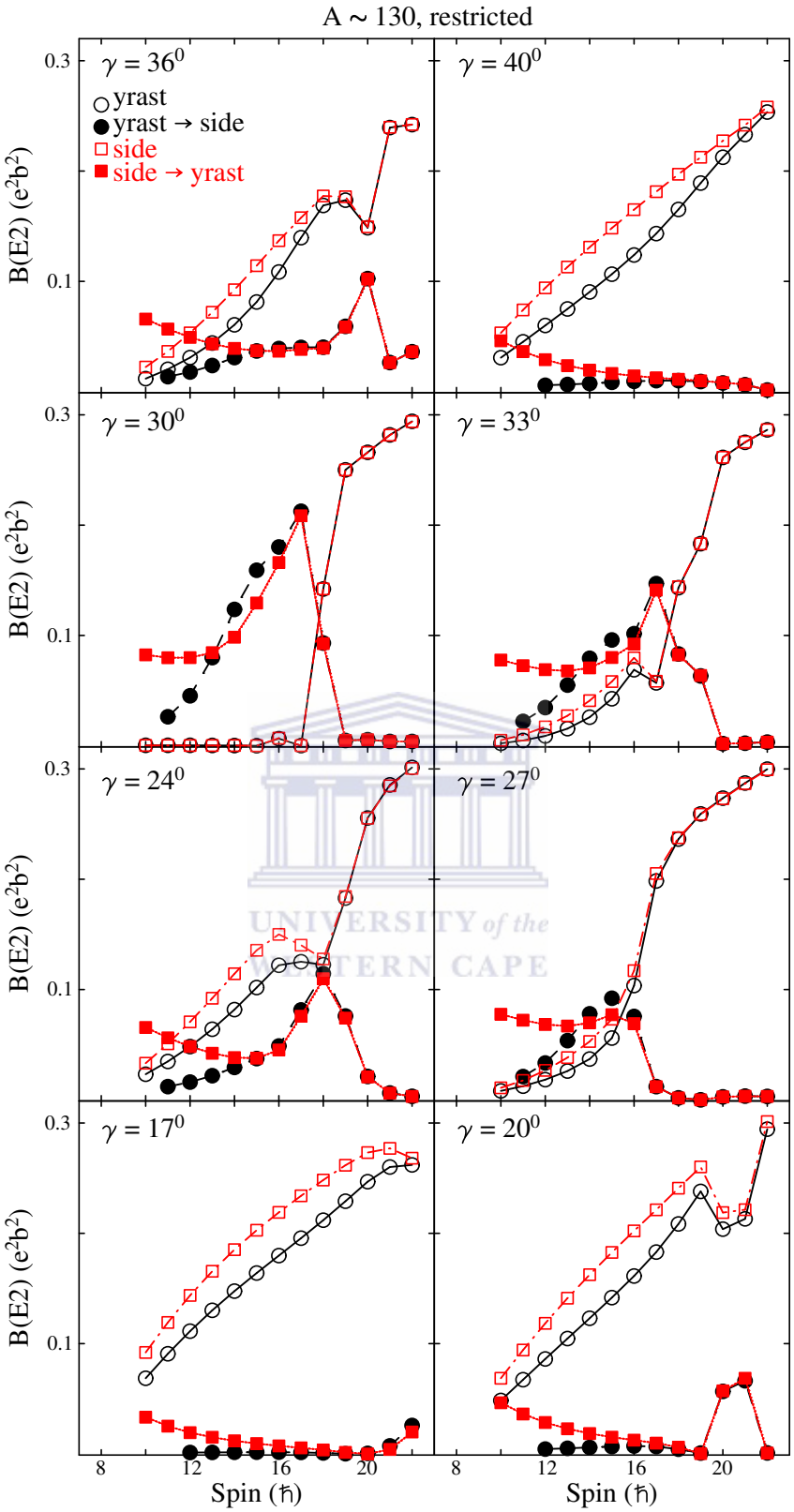

Figure 5.26: *Calculated intra- and inter-band $B(E2)$ reduced transition probabilities for the partner bands in A ~ 130 mass region. Open and filled symbols denote intra- and inter-band $B(E2)$ transitions respectively. The calculations were performed with ε_2 = 0.15 and γ = 17⁰, 20⁰, 24⁰, 27⁰, 30⁰, 33⁰, 36⁰, 40⁰.*

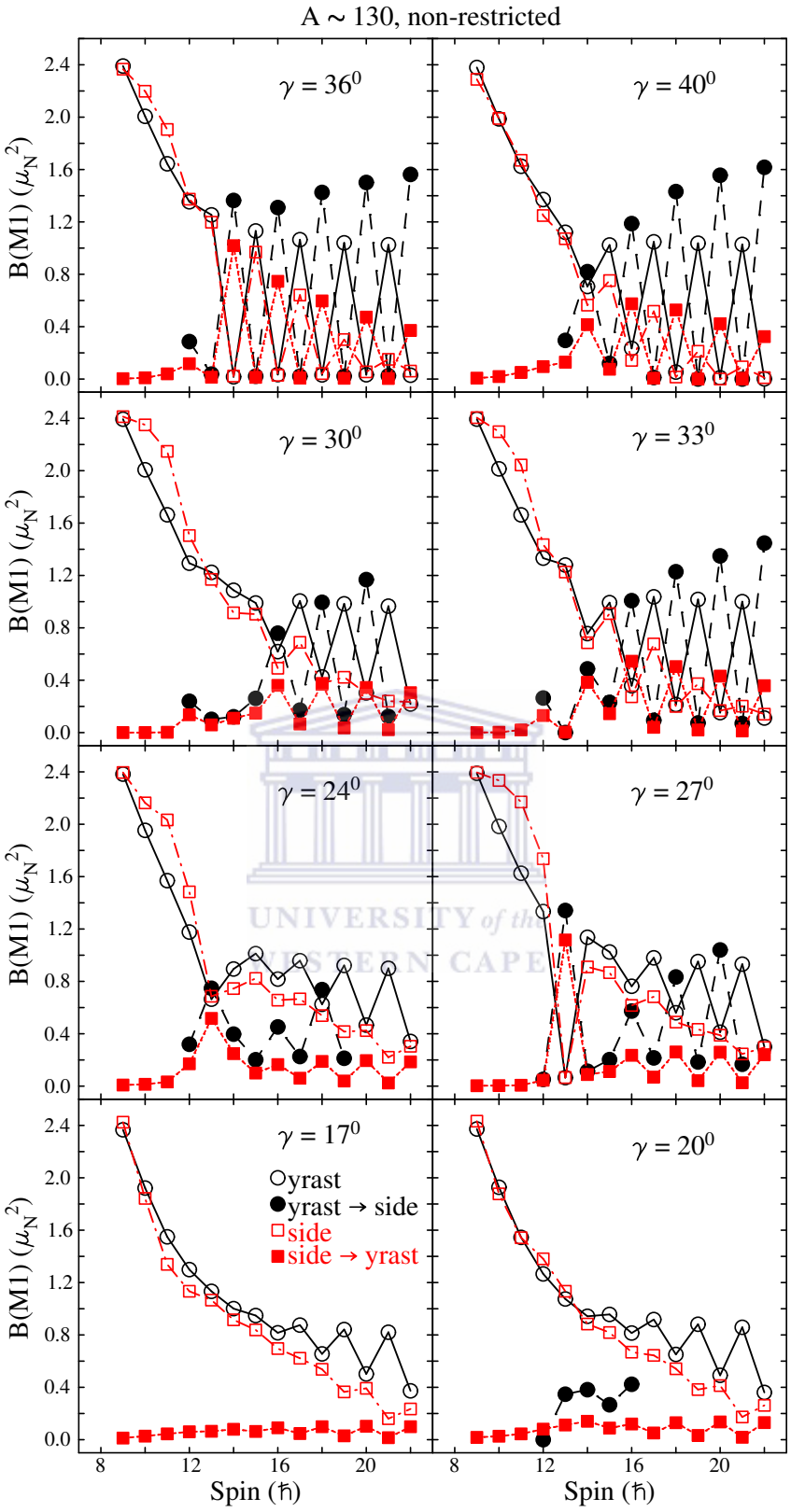

Figure 5.27: *Calculated intra- and inter-band $B(M1)$ reduced transition probabilities for the partner bands in A ~ 130 mass region. Open and filled symbols denote intra- and inter-band $B(M1)$ transitions respectively. The calculations were performed with ε_2 = 0.15 and γ = 17^0, 20^0, 24^0, 27^0, 30^0, 33^0, 36^0, 40^0.*

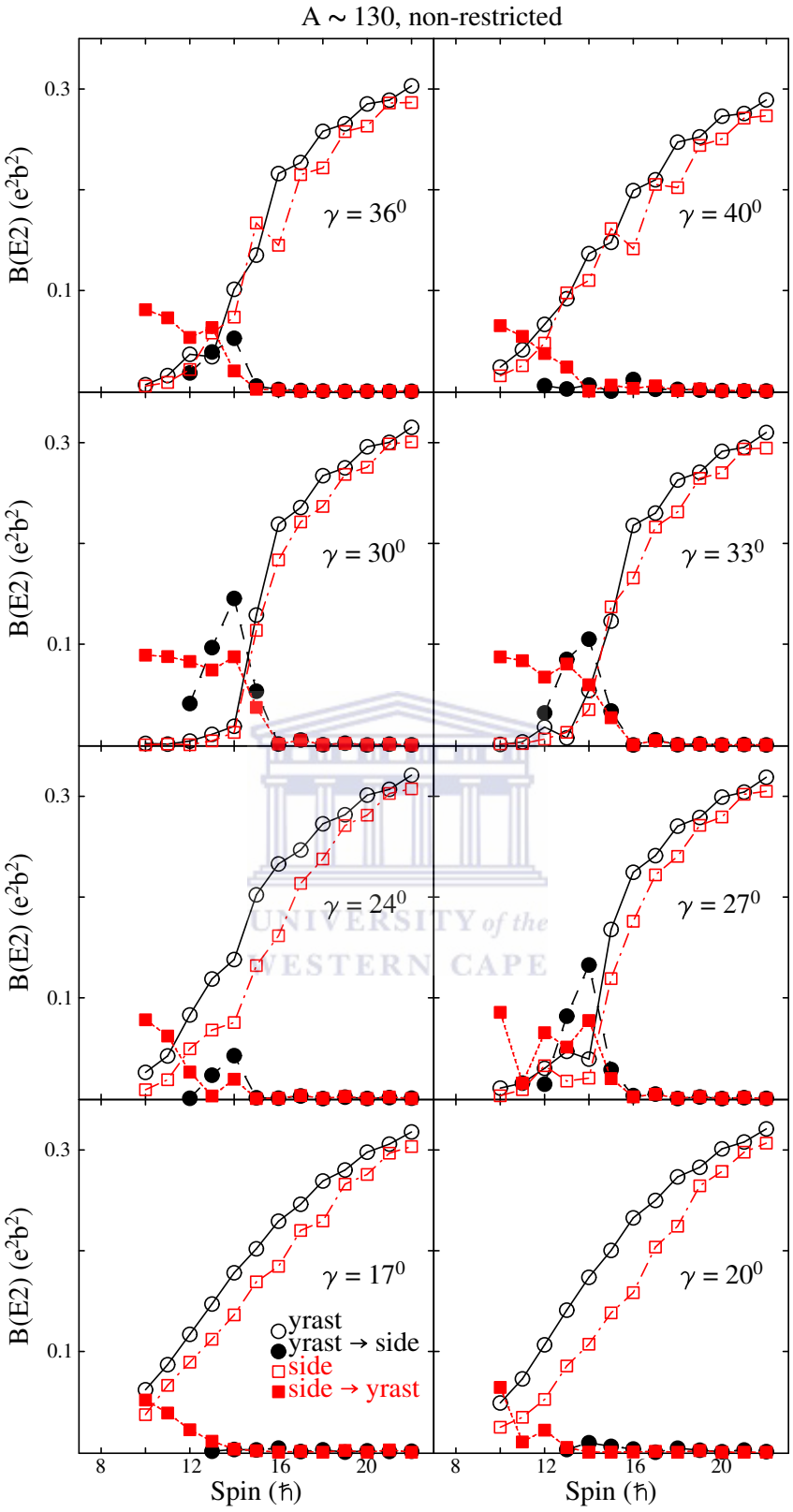

Figure 5.28: *Calculated intra- and inter-band $B(E2)$ reduced transition probabilities for the partner bands in A ~ 130 mass region. Open and filled symbols denote intra- and inter-band $B(E2)$ transitions respectively. The calculations were performed with ε_2 = 0.15 and γ = 17^0, 20^0, 24^0, 27^0, 30^0, 33^0, 36^0, 40^0.*

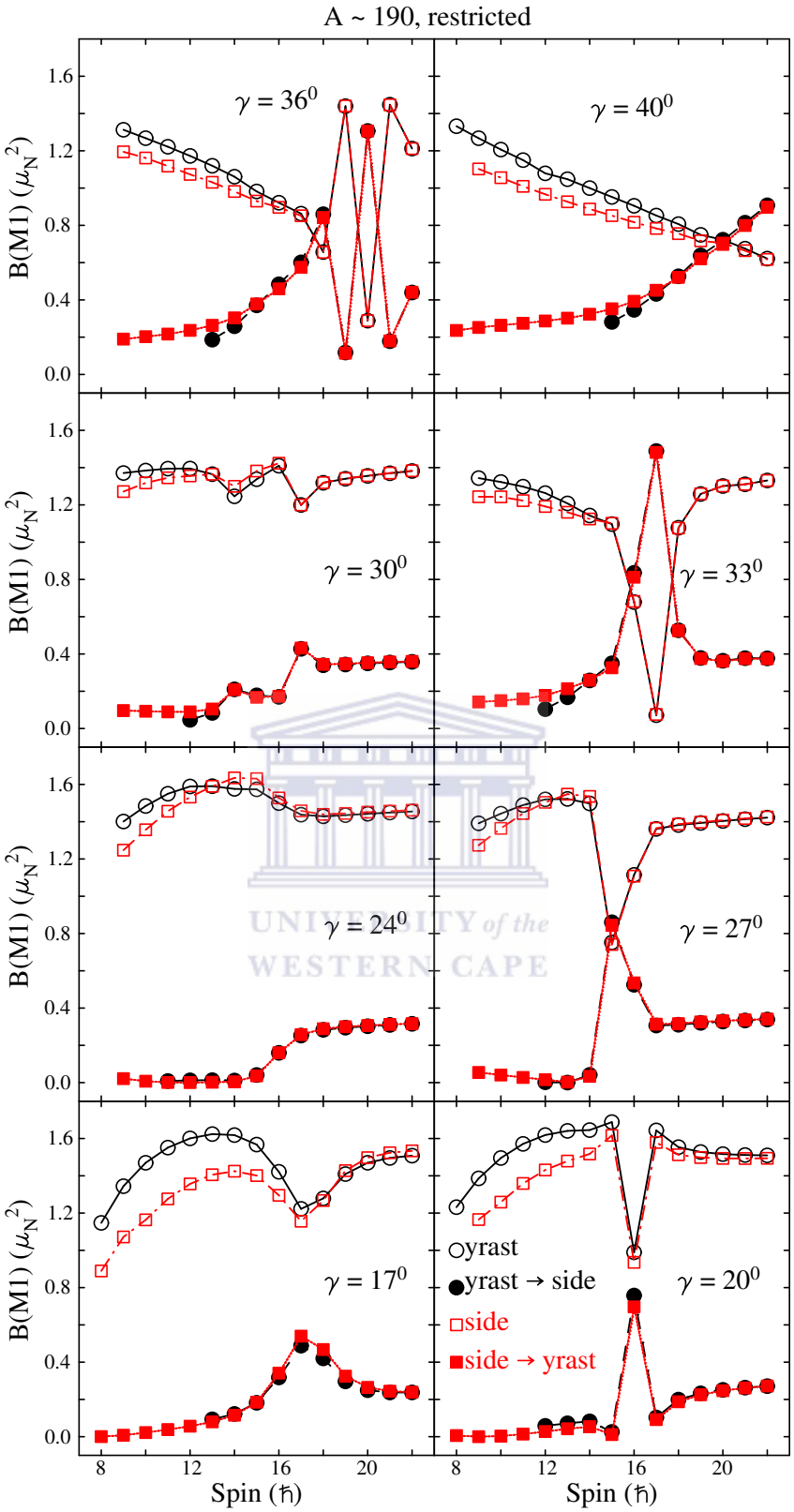

Figure 5.29: *Calculated intra- and inter-band $B(M1)$ reduced transition probabilities for the partner bands in A ~ 190 mass region. Open and filled symbols denote intra- and inter-band $B(M1)$ transitions respectively. The calculations were performed with ε_2 = 0.15 and γ = 17⁰, 20⁰, 24⁰, 27⁰, 30⁰, 33⁰, 36⁰, 40⁰.*

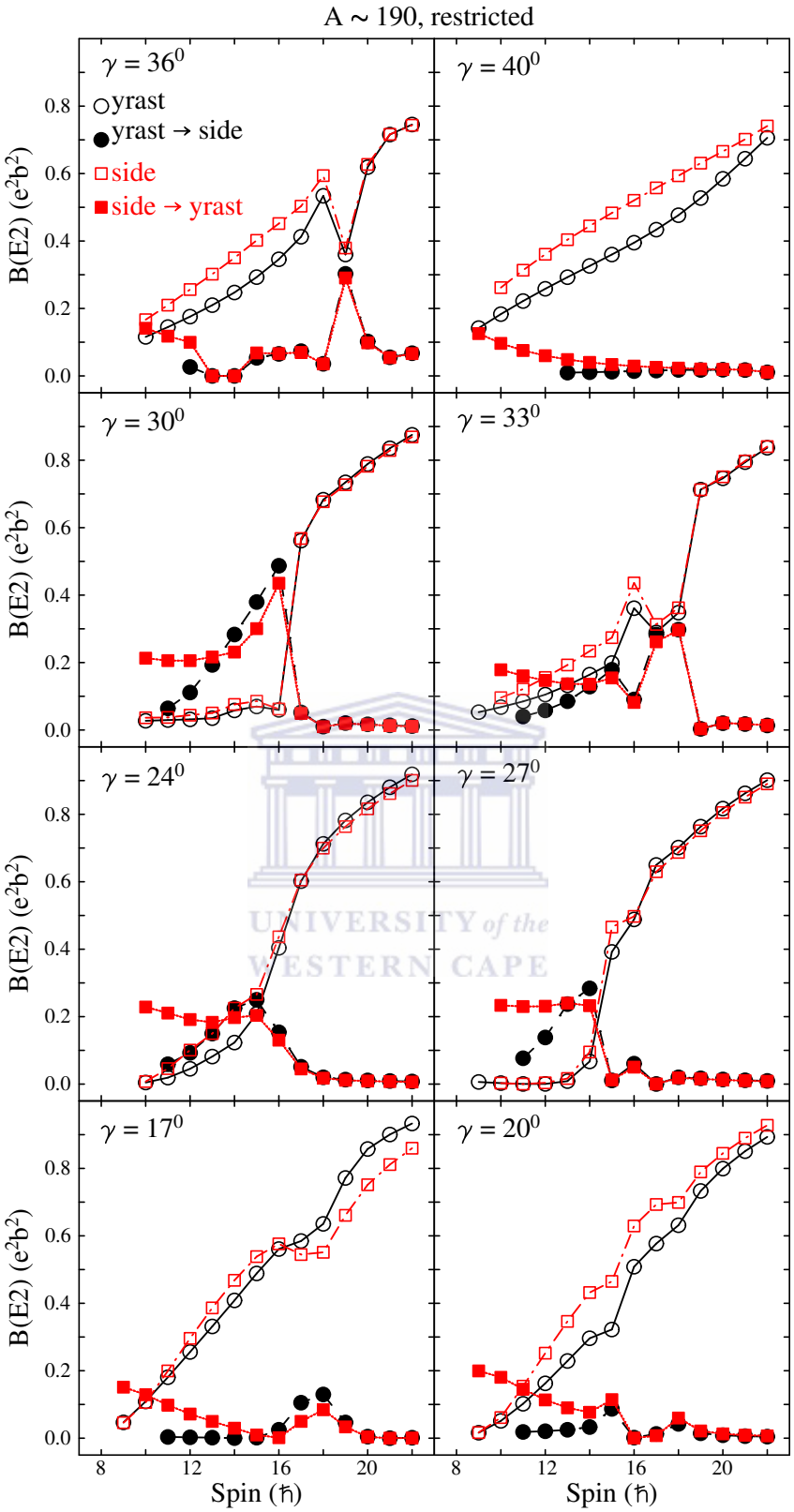

Figure 5.30: *Calculated intra- and inter-band $B(E2)$ reduced transition probabilities for the partner bands in A ~ 190 mass region. Open and filled symbols denote intra- and inter-band $B(E2)$ transitions respectively. The calculations were performed with ε_2 = 0.15 and γ = 17⁰, 20⁰, 24⁰, 27⁰, 30⁰, 33⁰, 36⁰, 40⁰.*

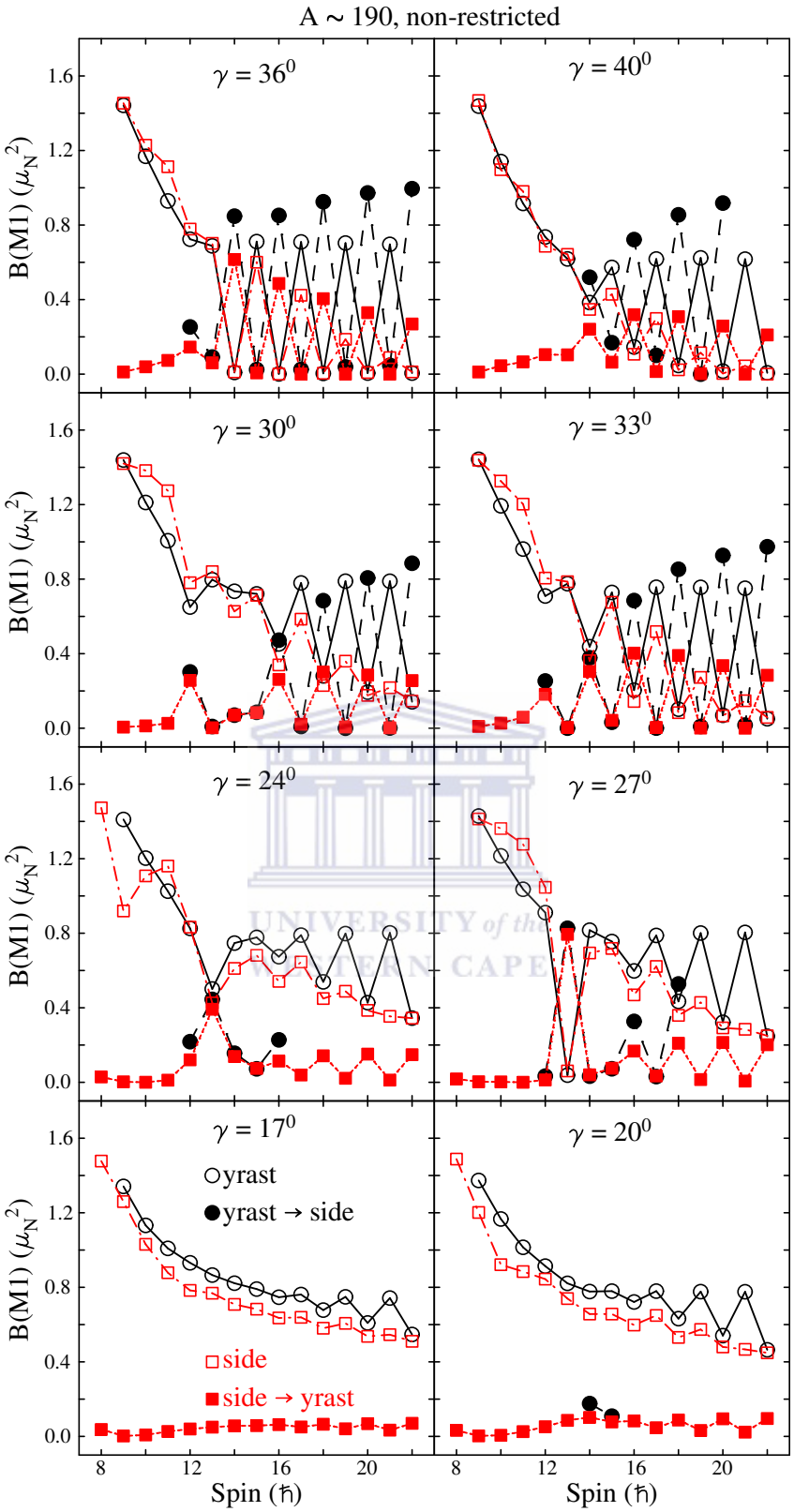

Figure 5.31: *Calculated intra- and inter-band $B(M1)$ reduced transition probabilities for the partner bands in A ~ 190 mass region. Open and filled symbols denote intra- and inter-band $B(M1)$ transitions respectively. The calculations were performed with ε_2 = 0.15 and γ = 17⁰, 20⁰, 24⁰, 27⁰, 30⁰, 33⁰, 36⁰, 40⁰.*

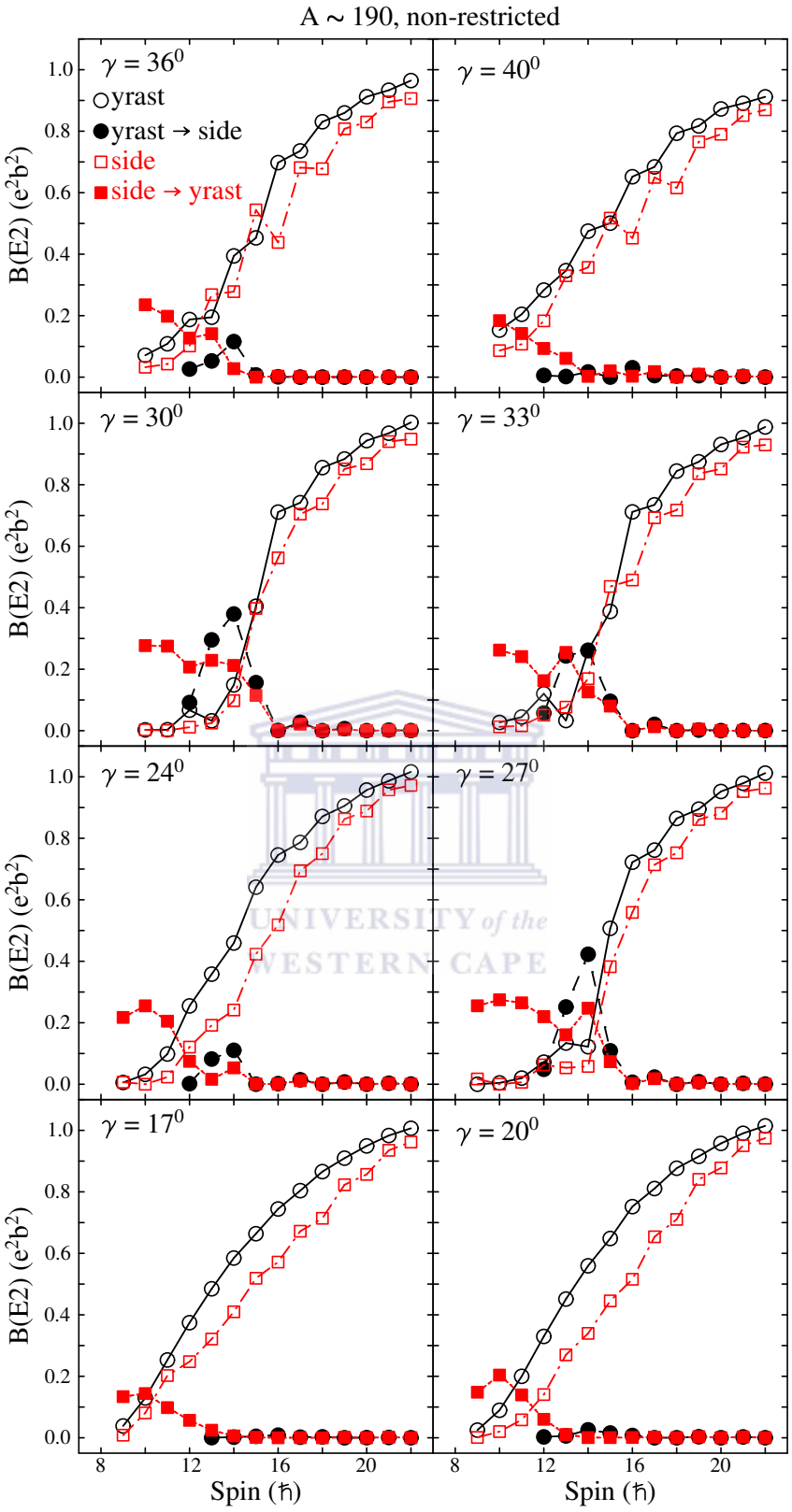

Figure 5.32: *Calculated intra- and inter-band $B(E2)$ reduced transition probabilities for the partner bands in A ~ 190 mass region. Open and filled symbols denote intra- and inter-band $B(E2)$ transitions respectively. The calculations were performed with ε_2 = 0.15 and γ = 17^0, 20^0, 24^0, 27^0, 30^0, 33^0, 36^0, 40^0.*

5.2.1 Calculations performed with quadrupole deformation of ε_2 = 0.25

In general the increase in ε_2 has largest impact on the properties of the partner bands calculated with non-restricted configurations (for example compare Figures 5.4 and 5.33 and Tables A.2, A.73). One can see first of all that the energy staggering parameter $S(I)$ is almost independent of the spin (see Figure 5.34), while substantial staggering was present in the previous "standard" calculations (see Figures 5.19 and Tables A.5, A.8, A.74). Such behaviour is expected and shows that by increasing the deformation the Coriolis effects become substantially smaller, which leads to the disappearance of the energy staggering. The calculations performed with restricted configurations show no significant impact on the values of the energy staggering parameter.

No significant impact on the values of the intra- and inter-band $B(M1)$ transitions was found, except that at $\gamma = 30^0$ the magnitude of $B(M1)$ staggering is a bit higher for restricted configurations than in the previous standard calculations (see Figures 5.25, 5.27, 5.35 and Tables A.49-50, A.62-63, A.75). In the case of non-restricted configuration, the magnitude of the $B(M1)$ staggering is reduced for $\varepsilon_2 = 0.25$, but at low spins where staggering is absent their values are comparable (see Figures 5.27, 5.35 and Tables A.49-50, A.75). The values of the $B(E2)$ transition probabilities are raised by a factor of ~3 for $\varepsilon_2 = 0.25$ reflecting the increase in the quadrupole moment (see Figures 5.26, 5.28, 5.36 and Tables A.51-52, A.64-65, A.76).

Therefore, the weakening of the Coriolis effects is not sufficient to ensure degeneracy in the chiral partner bands. One can notice that in fact the chiral partner bands at $\varepsilon_2 = 0.25$ do not show properties substantially closer to degeneracy (see Figure 5.33 and Tables A.73). Thus it seems that the lack of energy staggering does not necessarily prove that the conditions for chiral symmetry are considerably better.

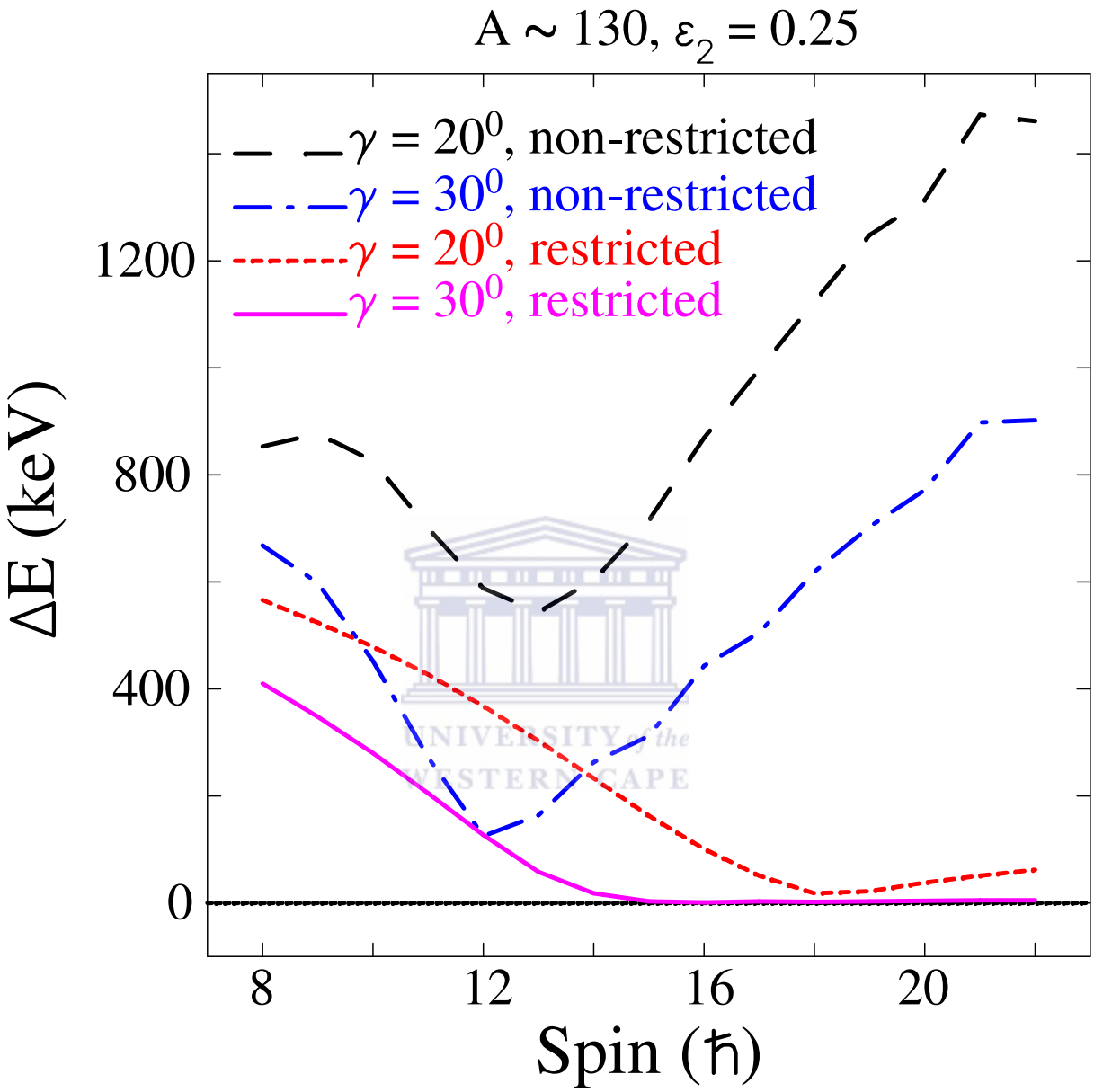

Figure 5.33: *Calculated relative excitation energy (ΔE), in A ~ 130 mass region for the four sets of parameters as described in the text, but with ε_2 = 0.25. The dashed, dash-dotted, dotted and solid lines correspond to cases (i), (ii), (ii) and (iv) respectively.*

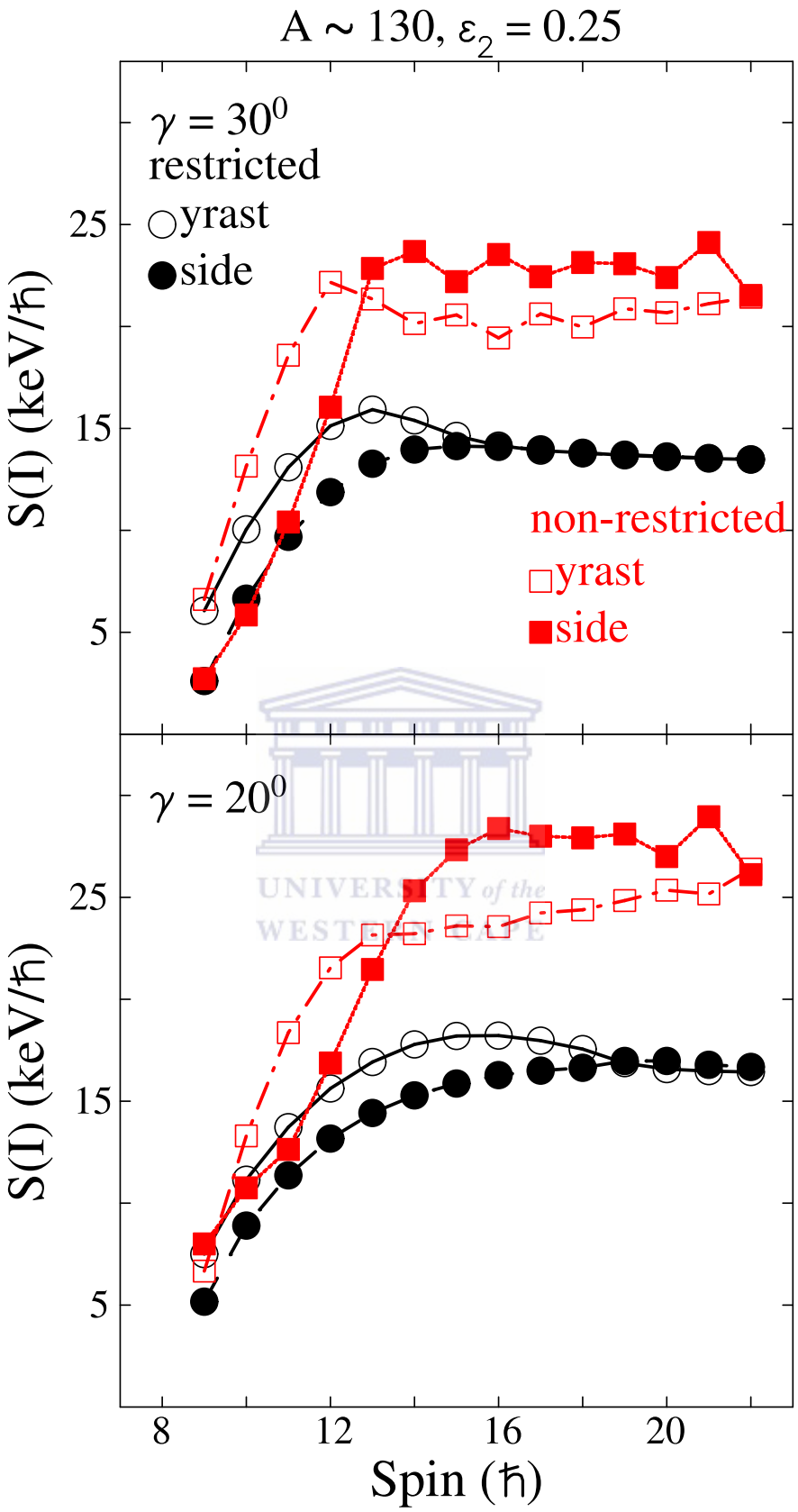

Figure 5.34: *Calculated energy staggering parameter $S(I)$ for the partner bands in A ~ 130 mass region. Open and filled symbols denote the yrast and side bands respectively. The calculations were performed with ε_2 = 0.25 and γ = 20^0, 30^0.*

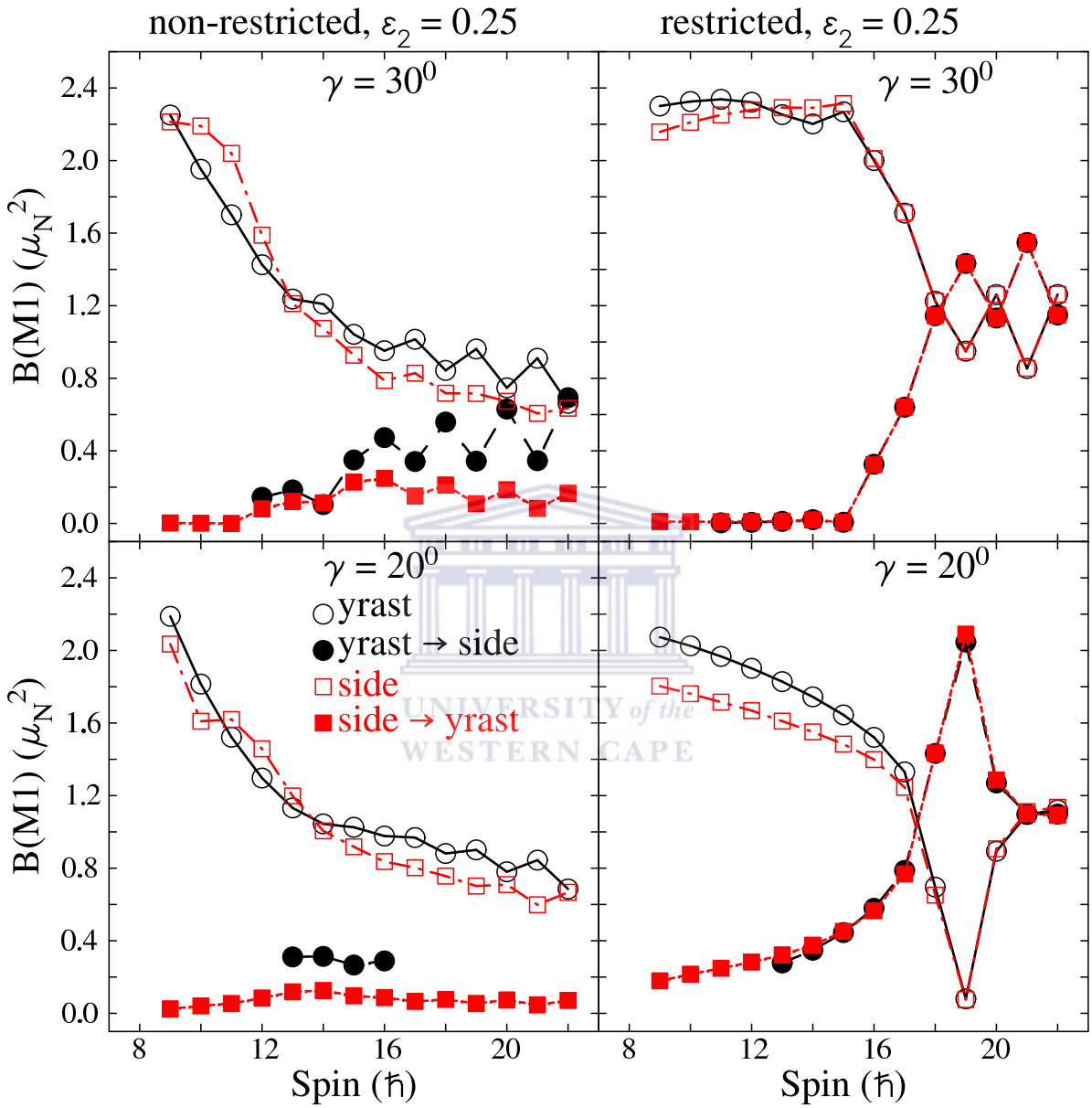

Figure 5.35: *Calculated intra- and inter-band $B(M1)$ reduced transition probabilities for the partner bands in A ~ 130 mass region. Open and filled symbols denote intra- and inter-band $B(M1)$ transitions respectively. The calculations were performed with $\varepsilon_2 = 0.25$ and $\gamma = 20^0, 30^0$.*

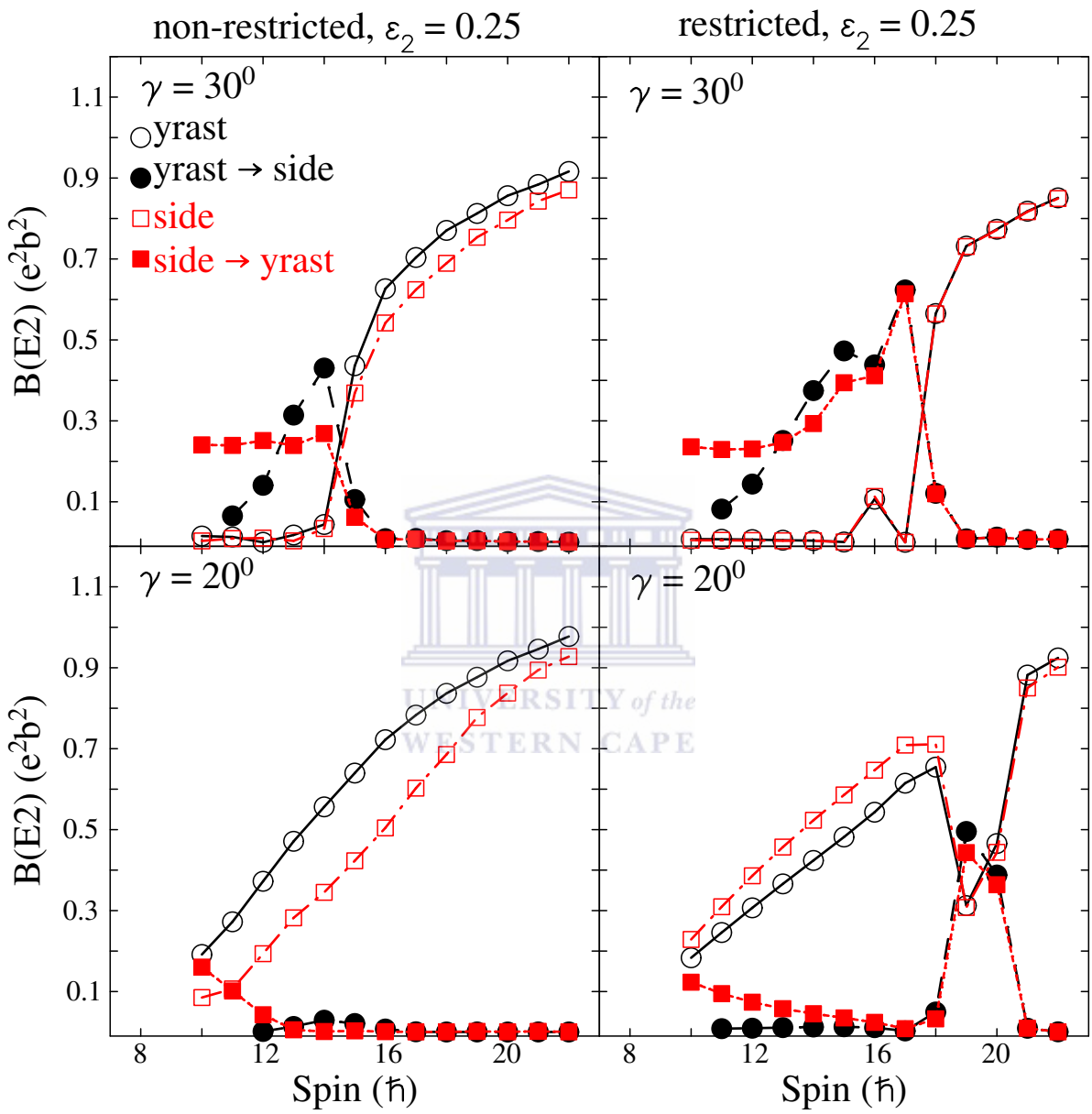

Figure 5.36: *Calculated intra- and inter-band $B(E2)$ reduced transition probabilities for the partner bands in A ~ 130 mass region. Open and filled symbols denote intra- and inter-band $B(E2)$ transitions respectively. The calculations were performed with $\varepsilon_2 = 0.25$ and $\gamma = 20^0, 30^0$.*

5.2.2 Calculations performed with Coriolis attenuation factor of ξ = 0.8

The calculations performed with restricted configuration and $\xi = 0.8$ show no impact in the degeneracy of all properties of the partner bands as compared to the previous standard calculations performed in A ~ 130 mass region (for example see Figures 5.4, 5.37 and Tables A.2, A.77). This is not a surprise because for restricted configuration lower projection of the angular momenta of the odd proton and odd neutron are not allowed. A small impact in the properties of the partner bands is found for the calculations performed with $\xi = 0.8$ and non-restricted configuration (for example see Figures 5.4, 5.37 and Tables A.2, A.77). The amplitude of the energy staggering parameter $S(I)$ for the partner bands is reduced for the calculations performed with $\xi = 0.8$ and non-restricted configurations, but this does not lead to significant improvement in the degeneracy of the partner bands (see Figures 5.19, 5.38 and Tables A.5, A.8, A.78). These calculations do not show significant impact in the amplitude of the $B(M1)$ staggering either. The values of the $B(M1)$ and $B(E2)$ transition probabilities for the partner bands are comparable between these calculations, i.e. standard calculation and calculations performed with $\xi = 0.8$ in A ~ 130 (see Figures 5.25-5.28, 4.39-4.40 and Tables A.61-65, A.79-80).

In summary it seems that there is no direct relation between the presence or lack of the energy staggering and how good the chiral symmetry is.

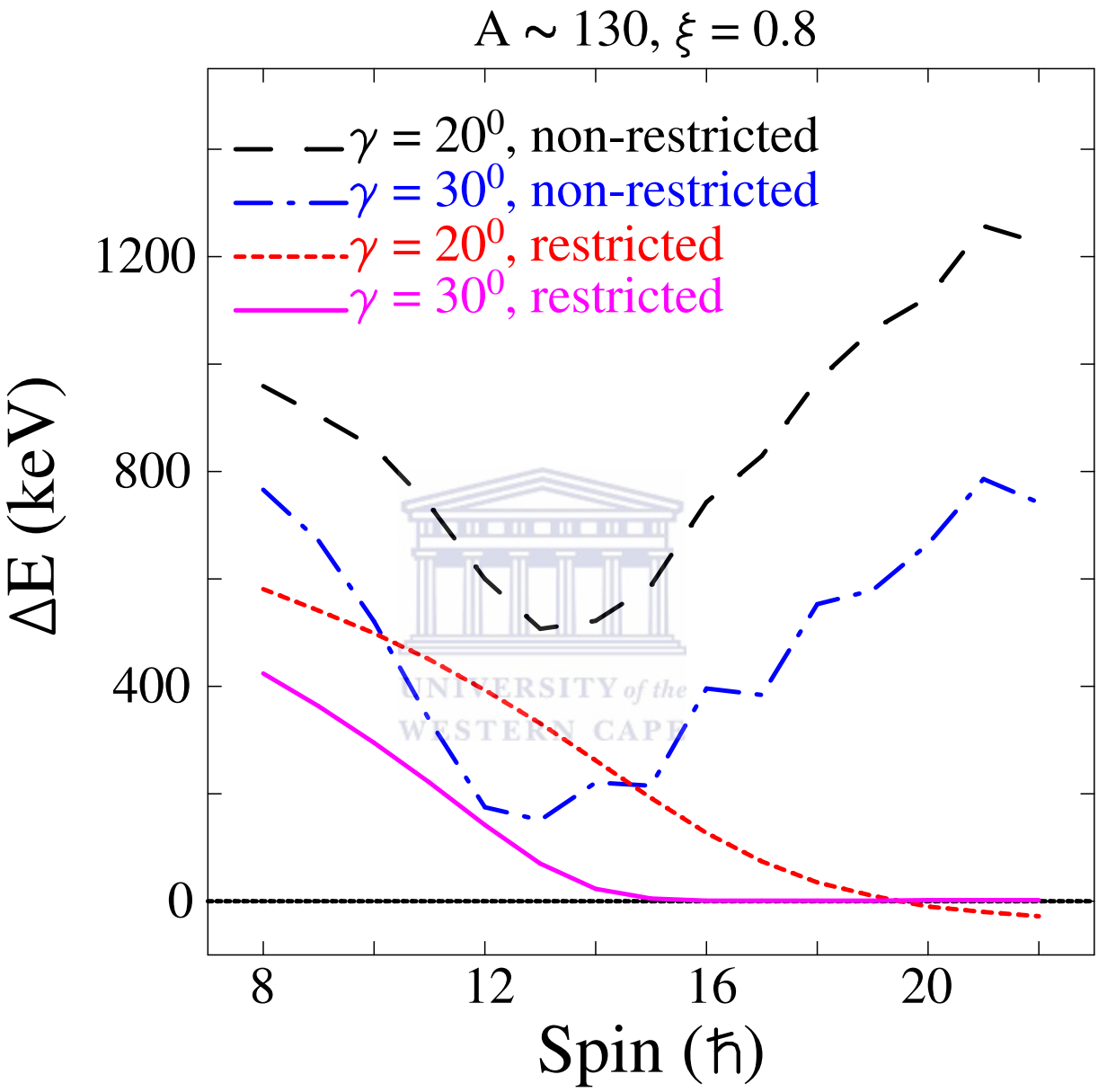

Figure 5.37: *Calculated relative excitation energy (ΔE), in A ~ 130 mass region for the four sets of parameters as described in the text, but with* $\varepsilon_2 = 0.15$, $\xi = 0.8$ *and* $\gamma = 20^0, 30^0$. *The dashed, dash-dotted, dotted and solid lines correspond to cases (i), (ii), (ii) and (iv) respectively.*

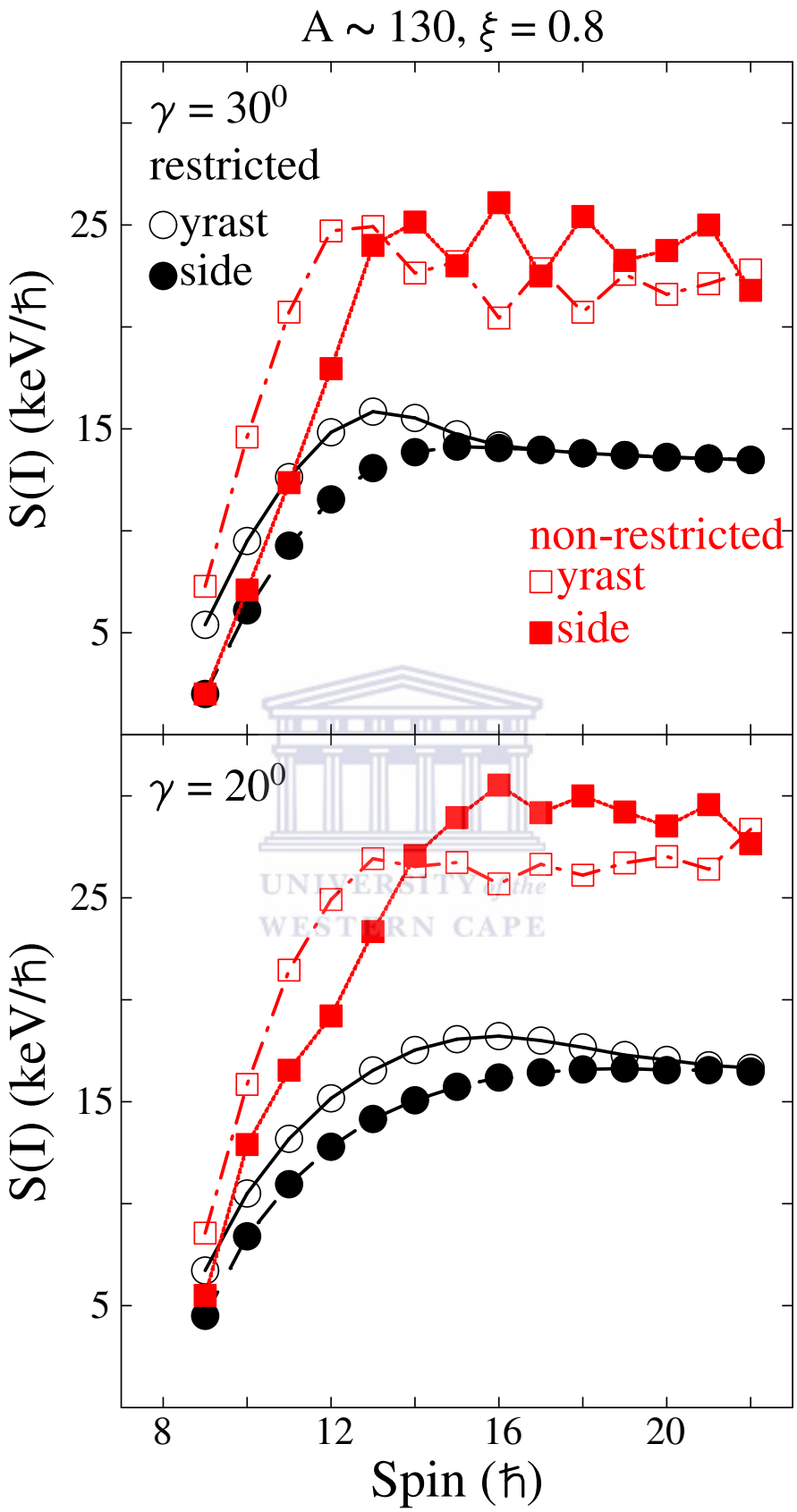

Figure 5.38: *Calculated energy staggering parameter $S(I)$ for the partner bands in A ~ 130 mass region. Open and filled symbols denote the yrast and side bands respectively. The calculations were performed with $\varepsilon_2 = 0.15$, $\xi = 0.8$ and $\gamma = 20^0, 30^0$.*

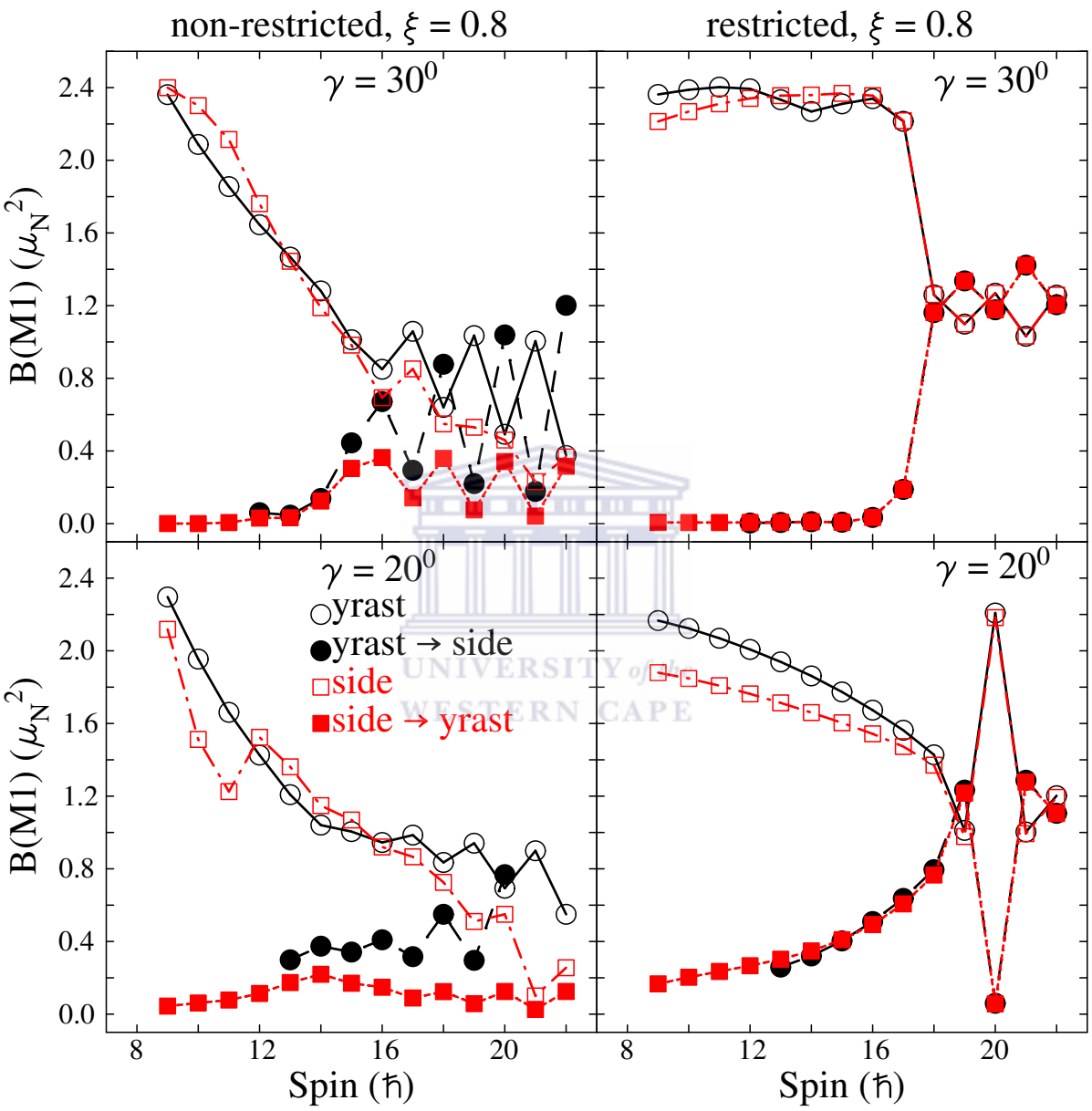

Figure 5.39: *Calculated intra- and inter-band $B(M1)$ reduced transition probabilities for the partner bands in A ~ 130 mass region. Open and filled symbols denote intra- and inter-band $B(M1)$ transitions respectively. The calculations were performed with $\varepsilon_2 = 0.15$, $\xi = 0.8$ and $\gamma = 20^0, 30^0$.*

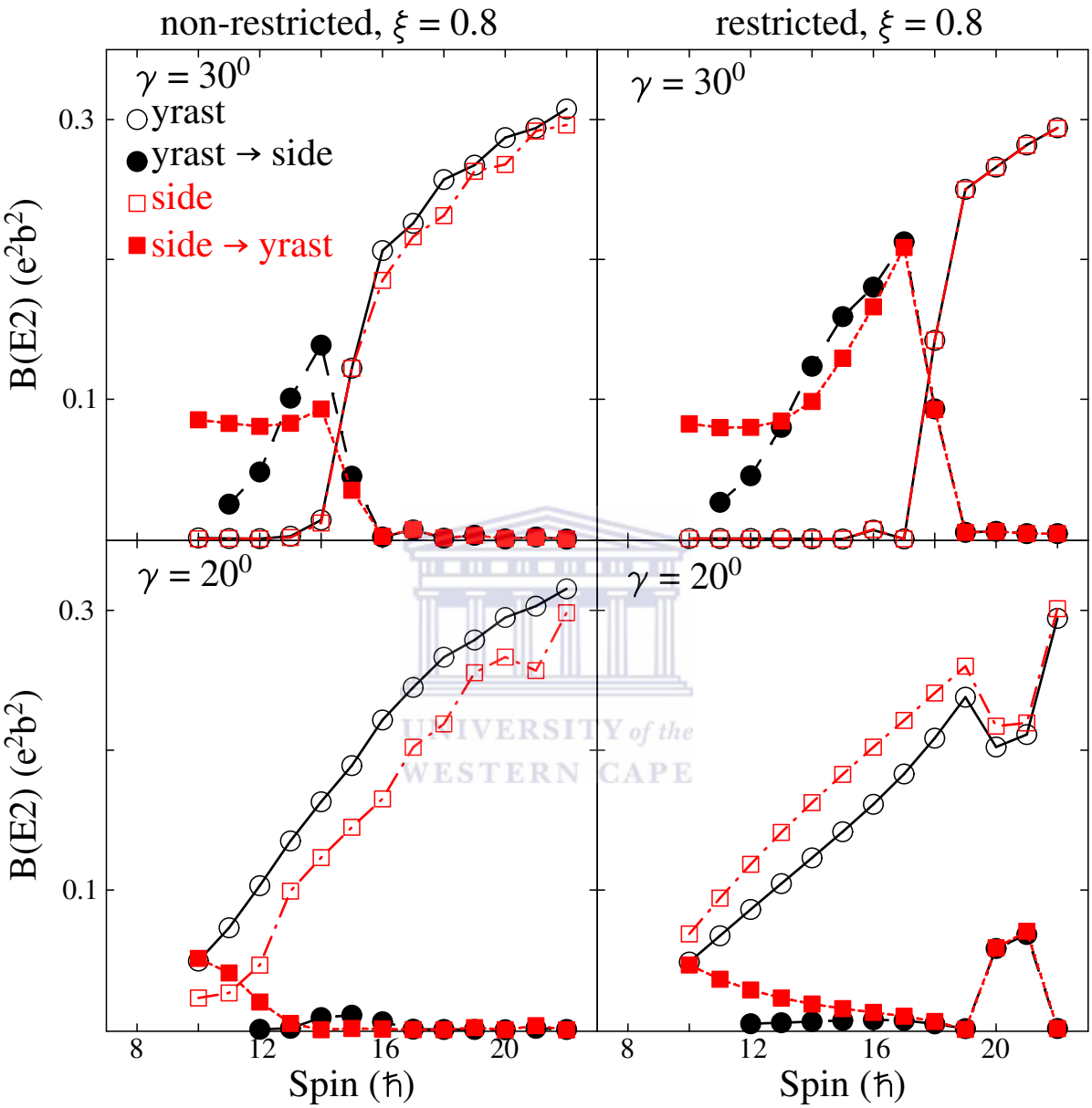

Figure 5.40: *Calculated intra- and inter-band $B(E2)$ reduced transition probabilities for the partner bands in A ~ 130 mass region. Open and filled symbols denote intra- and inter-band $B(E2)$ transitions respectively. The calculations were performed with ε_2 = 0.15, ξ = 0.8 and γ = 20⁰, 30⁰.*

5.2.3 Calculations performed with a change in the Fermi surface λ_F

The calculations performed with a change in the Fermi surface of either the proton, the neutron or both the proton and neutron show a significant impact in the degeneracy of the properties for the partner bands (see Figures 5.4, 5.41 and Tables A.2, A.81).

At $\gamma = 30^0$ (where we have best degeneracy for standard calculation) there is large displacement in the values of ΔE for the calculations performed with a change in the Fermi surface of either the proton, the neutron or both the proton and neutron (see Figures 5.4, 5.41 and Tables A.2, A.81). Better near-degeneracy is found at specific values of γ, but it is never as good as the previous standard calculations. Best near-degeneracy is found for $\gamma = 24^0, 27^0, 30^0$; $\gamma = 36^0, 40^0$; and $\gamma = 33^0, 36^0$ for the calculations performed with a change in the Fermi surface of the neutron, the proton and both the proton and neutron respectively (see Figure 5.41 and Table A.81)

In general, smooth dependence of the energy staggering parameter $S(I)$ within the partner bands was found for all values of γ which is expected for such restricted configurations. Interestingly some staggering was found for some values of γ close to 30^0 in the calculations performed with a change in Fermi surface of both the proton and the neutron (see Figures 5.42-5.44 and Tables A.82-84). It's origin is not well understood.

Staggering in the intra- and inter-band $B(M1)$ transitions was found for the cases when the partner bands are near-degenerate (see Figures 5.45, 5.47, 5.49 and Tables A.85-86, A.89-90, A.93-94). For calculations performed with a change in the Fermi surface of the proton, the largest $B(M1)$ staggering is found at $\gamma = 40^0$ (see Figures 5.45). For calculations performed with a change in the Fermi surface of the neutron, the largest $B(M1)$ staggering is found at $\gamma = 27^0$ (see Figure 5.47). For calculations performed with a change in the Fermi surface of both the proton and the neutron, the largest $B(M1)$ staggering is found at $\gamma = 33^0$ and 36^0 (see Figure 5.49). The phase of the $B(M1)$ staggering remains the same as in the standard calculations if there is a change in the Fermi surface of the neutron or both the proton and neutron. It is however opposite (high at odd spins and low at even spins) if the Fermi level of the proton is changed. The trend of behaviour for the intra- and inter-band $B(E2)$ transitions is similar to that found for the standard calculations (see Figures 5.26, 5.46, 5.48, 5.50).

In summary, a change in the Fermi surface of either the proton, the neutron or both the proton and the neutron hinders the degeneracy between the partner bands. Therefore, the optimal for chiral symmetry nucleon configuration is when the odd proton and the odd neutron occupy

the lowest- and the highest-energy orbitals of the high-j shell. It is interesting to note that to a certain extend the loss of degeneracy when the Fermi surface is changed can be compensated by a small change in γ away from $\gamma = 30^0$. Nevertheless one cannot obtain a similarity in the partner bands as good as that of the standard calculations. Staggering in the $B(M1)$ transition probabilities occurs when the partner bands exhibit best near-degeneracy and may gradually disappear when γ is changed.

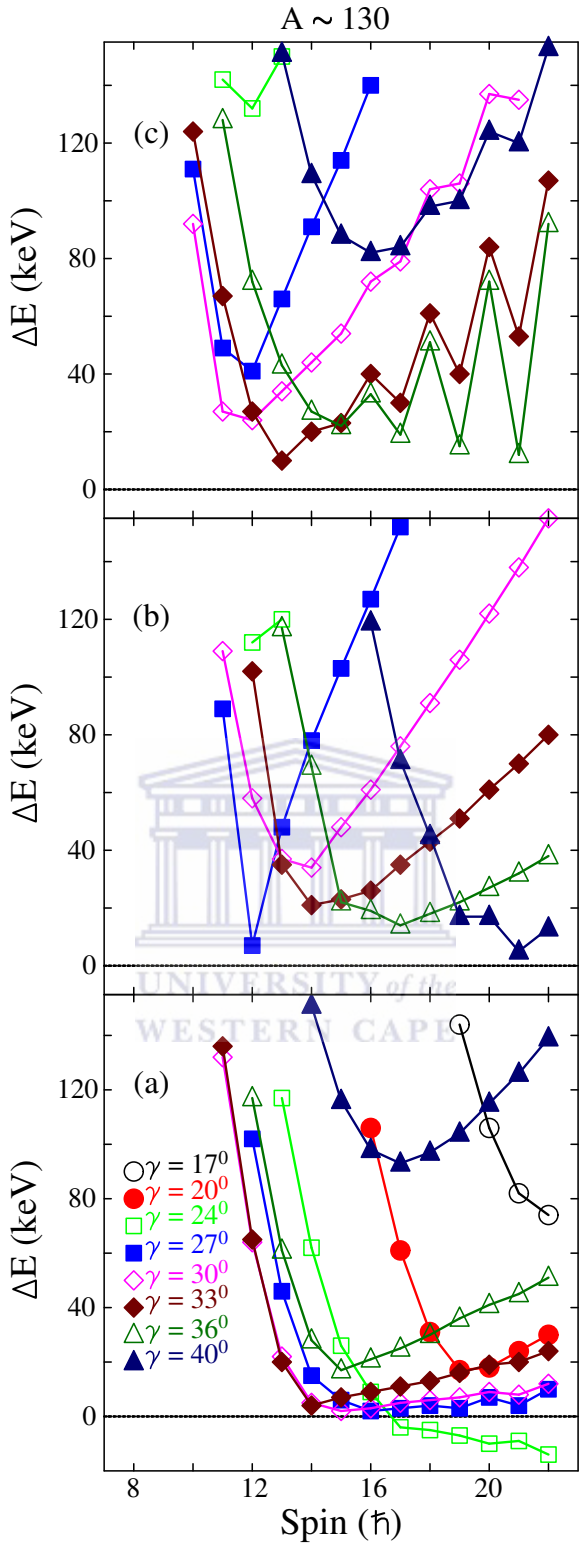

Figure 5.41: *Calculated relative excitation energy (ΔE) for the partner bands in A ~ 130 mass region. The bottom (a), middle (b) and top (c) panels correspond to the calculations performed with a change in the Fermi surface of the neutron, calculations performed with a change in the Fermi surface of the proton, and the calculations performed with a change in the Fermi surface of both the proton and neutron, respectively. The calculations were performed with* $\varepsilon_2 = 0.15$ *and* $\gamma = 17^0, 20^0, 24^0, 27^0, 30^0, 33^0, 36^0, 40^0$.

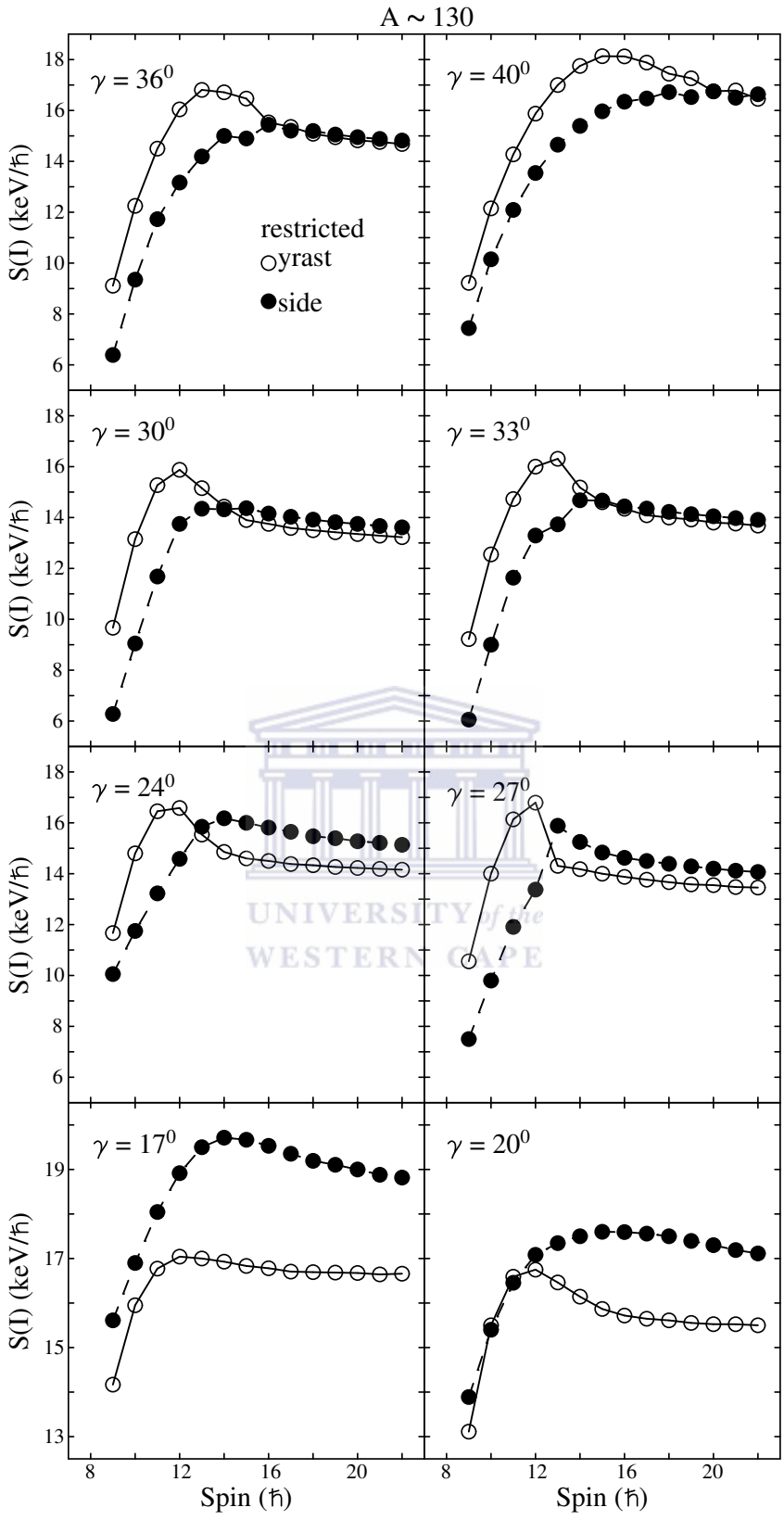

Figure 5.42: *Calculated energy staggering parameter $S(I)$ for the partner bands in A ~ 130 mass region. Open and filled symbols denote the yrast and side bands respectively. The calculations were performed with ε_2 = 0.15, γ = 17⁰, 20⁰, 24⁰, 27⁰, 30⁰, 33⁰, 36⁰, 40⁰ and a change in the Fermi surface of the proton.*

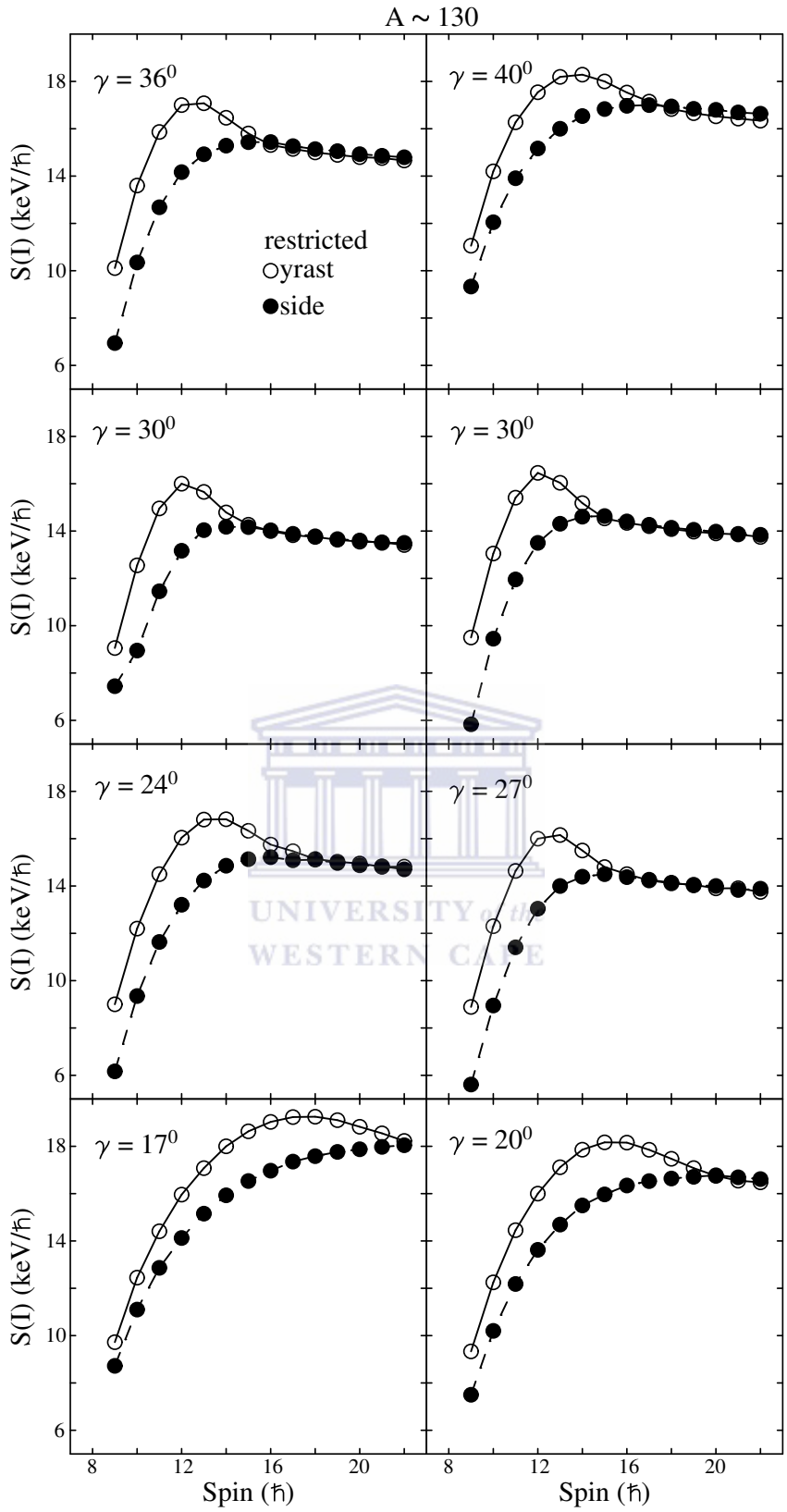

Figure 5.43: *Calculated energy staggering parameter $S(I)$ for the partner bands in A ~ 130 mass region. Open and filled symbols denote the yrast and side bands respectively. The calculations were performed with ε_2 = 0.15, γ = 17⁰, 20⁰, 24⁰, 27⁰, 30⁰, 33⁰, 36⁰, 40⁰ and a change in the Fermi surface of the neutron.*

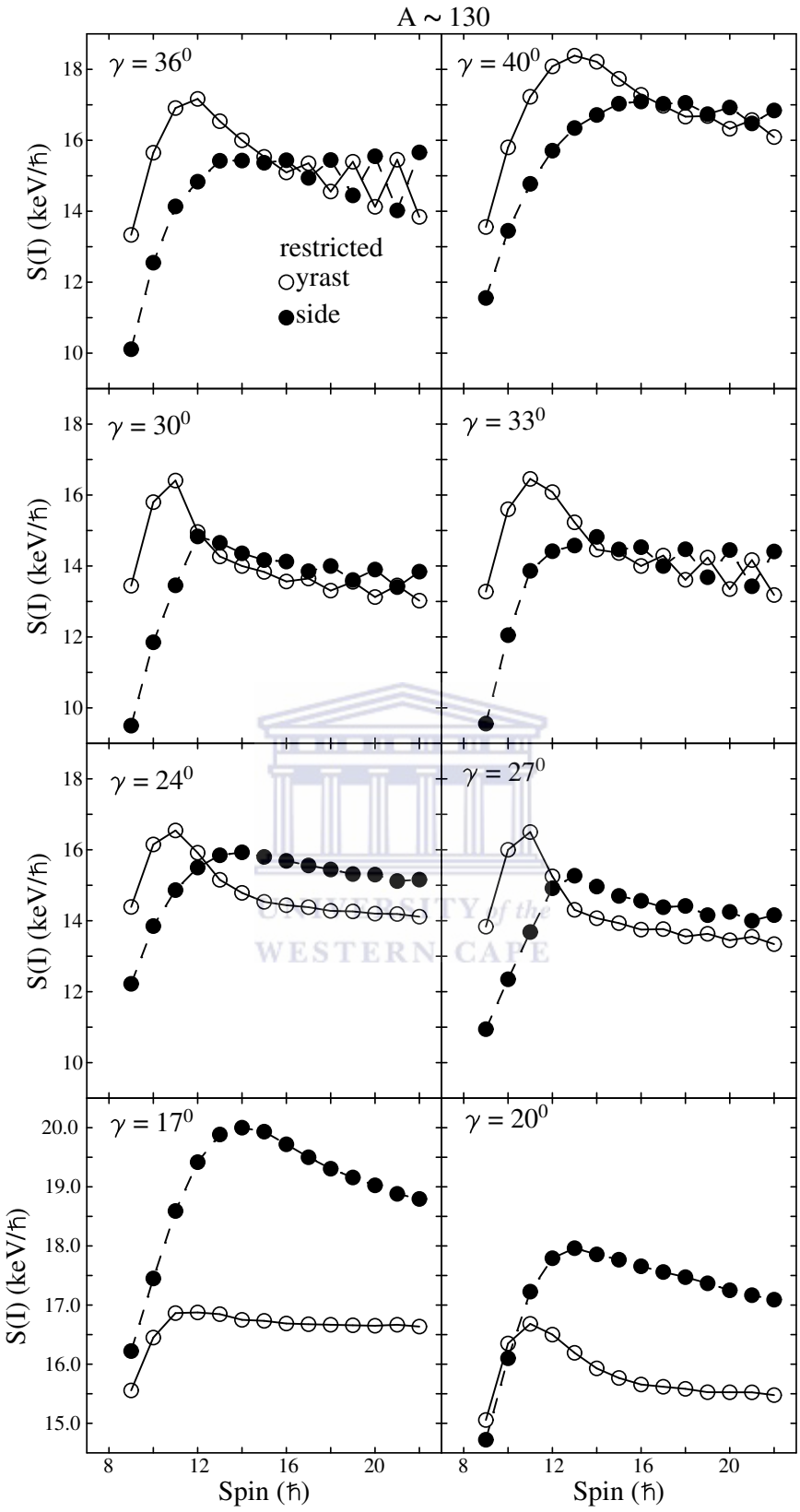

Figure 5.44: *Calculated energy staggering parameter $S(I)$ for the partner bands in A ~ 130 mass region. Open and filled symbols denote the yrast and side bands respectively. The calculations were performed with ε_2 = 0.15, γ = 17⁰, 20⁰, 24⁰, 27⁰, 30⁰, 33⁰, 36⁰, 40⁰ and a change in the Fermi surface of both the proton and the neutron.*

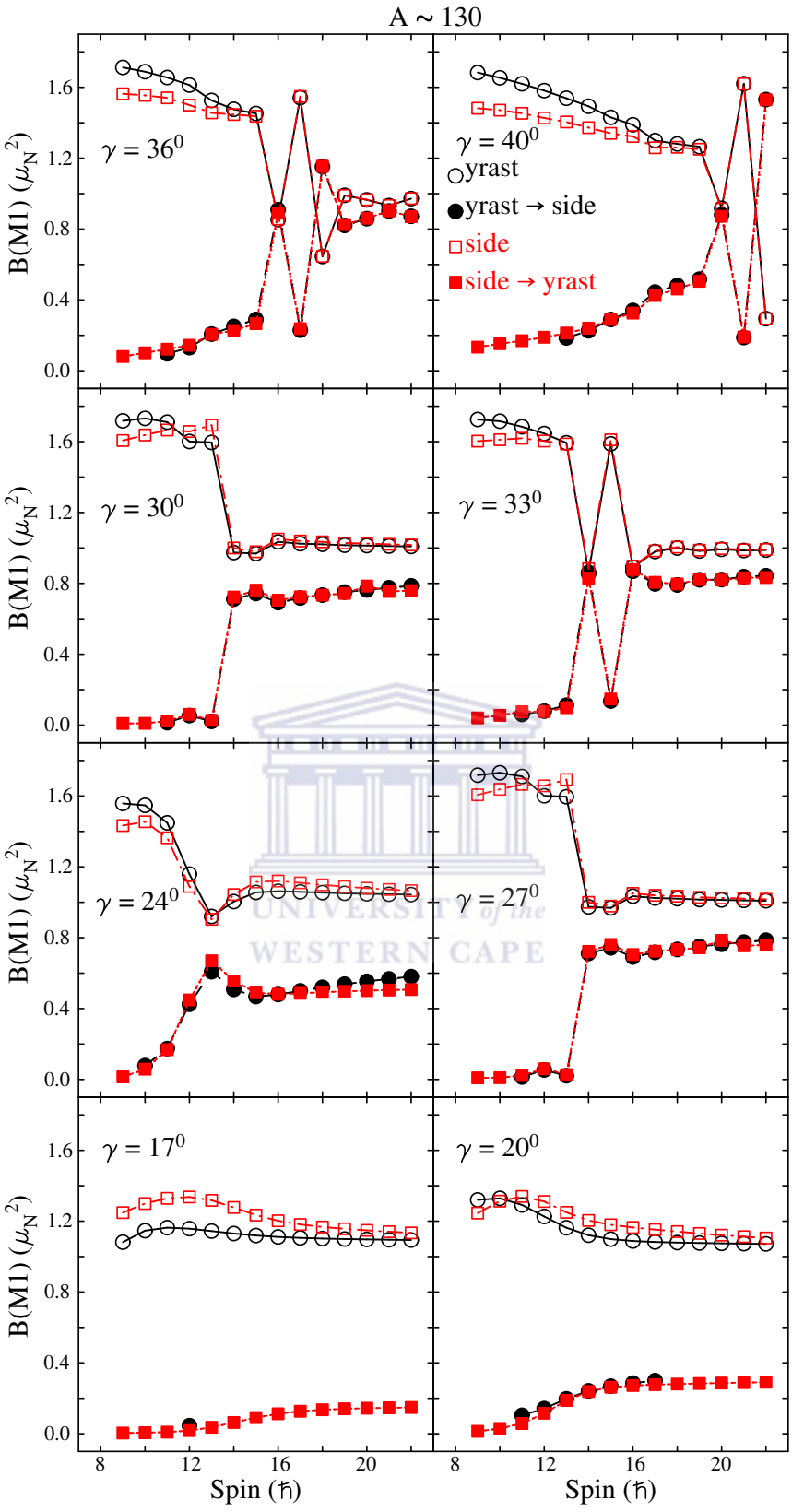

Figure 5.45: *Calculated intra- and inter-band $B(M1)$ reduced transition probabilities for the partner bands in A ~ 130 mass region. Open and filled symbols denote intra- and inter-band $B(M1)$ transitions respectively. The calculations were performed with $\varepsilon_2 = 0.15$, $\gamma = 17^0, 20^0, 24^0, 27^0, 30^0, 33^0, 36^0, 40^0$ and a change in the Fermi surface of the proton.*

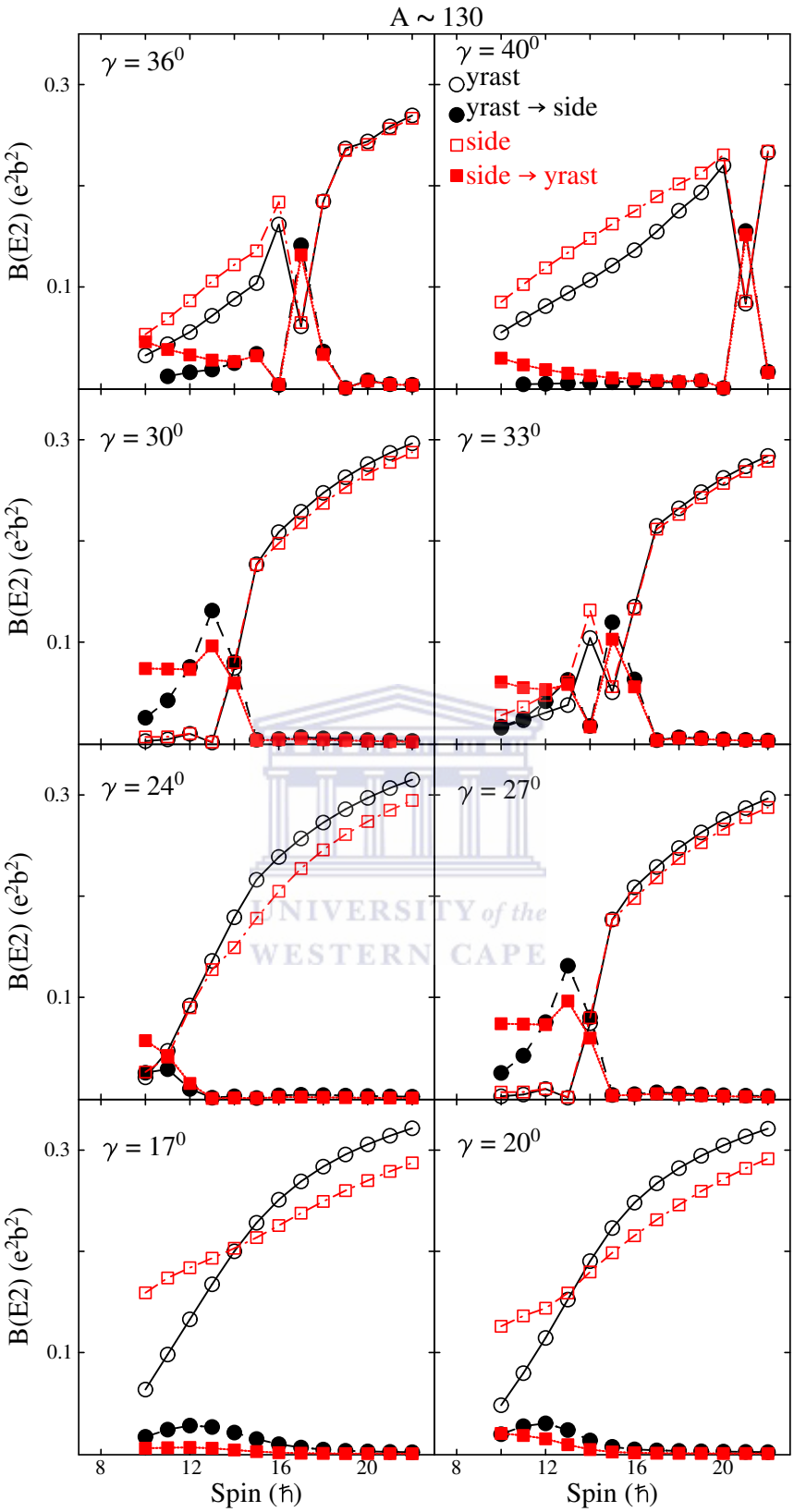

Figure 5.46: *Calculated intra- and inter-band $B(E2)$ reduced transition probabilities for the partner bands in A ~ 130 mass region. Open and filled symbols denote intra- and inter-band $B(E2)$ transitions respectively. The calculations were performed with ε_2 = 0.15, γ = 17^0, 20^0, 24^0, 27^0, 30^0, 33^0, 36^0, 40^0 and a change in the Fermi surface of the proton.*

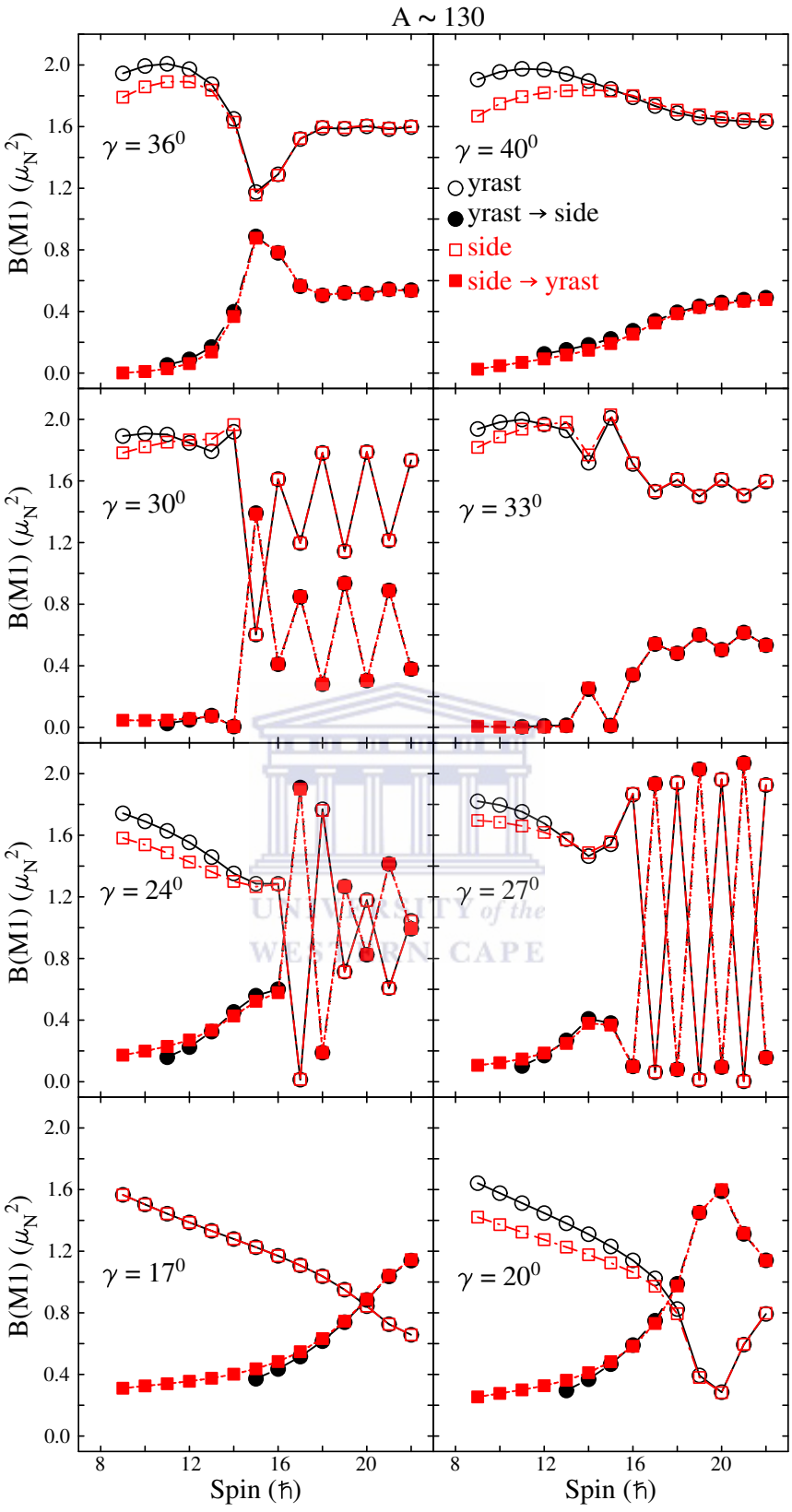

Figure 5.47: *Calculated intra- and inter-band $B(M1)$ reduced transition probabilities for the partner bands in A ~ 130 mass region. Open and filled symbols denote intra- and inter-band $B(M1)$ transitions respectively. The calculations were performed with $\varepsilon_2 = 0.15$, $\gamma = 17^0, 20^0, 24^0, 27^0, 30^0, 33^0, 36^0, 40^0$ and a change in the Fermi surface of the neutron.*

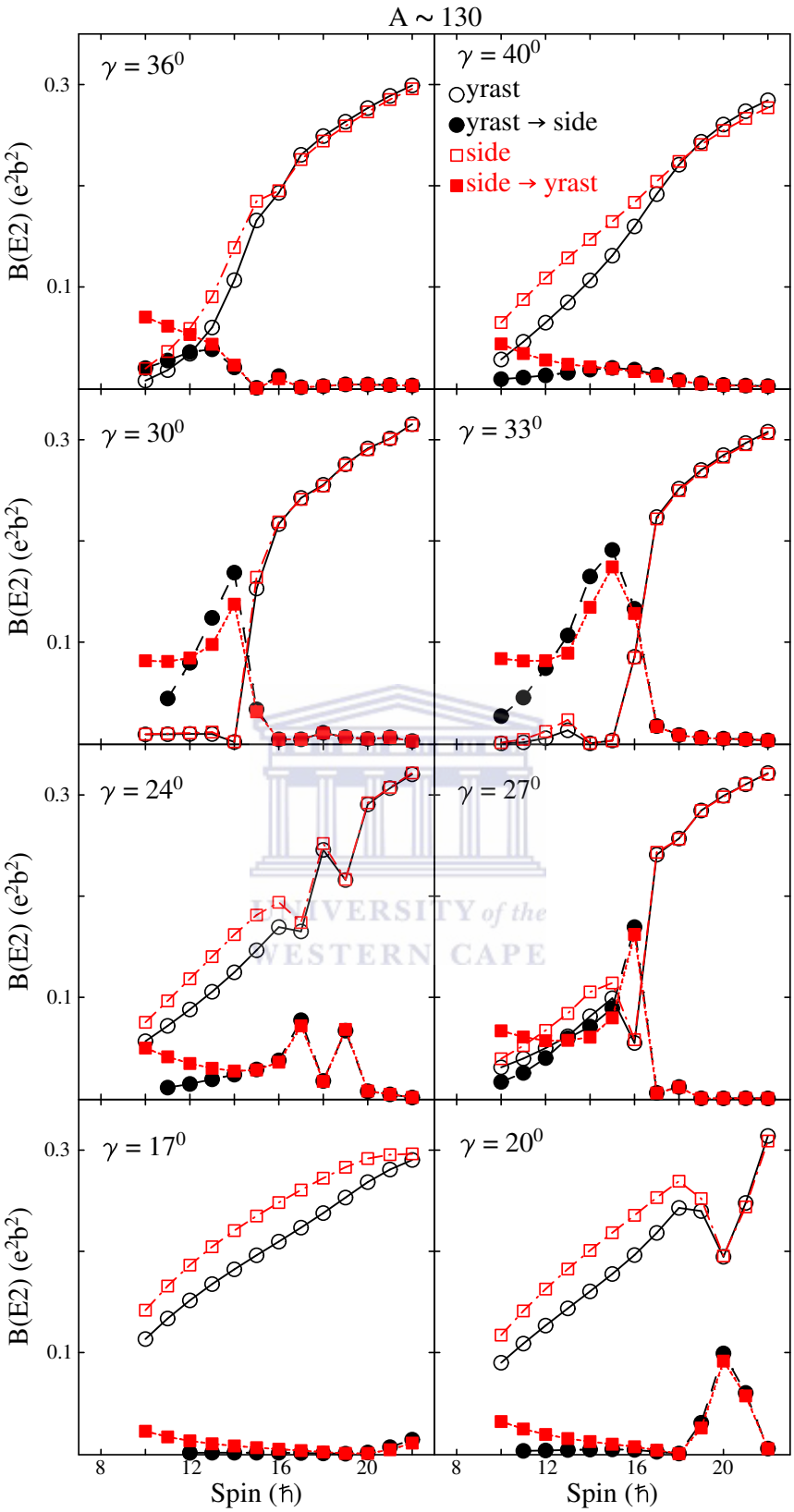

Figure 5.48: *Calculated intra- and inter-band $B(E2)$ reduced transition probabilities for the partner bands in A ~ 130 mass region. Open and filled symbols denote intra- and inter-band $B(E2)$ transitions respectively. The calculations were performed with $\varepsilon_2 = 0.15$, $\gamma = 17^0, 20^0, 24^0, 27^0, 30^0, 33^0, 36^0, 40^0$ and a change in the Fermi surface of the neutron.*

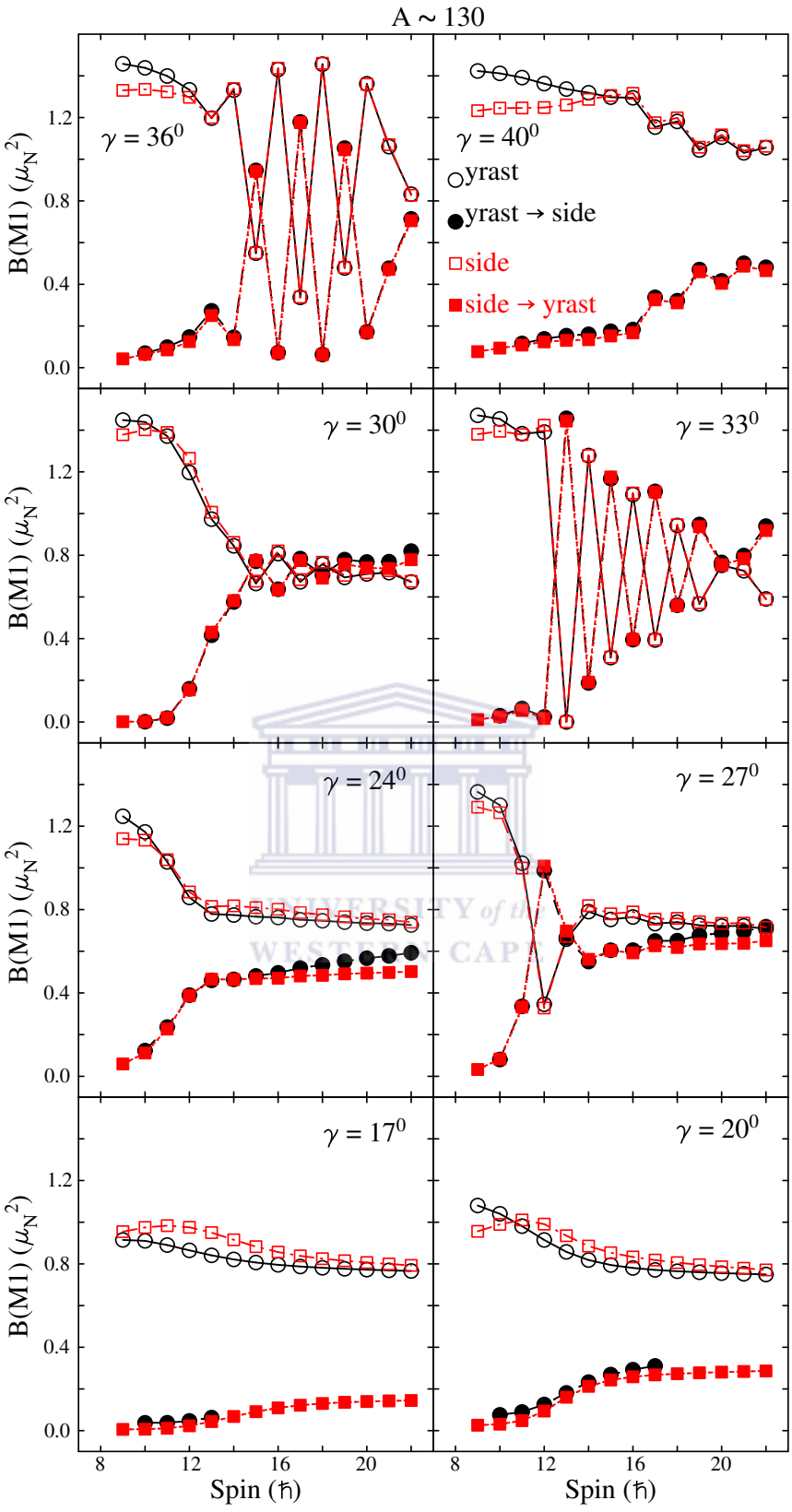

Figure 5.49: *Calculated intra- and inter-band $B(M1)$ reduced transition probabilities for the partner bands in A ~ 130 mass region. Open and filled symbols denote intra- and inter-band $B(M1)$ transitions respectively. The calculations were performed with $\varepsilon_2 = 0.15$, $\gamma = 17^0, 20^0, 24^0, 27^0, 30^0, 33^0, 36^0, 40^0$ and a change in the Fermi surface of both the proton and the neutron.*

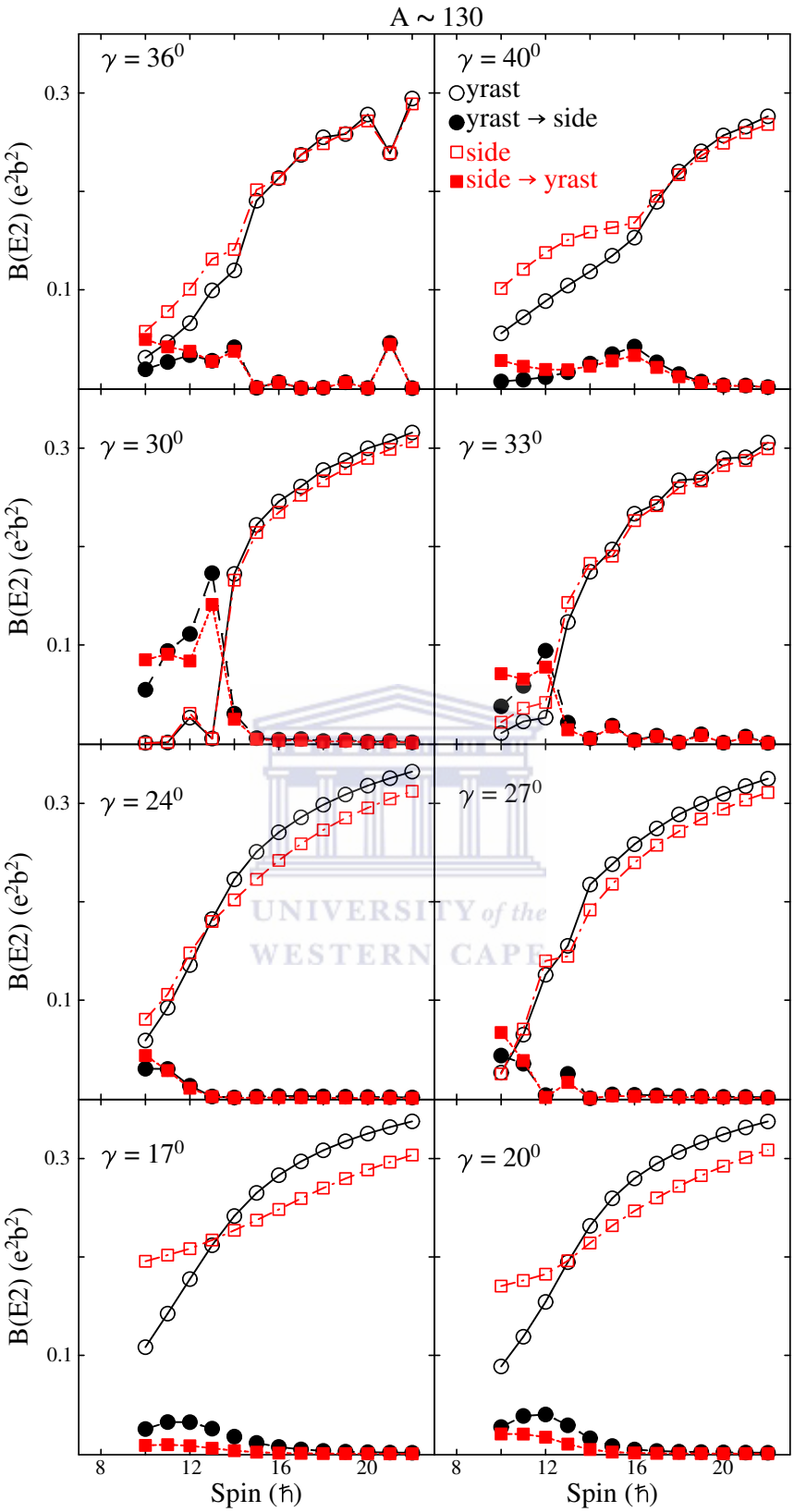

Figure 5.50: *Calculated intra- and inter-band $B(E2)$ reduced transition probabilities for the partner bands in A ~ 130 mass region. Open and filled symbols denote intra- and inter-band $B(E2)$ transitions respectively. The calculations were performed with $\varepsilon_2 = 0.15$, $\gamma = 17^0, 20^0, 24^0, 27^0, 30^0, 33^0, 36^0, 40^0$ and a change in the Fermi surface of both the proton and the neutron.*

CHAPTER 6 Summary

In this study the two-quasiparticle-plus-triaxial rotor (TQPRM) calculations were performed for the partner bands associated with $\pi g_{9/2}^{-1} \otimes \nu h_{11/2}$, $\pi h_{11/2} \otimes \nu h_{11/2}^{-1}$ and $\pi h_{9/2} \otimes \nu i_{13/2}^{-1}$ configurations in the A ~ 100, 130 and 190 mass regions. In summary, the calculations performed with "non-restricted" (the odd proton and the odd neutron span five orbitals each, while the Fermi surfaces are located at the lowest- and highest-energy orbitals of a high-j shells) and "restricted" (the odd proton and the odd neutron are restricted to one orbital each located at the lowest- and highest-energy orbitals or vice versa of a high-j shells) configurations show that the total angular momentum is aplanar in all three mass regions, having on average large projections on all three nuclear axes, with major contributions from the particle, the hole and the core angular momenta on the short, long and intermediate nuclear axes respectively. Thus the requirement for the formation of a chiral system is fulfilled.

Degeneracy between the partner bands was found only for the calculations performed with restricted configurations (i.e. the odd proton and the odd neutron are restricted to one orbital each located at the lowest- and highest-energy orbitals or vice versa of a high-j shells) in all three mass regions. The degeneracy occurs simultaneously in all properties of the partner bands. The calculations showed that for strongly broken chirality to occur, perfect alignment of the angular momenta of the two odd particles and the core along the nuclear axes is needed, i.e. three mutually orthogonal angular momenta. Even small contributions with lower alignments of the particle angular momenta lead to a loss of the degeneracy in all properties of the partner bands. The requirement for such perfect alignment seems to be unreachable for real nuclei, where components with vanishing rotation along the intermediate axis at low spins, and Coriolis effects at high spins destroy the degeneracy in the chiral bands. This might explain why no degenerate chiral bands are found so far in nuclei. Some of the results of this work for the symmetric $\pi h_{11/2} \otimes \nu h_{11/2}^{-1}$ nucleon configuration in A ~ 130 mass regions are published in reference [Law10a]. More results can be found in references [Shi11a-c].

Allowing a larger configuration space i.e. non-restricted configurations (the odd proton and the odd neutron span for instance five orbitals each, while the Fermi surfaces are located at the lowest- and highest-energy orbitals or vice versa of the high-j shells) has much larger effect in destroying the degeneracy than many others, (for example a change in non-axiality parameter γ to 20^0, a move of the Fermi levels of either nucleon or for both the proton and

neutron to the second lowest-energy and second highest-energy orbitals in the high-j shell, etc). The calculations also showed that optimal conditions for chirality may require γ slight different from 30^0 particularly for asymmetric configurations.

Other fingerprints of chirality such as intra- and inter-band $B(M1)$ reduced transition probabilities and energy staggering parameter $S(I)$ were studied in all three nuclear mass regions. The results suggested that spin independence of the energy staggering parameter $S(I)$ within two-quasiparticle chiral bands (previously suggested a fingerprint of chirality) is found only if the Coriolis interaction can be completely neglected. However, if the configuration is non-restricted the Coriolis interaction is often strong enough to create considerable energy staggering. It was found that staggering in the $B(M1)$ reduced transition probabilities (proposed as another fingerprint of chirality) occurs for a strongly broken chirality but also for systems with weakly broken chiral symmetry. For strongly broken chirality the phase of the $B(M1)$ staggering is specific for in A ~ 100, 130 mass regions, but not in A ~ 190 mass region. Thus the amplitude of the $B(M1)$ staggering does not seem related to how good the chirality is. The staggering may disappear completely for partner bands which are almost degenerate, and be large for bands which do not have so close excitation energies. Therefore, the use of the $B(M1)$ staggering as a fingerprint of strongly broken chiral symmetry seems rather risky, in particular if the phase of the staggering is not checked.

The ultimate goal of all theoretical investigations on chiral symmetry is to define specific measurable nuclear properties, which can directly and unambiguously prove whether a nucleus has chiral symmetry or not. This goal is not achieved so far, and thus remains an exciting project for future investigations.

REFERENCES

[And76] G. Andersson *et al*., Nucl. Phys. **A** 268, 205 (1976)

[Ari76] A. Arima and F. Iachello, Phys. Rev. **C** 14, 761 (1976)

[Bal04] D.L. Balabanski *et al*., Phys. Rev. **C** 70, 044305 (2004)

[Bal94] G. Baldsiefen *et al*., Nucl. Phys. **A** 574, 521 (1994)

[Bar01] R.A. Bark *et al*., Nucl. Phys. **A** 691, 577 (2001)

[Bar57] J. Bardeen, L.N. Cooper and J.R. Schrieffer, Phys. Rev. 108, 1175 (1957)

[Bar97] R.A. Bark *et al*., Phys. Lett. **B** 406, 193 (1997); Erratum Phys. Lett. **B** 416, 453 (1998)

[Ben85] T. Bengtsson and I. Ragnarsson, Nucl. Phys. **A** 436, 14 (1985)

[Boh52] A. Bohr, Mat. Fys. Medd. Dan. Vid. Selsk. 26, 14 (1952)

[Boh53] A. Bohr and B.R. Mottelson, Mat. Fys. Medd. Dan. Vid. Selsk. 27, 16 (1953)

[Boh69] A. Bohr and B.R. Mottelson, Nuclear Structure, Vol. I (W.A. Benjamin, New York, 1969)

[Boh81] A. Bohr and B.R. Mottelson, Phys. Scr. 24, 71 (1981)

[Bra04] S. Brant, D. Vretenar and A. Ventura, Phys. Rev. **C** 69, 017304 (2004)

[Bra08] S. Brant *et al*., Phys. Rev. **C** 78, 034301 (2008)

[Bra09] S. Brant and C.M. Petrache, Phys. Rev. **C** 79, 054326 (2009)

[Cas00] R.F. Casten, *Nuclear Structure from a Simple Perspective,* second edition, Copyright © 2000, by Oxford University, New York Inc

[Dav58] A.S. Davydov and G.F. Filippov, Nucl. Phys. 8, 237 (1958)

[Dav59a] A.S. Davydov and V. S. Rostovsky, Nucl. Phys. 12, 58 (1959)

[Dav59b] A.S. Davydov, Sov. Phys. JETP 9, 1103 (1959)

[Dav65] J.P. Davidson, Rev. Mod. Phys. 37, 105 (1965)

[Dim00] V.I. Dimitrov, S. Frauendorf and F. Dönau, Phys. Rev. Lett. 84, 5732 (2000)

[Don79] F. Dönau and U. Hagemann, Z. Phys. **A** 293, 31 (1979)

[Don77] F. Dönau and S. Frauendorf, Phys. Lett. **B** 71, 263 (1977)

[Dro09] Ch. Droste *et al*., Eur. Phys. J. **A** 42, 79 (2009)

[Edm57] A.R. Edmonds, *Angular Momentum in Quantum Mechanics*. Princeton Univ. Press, Princeton, (1957)

[Fae62] A. Faessler and W. Greiner, Z. Phys. 168, 425 (1962)

[Fae64a] A. Faessler and W. Greiner, Z. Phys. 177, 190 (1964)

[Fae64b] A. Faessler and W. Greiner, Nucl. Phys. 59, 177 (1964)

[Fae65a] A. Faessler, W. Greiner and R.K. Sheline, Nucl. Phys. 80, 417 (1965)

[Fae65b] A. Faessler, W. Greiner and R.K. Sheline, Nucl. Phys. 62, 241 (1965)

[Fae65c] A. Faessler, W. Greiner and R.K. Sheline, Nucl. Phys. 70, 33 (1965)

[Fir96a] R.B. Firestone, Table of Isotopes, 8th edition, Vol. 1, p. 14166 (1996)

[Fir96b] R.B. Firestone, Table of Isotopes, 8th edition, Vol. 1, p. 14164 (1996)

[Fir96c] R.B. Firestone, Table of Isotopes, 8th edition, Vol. 1, p. 14170 (1996)

[Fir96d] R.B. Firestone, Table of Isotopes, 8th edition, Vol. 1, p. 14172 (1996)

[Flü71] S. Flügge, *Practical Quantum Mechanics*, Springer-Verlag, Berlin, (1971)

[Fra01] S. Frauendorf, Rev. Mod. Phys. Vol. 73, No. 2, 463 (2001)

[Fra93] S. Frauendorf, Nucl. Phys. **A** 557, 259c (1993)

[Fra97] S. Frauendorf and J. Meng, Nucl. Phys. **A** 617, 131 (1997)

[Gan09] H.G. Ganev *et al*., Phys. Rev. **C** 79, 044322 (2009)

[Gro05] E. Grodner *et al*., Int. J. Mod. Phys. **E** 14, 347 (2005)

[Gro06] E. Grodner *et al*., Phys. Rev. Lett. 97, 172501 (2006); Int. J. Mod. Phys. **E** 15, 548 (2006)

[Gro62] L. Grodzins, Phys. Lett. 2, 88 (1962)

[Har01] D.J. Hartley *et al*., Phys. Rev. **C** 64, 031304 (2001)

[Har65] S.M. Harris, Phys. Rev. 138, B509 (1965)

[Hax49] O. Haxel, J.H.D. Jensen and H.E. Suess, Phys. Rev. 75, 1766 (1949)

[Hec01] A.A. Hecht *et al*., Phys. Rev. **C** 63, 051302 (2001)

[Hec03] A.A. Hecht *et al*., Phys. Rev. **C** 68, 054310 (2003)

[Hec62] K.T. Hecht and G.R. Satchler, Nucl. Phys. 32, 286 (1962)

[Hey99] K. Heyde, *Basic ideas and Concepts in Nuclear Physics, an introductory approach*, second edition, Copyright © 1999, by Institute of Physics, p. 361

[Hig05] K. Higashiyama, N. Yoshinaga and K. Tanabe, Phys. Rev. **C** 72, 024315 (2005)

[Hig07] K. Higashiyama and N. Yoshinaga, Eur. Phys. J. **A** 33, 355 (2007)

[Hil53] D.L. Hill and J.A. Wheeler, Phys. Rev. 89, 1102 (1953)

[Iac79] F. Iachello and O. Scholten, Phys. Rev. Lett. 43, 679 (1979)

[Jos04] P. Joshi *et al*., Phys. Lett. **B** 595, 135 (2004)

[Jos05a] P. Joshi *et al*., J. Phys. G: Nucl. Part. Phys. 31, S1895 (2005)

[Jos05b] P. Joshi *et al*., Eur. Phys. J. **A** 24, 23 (2005)

[Jos07] P. Joshi *et al*., Phys. Rev. Lett. 98, 102501 (2007)

[Jun08] A. Jungclaus *et al*., Phys. Rev. **C** 77, 024310 (2008)

[Koi01] T. Koike *et al*., Phys. Rev. **C** 63, 061304(R) (2001)

[Koi03a] T. Koike *et al*., Phys. Rev. **C** 67, 044319 (2003)

[Koi03b] T. Koike *et al*., in FNS2002, Berkeley. CA, 2002, AIP Conf. Proc. No. 656, edited by P. Fallon, R. Clark (AIP, Melville, NY, 2003), p. 160

[Koi04] T. Koike, K. Starosta and I. Hamamoto, Phys. Rev. Lett. 93, 172502 (2004)

[Koi05] T. Koike *et al*., J. Phys. G: Nucl. Part. Phys. 31, S1741 (2005)

[Kra98] K.S. Krane, *Introductory Nuclear Physics*, Copyright © 1998, by John Wiley and Sons, p. 152

[Lar78] S.E. Larsson, G. Leander and I. Ragnarsson, Nucl. Phys. **A** 307, 189 (1978)

[Law08] E.A. Lawrie *et al*., Phys.Rev. **C** 78, 021305 (2008)

[Law10a] E.A. Lawrie and O. Shirinda, Phys. Lett. **B** 689, 66 (2010)

[Law10b] E.A. Lawrie *et al*., Eur. Phys. J. **A** 45, 39 (2010)

[Luo09] Y.X. Luo *et al*., Phys. Lett. **B** 670, 307 (2009); Erratum Phys. Lett. **B** 691, 285 (2010)

[Mab03] G.K. Mabala, PhD thesis, University of Cape Town, (2003)

[Mar96] G. Maruhn, *Nuclear Models*, Copyright © 1996, by Springer-Verlag Berlin Heidelberg, p. 108

[Mas09] P.L. Masiteng *et al*., Acta Phys. Pol. **B** 40, 657 (2009)

[May49] M.G. Mayer, Phys. Rev. 75, 1969 (1949)

[Men06] J. Meng *et al*., Phys. Rev. **C** 73, 037303 (2006)

[Mer02] E. Mergel *et al*., Eur. Phys. J. **A** 15, 417 (2002)

[Mey74] J. Meyer-ter-Vehn, F.S. Stephens and R.M. Diamond, Phys. Rev. Lett. 32, 1383 (1974)

[Mey75] J. Meyer-ter-Vehn, Nucl. Phys. **A** 249, 141 (1975)

[Moo00a] C.-B. Moon, T. Komatsubara and K. Furuno, Nucl. Phys. **A** 674, 343 (2000)

[Moo00b] C.-B. Moon, T. Komatsubara and K. Furuno, Erratum Nucl. Phys. **A** 678, 457 (2000)

[Muk07] S. Mukhopadhyay *et al*., Phys. Rev. Lett. 99, 172501 (2007)

[Muk08] S. Mukhopadhyay *et al*., Phys. Rev. **C** 78, 034311 (2008)

[Nil55] S.G. Nilsson, Mat. Fys. Medd. Dan. Vid. Selsk, 29, 16 (1955)

[Nil69] S.G. Nilsson *et al*., Nucl. Phys. **A** 131, 1 (1969)

[Olb04] P. Olbratowski *et al*., Phys. Rev. Lett. 93, 052501 (2004)

[Pen03] J. Peng, J. Meng and S.Q. Zhang, Phys. Rev. **C** 68, 044324 (2003)

[Pen08] J. Peng *et al*., Phys. Rev. **C** 77, 024309 (2008)

[Pet02] C.M. Petrache *et al.*, Phys. Rev. **C** 65, 054324 (2002)

[Pet06] C.M. Petrache *et al*., Phys. Rev. Lett. 96, 112502 (2006)

[Pet96] C.M. Petrache *et al.*, Nucl. Phys. **A** 597, 106 (1996)

[Qi09a] B. Qi *et al*., Phys. Lett. **B** 675, 175 (2009)

[Qi09b] B. Qi *et al*., Phys. Rev. **C** 79, 041302(R) (2009)

[Rag08] I. Ragnarsson, private communication, 2008

[Rag88] I. Ragnarsson and P.B. Semmes, Hyperfine Interactions 43, 425 (1988)

[Rai03a] G. Rainovski *et al*., J. Phys. G: Nucl. Part. Phys. 29, 2763 (2003)

[Rai03b] G. Rainovski *et al*., Phys. Rev. **C** 68, 024318 (2003)

[Rin80] P. Ring and P. Schuck, *The Nuclear Many-Body Problem*, Copyright © 1980, by Springer-Verlag New York Inc, p. 111

[Sem90] P.B. Semmes and I. Ragnarsson, Conf. high spin physics and gamma-soft nuclei, Pittsburg, September 1990 (World Scientific, Singapore, 1991) p. 500

[Sem92] P.B. Semmes and I. Ragnarsson, AIP Conf. Proc. No. 259, p.566 (1992)

[Ser87] A. Servin, K. Heyde and J. Jolie, Phys. Rev. **C** 36, 2631 (1987)

[Shi11a] O. Shirinda and E.A. Lawrie, XVII Nuclear Physics Workshop "Marie and Pierre Curie", 22-26 September 2010, Symmetry and Symmetry Breaking in Nuclear Physics, Kazimierz Dolny, Poland, Int. J. Mod. Phys. **E**. Vol. 20, No. 2, 358 (2011)

[Shi11b] O. Shirinda and E.A. Lawrie, Third International Conference on Frontiers in Nuclear Structure, Astrophysics and Reactions (FINUSTAR3), 23-27 August 2010, Rhodos, Greece, AIP Conf. Proc. (2011), in print

[Shi11c] O. Shirinda and E.A. Lawrie, Third International Conference on Frontiers in Nuclear Structure, Astrophysics and Reactions (FINUSTAR3), 23-27 August 2010, Rhodos, Greece, AIP Conf. Proc. (2011), in print

[Sim05] A.J. Simons *et al*., J. Phys. G: Nucl. Part. Phys. 31, 541 (2005)

[Sta01a] K. Starosta *et al*., Phys. Rev. Lett. 86, 971 (2001)

[Sta01b] K. Starosta *et al*., Nucl .Phys. **A** 682, 375c (2001)

[Sta02] K. Starosta *et al*., Phys. Rev. **C** 65, 044328 (2002)

[Ste75] F.S. Stephens, Rev. Mod. Phys. 47, 43 (1975)

[Suz08] T. Suzuki *et al*., Phys. Rev. **C** 78, 031302(R) (2008)

[Taj94] N. Tajima, Nucl. Phys. **A** 572, 365 (1994)

[Tim04] J. Timar *et al*., Phys. Lett. **B** 598, 178 (2004)

[Tim06] J. Timar *et al.*, Phys. Rev. **C** 73, 011301(R) (2006)

[Tim07] J. Timar *et al.*, Phys. Rev. **C** 76, 024307 (2007)

[Ton06] D. Tonev *et al.*, Phys. Rev. Lett. 96, 052501 (2006)

[Ton07] D. Tonev *et al.*, Phys. Rev. **C** 76, 044313 (2007)

[Vam04] C. Vaman *et al.*, Phys. Rev. Lett. 92, 032501 (2004)

[Wan06] S. Wang *et al.*, Phys. Rev. **C** 74, 017302 (2006)

[Wan07] S.Y. Wang *et al.*, Phys. Rev. **C** 75, 024309 (2007)

[Wan08] S.Y. Wang *et al.*, Phys. Rev. **C** 77, 034314 (2008)

[Wan09] L.-L. Wang et al., Chin. Phys. **C** 33, Supplement 1, 173 (2009)

[Woo54] R.D. Woods and D.S. Saxon, Phys. Rev. 95, 577 (1954)

[Yao09] J.M. Yao *et al.*, Phys. Rev. **C** 79, 067302 (2009)

[Yon05] Yong-Nam U *et al.*, J. Phys. G: Nucl. Part. Phys. 31, B1 (2005)

[Yos04] N. Yoshinaga and K. Higashiyama, Phys. Rev. **C** 69, 054309 (2004)

[Yos05] N. Yoshinaga and K. Higashiyama, J. Phys. G: Nucl. Part. Phys. 31, S1455 (2005)

[Yos06] N. Yoshinaga and K. Higashiyama, Eur. Phys. J. **A** 30, 343 (2006); Erratum Eur. Phys. J. **A** 31, 395 (2007)

[Zha07] S.Q. Zhang *et al.*, Phys. Rev. **C** 75, 044307 (2007)

[Zhu03] S. Zhu *et al.*, Phys. Rev. Lett. 91, 132501 (2003)

[Zhu05] S.J. Zhu *et al.*, Eur. Phys. J. **A** 25, s01, 459 (2005)

APPENDIX A Tables of results from TQPRM calculations

Table A.1-3: *Calculated relative excitation energy (ΔE) for the partner bands in A ~ 100, 130 and 190 mass regions at ε_2 = 0.15 and γ = 17^0, 20^0, 24^0, 27^0, 30^0, 33^0, 36^0, 40^0.*

Table A.1

A ~ 100								
Spin I ($\hbar$)	Non-restricted configuration							
	$\Delta E = E_{side} - E_{yrast}$ (keV)							
	$\gamma = 17^0$	$\gamma = 20^0$	$\gamma = 24^0$	$\gamma = 27^0$	$\gamma = 30^0$	$\gamma = 33^0$	$\gamma = 36^0$	$\gamma = 40^0$
8	880.000	826.000	705.000	627.000	591.000	597.000	634.000	697.000
9	899.000	789.000	600.000	510.000	474.000	485.000	535.000	639.000
10	928.000	712.000	440.000	334.000	295.000	310.000	385.000	573.000
11	966.000	646.000	300.000	152.000	88.000	111.000	219.000	503.000
12	933.000	553.000	185.000	24.000	55.000	50.000	75.000	388.000
13	987.000	614.000	344.000	301.000	306.000	299.000	298.000	469.000
14	967.000	622.000	377.000	281.000	209.000	180.000	225.000	421.000
15	1052.000	793.000	607.000	517.000	462.000	461.000	509.000	631.000
16	1100.000	859.000	643.000	518.000	436.000	417.000	462.000	606.000
17	1122.000	932.000	745.000	636.000	568.000	556.000	595.000	710.000
18	1256.000	1118.000	897.000	760.000	678.000	669.000	726.000	866.000
19	1176.000	1014.000	831.000	719.000	647.000	625.000	651.000	1045.000
20	1398.000	1328.000	1147.000	1006.000	924.000	927.000	1003.000	1164.000
21	1216.000	1069.000	893.000	784.000	709.000	681.000	696.000	768.000
22	1579.000	1495.000	1379.000	1252.000	1174.000	1191.000	1288.000	1479.000
	Restricted configuration							
8	762.000	606.000	475.000	418.000	393.000	402.000	441.000	541.000
9	740.000	566.000	416.000	349.000	319.000	327.000	372.000	492.000
10	707.000	517.000	352.000	275.000	238.000	245.000	297.000	436.000
11	666.000	460.000	279.000	193.000	152.000	160.000	218.000	372.000
12	616.000	395.000	201.000	113.000	74.000	82.000	139.000	301.000
13	556.000	323.000	125.000	50.000	24.000	29.000	73.000	227.000
14	490.000	247.000	64.000	17.000	5.000	8.000	31.000	155.000
15	418.000	172.000	25.000	6.000	1.000	3.000	12.000	94.000
16	344.000	108.000	8.000	4.000	1.000	2.000	5.000	50.000
17	272.000	59.000	-7.000	5.000	2.000	1.000	4.000	22.000
18	207.000	29.000	-10.000	4.000	2.000	1.000	4.000	6.000
19	156.000	23.000	-13.000	6.000	3.000	3.000	5.000	-6.000
20	121.000	33.000	-16.000	7.000	3.000	2.000	5.000	-11.000
21	106.000	44.000	-19.000	9.000	5.000	4.000	7.000	-15.000
22	108.000	52.000	-21.000	9.000	3.000	1.000	6.000	-18.000

Table A.2

A ~ 130								
Spin I ($\hbar$)	Non-restricted configuration							
	$\Delta E = E_{side} - E_{yrast}$ (keV)							
	$\gamma = 17^0$	$\gamma = 20^0$	$\gamma = 24^0$	$\gamma = 27^0$	$\gamma = 30^0$	$\gamma = 33^0$	$\gamma = 36^0$	$\gamma = 40^0$
8	808.000	786.000	724.000	661.000	623.000	623.000	650.000	703.000
9	798.000	764.000	672.000	599.000	562.000	566.000	601.000	672.000
10	812.000	727.000	549.000	462.000	432.000	447.000	498.000	611.000
11	854.000	645.000	367.000	269.000	256.000	292.000	369.000	546.000
12	877.000	550.000	199.000	58.000	101.000	181.000	278.000	505.000
13	874.000	494.000	170.000	118.000	153.000	147.000	124.000	343.000
14	914.000	569.000	367.000	337.000	312.000	263.000	241.000	426.000
15	938.000	639.000	454.000	363.000	266.000	183.000	149.000	301.000
16	1038.000	813.000	648.000	551.000	483.000	466.000	493.000	591.000
17	1099.000	882.000	685.000	558.000	458.000	398.000	388.000	483.000

Table A.2 continues

A ~ 130								
Spin I ($\hbar$)	**Non-restricted configuration**							
	$\Delta E = E_{side} - E_{yrast}$ (keV)							
	$\gamma = 17^0$	$\gamma = 20^0$	$\gamma = 24^0$	$\gamma = 27^0$	$\gamma = 30^0$	$\gamma = 33^0$	$\gamma = 36^0$	$\gamma = 40^0$
18	1167.000	984.000	796.000	682.000	606.000	581.000	606.000	707.000
19	1299.000	1110.000	898.000	761.000	666.000	630.000	655.000	763.000
20	1244.000	1070.000	880.000	765.000	687.000	656.000	672.000	762.000
21	1520.000	1336.000	1113.000	973.000	885.000	872.000	929.000	1076.000
22	1286.000	1116.000	931.000	820.000	743.000	709.000	720.000	797.000
	Restricted configuration							
8	703.000	581.000	481.000	439.000	424.000	440.000	485.000	584.000
9	680.000	541.000	426.000	378.000	363.000	381.000	431.000	547.000
10	654.000	499.000	367.000	313.000	295.000	315.000	373.000	507.000
11	620.000	450.000	303.000	241.000	221.000	244.000	309.000	460.000
12	578.000	393.000	233.000	165.000	142.000	168.000	240.000	405.000
13	527.000	330.000	161.000	93.000	70.000	94.000	168.000	344.000
14	470.000	262.000	95.000	39.000	23.000	40.000	100.000	277.000
15	406.000	193.000	45.000	13.000	5.000	13.000	50.000	208.000
16	338.000	127.000	19.000	4.000	1.000	3.000	21.000	144.000
17	270.000	75.000	8.000	3.000	1.000	-1.000	8.000	91.000
18	204.000	35.000	7.000	3.000	1.000	-1.000	2.000	52.000
19	147.000	10.000	7.000	3.000	1.000	-1.000	2.000	27.000
20	100.000	-10.000	9.000	4.000	2.000	-1.000	0.000	13.000
21	71.000	-20.000	10.000	4.000	2.000	-1.000	0.000	5.000
22	59.000	-28.000	11.000	5.000	2.000	-1.000	1.000	1.000

Table A.3

A ~ 190								
Spin I ($\hbar$)	**Non-restricted configuration**							
	$\Delta E = E_{side} - E_{yrast}$ (keV)							
	$\gamma = 17^0$	$\gamma = 20^0$	$\gamma = 24^0$	$\gamma = 27^0$	$\gamma = 30^0$	$\gamma = 33^0$	$\gamma = 36^0$	$\gamma = 40^0$
8	500.000	521.000	556.000	574.000	538.000	531.000	545.000	578.000
9	618.000	609.000	581.000	535.000	507.000	512.000	540.000	592.000
10	747.000	653.000	483.000	406.000	385.000	406.000	464.000	573.000
11	837.000	586.000	311.000	219.000	216.000	267.000	360.000	552.000
12	874.000	509.000	168.000	20.000	98.000	187.000	301.000	541.000
13	865.000	465.000	165.000	136.000	154.000	120.000	126.000	391.000
14	902.000	545.000	370.000	351.000	322.000	275.000	284.000	505.000
15	931.000	611.000	420.000	318.000	220.000	147.000	153.000	357.000
16	1052.000	805.000	650.000	560.000	505.000	503.000	541.000	663.000
17	1116.000	851.000	626.000	494.000	400.000	359.000	383.000	524.000
18	1279.000	1037.000	807.000	688.000	620.000	611.000	658.000	790.000
19	1350.000	1088.000	839.000	701.000	617.000	600.000	651.000	790.000
20	1480.000	1185.000	899.000	762.000	685.000	669.000	714.000	845.000
21	1602.000	1332.000	1070.000	929.000	851.000	854.000	930.000	1089.000
22	1637.000	1285.000	954.000	805.000	723.000	706.000	749.000	877.000
	Restricted configuration							
8	1469.000	1209.000	1018.000	947.000	937.000	997.000	1123.000	1394.000
9	1239.000	982.000	824.000	782.000	797.000	878.000	1028.000	1340.000
10	1099.000	826.000	660.000	623.000	653.000	752.000	923.000	1272.000
11	972.000	681.000	502.000	463.000	499.000	612.000	804.000	1189.000
12	838.000	528.000	346.000	298.000	329.000	456.000	668.000	1088.000
13	692.000	365.000	207.000	149.000	163.000	296.000	522.000	971.000
14	540.000	202.000	120.000	51.000	57.000	159.000	367.000	838.000
15	394.000	58.000	90.000	23.000	28.000	59.000	226.000	694.000

Table A.3 continues

A ~ 190								
Spin I ($\hbar$)	Restricted configuration							
	$\Delta E = E_{side} - E_{yrast}$ (keV)							
	$\gamma = 17^0$	$\gamma = 20^0$	$\gamma = 24^0$	$\gamma = 27^0$	$\gamma = 30^0$	$\gamma = 33^0$	$\gamma = 36^0$	$\gamma = 40^0$
16	284.000	-73.000	90.000	38.000	20.000	21.000	121.000	543.000
17	259.000	-163.000	102.000	51.000	24.000	-16.000	49.000	398.000
18	320.000	-232.000	120.000	62.000	31.000	-13.000	25.000	269.000
19	415.000	-288.000	140.000	74.000	38.000	-18.000	9.000	167.000
20	511.000	-337.000	161.000	87.000	45.000	-22.000	9.000	99.000
21	602.000	-383.000	183.000	99.000	52.000	-26.000	12.000	51.000
22	685.000	-427.000	204.000	111.000	59.000	-30.000	14.000	31.000

Table A.4-9: *Calculated energy staggering parameter* $S(I)$ *for the partner bands in A ~ 100, 130 and 190 mass regions at* ε_2 *= 0.15 and* γ *= 17*^{0}*, 20*^{0}*, 24*^{0}*, 27*^{0}*, 30*^{0}*, 33*^{0}*, 36*^{0}*, 40*^{0}*.*

Table A.4

A ~ 100								
Spin I ($\hbar$)	Non-restricted configuration							
	$S(I) = [E(I) - E(I-1)]/2I$ ($keV/\hbar$), yrast band							
	$\gamma = 17^0$	$\gamma = 20^0$	$\gamma = 24^0$	$\gamma = 27^0$	$\gamma = 30^0$	$\gamma = 33^0$	$\gamma = 36^0$	$\gamma = 40^0$
9	10.667	10.611	10.556	10.500	10.444	10.556	10.667	10.667
10	16.600	16.750	16.950	17.000	17.150	17.400	17.700	17.650
11	19.045	19.227	19.955	20.818	21.591	21.864	21.636	21.227
12	23.750	23.583	23.500	23.750	22.083	23.125	25.250	25.208
13	22.462	21.385	18.885	16.269	16.654	16.923	18.038	21.962
14	26.857	25.036	22.571	22.000	22.464	23.321	24.036	26.000
15	23.733	21.433	18.633	17.200	16.367	16.400	17.600	20.833
16	27.594	25.344	23.125	22.156	21.938	22.563	23.719	25.688
17	25.147	22.618	20.029	18.618	17.971	18.324	19.647	22.500
18	27.222	25.306	23.139	21.972	21.472	21.833	22.806	24.556
19	27.263	24.526	21.737	20.316	19.763	20.421	22.105	25.474
20	26.325	24.700	22.725	21.525	20.950	21.100	21.750	23.000
21	29.976	26.976	23.762	22.167	21.667	22.571	24.714	28.786
22	25.023	23.705	21.955	20.886	20.273	20.227	20.591	21.386
	$S(I) = [E(I) - E(I-1)]/2I$ ($keV/\hbar$), side band							
9	11.722	8.556	4.722	4.000	3.944	4.333	5.167	7.444
10	18.050	12.900	8.950	8.200	8.200	8.650	10.200	14.350
11	20.773	16.227	13.591	12.545	12.182	12.818	14.091	18.045
12	22.375	19.708	18.708	18.417	20.708	20.583	19.250	20.417
13	24.538	23.731	25.000	26.923	26.308	26.500	26.615	25.077
14	26.143	25.321	23.750	21.286	19.000	19.071	21.429	24.286
15	26.567	27.133	26.300	25.067	24.800	25.767	27.067	27.833
16	29.094	27.406	24.250	22.188	21.125	21.188	22.250	24.906
17	25.794	24.765	23.029	22.088	21.853	22.412	23.559	25.559
18	30.944	30.472	27.361	25.417	24.528	24.972	26.444	28.889
19	25.158	21.789	20.000	19.237	18.947	19.263	20.132	30.184
20	31.875	32.550	30.625	28.700	27.875	28.650	30.550	25.975
21	25.643	20.810	17.714	16.881	16.548	16.714	17.405	19.357
22	33.273	33.386	33.000	31.523	30.841	31.818	34.045	37.545

Table A.5

A ~ 130								
Spin I ($\hbar$)	**Non-restricted configuration**							
	$S(I)=[E(I)-E(I-1)]/2I$ **($keV/\hbar$), yrast band**							
	$\gamma=17^0$	$\gamma=20^0$	$\gamma=24^0$	$\gamma=27^0$	$\gamma=30^0$	$\gamma=33^0$	$\gamma=36^0$	$\gamma=40^0$
9	4.556	4.667	4.611	4.556	4.556	4.611	4.722	4.833
10	10.300	10.500	10.400	10.300	10.150	10.200	10.250	10.300
11	15.818	15.773	15.909	15.818	15.545	15.455	15.500	15.500
12	20.000	18.875	19.292	20.000	18.958	18.375	18.417	18.208
13	18.231	21.192	20.077	18.231	18.538	20.385	22.692	22.962
14	16.143	20.429	17.250	16.143	16.536	17.071	17.464	19.214
15	19.300	22.067	19.833	19.300	19.667	20.733	22.333	24.767
16	16.813	20.688	18.156	16.813	15.781	15.125	15.125	17.438
17	19.882	22.676	20.765	19.882	19.765	20.676	22.176	24.382
18	17.778	21.917	19.278	17.778	16.861	16.639	17.139	19.056
19	20.000	22.789	20.947	20.000	19.737	20.289	21.421	23.342
20	19.150	23.675	20.775	19.150	18.300	18.475	19.600	22.050
21	19.738	22.286	20.643	19.738	19.405	19.738	20.524	22.000
22	20.773	25.909	22.591	20.773	19.977	20.455	22.068	25.273
	$S(I)=[E(I)-E(I-1)]/2I$ **($keV/\hbar$), side band**							
9	4.222	3.444	1.722	1.111	1.167	1.444	2.000	3.111
10	11.200	8.650	4.250	3.450	3.650	4.250	5.100	7.250
11	17.636	12.045	7.636	7.045	7.545	8.409	9.636	12.545
12	19.917	14.917	12.292	11.208	12.500	13.750	14.625	16.500
13	21.577	19.038	18.962	20.538	20.538	19.077	16.769	16.731
14	23.571	23.107	24.286	23.964	22.214	21.214	21.643	22.179
15	24.833	24.400	22.733	20.167	18.133	18.067	19.267	20.600
16	26.313	26.125	24.219	22.688	22.563	23.969	25.875	26.500
17	26.500	24.706	21.853	20.088	19.029	18.676	19.088	21.206
18	26.222	24.750	22.361	21.222	20.972	21.722	23.194	25.278
19	28.105	26.105	23.632	22.079	21.316	21.579	22.711	24.816
20	24.825	22.675	20.325	19.250	18.825	19.125	20.025	22.025
21	30.500	28.619	26.190	24.690	24.119	24.881	26.643	29.476
22	23.364	20.909	18.455	17.295	16.750	16.750	17.318	18.932

Table A.6

A ~ 190								
Spin I ($\hbar$)	**Non-restricted configuration**							
	$S(I)=[E(I)-E(I-1)]/2I$ **($keV/\hbar$), yrast band**							
	$\gamma=17^0$	$\gamma=20^0$	$\gamma=24^0$	$\gamma=27^0$	$\gamma=30^0$	$\gamma=33^0$	$\gamma=36^0$	$\gamma=40^0$
9	3.889	3.944	4.000	3.944	3.833	3.889	4.000	4.222
10	9.950	9.650	9.200	8.950	8.750	8.650	8.550	8.500
11	14.455	14.409	14.545	14.500	14.136	13.818	13.773	13.727
12	17.333	17.250	17.583	18.458	16.667	15.958	15.667	15.333
13	19.654	19.269	18.115	15.769	16.962	19.192	21.115	20.769
14	20.429	18.643	15.393	14.464	14.607	14.607	14.857	16.571
15	21.767	20.033	18.300	18.100	18.567	19.667	21.067	22.867
16	21.594	19.031	16.375	14.875	13.688	12.969	13.375	16.000
17	22.471	20.500	18.882	18.265	18.353	19.176	20.294	22.029
18	22.722	20.472	17.917	16.333	15.306	15.167	15.889	18.056
19	22.737	20.553	18.553	17.737	17.553	18.026	18.921	20.500
20	24.325	22.425	19.975	18.400	17.550	17.750	18.900	21.375
21	22.667	20.143	17.786	16.810	16.500	16.762	17.429	18.738
22	26.205	24.545	22.227	20.659	19.886	20.341	21.864	24.795

Table A.6 continues

A ~ 190								
Spin I ($\hbar$)	**Non-restricted configuration**							
	$S(I) = [E(I) - E(I-1)]/2I$ **($keV/\hbar$), side band**							
	$\gamma = 17^0$	$\gamma = 20^0$	$\gamma = 24^0$	$\gamma = 27^0$	$\gamma = 30^0$	$\gamma = 33^0$	$\gamma = 36^0$	$\gamma = 40^0$
9	10.444	8.833	5.389	1.778	2.111	2.833	3.722	5.000
10	16.400	11.850	4.300	2.500	2.650	3.350	4.750	7.550
11	18.545	11.364	6.727	6.000	6.455	7.500	9.045	12.773
12	18.875	14.042	11.625	10.167	11.750	12.625	13.208	14.875
13	19.308	17.577	18.000	20.231	19.115	16.615	14.385	15.000
14	21.750	21.500	22.714	22.143	20.607	20.143	20.500	20.643
15	22.733	22.233	19.967	17.000	15.167	15.400	16.700	17.933
16	25.375	25.094	23.563	22.438	22.594	24.094	25.500	25.563
17	24.353	21.853	18.176	16.324	15.265	14.941	15.647	17.941
18	27.250	25.639	22.944	21.722	21.417	22.167	23.528	25.444
19	24.605	21.895	19.395	18.079	17.474	17.737	18.737	20.500
20	27.575	24.850	21.475	19.925	19.250	19.475	20.475	22.750
21	25.571	23.643	21.857	20.786	20.452	21.167	22.571	24.548
22	27.000	23.477	19.591	17.841	16.977	16.977	17.750	19.977

Table A.7

A ~ 100								
Spin I ($\hbar$)	**Restricted configuration**							
	$S(I) = [E(I) - E(I-1)]/2I$ **($keV/\hbar$), yrast band**							
	$\gamma = 17^0$	$\gamma = 20^0$	$\gamma = 24^0$	$\gamma = 27^0$	$\gamma = 30^0$	$\gamma = 33^0$	$\gamma = 36^0$	$\gamma = 40^0$
9	11.389	10.889	10.389	10.167	10.167	10.556	11.111	11.889
10	14.450	14.200	13.950	13.950	14.150	14.600	15.100	15.550
11	16.591	16.545	16.591	16.682	16.955	17.318	17.682	17.955
12	18.292	18.333	18.292	18.167	18.125	18.542	19.167	19.625
13	19.615	19.538	19.115	18.308	17.769	18.231	19.385	20.538
14	20.536	20.321	19.036	17.536	16.786	17.250	18.786	20.929
15	21.233	20.667	18.467	16.767	16.167	16.633	18.033	20.767
16	21.656	20.563	17.813	16.375	15.875	16.313	17.563	20.313
17	21.824	20.206	17.529	16.147	15.706	16.147	17.265	19.853
18	21.806	19.722	17.194	16.028	15.583	16.000	17.083	19.417
19	21.553	19.211	17.026	15.868	15.474	15.868	16.974	19.211
20	21.225	18.850	16.925	15.800	15.375	15.800	16.850	18.975
21	20.857	18.714	16.833	15.690	15.286	15.690	16.762	18.833
22	20.523	18.636	16.750	15.659	15.273	15.682	16.705	18.727
	$S(I) = [E(I) - E(I-1)]/2I$ **($keV/\hbar$), side band**							
9	10.167	8.667	7.111	6.333	6.056	6.389	7.278	9.167
10	12.800	11.750	10.750	10.250	10.100	10.500	11.350	12.750
11	14.727	13.955	13.273	12.955	13.045	13.455	14.091	15.045
12	16.208	15.625	15.042	14.833	14.875	15.292	15.875	16.667
13	17.308	16.769	16.192	15.885	15.846	16.192	16.846	17.692
14	18.179	17.607	16.857	16.357	16.107	16.500	17.286	18.357
15	18.833	18.167	17.167	16.400	16.033	16.467	17.400	18.733
16	19.344	18.563	17.281	16.313	15.875	16.281	17.344	18.938
17	19.706	18.765	17.294	16.176	15.735	16.118	17.235	19.029
18	20.000	18.889	17.194	16.000	15.583	16.000	17.083	18.972
19	20.211	19.053	17.026	15.921	15.500	15.921	17.000	18.895
20	20.350	19.100	16.925	15.825	15.375	15.775	16.850	18.850
21	20.500	18.976	16.833	15.738	15.333	15.738	16.810	18.738
22	20.568	18.818	16.750	15.659	15.227	15.614	16.682	18.659

Table A.8

A ~ 130								
Spin I ($\hbar$)	**Restricted configuration**							
	$S(I)=[E(I)-E(I-1)]/2I$ **($keV/\hbar$), yrast band**							
	$\gamma=17^0$	$\gamma=20^0$	$\gamma=24^0$	$\gamma=27^0$	$\gamma=30^0$	$\gamma=33^0$	$\gamma=36^0$	$\gamma=40^0$
9	7.500	6.778	5.944	5.611	5.389	5.500	5.833	6.444
10	10.900	10.450	10.000	9.650	9.500	9.600	9.850	10.200
11	13.364	13.182	12.955	12.773	12.636	12.682	12.818	12.955
12	15.208	15.167	15.042	14.917	14.833	14.833	14.917	14.958
13	16.577	16.577	16.346	16.000	15.846	16.038	16.269	16.385
14	17.607	17.500	16.857	16.000	15.536	16.000	16.857	17.393
15	18.400	18.067	16.633	15.267	14.733	15.267	16.633	18.000
16	18.906	18.219	16.031	14.688	14.188	14.719	16.063	18.156
17	19.206	18.000	15.529	14.353	13.971	14.412	15.588	18.000
18	19.306	17.667	15.194	14.194	13.806	14.194	15.278	17.667
19	19.184	17.289	15.053	14.079	13.711	14.079	15.053	17.289
20	18.975	17.050	14.925	13.975	13.600	13.975	14.975	16.975
21	18.643	16.786	14.833	13.905	13.548	13.905	14.857	16.786
22	18.318	16.659	14.773	13.818	13.477	13.841	14.773	16.614
	$S(I)=[E(I)-E(I-1)]/2I$ **($keV/\hbar$), side band**							
9	6.222	4.556	2.889	2.222	2.000	2.222	2.833	4.389
10	9.600	8.350	7.050	6.400	6.100	6.300	6.950	8.200
11	11.818	10.955	10.045	9.500	9.273	9.455	9.909	10.818
12	13.458	12.792	12.125	11.750	11.542	11.667	12.042	12.667
13	14.615	14.154	13.577	13.231	13.077	13.192	13.500	14.038
14	15.571	15.071	14.500	14.071	13.857	14.071	14.429	15.000
15	16.267	15.767	14.967	14.400	14.133	14.367	14.967	15.700
16	16.781	16.156	15.219	14.406	14.063	14.406	15.156	16.156
17	17.206	16.471	15.206	14.324	13.971	14.294	15.206	16.441
18	17.472	16.556	15.167	14.194	13.806	14.194	15.111	16.583
19	17.684	16.632	15.053	14.079	13.711	14.079	15.053	16.632
20	17.800	16.550	14.975	14.000	13.625	13.975	14.925	16.625
21	17.952	16.548	14.857	13.905	13.548	13.905	14.857	16.595
22	18.045	16.477	14.795	13.841	13.477	13.841	14.795	16.523

Table A.9

A ~ 190								
Spin I ($\hbar$)	**Restricted configuration**							
	$S(I)=[E(I)-E(I-1)]/2I$ **($keV/\hbar$), yrast band**							
	$\gamma=17^0$	$\gamma=20^0$	$\gamma=24^0$	$\gamma=27^0$	$\gamma=30^0$	$\gamma=33^0$	$\gamma=36^0$	$\gamma=40^0$
8	6.313	...	...	...	...	...	...	...
9	20.333	17.056	13.611	11.778	10.667	10.333	10.500	11.222
10	28.550	26.450	23.400	21.200	19.550	18.700	18.450	18.600
11	33.818	32.545	30.364	28.318	26.455	25.227	24.591	24.227
12	37.375	36.542	34.708	33.042	31.375	30.042	29.292	28.625
13	39.769	39.000	36.577	34.923	33.923	33.192	32.654	32.077
14	41.250	40.071	35.893	34.107	33.464	34.250	34.893	34.679
15	41.900	39.967	34.367	32.167	31.533	33.600	35.667	36.600
16	41.688	39.406	33.219	30.906	30.531	32.031	35.250	37.875
17	40.412	38.235	32.618	30.529	29.912	31.471	34.324	38.441
18	39.056	37.444	32.194	30.278	29.583	30.528	33.167	38.417
19	38.368	36.842	31.947	30.026	29.342	30.342	32.684	37.921
20	38.100	36.450	31.750	29.825	29.150	30.125	32.200	37.175
21	37.929	36.143	31.548	29.690	29.000	29.929	31.929	36.595
22	37.818	35.909	31.432	29.545	28.841	29.773	31.773	35.977

Table A.9 continues

A ~ 190								
Spin I ($\hbar$)	**Restricted configuration**							
	$S(I) = [E(I) - E(I-1)]/2I$ **($keV/\hbar$), side band**							
	$\gamma = 17^0$	$\gamma = 20^0$	$\gamma = 24^0$	$\gamma = 27^0$	$\gamma = 30^0$	$\gamma = 33^0$	$\gamma = 36^0$	$\gamma = 40^0$
8	4.375	...	...	...	...	...	...	...
9	7.556	4.444	2.833	2.611	2.889	3.722	5.222	8.222
10	21.550	18.650	15.200	13.250	12.350	12.400	13.200	15.200
11	28.045	25.955	23.182	21.045	19.455	18.864	19.182	20.455
12	31.792	30.167	28.208	26.167	24.292	23.542	23.625	24.417
13	34.154	32.731	31.231	29.192	27.538	27.038	27.038	27.577
14	35.821	34.250	32.786	30.607	29.679	29.357	29.357	29.929
15	37.033	35.167	33.367	31.233	30.567	30.267	30.967	31.800
16	38.250	35.313	33.219	31.375	30.281	30.844	31.969	33.156
17	39.676	35.588	32.971	30.912	30.029	30.382	32.206	34.176
18	40.750	35.528	32.694	30.583	29.778	30.611	32.500	34.833
19	40.868	35.368	32.474	30.342	29.526	30.211	32.263	35.237
20	40.500	35.225	32.275	30.150	29.325	30.025	32.200	35.475
21	40.095	35.048	32.071	29.976	29.167	29.833	32.000	35.452
22	39.705	34.909	31.909	29.818	29.000	29.682	31.818	35.523

Table A.10-21: *Calculated projections of the angular momenta of the proton (j_p), neutron (j_n) and the core (j_R) for the partner bands in A ~ 100, 130 and 190 mass regions at ε_2 = 0.15 and $\gamma = 20^0$, 30^0, 36^0.*

Table A.10

A ~ 100, non-restricted configuration						
Spin I ($\hbar$)	$\gamma = 20^0$**, yrast band**			$\gamma = 20^0$**, side band**		
	$\sqrt{\langle j_{px}^2 \rangle}$ ($\hbar$)	$\sqrt{\langle j_{py}^2 \rangle}$ ($\hbar$)	$\sqrt{\langle j_{pz}^2 \rangle}$ ($\hbar$)	$\sqrt{\langle j_{px}^2 \rangle}$ ($\hbar$)	$\sqrt{\langle j_{py}^2 \rangle}$ ($\hbar$)	$\sqrt{\langle j_{pz}^2 \rangle}$ ($\hbar$)
8	1.256	1.444	4.398	1.352	1.701	4.274
9	1.385	1.503	4.338	1.325	1.742	4.266
10	1.504	1.553	4.280	1.315	1.746	4.267
11	1.673	1.760	4.136	1.416	1.704	4.252
12	1.747	1.762	4.104	1.482	1.906	4.142
13	1.769	2.134	3.915	1.735	1.902	4.046
14	1.770	2.117	3.924	1.691	2.288	3.860
15	1.733	2.458	3.738	2.000	2.291	3.716
16	1.706	2.521	3.707	1.609	2.740	3.592
17	1.754	2.691	3.565	2.028	2.763	3.372
18	1.633	2.913	3.445	1.536	3.063	3.358
19	1.809	2.858	3.408	1.956	3.100	3.156
20	1.568	3.246	3.169	2.099	3.041	3.087
21	1.869	2.978	3.273	1.881	3.333	2.913
22	1.523	3.502	2.912	2.512	2.738	3.077
	$\sqrt{\langle j_{nx}^2 \rangle}$ ($\hbar$)	$\sqrt{\langle j_{ny}^2 \rangle}$ ($\hbar$)	$\sqrt{\langle j_{nz}^2 \rangle}$ ($\hbar$)	$\sqrt{\langle j_{nx}^2 \rangle}$ ($\hbar$)	$\sqrt{\langle j_{ny}^2 \rangle}$ ($\hbar$)	$\sqrt{\langle j_{nz}^2 \rangle}$ ($\hbar$)
8	4.672	3.248	1.428	4.741	2.865	1.990
9	4.627	3.255	1.562	4.767	2.812	2.007
10	4.574	3.298	1.628	4.710	2.961	1.910
11	4.450	3.455	1.637	4.620	3.104	1.895
12	4.274	3.667	1.632	4.613	3.147	1.835
13	3.995	3.969	1.605	4.728	2.955	1.872
14	3.789	4.161	1.603	4.693	3.062	1.774
15	3.561	4.355	1.592	4.697	2.958	1.949

Table A.10 continues

A ~ 100, non-restricted configuration						
Spin I ($\hbar$)	$\gamma = 20^0$, **yrast band**			$\gamma = 20^0$, **side band**		
	$\sqrt{\langle j_{nx}^2 \rangle}$ ($\hbar$)	$\sqrt{\langle j_{ny}^2 \rangle}$ ($\hbar$)	$\sqrt{\langle j_{nz}^2 \rangle}$ ($\hbar$)	$\sqrt{\langle j_{nx}^2 \rangle}$ ($\hbar$)	$\sqrt{\langle j_{ny}^2 \rangle}$ ($\hbar$)	$\sqrt{\langle j_{nz}^2 \rangle}$ ($\hbar$)
16	3.469	4.434	1.569	4.576	3.223	1.784
17	3.291	4.560	1.581	4.466	3.210	2.086
18	3.264	4.595	1.530	4.220	3.662	1.787
19	3.101	4.688	1.579	4.269	3.412	2.170
20	3.101	4.711	1.502	3.364	4.497	1.618
21	2.956	4.776	1.585	4.112	3.563	2.227
22	2.957	4.804	1.489	2.832	4.846	1.593
	$\sqrt{\langle j_{Rx}^2 \rangle}$ ($\hbar$)	$\sqrt{\langle j_{Ry}^2 \rangle}$ ($\hbar$)	$\sqrt{\langle j_{Rz}^2 \rangle}$ ($\hbar$)	$\sqrt{\langle j_{Rx}^2 \rangle}$ ($\hbar$)	$\sqrt{\langle j_{Ry}^2 \rangle}$ ($\hbar$)	$\sqrt{\langle j_{Rz}^2 \rangle}$ ($\hbar$)
8	1.438	1.969	0.501	2.050	2.987	0.841
9	1.660	2.146	0.493	1.829	3.288	1.101
10	2.134	2.571	0.474	1.619	3.581	1.436
11	2.534	3.069	0.406	1.767	3.843	1.649
12	2.969	3.954	0.428	2.258	4.239	1.723
13	3.071	4.742	0.593	2.993	4.828	1.695
14	3.168	5.822	0.809	3.440	5.638	1.686
15	3.224	6.646	1.007	3.592	6.939	1.519
16	3.280	7.606	1.114	4.003	7.764	1.642
17	3.453	8.532	1.251	3.596	9.046	1.497
18	3.478	9.317	1.305	4.166	9.943	1.634
19	3.720	10.438	1.422	3.761	10.910	1.571
20	3.713	11.031	1.454	4.148	11.887	1.577
21	3.987	12.369	1.566	3.990	12.755	1.667
22	3.962	12.794	1.585	4.285	13.909	1.650

Table A.11

A ~ 100, non-restricted configuration						
Spin I ($\hbar$)	$\gamma = 30^0$, **yrast band**			$\gamma = 30^0$, **side band**		
	$\sqrt{\langle j_{px}^2 \rangle}$ ($\hbar$)	$\sqrt{\langle j_{py}^2 \rangle}$ ($\hbar$)	$\sqrt{\langle j_{pz}^2 \rangle}$ ($\hbar$)	$\sqrt{\langle j_{px}^2 \rangle}$ ($\hbar$)	$\sqrt{\langle j_{py}^2 \rangle}$ ($\hbar$)	$\sqrt{\langle j_{pz}^2 \rangle}$ ($\hbar$)
8	1.239	1.727	4.314	1.307	1.742	4.287
9	1.411	1.732	4.259	1.333	1.811	4.250
10	1.557	1.715	4.215	1.342	1.986	4.166
11	1.662	1.828	4.126	1.500	2.134	4.039
12	1.531	2.025	4.082	1.754	2.134	3.938
13	1.502	2.499	3.819	1.762	1.983	4.012
14	1.614	2.363	3.862	1.462	2.584	3.776
15	1.479	2.792	3.618	1.847	2.291	3.806
16	1.527	2.741	3.637	1.408	2.773	3.657
17	1.518	2.974	3.453	1.856	2.657	3.555
18	1.434	3.045	3.423	1.425	2.912	3.541
19	1.584	3.100	3.310	1.815	2.946	3.339
20	1.354	3.298	3.212	1.478	3.016	3.431
21	1.653	3.193	3.187	1.772	3.159	3.162
22	1.296	3.504	3.011	1.551	3.091	3.333
	$\sqrt{\langle j_{nx}^2 \rangle}$ ($\hbar$)	$\sqrt{\langle j_{ny}^2 \rangle}$ ($\hbar$)	$\sqrt{\langle j_{nz}^2 \rangle}$ ($\hbar$)	$\sqrt{\langle j_{nx}^2 \rangle}$ ($\hbar$)	$\sqrt{\langle j_{ny}^2 \rangle}$ ($\hbar$)	$\sqrt{\langle j_{nz}^2 \rangle}$ ($\hbar$)
8	5.190	2.390	1.455	5.100	2.539	1.513
9	5.153	2.390	1.588	5.002	2.710	1.533
10	5.127	2.367	1.711	4.840	2.954	1.585
11	5.089	2.408	1.768	4.620	3.217	1.711
12	4.748	3.002	1.770	4.718	3.055	1.752

Table A.11 continues

A ~ 100, non-restricted configuration						
Spin I ($\hbar$)	$\gamma = 30^0$, **yrast band**			$\gamma = 30^0$, **side band**		
	$\sqrt{\langle j_{nx}^2 \rangle}$ ($\hbar$)	$\sqrt{\langle j_{ny}^2 \rangle}$ ($\hbar$)	$\sqrt{\langle j_{nz}^2 \rangle}$ ($\hbar$)	$\sqrt{\langle j_{nx}^2 \rangle}$ ($\hbar$)	$\sqrt{\langle j_{ny}^2 \rangle}$ ($\hbar$)	$\sqrt{\langle j_{nz}^2 \rangle}$ ($\hbar$)
13	4.280	3.647	1.694	4.834	2.842	1.813
14	4.065	3.861	1.733	4.689	3.129	1.692
15	3.852	4.100	1.637	4.606	3.127	1.919
16	3.738	4.189	1.669	4.495	3.388	1.698
17	3.545	4.364	1.620	4.409	3.355	1.983
18	3.483	4.416	1.608	4.340	3.556	1.747
19	3.320	4.530	1.622	4.241	3.535	2.023
20	3.269	4.585	1.559	4.204	3.677	1.817
21	3.153	4.639	1.634	4.095	3.680	2.055
22	3.084	4.716	1.526	4.076	3.783	1.884
	$\sqrt{\langle j_{Rx}^2 \rangle}$ ($\hbar$)	$\sqrt{\langle j_{Ry}^2 \rangle}$ ($\hbar$)	$\sqrt{\langle j_{Rz}^2 \rangle}$ ($\hbar$)	$\sqrt{\langle j_{Rx}^2 \rangle}$ ($\hbar$)	$\sqrt{\langle j_{Ry}^2 \rangle}$ ($\hbar$)	$\sqrt{\langle j_{Rz}^2 \rangle}$ ($\hbar$)
8	1.129	2.177	1.100	1.528	3.073	1.727
9	1.277	2.294	1.199	1.484	3.265	1.679
10	1.604	2.596	1.448	1.489	3.470	1.631
11	2.027	3.031	1.683	1.457	3.809	1.593
12	1.984	4.081	2.014	1.970	4.670	1.442
13	1.852	5.206	1.711	2.273	5.741	2.000
14	1.968	6.364	1.714	2.295	6.372	2.307
15	2.059	7.002	1.910	2.231	7.801	2.189
16	2.091	8.042	1.923	2.530	8.438	2.571
17	2.253	8.838	2.140	2.308	9.633	2.289
18	2.249	9.733	2.136	2.710	10.495	2.756
19	2.439	10.726	2.348	2.445	11.419	2.431
20	2.414	11.456	2.334	2.857	12.531	2.899
21	2.616	12.647	2.539	2.604	13.228	2.588
22	2.583	13.219	2.520	2.992	14.546	3.021

Table A.12

A ~ 130, non-restricted configuration						
Spin I ($\hbar$)	$\gamma = 20^0$, **yrast band**			$\gamma = 20^0$, **side band**		
	$\sqrt{\langle j_{px}^2 \rangle}$ ($\hbar$)	$\sqrt{\langle j_{py}^2 \rangle}$ ($\hbar$)	$\sqrt{\langle j_{pz}^2 \rangle}$ ($\hbar$)	$\sqrt{\langle j_{px}^2 \rangle}$ ($\hbar$)	$\sqrt{\langle j_{py}^2 \rangle}$ ($\hbar$)	$\sqrt{\langle j_{pz}^2 \rangle}$ ($\hbar$)
8	4.614	3.375	1.361	4.565	3.127	1.979
9	4.575	3.344	1.559	4.594	2.958	2.179
10	4.510	3.341	1.748	4.633	2.884	2.200
11	4.440	3.400	1.815	4.571	3.092	2.032
12	4.292	3.591	1.802	4.491	3.210	2.028
13	4.054	3.868	1.778	4.566	3.121	1.999
14	3.775	4.154	1.746	4.679	2.964	1.975
15	3.556	4.345	1.741	4.690	2.989	1.908
16	3.407	4.476	1.705	4.636	2.996	2.033
17	3.283	4.573	1.688	4.543	3.201	1.923
18	3.186	4.651	1.660	4.396	3.229	2.211
19	3.112	4.711	1.629	4.286	3.527	1.943
20	3.023	4.769	1.629	4.224	3.428	2.306
21	2.981	4.810	1.583	3.957	3.912	1.900
22	2.896	4.853	1.613	4.037	3.578	2.357

Table A.12 continues

A ~ 130, non-restricted configuration						
Spin I ($\hbar$)	$\gamma = 20^0$, **yrast band**			$\gamma = 20^0$, **side band**		
	$\sqrt{\langle j_{nx}^2 \rangle}$ ($\hbar$)	$\sqrt{\langle j_{ny}^2 \rangle}$ ($\hbar$)	$\sqrt{\langle j_{nz}^2 \rangle}$ ($\hbar$)	$\sqrt{\langle j_{nx}^2 \rangle}$ ($\hbar$)	$\sqrt{\langle j_{ny}^2 \rangle}$ ($\hbar$)	$\sqrt{\langle j_{nz}^2 \rangle}$ ($\hbar$)
8	1.442	1.681	5.389	1.615	1.917	5.257
9	1.495	1.704	4.486	1.594	1.924	5.261
10	1.615	1.769	5.310	1.577	1.962	5.252
11	1.764	1.854	5.233	1.552	1.967	5.257
12	1.905	2.029	5.117	1.629	1.978	5.229
13	1.963	2.137	5.051	1.793	2.116	5.121
14	1.944	2.432	4.921	2.010	2.204	5.003
15	1.929	2.508	4.887	2.049	2.591	4.795
16	1.898	2.798	4.737	2.179	2.660	4.702
17	1.908	2.915	4.661	1.932	3.171	4.477
18	1.903	3.093	4.545	2.163	3.202	4.353
19	1.887	3.335	4.374	1.807	3.551	4.231
20	1.930	3.322	4.367	2.108	3.630	4.026
21	1.853	3.714	4.067	1.841	3.745	4.042
22	1.964	3.496	4.213	2.049	3.932	3.757
	$\sqrt{\langle j_{Rx}^2 \rangle}$ ($\hbar$)	$\sqrt{\langle j_{Ry}^2 \rangle}$ ($\hbar$)	$\sqrt{\langle j_{Rz}^2 \rangle}$ ($\hbar$)	$\sqrt{\langle j_{Rx}^2 \rangle}$ ($\hbar$)	$\sqrt{\langle j_{Ry}^2 \rangle}$ ($\hbar$)	$\sqrt{\langle j_{Rz}^2 \rangle}$ ($\hbar$)
8	1.473	1.865	0.358	2.273	2.951	0.559
9	1.518	1.938	0.366	2.177	3.037	0.663
10	1.747	2.164	0.371	1.958	3.333	1.007
11	2.205	2.633	0.352	1.649	3.567	1.474
12	2.630	3.295	0.311	1.804	3.696	1.720
13	2.960	4.209	0.434	2.444	4.080	1.774
14	2.995	5.121	0.724	3.232	4.765	1.719
15	3.090	6.117	0.940	3.605	5.799	1.660
16	3.161	6.982	1.112	3.764	7.201	1.570
17	3.252	7.899	1.208	3.917	8.142	1.627
18	3.437	8.835	1.325	3.625	9.479	1.570
19	3.460	9.626	1.377	4.093	10.269	1.679
20	3.727	10.721	1.487	3.699	11.343	1.644
21	3.684	11.348	1.516	4.288	12.271	1.756
22	4.004	12.637	1.630	3.895	13.156	1.738

Table A.13

A ~ 130, non-restricted configuration						
Spin I ($\hbar$)	$\gamma = 30^0$, **yrast band**			$\gamma = 30^0$, **side band**		
	$\sqrt{\langle j_{px}^2 \rangle}$ ($\hbar$)	$\sqrt{\langle j_{py}^2 \rangle}$ ($\hbar$)	$\sqrt{\langle j_{pz}^2 \rangle}$ ($\hbar$)	$\sqrt{\langle j_{px}^2 \rangle}$ ($\hbar$)	$\sqrt{\langle j_{py}^2 \rangle}$ ($\hbar$)	$\sqrt{\langle j_{pz}^2 \rangle}$ ($\hbar$)
8	5.170	2.444	1.369	5.035	2.644	1.488
9	5.138	2.428	1.508	5.040	2.631	1.494
10	5.094	2.401	1.689	4.820	3.005	1.509
11	5.064	2.358	1.835	4.589	3.283	1.644
12	4.842	2.703	1.954	4.573	3.241	1.776
13	4.355	3.452	1.920	4.827	2.804	1.848
14	4.020	3.886	1.815	4.740	2.897	1.927
15	3.738	4.155	1.822	4.677	3.051	1.836
16	3.596	4.313	1.737	4.560	3.126	2.003
17	3.449	4.424	1.756	4.495	3.333	1.799
18	3.323	4.544	1.690	4.390	3.315	2.080
19	3.260	4.591	1.686	4.322	3.549	1.811
20	3.132	4.686	1.666	4.234	3.483	2.132
21	3.106	4.716	1.627	4.156	3.727	1.841

Table A.13 continues

A ~ 130, non-restricted configuration						
Spin I ($\hbar$)	$\gamma = 30^0$, **yrast band**			$\gamma = 30^0$, **side band**		
	$\sqrt{\langle j_{px}^2 \rangle}$ ($\hbar$)	$\sqrt{\langle j_{py}^2 \rangle}$ ($\hbar$)	$\sqrt{\langle j_{pz}^2 \rangle}$ ($\hbar$)	$\sqrt{\langle j_{px}^2 \rangle}$ ($\hbar$)	$\sqrt{\langle j_{py}^2 \rangle}$ ($\hbar$)	$\sqrt{\langle j_{pz}^2 \rangle}$ ($\hbar$)
22	2.993	4.779	1.660	4.091	3.630	2.166
	$\sqrt{\langle j_{nx}^2 \rangle}$ ($\hbar$)	$\sqrt{\langle j_{ny}^2 \rangle}$ ($\hbar$)	$\sqrt{\langle j_{nz}^2 \rangle}$ ($\hbar$)	$\sqrt{\langle j_{nx}^2 \rangle}$ ($\hbar$)	$\sqrt{\langle j_{ny}^2 \rangle}$ ($\hbar$)	$\sqrt{\langle j_{nz}^2 \rangle}$ ($\hbar$)
8	1.438	2.046	5.294	1.570	2.117	5.227
9	1.522	2.048	5.270	1.601	2.111	5.220
10	1.666	2.065	5.220	1.612	2.150	5.201
11	1.808	2.073	5.170	1.647	2.254	5.144
12	1.801	2.125	5.151	1.865	2.471	4.965
13	1.747	2.311	5.085	2.020	2.562	4.857
14	1.741	2.781	4.835	1.929	2.465	4.944
15	1.803	2.661	4.884	1.749	3.073	4.644
16	1.701	3.136	4.617	2.020	2.809	4.713
17	1.765	3.087	4.629	1.639	3.391	4.447
18	1.716	3.393	4.418	2.042	3.254	4.393
19	1.694	3.487	4.349	1.602	3.597	4.289
20	1.755	3.591	4.236	2.007	3.630	4.091
21	1.616	3.835	4.063	1.631	3.735	4.153
22	1.802	3.745	4.075	1.961	3.900	3.846
	$\sqrt{\langle j_{Rx}^2 \rangle}$ ($\hbar$)	$\sqrt{\langle j_{Ry}^2 \rangle}$ ($\hbar$)	$\sqrt{\langle j_{Rz}^2 \rangle}$ ($\hbar$)	$\sqrt{\langle j_{Rx}^2 \rangle}$ ($\hbar$)	$\sqrt{\langle j_{Ry}^2 \rangle}$ ($\hbar$)	$\sqrt{\langle j_{Rz}^2 \rangle}$ ($\hbar$)
8	1.251	2.129	0.943	1.632	2.917	1.696
9	1.283	2.201	0.986	1.620	3.136	1.656
10	1.409	2.353	1.157	1.570	3.254	1.618
11	1.652	2.637	1.512	1.610	3.482	1.508
12	1.728	3.118	2.033	1.941	3.932	1.085
13	1.873	4.302	1.944	2.188	4.729	1.577
14	1.913	5.344	1.730	2.186	5.827	2.243
15	2.063	6.436	1.812	2.184	6.562	2.403
16	2.070	7.160	1.978	2.277	7.917	2.364
17	2.154	8.175	2.020	2.464	8.574	2.615
18	2.259	8.994	2.211	2.325	9.803	2.428
19	2.286	9.883	2.217	2.671	10.592	2.790
20	2.442	10.874	2.421	2.435	11.587	2.531
21	2.433	11.599	2.401	2.842	12.602	2.931
22	2.616	12.787	2.614	2.581	13.385	2.662

Table A.14

A ~ 190, non-restricted configuration						
Spin I ($\hbar$)	$\gamma = 36^0$, **yrast band**			$\gamma = 36^0$, **side band**		
	$\sqrt{\langle j_{px}^2 \rangle}$ ($\hbar$)	$\sqrt{\langle j_{py}^2 \rangle}$ ($\hbar$)	$\sqrt{\langle j_{pz}^2 \rangle}$ ($\hbar$)	$\sqrt{\langle j_{px}^2 \rangle}$ ($\hbar$)	$\sqrt{\langle j_{py}^2 \rangle}$ ($\hbar$)	$\sqrt{\langle j_{pz}^2 \rangle}$ ($\hbar$)
8	4.337	1.968	1.329	4.161	2.228	1.414
9	4.324	1.973	1.368	4.176	2.230	1.376
10	4.276	1.987	1.489	4.068	2.415	1.375
11	4.216	2.043	1.580	4.042	2.431	1.426
12	3.987	2.341	1.717	4.159	2.181	1.526
13	3.967	2.314	1.803	3.978	2.503	1.477
14	3.638	2.869	1.616	3.997	2.297	1.762
15	3.589	2.882	1.701	3.775	2.755	1.523
16	3.446	3.116	1.541	3.796	2.557	1.817
17	3.298	3.239	1.588	3.636	2.935	1.498
18	3.297	3.271	1.520	3.489	2.828	1.846

Table A.14 continues

A ~ 190, non-restricted configuration						
Spin I ($\hbar$)	$\gamma = 36^0$, **yrast band**			$\gamma = 36^0$, **side band**		
	$\sqrt{\langle j_{px}^2 \rangle}$ ($\hbar$)	$\sqrt{\langle j_{py}^2 \rangle}$ ($\hbar$)	$\sqrt{\langle j_{pz}^2 \rangle}$ ($\hbar$)	$\sqrt{\langle j_{px}^2 \rangle}$ ($\hbar$)	$\sqrt{\langle j_{py}^2 \rangle}$ ($\hbar$)	$\sqrt{\langle j_{pz}^2 \rangle}$ ($\hbar$)
19	3.057	3.481	1.511	3.576	2.992	1.522
20	3.189	3.366	1.526	3.385	3.030	1.839
21	2.863	3.650	1.459	3.540	3.003	1.587
22	3.108	3.426	1.545	3.246	3.176	1.823
	$\sqrt{\langle j_{nx}^2 \rangle}$ ($\hbar$)	$\sqrt{\langle j_{ny}^2 \rangle}$ ($\hbar$)	$\sqrt{\langle j_{nz}^2 \rangle}$ ($\hbar$)	$\sqrt{\langle j_{nx}^2 \rangle}$ ($\hbar$)	$\sqrt{\langle j_{ny}^2 \rangle}$ ($\hbar$)	$\sqrt{\langle j_{nz}^2 \rangle}$ ($\hbar$)
8	1.810	2.948	5.957	2.366	2.903	5.794
9	1.939	2.968	5.908	2.341	2.801	5.856
10	2.082	3.020	5.834	2.271	2.894	5.834
11	2.135	3.010	5.822	2.293	3.192	5.662
12	2.095	3.211	5.722	2.383	3.541	5.404
13	2.162	3.297	5.647	2.173	3.748	5.342
14	2.039	4.147	5.077	2.279	3.179	5.676
15	2.128	4.171	5.022	2.067	3.923	5.250
16	2.025	4.569	4.689	2.359	3.524	5.426
17	2.050	4.644	4.601	2.000	4.222	5.028
18	2.003	4.830	4.417	2.458	3.914	5.094
19	1.967	4.958	4.281	1.991	4.489	4.784
20	1.996	5.011	4.203	2.471	4.186	4.857
21	1.902	5.190	4.015	1.999	4.694	4.573
22	1.997	5.143	4.030	2.466	4.376	4.683
	$\sqrt{\langle j_{Rx}^2 \rangle}$ ($\hbar$)	$\sqrt{\langle j_{Ry}^2 \rangle}$ ($\hbar$)	$\sqrt{\langle j_{Rz}^2 \rangle}$ ($\hbar$)	$\sqrt{\langle j_{Rx}^2 \rangle}$ ($\hbar$)	$\sqrt{\langle j_{Ry}^2 \rangle}$ ($\hbar$)	$\sqrt{\langle j_{Rz}^2 \rangle}$ ($\hbar$)
8	1.228	2.352	1.342	1.332	3.176	2.056
9	1.229	2.474	1.391	1.421	3.390	2.022
10	1.240	2.641	1.640	1.572	3.547	1.823
11	1.281	2.984	2.148	1.792	3.793	1.557
12	1.251	3.429	2.507	1.959	4.195	1.777
13	1.380	4.359	2.916	1.847	4.824	2.342
14	1.421	5.391	2.636	1.928	5.212	3.268
15	1.536	6.471	2.680	1.972	6.378	3.130
16	1.689	7.209	2.797	1.906	7.917	3.346
17	1.710	8.127	2.724	2.092	8.432	3.575
18	1.858	9.087	3.074	1.987	10.023	3.183
19	1.843	9.796	2.922	2.241	10.550	3.821
20	2.014	11.018	3.324	2.085	11.876	3.291
21	1.948	11.538	3.155	2.355	12.649	4.021
22	2.224	12.977	3.554	2.175	13.719	3.490

Table A.15

A ~ 190, non-restricted configuration						
Spin I ($\hbar$)	$\gamma = 30^0$, **yrast band**			$\gamma = 30^0$, **side band**		
	$\sqrt{\langle j_{px}^2 \rangle}$ ($\hbar$)	$\sqrt{\langle j_{py}^2 \rangle}$ ($\hbar$)	$\sqrt{\langle j_{pz}^2 \rangle}$ ($\hbar$)	$\sqrt{\langle j_{px}^2 \rangle}$ ($\hbar$)	$\sqrt{\langle j_{py}^2 \rangle}$ ($\hbar$)	$\sqrt{\langle j_{pz}^2 \rangle}$ ($\hbar$)
8	4.229	2.199	1.235	4.154	2.269	1.346
9	4.218	2.184	1.302	4.162	2.279	1.309
10	4.191	2.155	1.439	3.991	2.557	1.287
11	4.178	2.117	1.534	3.837	2.741	1.350
12	3.910	2.506	1.610	3.942	2.530	1.480
13	3.646	2.876	1.561	4.046	2.332	1.555
14	3.452	3.132	1.467	3.979	2.406	1.610
15	3.190	3.374	1.482	3.969	2.480	1.513

Table A.15 continues

A ~ 190, non-restricted configuration						
Spin I ($\hbar$)	$\gamma = 30^0$, **yrast band**			$\gamma = 30^0$, **side band**		
	$\sqrt{\langle j_{px}^2 \rangle}$ ($\hbar$)	$\sqrt{\langle j_{py}^2 \rangle}$ ($\hbar$)	$\sqrt{\langle j_{pz}^2 \rangle}$ ($\hbar$)	$\sqrt{\langle j_{px}^2 \rangle}$ ($\hbar$)	$\sqrt{\langle j_{py}^2 \rangle}$ ($\hbar$)	$\sqrt{\langle j_{pz}^2 \rangle}$ ($\hbar$)
16	3.207	3.389	1.406	3.864	2.529	1.688
17	2.997	3.557	1.422	3.839	2.677	1.488
18	3.048	3.533	1.378	3.713	2.682	1.776
19	2.856	3.682	1.370	3.725	2.813	1.511
20	2.934	3.623	1.374	3.574	2.827	1.821
21	2.731	3.781	1.333	3.634	2.901	1.555
22	2.849	3.683	1.384	3.457	2.947	1.844
	$\sqrt{\langle j_{nx}^2 \rangle}$ ($\hbar$)	$\sqrt{\langle j_{ny}^2 \rangle}$ ($\hbar$)	$\sqrt{\langle j_{nz}^2 \rangle}$ ($\hbar$)	$\sqrt{\langle j_{nx}^2 \rangle}$ ($\hbar$)	$\sqrt{\langle j_{ny}^2 \rangle}$ ($\hbar$)	$\sqrt{\langle j_{nz}^2 \rangle}$ ($\hbar$)
8	1.859	2.528	6.165	2.267	2.606	5.999
9	1.988	2.585	6.101	2.123	2.638	6.034
10	2.172	2.665	6.005	2.100	2.734	5.997
11	2.310	2.680	5.948	2.163	2.967	5.858
12	2.208	2.785	5.935	2.462	3.298	5.552
13	2.245	3.056	5.781	2.457	3.453	5.455
14	2.243	3.707	5.367	2.353	3.221	5.645
15	2.269	3.569	5.456	2.237	4.011	5.135
16	2.197	4.112	5.068	2.453	3.583	5.369
17	2.233	4.100	5.064	2.139	4.308	4.918
18	2.185	4.382	4.830	2.474	3.972	5.063
19	2.167	4.517	4.705	2.102	4.480	4.771
20	2.185	4.575	4.638	2.449	4.286	4.797
21	2.101	4.827	4.400	2.104	4.594	4.654
22	2.191	4.719	4.481	2.414	4.514	4.589
	$\sqrt{\langle j_{Rx}^2 \rangle}$ ($\hbar$)	$\sqrt{\langle j_{Ry}^2 \rangle}$ ($\hbar$)	$\sqrt{\langle j_{Rz}^2 \rangle}$ ($\hbar$)	$\sqrt{\langle j_{Rx}^2 \rangle}$ ($\hbar$)	$\sqrt{\langle j_{Ry}^2 \rangle}$ ($\hbar$)	$\sqrt{\langle j_{Rz}^2 \rangle}$ ($\hbar$)
8	1.509	2.406	1.099	1.719	3.294	1.837
9	1.515	2.518	1.138	1.839	3.423	1.779
10	1.594	2.682	1.318	1.822	3.495	1.715
11	1.802	2.983	1.718	1.887	3.706	1.564
12	1.767	3.464	2.212	2.237	4.163	1.273
13	2.114	4.532	2.063	2.225	5.150	1.892
14	2.090	5.641	1.894	2.350	6.025	2.542
15	2.265	6.656	1.989	2.332	6.854	2.533
16	2.263	7.462	2.153	2.531	8.261	2.558
17	2.321	8.398	2.159	2.668	8.818	2.750
18	2.468	9.330	2.379	2.548	10.257	2.597
19	2.429	10.114	2.335	2.915	10.841	2.942
20	2.659	11.244	2.587	2.630	12.105	2.689
21	2.561	11.867	2.509	3.111	12.885	3.106
22	2.838	13.188	2.777	2.758	13.940	2.814

Table A.16

A ~ 100, restricted configuration						
Spin I ($\hbar$)	$\gamma = 20^0$, **yrast band**			$\gamma = 20^0$, **side band**		
	$\sqrt{\langle j_{px}^2 \rangle}$ ($\hbar$)	$\sqrt{\langle j_{py}^2 \rangle}$ ($\hbar$)	$\sqrt{\langle j_{pz}^2 \rangle}$ ($\hbar$)	$\sqrt{\langle j_{px}^2 \rangle}$ ($\hbar$)	$\sqrt{\langle j_{py}^2 \rangle}$ ($\hbar$)	$\sqrt{\langle j_{pz}^2 \rangle}$ ($\hbar$)
8 to 22	1.133	1.310	4.780	1.133	1.310	4.780
	$\sqrt{\langle j_{nx}^2 \rangle}$ ($\hbar$)	$\sqrt{\langle j_{ny}^2 \rangle}$ ($\hbar$)	$\sqrt{\langle j_{nz}^2 \rangle}$ ($\hbar$)	$\sqrt{\langle j_{nx}^2 \rangle}$ ($\hbar$)	$\sqrt{\langle j_{ny}^2 \rangle}$ ($\hbar$)	$\sqrt{\langle j_{nz}^2 \rangle}$ ($\hbar$)
8 to 22	5.267	2.372	1.058	5.267	2.372	1.058

Table A.16 continues

A ~ 100, restricted configuration						
Spin I ($\hbar$)	$\gamma = 20^0$, **yrast band**			$\gamma = 20^0$, **side band**		
	$\sqrt{\langle j_{Rx}^2 \rangle}$ ($\hbar$)	$\sqrt{\langle j_{Ry}^2 \rangle}$ ($\hbar$)	$\sqrt{\langle j_{Rz}^2 \rangle}$ ($\hbar$)	$\sqrt{\langle j_{Rx}^2 \rangle}$ ($\hbar$)	$\sqrt{\langle j_{Ry}^2 \rangle}$ ($\hbar$)	$\sqrt{\langle j_{Rz}^2 \rangle}$ ($\hbar$)
8	2.005	4.131	1.481	2.299	5.492	2.116
9	2.652	4.519	1.518	2.306	6.121	2.163
10	3.445	4.980	1.544	2.632	6.806	2.190
11	4.265	5.537	1.559	3.131	7.549	2.200
12	5.052	6.222	1.566	3.688	8.354	2.199
13	5.757	7.077	1.572	4.239	9.225	2.190
14	6.328	8.147	1.588	4.746	10.166	2.179
15	6.710	9.453	1.633	5.189	11.174	2.171
16	6.877	10.947	1.715	5.560	12.238	2.173
17	6.866	12.520	1.824	5.870	13.335	2.189
18	6.718	14.106	1.948	6.185	14.396	2.216
19	6.463	15.631	2.083	6.555	15.429	2.218
20	6.444	16.885	2.180	6.680	16.645	2.254
21	6.513	18.062	2.242	6.733	17.865	2.314
22	6.592	19.216	2.295	6.788	19.052	2.376

Table A.17

A ~ 100, restricted configuration						
Spin I ($\hbar$)	$\gamma = 30^0$, **yrast band**			$\gamma = 30^0$, **side band**		
	$\sqrt{\langle j_{px}^2 \rangle}$ ($\hbar$)	$\sqrt{\langle j_{py}^2 \rangle}$ ($\hbar$)	$\sqrt{\langle j_{pz}^2 \rangle}$ ($\hbar$)	$\sqrt{\langle j_{px}^2 \rangle}$ ($\hbar$)	$\sqrt{\langle j_{py}^2 \rangle}$ ($\hbar$)	$\sqrt{\langle j_{pz}^2 \rangle}$ ($\hbar$)
8 to 22	1.136	1.461	4.443	1.136	1.461	4.443
	$\sqrt{\langle j_{nx}^2 \rangle}$ ($\hbar$)	$\sqrt{\langle j_{ny}^2 \rangle}$ ($\hbar$)	$\sqrt{\langle j_{nz}^2 \rangle}$ ($\hbar$)	$\sqrt{\langle j_{nx}^2 \rangle}$ ($\hbar$)	$\sqrt{\langle j_{ny}^2 \rangle}$ ($\hbar$)	$\sqrt{\langle j_{nz}^2 \rangle}$ ($\hbar$)
8 to 22	5.382	2.084	1.212	5.382	2.084	1.212
	$\sqrt{\langle j_{Rx}^2 \rangle}$ ($\hbar$)	$\sqrt{\langle j_{Ry}^2 \rangle}$ ($\hbar$)	$\sqrt{\langle j_{Rz}^2 \rangle}$ ($\hbar$)	$\sqrt{\langle j_{Rx}^2 \rangle}$ ($\hbar$)	$\sqrt{\langle j_{Ry}^2 \rangle}$ ($\hbar$)	$\sqrt{\langle j_{Rz}^2 \rangle}$ ($\hbar$)
8	1.733	3.789	1.764	2.133	5.094	2.368
9	2.127	4.153	2.026	2.209	5.623	2.406
10	2.611	4.699	2.367	2.434	6.271	2.527
11	3.063	5.595	2.702	2.723	7.080	2.692
12	3.337	7.052	2.938	2.997	8.086	2.858
13	3.385	8.861	3.042	3.199	9.279	3.000
14	3.398	10.472	3.110	3.323	10.574	3.119
15	3.443	11.859	3.192	3.417	11.867	3.214
16	3.499	13.130	3.289	3.505	13.127	3.290
17	3.571	14.352	3.367	3.577	14.340	3.378
18	3.646	15.530	3.449	3.645	15.529	3.457
19	3.712	16.693	3.523	3.719	16.680	3.539
20	3.786	17.824	3.601	3.783	17.823	3.612
21	3.849	18.949	3.670	3.856	18.938	3.689
22	3.920	20.052	3.743	3.917	20.049	3.759

Table A.18

A ~ 130, restricted configuration						
Spin I ($\hbar$)	$\gamma = 20^0$, **yrast band**			$\gamma = 20^0$, **side band**		
	$\sqrt{\langle j_{px}^2 \rangle}$ ($\hbar$)	$\sqrt{\langle j_{py}^2 \rangle}$ ($\hbar$)	$\sqrt{\langle j_{pz}^2 \rangle}$ ($\hbar$)	$\sqrt{\langle j_{px}^2 \rangle}$ ($\hbar$)	$\sqrt{\langle j_{py}^2 \rangle}$ ($\hbar$)	$\sqrt{\langle j_{pz}^2 \rangle}$ ($\hbar$)
8 to 22	5.320	2.265	1.074	5.320	2.265	1.074
	$\sqrt{\langle j_{nx}^2 \rangle}$ ($\hbar$)	$\sqrt{\langle j_{ny}^2 \rangle}$ ($\hbar$)	$\sqrt{\langle j_{nz}^2 \rangle}$ ($\hbar$)	$\sqrt{\langle j_{nx}^2 \rangle}$ ($\hbar$)	$\sqrt{\langle j_{ny}^2 \rangle}$ ($\hbar$)	$\sqrt{\langle j_{nz}^2 \rangle}$ ($\hbar$)
8 to 22	8 to 22	1.330	1.516	5.468	1.330	1.516
	$\sqrt{\langle j_{Rx}^2 \rangle}$ ($\hbar$)	$\sqrt{\langle j_{Ry}^2 \rangle}$ ($\hbar$)	$\sqrt{\langle j_{Rz}^2 \rangle}$ ($\hbar$)	$\sqrt{\langle j_{Rx}^2 \rangle}$ ($\hbar$)	$\sqrt{\langle j_{Ry}^2 \rangle}$ ($\hbar$)	$\sqrt{\langle j_{Rz}^2 \rangle}$ ($\hbar$)
8	1.895	3.951	1.456	2.754	5.202	2.050
9	2.267	4.299	1.515	2.456	5.785	2.125
10	2.970	4.714	1.569	2.536	6.443	2.181
11	3.788	5.214	1.610	2.910	7.163	2.214
12	4.617	5.825	1.637	3.430	7.946	2.230
13	5.396	6.585	1.656	3.992	8.796	2.232
14	6.072	7.541	1.674	4.536	9.717	2.226
15	6.583	8.735	1.707	5.026	10.710	2.218
16	6.881	10.161	1.771	5.445	11.771	2.213
17	6.967	11.731	1.870	5.786	12.889	2.216
18	6.922	13.306	1.987	6.053	14.045	2.232
19	6.826	14.826	2.088	6.279	15.188	2.271
20	6.764	16.143	2.252	6.452	16.432	2.243
21	6.789	17.425	2.317	6.542	17.624	2.302
22	6.822	18.653	2.386	6.638	18.798	2.350

Table A.19

A ~ 130, restricted configuration						
Spin I ($\hbar$)	$\gamma = 30^0$, **yrast band**			$\gamma = 30^0$, **side band**		
	$\sqrt{\langle j_{px}^2 \rangle}$ ($\hbar$)	$\sqrt{\langle j_{py}^2 \rangle}$ ($\hbar$)	$\sqrt{\langle j_{pz}^2 \rangle}$ ($\hbar$)	$\sqrt{\langle j_{px}^2 \rangle}$ ($\hbar$)	$\sqrt{\langle j_{py}^2 \rangle}$ ($\hbar$)	$\sqrt{\langle j_{pz}^2 \rangle}$ ($\hbar$)
8 to 22	5.170	2.444	1.369	5.170	2.444	1.369
	$\sqrt{\langle j_{nx}^2 \rangle}$ ($\hbar$)	$\sqrt{\langle j_{ny}^2 \rangle}$ ($\hbar$)	$\sqrt{\langle j_{nz}^2 \rangle}$ ($\hbar$)	$\sqrt{\langle j_{nx}^2 \rangle}$ ($\hbar$)	$\sqrt{\langle j_{ny}^2 \rangle}$ ($\hbar$)	$\sqrt{\langle j_{nz}^2 \rangle}$ ($\hbar$)
8 to 22	1.438	2.046	5.294	1.438	2.046	5.294
	$\sqrt{\langle j_{Rx}^2 \rangle}$ ($\hbar$)	$\sqrt{\langle j_{Ry}^2 \rangle}$ ($\hbar$)	$\sqrt{\langle j_{Rz}^2 \rangle}$ ($\hbar$)	$\sqrt{\langle j_{Rx}^2 \rangle}$ ($\hbar$)	$\sqrt{\langle j_{Ry}^2 \rangle}$ ($\hbar$)	$\sqrt{\langle j_{Rz}^2 \rangle}$ ($\hbar$)
8	1.810	3.744	1.624	2.477	5.016	2.341
9	1.993	4.026	1.828	2.429	5.472	2.288
10	2.336	4.411	2.201	2.518	6.016	2.383
11	2.747	4.987	2.639	2.704	6.681	2.585
12	3.134	5.920	3.043	2.933	7.509	2.826
13	3.383	7.414	3.300	3.150	8.537	3.056
14	3.454	9.272	3.370	3.320	9.751	3.234
15	3.480	10.941	3.403	3.443	11.070	3.352
16	3.531	12.369	3.463	3.538	12.391	3.440
17	3.608	13.676	3.525	3.608	13.675	3.529
18	3.682	14.920	3.598	3.681	14.915	3.606
19	3.753	16.125	3.671	3.754	16.120	3.679
20	3.823	17.302	3.742	3.824	17.297	3.751
21	3.892	18.456	3.812	3.893	18.451	3.821
22	3.958	19.593	3.879	3.960	19.587	3.891

Table A.20

A ~ 190, restricted configuration						
Spin I ($\hbar$)	$\gamma = 36^0$, **yrast band**			$\gamma = 36^0$, **side band**		
	$\sqrt{\langle j_{px}^2 \rangle}$ ($\hbar$)	$\sqrt{\langle j_{py}^2 \rangle}$ ($\hbar$)	$\sqrt{\langle j_{pz}^2 \rangle}$ ($\hbar$)	$\sqrt{\langle j_{px}^2 \rangle}$ ($\hbar$)	$\sqrt{\langle j_{py}^2 \rangle}$ ($\hbar$)	$\sqrt{\langle j_{pz}^2 \rangle}$ ($\hbar$)
8 to 22	4.422	1.868	1.193	4.422	1.868	1.193
	$\sqrt{\langle j_{nx}^2 \rangle}$ ($\hbar$)	$\sqrt{\langle j_{ny}^2 \rangle}$ ($\hbar$)	$\sqrt{\langle j_{nz}^2 \rangle}$ ($\hbar$)	$\sqrt{\langle j_{nx}^2 \rangle}$ ($\hbar$)	$\sqrt{\langle j_{ny}^2 \rangle}$ ($\hbar$)	$\sqrt{\langle j_{nz}^2 \rangle}$ ($\hbar$)
8 to 22	1.534	2.079	6.395	1.534	2.079	6.395
	$\sqrt{\langle j_{Rx}^2 \rangle}$ ($\hbar$)	$\sqrt{\langle j_{Ry}^2 \rangle}$ ($\hbar$)	$\sqrt{\langle j_{Rz}^2 \rangle}$ ($\hbar$)	$\sqrt{\langle j_{Rx}^2 \rangle}$ ($\hbar$)	$\sqrt{\langle j_{Ry}^2 \rangle}$ ($\hbar$)	$\sqrt{\langle j_{Rz}^2 \rangle}$ ($\hbar$)
8	1.986	3.957	1.611	2.623	5.269	2.368
9	2.024	4.242	1.928	2.663	5.751	2.105
10	2.071	4.596	2.571	2.698	6.313	2.194
11	2.118	5.045	3.336	2.723	6.934	2.583
12	2.157	5.632	4.117	2.735	7.655	3.101
13	2.190	6.437	4.833	2.734	8.476	3.655
14	2.231	7.550	5.401	2.722	9.403	4.182
15	2.302	9.014	5.725	2.719	10.466	4.604
16	2.429	10.733	5.751	2.719	11.602	4.962
17	2.572	12.388	5.666	2.740	12.829	5.190
18	2.691	13.894	5.583	2.788	14.076	5.347
19	2.817	15.278	5.513	2.814	15.298	5.509
20	2.880	16.541	5.562	2.891	16.538	5.564
21	2.952	17.757	5.608	2.949	17.748	5.634
22	3.014	18.944	5.665	3.010	18.930	5.700

Table A.21

A ~ 190, restricted configuration						
Spin I ($\hbar$)	$\gamma = 30^0$, **yrast band**			$\gamma = 30^0$, **side band**		
	$\sqrt{\langle j_{px}^2 \rangle}$ ($\hbar$)	$\sqrt{\langle j_{py}^2 \rangle}$ ($\hbar$)	$\sqrt{\langle j_{pz}^2 \rangle}$ ($\hbar$)	$\sqrt{\langle j_{px}^2 \rangle}$ ($\hbar$)	$\sqrt{\langle j_{py}^2 \rangle}$ ($\hbar$)	$\sqrt{\langle j_{pz}^2 \rangle}$ ($\hbar$)
8 to 22	4.373	1.985	1.105	4.373	1.985	1.105
	$\sqrt{\langle j_{nx}^2 \rangle}$ ($\hbar$)	$\sqrt{\langle j_{ny}^2 \rangle}$ ($\hbar$)	$\sqrt{\langle j_{nz}^2 \rangle}$ ($\hbar$)	$\sqrt{\langle j_{nx}^2 \rangle}$ ($\hbar$)	$\sqrt{\langle j_{ny}^2 \rangle}$ ($\hbar$)	$\sqrt{\langle j_{nz}^2 \rangle}$ ($\hbar$)
8 to 22	1.604	2.000	6.428	1.604	2.000	6.428
	$\sqrt{\langle j_{Rx}^2 \rangle}$ ($\hbar$)	$\sqrt{\langle j_{Ry}^2 \rangle}$ ($\hbar$)	$\sqrt{\langle j_{Rz}^2 \rangle}$ ($\hbar$)	$\sqrt{\langle j_{Rx}^2 \rangle}$ ($\hbar$)	$\sqrt{\langle j_{Ry}^2 \rangle}$ ($\hbar$)	$\sqrt{\langle j_{Rz}^2 \rangle}$ ($\hbar$)
8	2.134	3.877	1.492	2.856	5.129	2.130
9	2.218	4.137	1.770	2.842	5.525	2.013
10	2.397	4.496	2.276	2.870	6.087	2.135
11	2.635	5.040	2.846	2.946	6.720	2.464
12	2.887	5.913	3.366	3.032	7.497	2.869
13	3.091	7.302	3.707	3.135	8.518	3.191
14	3.185	9.130	3.791	3.288	9.728	3.380
15	3.311	10.879	3.690	3.352	10.993	3.603
16	3.436	12.342	3.659	3.407	12.298	3.747
17	3.504	13.646	3.731	3.513	13.599	3.796
18	3.585	14.890	3.793	3.597	14.850	3.859
19	3.664	16.098	3.853	3.676	16.060	3.927
20	3.740	17.276	3.914	3.752	17.241	3.994
21	3.813	18.432	3.975	3.826	18.399	4.060
22	3.884	19.568	4.035	3.898	19.539	4.125

Table A.22-23: *Calculated relative angular momenta of the proton, neutron and the core for the partner bands in A ~ 100, 130 and 190 mass regions at* ε_2 *= 0.15 and* γ *= 20⁰, 30⁰, 36⁰.*

Table A.22

Non-restricted configuration						
Spin I ($\hbar$)	$\Delta j_{p,l} = \sqrt{\langle j^2_{p,l} \rangle_{side}} - \sqrt{\langle j^2_{p,l} \rangle_{yrast}}$ ($\hbar$)		$\Delta j_{p,s} = \sqrt{\langle j^2_{p,s} \rangle_{side}} - \sqrt{\langle j^2_{p,s} \rangle_{yrast}}$ ($\hbar$)			
	A ~ 100		**A ~ 130**		**A ~ 190**	
	$\gamma = 20^0$	$\gamma = 30^0$	$\gamma = 20^0$	$\gamma = 30^0$	$\gamma = 36^0$	$\gamma = 30^0$
8	-0.124	-0.027	-0.049	-0.134	-0.176	-0.074
9	-0.072	-0.009	0.019	-0.098	-0.148	-0.056
10	-0.013	-0.049	0.123	-0.274	-0.208	-0.200
11	0.116	-0.087	0.131	-0.475	-0.174	-0.342
12	0.038	-0.144	0.199	-0.269	0.172	0.032
13	0.131	0.193	0.511	0.472	0.011	0.400
14	-0.063	-0.086	0.904	0.719	0.359	0.527
15	-0.021	0.188	1.135	0.939	0.186	0.779
16	-0.115	0.020	1.229	0.964	0.350	0.657
17	-0.193	0.102	1.260	1.046	0.338	0.842
18	-0.086	0.117	1.210	1.067	0.192	0.665
19	-0.252	0.030	1.174	1.062	0.518	0.870
20	-0.081	0.219	1.201	1.102	0.196	0.640
21	-0.360	-0.025	0.977	1.050	0.676	0.903
22	0.165	0.322	1.142	1.099	0.139	0.608
	$\Delta j_{n,s} = \sqrt{\langle j^2_{n,s} \rangle_{side}} - \sqrt{\langle j^2_{n,s} \rangle_{yrast}}$ ($\hbar$)		$\Delta j_{n,l} = \sqrt{\langle j^2_{n,l} \rangle_{side}} - \sqrt{\langle j^2_{n,l} \rangle_{yrast}}$ ($\hbar$)			
8	0.069	-0.090	-0.132	-0.067	-0.163	-0.166
9	0.140	-0.151	0.775	-0.049	-0.052	-0.067
10	0.136	-0.287	-0.059	-0.019	0.000	-0.008
11	0.170	-0.469	0.024	-0.027	-0.160	-0.090
12	0.339	-0.030	0.112	-0.186	-0.319	-0.383
13	0.733	0.554	0.070	-0.228	-0.306	-0.326
14	0.904	0.625	0.083	0.109	0.599	0.277
15	1.135	0.754	-0.092	-0.240	0.228	-0.321
16	1.107	0.757	-0.035	0.095	0.737	0.300
17	1.174	0.864	-0.183	-0.182	0.426	-0.145
18	0.956	0.857	-0.192	-0.025	0.677	0.233
19	1.168	0.922	-0.144	-0.060	0.503	0.066
20	0.264	0.935	-0.341	-0.145	0.654	0.159
21	1.155	0.943	-0.025	0.090	0.558	0.254
22	-0.125	0.992	-0.455	-0.230	0.654	0.108

Table A.23

Non-restricted configuration						
Spin I ($\hbar$)	$\Delta j_{R,i} = \sqrt{\langle j^2_{R,i} \rangle_{side}} - \sqrt{\langle j^2_{R,i} \rangle_{yrast}}$ ($\hbar$)					
	A ~ 100		**A ~ 130**		**A ~ 190**	
	$\gamma = 20^0$	$\gamma = 30^0$	$\gamma = 20^0$	$\gamma = 30^0$	$\gamma = 36^0$	$\gamma = 30^0$
8	1.018	0.897	1.086	0.788	0.824	0.889
9	1.142	0.971	1.098	0.935	0.916	0.905
10	1.010	0.874	1.169	0.901	0.906	0.813
11	0.774	0.777	0.935	0.845	0.809	0.723
12	0.285	0.589	0.401	0.814	0.766	0.699
13	0.087	0.536	-0.129	0.426	0.465	0.618
14	-0.184	0.008	-0.357	0.483	-0.179	0.384
15	0.293	0.799	-0.317	0.126	-0.094	0.198

Table A.23 continues

Spin I ($\hbar$)	Non-restricted configuration: $\Delta j_{R,i} = \sqrt{\langle j^2_{R,i} \rangle_{side}} - \sqrt{\langle j^2_{R,i} \rangle_{yrast}}$ ($\hbar$)					
	A ~ 100		A ~ 130		A ~ 190	
	$\gamma = 20^0$	$\gamma = 30^0$	$\gamma = 20^0$	$\gamma = 30^0$	$\gamma = 36^0$	$\gamma = 30^0$
16	0.159	0.396	0.219	0.758	0.708	0.799
17	0.514	0.795	0.243	0.398	0.305	0.420
18	0.626	0.762	0.644	0.809	0.937	0.927
19	0.472	0.694	0.643	0.710	0.754	0.727
20	0.856	1.075	0.622	0.713	0.858	0.861
21	0.387	0.581	0.923	1.003	1.111	1.018
22	1.116	1.328	0.519	0.597	0.741	0.752
	Restricted configuration					
8	1.361	1.306	1.251	1.272	1.312	1.251
9	1.602	1.470	1.486	1.446	1.508	1.388
10	1.826	1.571	1.729	1.605	1.718	1.592
11	2.012	1.484	1.949	1.694	1.889	1.680
12	2.132	1.034	2.121	1.590	2.023	1.584
13	2.148	0.418	2.211	1.123	2.039	1.217
14	2.019	0.102	2.176	0.480	1.853	0.598
15	1.721	0.008	1.975	0.129	1.452	0.114
16	1.291	-0.002	1.610	0.022	0.870	-0.044
17	0.814	-0.012	1.158	-0.001	0.441	-0.047
18	0.290	-0.001	0.738	-0.005	0.182	-0.040
19	-0.202	-0.013	0.361	-0.005	0.019	-0.038
20	-0.240	-0.001	0.290	-0.006	-0.004	-0.036
21	-0.197	-0.012	0.199	-0.005	-0.008	-0.033
22	-0.164	-0.004	0.145	-0.006	-0.014	-0.030

Table A.24-26: *Calculated relative projections of the total angular momenta of the system in A ~ 100, 130 and 190 mass regions at* $\varepsilon_2 = 0.15$ *and* $\gamma = 20^0, 30^0, 36^0$.

Table A.24

Spin I ($\hbar$)	Non-restricted configuration: $\Delta I_s = \sqrt{\langle I_s \rangle^2_{side}} - \sqrt{\langle I_s \rangle^2_{yrast}}$ ($\hbar$)					
	A ~ 100		A ~ 130		A ~ 190	
	$\gamma = 20^0$	$\gamma = 30^0$	$\gamma = 20^0$	$\gamma = 30^0$	$\gamma = 36^0$	$\gamma = 30^0$
8	-0.572	-0.710	-0.210	-0.476	0.024	-0.089
9	-0.944	-0.989	-0.469	-0.725	-0.253	-0.674
10	-1.390	-1.270	-0.952	-1.243	-0.389	-1.174
11	-1.381	-1.744	-1.560	-1.510	0.318	-1.204
12	-0.721	0.079	-1.351	-0.103	1.525	1.002
13	0.652	1.165	-0.172	1.399	0.532	1.013
14	1.360	1.051	1.403	1.210	1.557	1.006
15	1.991	1.385	2.153	1.532	0.622	1.413
16	1.819	1.010	2.318	1.622	0.841	1.286
17	1.864	1.585	2.118	1.451	0.373	1.353
18	1.025	0.902	1.731	1.746	0.857	1.156
19	1.670	1.667	1.451	1.164	0.386	1.152
20	-0.127	0.764	1.373	1.773	0.874	1.063
21	1.511	1.675	0.775	0.862	0.411	0.973
22	-0.277	0.606	1.181	1.739	0.840	0.993

Table A.24 continues

Restricted configuration						
Spin I ($\hbar$)	$\Delta I_s = \sqrt{\langle I_s \rangle^2_{side}} - \sqrt{\langle I_s \rangle^2_{yrast}}$ ($\hbar$)					
	A ~ 100		A ~ 130		A ~ 190	
	$\gamma = 20^0$	$\gamma = 30^0$	$\gamma = 20^0$	$\gamma = 30^0$	$\gamma = 36^0$	$\gamma = 30^0$
8	-1.310	-0.666	-1.158	-0.508	0.068	-0.161
9	-1.454	-0.725	-1.339	-0.563	0.077	-0.266
10	-1.593	-0.782	-1.491	-0.624	-0.528	-0.304
11	-1.730	-0.788	-1.635	-0.681	0.073	-0.350
12	-1.852	-0.628	-1.773	-0.694	0.057	-0.429
13	-1.936	-0.307	-1.888	-0.566	0.053	-0.402
14	-1.940	-0.108	-1.948	-0.290	0.033	-0.098
15	-1.814	-0.032	-1.904	-0.086	0.049	0.025
16	-1.538	0.010	-1.713	-0.001	0.045	0.025
17	-1.140	0.016	-1.388	0.004	0.014	0.085
18	-0.569	0.008	-1.016	0.007	0.060	0.096
19	0.196	0.021	-0.635	0.009	-0.031	0.105
20	0.375	0.012	-0.416	0.011	0.044	0.115
21	0.368	0.025	-0.350	0.012	0.019	0.124
22	0.353	0.019	-0.290	0.015	0.028	0.132

Table A.25

Non-restricted configuration						
Spin I ($\hbar$)	$\Delta I_i = \sqrt{\langle I_i \rangle^2_{side}} - \sqrt{\langle I_i \rangle^2_{yrast}}$ ($\hbar$)					
	A ~ 100		A ~ 130		A ~ 190	
	$\gamma = 20^0$	$\gamma = 30^0$	$\gamma = 20^0$	$\gamma = 30^0$	$\gamma = 36^0$	$\gamma = 30^0$
8	0.618	1.423	0.401	1.507	0.630	1.050
9	0.745	1.595	0.525	1.541	0.896	1.318
10	0.688	1.978	0.727	1.817	1.303	1.608
11	0.127	2.312	0.537	2.302	1.687	2.251
12	-0.374	0.911	-0.305	2.071	0.959	1.499
13	-1.529	-0.960	-1.242	-0.012	1.246	0.341
14	-1.462	-0.677	-2.185	-1.017	-2.258	-1.214
15	-1.601	-0.858	-1.952	-0.746	-0.610	-0.506
16	-1.105	-0.518	-1.689	-0.920	-1.251	-0.916
17	-1.054	-0.748	-1.115	-0.529	-0.627	-0.479
18	-0.394	-0.366	-0.881	-0.729	-0.736	-0.632
19	-0.806	-0.671	-0.520	-0.346	-0.473	-0.414
20	0.141	-0.252	-0.586	-0.617	-0.587	-0.494
21	-0.664	-0.605	-0.175	-0.219	-0.351	-0.350
22	0.106	-0.168	-0.457	-0.541	-0.517	-0.422
	Restricted configuration					
8	1.647	1.606	1.557	1.604	1.664	1.611
9	1.866	1.732	1.773	1.749	1.835	1.727
10	2.063	1.781	1.991	1.868	2.013	1.897
11	2.218	1.623	2.181	1.903	2.146	1.919
12	2.304	1.098	2.319	1.730	2.238	1.747
13	2.285	0.435	2.373	1.189	2.203	1.309
14	2.121	0.105	2.302	0.499	1.965	0.628
15	1.793	0.009	2.067	0.133	1.517	0.107
16	1.339	-0.004	1.673	0.022	0.896	-0.059
17	0.844	-0.014	1.201	-0.002	0.455	-0.066
18	0.296	-0.003	0.769	-0.006	0.183	-0.062
19	-0.230	-0.016	0.383	-0.006	0.015	-0.063
20	-0.280	-0.004	0.316	-0.007	-0.009	-0.063

Table A.25 continues

Restricted configuration						
Spin I ($\hbar$)	$\Delta I_i = \sqrt{\langle I_i \rangle^2_{side}} - \sqrt{\langle I_i \rangle^2_{yrast}}$ ($\hbar$)					
	A ~ 100		A ~ 130		A ~ 190	
	$\gamma = 20^0$	$\gamma = 30^0$	$\gamma = 20^0$	$\gamma = 30^0$	$\gamma = 36^0$	$\gamma = 30^0$
21	-0.241	-0.016	0.228	-0.007	-0.014	-0.063
22	-0.213	-0.007	0.176	-0.008	-0.021	-0.063

Table A.26

Non-restricted configuration						
Spin I ($\hbar$)	$\Delta I_l = \sqrt{\langle I_l \rangle^2_{side}} - \sqrt{\langle I_l \rangle^2_{yrast}}$ ($\hbar$)					
	A ~ 100		A ~ 130		A ~ 190	
	$\gamma = 20^0$	$\gamma = 30^0$	$\gamma = 20^0$	$\gamma = 30^0$	$\gamma = 36^0$	$\gamma = 30^0$
8	0.042	-0.373	-0.113	-0.676	-0.436	-0.603
9	0.291	-0.257	0.000	-0.461	-0.412	-0.369
10	0.818	-0.369	0.229	-0.260	-0.652	-0.237
11	1.488	-0.385	-1.291	-0.484	-1.595	-0.743
12	1.437	-1.249	1.629	-1.820	-2.072	-2.184
13	1.518	0.191	1.640	-1.330	-1.622	-1.233
14	0.756	0.081	1.368	0.298	1.463	0.787
15	0.525	0.284	0.576	-0.177	0.441	-0.346
16	-0.018	0.113	0.352	0.229	1.422	0.580
17	0.135	0.212	-0.227	-0.206	0.901	-0.146
18	-0.332	0.063	0.004	0.076	0.910	0.451
19	0.155	0.241	-0.451	-0.188	0.798	0.052
20	-0.382	0.018	-0.013	0.038	0.813	0.415
21	0.244	0.298	-0.462	-0.141	0.644	0.180
22	-0.049	-0.010	0.035	0.071	0.842	0.438
	Restricted configuration					
8	0.161	-0.391	0.022	-0.516	-1.061	-0.783
9	0.182	-0.456	0.081	-0.569	-1.149	-0.769
10	0.187	-0.525	0.096	-0.631	-1.264	-0.880
11	0.186	-0.543	0.096	-0.690	-1.361	-0.934
12	0.186	-0.441	0.090	-0.702	-1.466	-0.890
13	0.190	-0.206	0.086	-0.568	-1.538	-0.766
14	0.202	-0.035	0.084	-0.284	-1.497	-1.049
15	0.222	0.023	0.089	-0.094	-1.319	-0.139
16	0.252	-0.003	0.097	-0.033	-0.900	0.060
17	0.298	0.011	0.107	0.000	-0.514	0.035
18	0.367	-0.001	0.120	0.004	-0.259	0.030
19	0.258	0.015	0.196	0.004	-0.007	0.032
20	0.110	-0.002	-0.082	0.004	-0.010	0.033
21	0.058	0.016	-0.020	0.004	0.013	0.034
22	0.039	-0.001	-0.013	0.006	0.020	0.035

Table A.27-29: *Calculated average angles (in degree) between the angular momenta of the proton (j_p), neutron (j_n) and the core (j_R) for the partner bands in A ~ 100, 130 and 190 mass regions at ε_2 = 0.15 and γ = 20^0, 30^0, 36^0.*

Table A.27

A ~ 100								
Spin I ($\hbar$)	**Non-restricted configuration**				**Restricted configuration**			
	$\alpha(p,n)$ **, yrast band**		$\alpha(p,n)$ **, side band**		$\alpha(p,n)$ **, yrast band**		$\alpha(p,n)$ **, side band**	
	$\gamma = 20^0$	$\gamma = 30^0$	$\gamma = 20^0$	$\gamma = 30^0$	$\gamma = 20^0$	$\gamma = 30^0$	$\gamma = 20^0$	$\gamma = 30^0$
8	82.206	82.282	88.246	89.210	89.994	90.000	90.029	90.000
9	76.074	75.496	84.046	84.618	89.994	90.000	90.027	90.000
10	71.987	70.812	78.607	77.710	89.994	90.000	90.024	90.000
11	68.281	68.065	73.407	69.977	89.994	90.000	90.022	90.000
12	66.034	68.968	70.766	64.340	89.992	90.000	90.020	90.000
13	65.031	66.167	65.269	66.036	89.990	90.000	90.022	90.000
14	61.841	61.169	67.154	70.441	89.988	90.000	90.022	90.000
15	63.422	65.199	58.650	59.925	89.984	89.998	90.024	90.002
16	57.472	57.227	68.951	72.323	89.976	90.002	90.029	89.998
17	62.157	64.348	53.409	54.590	89.966	89.996	90.037	90.004
18	52.906	53.694	72.942	73.880	89.949	90.004	90.051	89.996
19	61.255	63.669	50.145	50.896	89.955	89.994	90.041	90.006
20	48.635	50.358	71.514	75.181	89.976	90.004	90.020	89.996
21	60.631	63.139	47.759	48.187	89.984	89.994	90.012	90.006
22	45.065	47.333	67.010	76.336	89.986	90.004	90.008	89.996
	$\alpha(R,p)$ **, yrast band**		$\alpha(R,p)$ **, side band**		$\alpha(R,p)$ **, yrast band**		$\alpha(R,p)$ **, side band**	
8	93.622	89.905	85.442	90.739	92.532	92.310	94.027	98.074
9	88.650	80.992	79.643	81.111	91.266	86.057	92.424	93.025
10	83.954	72.827	72.772	74.507	90.478	81.866	91.385	89.143
11	77.365	66.013	67.549	68.270	90.024	80.094	90.704	86.582
12	75.374	60.515	63.099	69.685	89.797	81.048	90.263	85.305
13	68.412	59.287	62.330	67.187	89.749	83.439	89.976	85.078
14	67.689	63.883	58.553	56.372	89.833	85.114	89.785	85.412
15	61.637	54.736	60.714	64.105	89.988	85.961	89.666	85.902
16	60.596	57.922	55.494	53.928	90.215	86.403	89.570	86.415
17	57.150	51.604	55.933	59.506	90.454	86.784	89.475	86.760
18	53.839	52.554	53.651	52.206	90.358	87.047	89.331	87.070
19	54.089	49.449	50.655	54.949	90.143	87.321	89.511	87.285
20	47.609	47.746	57.824	50.854	90.060	87.488	89.797	87.511
21	51.901	47.873	46.283	51.105	90.036	87.678	89.905	87.654
22	42.387	43.522	62.055	49.890	92.532	87.809	89.964	87.821
	$\alpha(R,n)$ **, yrast band**		$\alpha(R,n)$ **, side band**		$\alpha(R,n)$ **, yrast band**		$\alpha(R,n)$ **, side band**	
8	85.552	91.399	95.283	91.186	95.247	95.010	106.564	101.334
9	70.553	81.223	84.571	83.500	85.497	87.318	98.639	95.176
10	59.092	71.892	76.041	74.807	78.407	82.076	92.421	90.408
11	51.278	63.674	66.611	66.979	73.579	79.715	87.765	87.191
12	47.749	59.435	58.064	62.858	70.615	80.602	84.430	85.527
13	42.982	54.169	55.728	62.973	69.275	83.222	82.180	85.146
14	42.779	52.758	51.382	58.422	69.421	84.990	80.789	85.527
15	38.593	47.068	56.147	61.088	70.853	85.906	80.076	86.023
16	39.422	47.181	50.126	55.479	73.151	86.471	79.868	86.452
17	35.785	42.584	56.154	58.540	75.704	86.860	79.957	86.812
18	36.919	42.941	47.076	53.671	78.218	87.143	79.967	87.133
19	33.990	39.755	54.580	56.014	80.492	87.405	79.789	87.347
20	56.328	39.603	36.793	52.335	81.529	87.590	80.472	87.571

Table A.27 continues

A ~ 100								
Spin I ($\hbar$)	Non-restricted configuration				Restricted configuration			
	$\alpha(R,n)$, yrast band		$\alpha(R,n)$, side band		$\alpha(R,n)$, yrast band		$\alpha(R,n)$, side band	
	$\gamma = 20^0$	$\gamma = 30^0$	$\gamma = 20^0$	$\gamma = 30^0$	$\gamma = 20^0$	$\gamma = 30^0$	$\gamma = 20^0$	$\gamma = 30^0$
21	32.798	37.897	52.976	53.799	82.150	87.775	81.253	87.726
22	33.140	36.960	31.404	51.127	82.672	87.911	81.904	87.882

Table A.28

A ~ 130								
Spin I ($\hbar$)	Non-restricted configuration				Restricted configuration			
	$\alpha(p,n)$, yrast band		$\alpha(p,n)$, side band		$\alpha(p,n)$, yrast band		$\alpha(p,n)$, side band	
	$\gamma = 20^0$	$\gamma = 30^0$	$\gamma = 20^0$	$\gamma = 30^0$	$\gamma = 20^0$	$\gamma = 30^0$	$\gamma = 20^0$	$\gamma = 30^0$
8	87.239	87.521	92.209	91.623	89.995	90.000	90.027	90.000
9	79.372	79.991	84.872	88.162	89.995	90.000	90.023	90.000
10	73.040	73.457	80.462	83.133	89.997	90.000	90.018	90.000
11	68.903	68.892	76.090	75.434	89.997	90.000	90.015	90.000
12	66.053	67.158	70.840	67.004	89.997	90.000	90.012	90.000
13	64.410	66.381	66.252	63.557	89.995	90.000	90.012	90.000
14	63.462	64.374	63.858	65.586	89.995	90.000	90.010	90.000
15	61.436	61.948	63.827	66.359	89.993	90.000	90.008	90.000
16	61.723	63.110	60.464	60.727	89.993	90.002	90.008	89.998
17	57.727	57.733	65.868	68.461	89.992	90.000	90.008	90.000
18	60.372	62.057	56.311	55.509	89.988	89.998	90.010	90.000
19	53.726	53.941	69.039	70.419	89.975	90.000	90.023	90.000
20	59.461	61.294	52.729	51.517	90.017	89.998	89.980	90.002
21	49.930	50.445	71.648	72.117	90.007	90.000	89.990	90.000
22	58.872	60.758	50.161	48.684	90.007	89.998	89.990	90.002
	$\alpha(R,p)$, yrast band		$\alpha(R,p)$, side band		$\alpha(R,p)$, yrast band		$\alpha(R,p)$, side band	
8	94.998	95.739	103.030	91.696	102.191	99.915	111.778	104.128
9	80.461	86.851	92.768	87.426	90.516	91.890	102.880	98.101
10	65.863	77.376	81.970	79.857	81.543	85.564	95.425	92.962
11	55.241	69.605	72.597	69.743	75.184	81.338	89.669	89.007
12	48.549	63.798	62.020	59.940	71.008	79.541	85.456	86.375
13	44.904	54.906	54.534	61.661	68.683	80.471	82.516	85.056
14	41.333	49.804	51.707	61.461	67.991	82.912	80.625	84.812
15	40.135	47.163	50.654	58.689	68.788	84.675	79.567	85.154
16	37.017	43.126	54.029	59.719	70.781	85.604	79.141	85.643
17	37.126	42.757	50.861	55.337	73.362	86.141	79.181	86.131
18	34.230	39.090	55.728	58.110	75.848	86.531	79.518	86.511
19	35.046	39.627	48.822	52.931	77.948	86.843	79.904	86.814
20	32.432	36.643	54.718	56.037	79.320	87.097	80.566	87.067
21	33.392	37.173	44.860	50.915	80.319	87.301	81.227	87.282
22	31.227	35.133	53.230	53.996	81.119	87.487	81.799	87.467
	$\alpha(R,n)$, yrast band		$\alpha(R,n)$, side band		$\alpha(R,n)$, yrast band		$\alpha(R,n)$, side band	
8	96.327	96.877	87.422	100.005	96.839	98.608	96.463	103.260
9	94.263	90.069	85.963	87.866	93.807	90.587	93.817	97.196
10	89.725	81.703	80.622	78.691	91.770	84.319	92.144	92.073
11	84.602	72.502	72.564	75.433	90.501	80.164	91.082	88.161
12	79.546	62.422	66.674	75.408	89.764	78.482	90.413	85.576
13	76.296	53.171	63.527	69.280	89.361	79.588	90.010	84.300
14	71.174	63.118	63.336	65.722	89.204	82.202	89.764	84.103
15	69.036	65.408	61.112	57.803	89.214	84.034	89.627	84.555
16	64.711	58.692	62.839	63.100	89.332	85.007	89.558	85.144
17	62.863	60.378	57.644	53.945	89.499	85.625	89.538	85.635
18	60.303	55.159	58.783	58.793	89.676	86.066	89.518	86.056

Table A.28 continues

A ~ 130								
Spin I ($\hbar$)	Non-restricted configuration				Restricted configuration			
	$\alpha(R,n)$, yrast band		$\alpha(R,n)$, side band		$\alpha(R,n)$, yrast band		$\alpha(R,n)$, side band	
	$\gamma = 20^0$	$\gamma = 30^0$	$\gamma = 20^0$	$\gamma = 30^0$	$\gamma = 20^0$	$\gamma = 30^0$	$\gamma = 20^0$	$\gamma = 30^0$
19	57.001	55.008	54.448	51.567	89.931	86.399	89.400	86.399
20	57.115	52.432	53.618	54.138	89.558	86.683	89.882	86.683
21	51.469	49.887	53.447	50.079	89.715	86.918	89.794	86.918
22	54.735	50.301	49.221	50.210	89.774	87.124	89.803	87.114

Table A.29

A ~ 190								
Spin I ($\hbar$)	Non-restricted configuration				Restricted configuration			
	$\alpha(p,n)$, yrast band		$\alpha(p,n)$, side band		$\alpha(p,n)$, yrast band		$\alpha(p,n)$, side band	
	$\gamma = 36^0$	$\gamma = 30^0$	$\gamma = 36^0$	$\gamma = 30^0$	$\gamma = 36^0$	$\gamma = 30^0$	$\gamma = 36^0$	$\gamma = 30^0$
8	88.735	88.607	90.996	91.516	90.000	89.997	90.002	90.020
9	80.400	79.829	87.894	89.362	90.000	89.998	90.000	90.007
10	74.221	73.151	83.513	84.215	90.000	89.998	89.998	89.985
11	70.742	69.399	74.429	75.020	90.000	89.997	90.002	89.993
12	66.747	67.884	70.300	66.937	90.000	89.993	89.998	90.008
13	63.213	66.423	71.821	65.582	90.000	89.997	89.998	89.997
14	65.489	65.150	64.933	67.630	89.998	90.012	90.002	89.975
15	57.796	61.223	71.170	69.245	90.002	89.990	89.995	90.002
16	64.835	64.602	60.585	62.994	89.997	89.980	90.003	90.012
17	53.866	56.816	73.498	72.142	90.000	89.982	90.000	90.010
18	64.671	64.313	54.737	57.950	90.002	89.980	89.997	90.012
19	50.771	53.555	75.602	74.261	89.988	89.978	90.012	90.014
20	64.640	64.214	51.559	54.490	89.998	89.977	90.000	90.015
21	48.331	50.991	77.196	75.855	89.993	89.975	90.005	90.017
22	64.664	64.220	49.652	52.208	89.993	89.973	90.005	90.019
	$\alpha(R,p)$, yrast band		$\alpha(R,p)$, side band		$\alpha(R,p)$, yrast band		$\alpha(R,p)$, side band	
8	100.239	100.260	92.128	94.919	101.674	102.885	100.789	104.513
9	96.700	93.935	90.570	93.331	98.041	96.607	98.065	100.251
10	90.985	85.752	83.544	86.054	95.138	91.407	95.743	95.846
11	85.638	78.614	75.906	76.776	93.001	87.593	94.022	92.442
12	77.708	72.343	72.061	67.955	91.564	85.438	92.769	90.279
13	74.590	62.516	69.961	71.325	90.672	85.298	91.854	88.930
14	65.821	58.612	68.235	68.743	90.220	86.894	91.321	88.035
15	65.151	55.108	63.347	66.437	90.174	87.965	90.915	88.093
16	58.274	52.152	67.582	66.852	90.278	88.419	90.730	88.372
17	57.054	50.724	60.666	62.246	90.394	88.721	90.649	88.535
18	54.323	48.199	63.609	64.976	90.544	88.884	90.521	88.721
19	51.056	47.083	59.708	59.705	90.452	89.000	90.602	88.872
20	51.961	45.761	59.707	62.447	90.556	89.093	90.487	88.989
21	46.637	44.073	59.536	58.142	90.510	89.163	90.521	89.093
22	50.560	44.208	56.570	60.030	90.498	89.221	90.498	89.175
	$\alpha(R,n)$, yrast band		$\alpha(R,n)$, side band		$\alpha(R,n)$, yrast band		$\alpha(R,n)$, side band	
8	97.046	97.744	103.923	102.092	101.372	100.465	109.039	105.934
9	89.060	92.560	91.586	88.716	90.673	91.374	100.873	98.509
10	78.898	84.934	82.863	80.506	81.941	84.037	93.957	92.907
11	68.707	75.858	79.526	77.877	75.448	79.047	88.280	88.319
12	62.149	66.161	71.571	76.767	71.119	76.786	84.058	84.877
13	61.230	66.877	60.871	69.801	68.954	77.542	81.185	83.329
14	55.454	63.860	60.214	66.012	69.007	80.225	79.381	83.371
15	58.211	65.349	53.746	58.410	71.040	82.820	78.738	83.521

Table A.29 continues

A ~ 190								
Spin I ($\hbar$)	Non-restricted configuration				Restricted configuration			
	$\alpha(R,n)$, yrast band		$\alpha(R,n)$, side band		$\alpha(R,n)$, yrast band		$\alpha(R,n)$, side band	
	$\gamma = 36^0$	$\gamma = 30^0$	$\gamma = 36^0$	$\gamma = 30^0$	$\gamma = 36^0$	$\gamma = 30^0$	$\gamma = 36^0$	$\gamma = 30^0$
16	50.392	58.482	62.264	64.653	74.286	84.195	78.679	84.004
17	52.539	59.709	50.378	54.172	77.090	84.827	79.187	84.727
18	46.839	54.827	61.492	61.883	79.035	85.326	79.964	85.259
19	47.611	54.369	48.150	51.989	80.520	85.733	80.537	85.674
20	44.480	52.258	58.834	58.545	81.319	86.065	81.370	86.015
21	43.716	49.958	46.407	50.693	82.016	86.347	81.999	86.297
22	42.882	50.376	56.335	55.582	82.578	86.587	82.553	86.546

Table A.30-44: *Calculated distributions (%) of the projection of the angular momenta of the proton (j_p), neutron (j_n) and the core (j_R) for the partner bands in A ~ 100, 130 and 190 mass regions at ε_2 = 0.15 and γ = 20^0, 30^0, 36^0.*

Table A.30

A ~ 100, non-restricted configuration						
Spin projection Ω ($\hbar$)	Distributions (%) for the angular momentum of the proton at I = 8					
	yrast band			side band		
	$\gamma = 20^0$, long axis	$\gamma = -100^0$, intermediate axis	$\gamma = 40^0$, short axis	$\gamma = 20^0$, long axis	$\gamma = -100^0$, intermediate axis	$\gamma = 40^0$, short axis
0.5	0.0800	42.6400	49.5500	0.3900	38.5700	45.2000
1.5	0.2300	31.9500	32.9000	0.7300	30.7700	32.8300
2.5	1.6800	17.4800	13.8700	3.4600	19.1500	16.4300
3.5	7.2300	6.5100	3.3300	15.0600	8.7500	4.8400
4.5	90.7700	1.4200	0.3600	80.3500	2.7600	0.7100
	Distributions (%) for the angular momentum of the proton at I = 16					
0.5	2.9800	25.2900	31.3400	3.4200	23.9000	30.1400
1.5	5.3200	24.8900	29.7600	6.7400	23.7500	28.8400
2.5	14.6700	22.6600	23.9100	17.1400	22.4700	24.3700
3.5	32.5800	16.9100	12.3500	32.1800	17.9500	13.9700
4.5	44.4500	10.2500	2.6400	40.5300	11.9400	2.6700
	Distributions (%) for the angular momentum of the proton at I = 20					
0.5	5.7100	18.5000	24.8700	12.8700	21.8200	25.9400
1.5	11.7500	19.8800	25.6100	22.6400	21.6000	24.3000
2.5	25.0800	22.2800	26.2300	15.9900	19.4700	17.5700
3.5	32.4800	21.7000	19.4600	15.8700	17.6100	22.4900
4.5	24.9800	17.6300	3.8400	32.6300	19.5000	9.7000

Table A.31

A ~ 100, non-restricted configuration						
Spin projection Ω ($\hbar$)	Distributions (%) for the angular momentum of the neutron at I = 8					
	yrast band			side band		
	$\gamma = 20^0$, long axis	$\gamma = -100^0$, intermediate axis	$\gamma = 40^0$, short axis	$\gamma = 20^0$, long axis	$\gamma = -100^0$, intermediate axis	$\gamma = 40^0$, short axis
0.5	49.0900	20.8600	4.1400	41.2000	18.3300	6.4000
1.5	33.2400	19.7800	4.9000	30.3400	17.6200	7.0500
2.5	14.1300	17.6800	6.6200	19.0400	16.2000	8.2200
3.5	3.2100	15.5800	11.3200	8.3900	15.9100	14.0500
4.5	0.3200	11.7400	16.8500	0.9900	14.5300	18.8800
5.5	0.0100	14.3600	56.1700	0.0300	17.4100	45.4100
	Distributions (%) for the angular momentum of the neutron at I = 16					
0.5	29.1900	12.0600	8.7200	42.3700	18.4200	5.8100
1.5	34.4000	13.4100	10.2000	33.3100	17.5700	5.9000
2.5	26.7800	14.8000	11.8500	15.4900	17.0900	9.1200
3.5	8.2100	16.5600	14.3900	7.2000	16.6700	12.3400
4.5	1.4000	18.0800	29.3400	1.6100	13.6400	20.3800
5.5	0.0300	25.0900	25.4900	0.0200	16.6200	46.4600
	Distributions (%) for the angular momentum of the neutron at I = 20					
0.5	25.5100	10.2400	9.5200	27.4400	11.4400	9.1800
1.5	34.9500	12.2200	11.3600	34.1400	12.8800	10.5900
2.5	29.8500	14.1800	12.6700	27.5100	14.5700	12.3700
3.5	8.3800	16.5600	14.8600	9.2000	16.7400	14.8000
4.5	1.2900	19.3100	32.0500	1.6900	18.6300	30.0700
5.5	0.0300	27.5100	19.5400	0.0300	25.7400	23.0000

Table A.32

A ~ 100, non-restricted configuration						
Spin projection Ω ($\hbar$)	Distributions (%) for the angular momentum of the proton at I = 8					
	yrast band			side band		
	$\gamma = 30^0$, long axis	$\gamma = -90^0$, intermediate axis	$\gamma = 30^0$, short axis	$\gamma = 30^0$, long axis	$\gamma = -90^0$, intermediate axis	$\gamma = 30^0$, short axis
0.5	0.3600	39.1400	51.0300	0.4500	37.9500	49.6500
1.5	0.7900	30.7900	32.9500	1.1100	30.5000	33.2600
2.5	3.6400	18.7700	13.0000	3.6400	19.2700	13.6100
3.5	9.5500	8.4300	2.7600	12.0400	9.0200	3.1500
4.5	85.6600	2.8800	0.2700	82.7600	3.2500	0.3300
	Distributions (%) for the angular momentum of the proton at I = 16					
0.5	4.2500	24.4100	34.3500	3.8000	24.7900	34.8700
1.5	5.7000	23.4900	31.2500	4.9200	23.8400	31.8000
2.5	14.6800	21.5200	23.6200	13.9500	21.6500	23.6200
3.5	30.1800	17.2900	9.3000	30.9400	17.0500	8.3800
4.5	45.1900	13.3000	1.4800	46.3900	12.6700	1.3300
	Distributions (%) for the angular momentum of the proton at I = 20					
0.5	6.4400	19.2400	28.8600	5.3100	21.2900	30.7400
1.5	7.7200	19.4900	28.5600	7.1400	21.8400	30.5700
2.5	22.8200	21.1100	28.5600	17.3000	21.9800	25.7100
3.5	33.4000	20.9600	12.3400	33.7800	19.1800	11.1200
4.5	29.6200	19.2000	1.6900	36.4800	15.7200	1.8600

Table A.33

A ~ 100, non-restricted configuration						
Spin projection Ω ($\hbar$)	Distributions (%) for the angular momentum of the neutron at I = 8					
	yrast band			side band		
	$\gamma = 30^0$, long axis	$\gamma = -90^0$, intermediate axis	$\gamma = 30^0$, short axis	$\gamma = 30^0$, long axis	$\gamma = -90^0$, intermediate axis	$\gamma = 30^0$, short axis
0.5	51.9500	29.2600	0.9400	49.0200	27.3100	1.3000
1.5	32.6600	25.7000	1.2500	33.5700	24.5000	1.4900
2.5	12.2200	19.7600	2.4600	13.2800	19.8200	3.5200
3.5	2.8200	13.3900	6.8000	3.5700	14.3600	6.8300
4.5	0.3400	7.2100	11.0700	0.5400	8.2300	15.3000
5.5	0.0100	4.6800	77.4700	0.0200	5.7700	71.5700
	Distributions (%) for the angular momentum of the neutron at I = 16					
0.5	28.3100	13.8700	7.1300	36.0100	18.6400	3.9000
1.5	28.6200	14.8900	9.2300	33.9300	18.8100	4.6300
2.5	27.8800	15.5400	9.7000	20.5700	18.5800	7.7100
3.5	12.3700	16.8900	18.3900	7.6800	17.2800	10.7100
4.5	2.7000	17.5900	28.9600	1.7400	13.6400	28.9600
5.5	0.1100	21.1300	26.6000	0.0600	13.2200	44.1000
	Distributions (%) for the angular momentum of the neutron at I = 20					
0.5	24.6800	11.3500	8.4800	30.9800	15.8100	5.4300
1.5	26.5100	12.9600	11.4500	32.6400	16.6700	6.1100
2.5	31.9900	14.1100	10.3900	22.6400	17.7700	9.7100
3.5	13.8900	16.8400	22.0000	10.7900	18.1600	12.9300
4.5	2.8100	19.5800	29.8400	2.8600	15.5500	31.6100
5.5	0.1300	25.1600	17.8400	0.0900	16.0500	34.2000

Table A.34

A ~ 130, non-restricted configuration						
Spin projection Ω ($\hbar$)	Distributions (%) for the angular momentum of the proton at I = 8					
	yrast band			side band		
	$\gamma = 20^0$, long axis	$\gamma = -100^0$, intermediate axis	$\gamma = 40^0$, short axis	$\gamma = 20^0$, long axis	$\gamma = -100^0$, intermediate axis	$\gamma = 40^0$, short axis
0.5	46.6700	20.6400	3.8200	36.5400	16.0000	6.4100
1.5	33.8100	19.7100	4.7100	32.3000	16.3600	8.0100
2.5	15.8100	17.7600	6.3700	23.1300	15.8500	8.7600
3.5	3.2800	15.2600	10.1200	6.7600	15.4300	13.4200
4.5	0.4200	12.1400	19.0300	1.2500	15.8100	24.2300
5.5	0.0100	14.5000	55.9600	0.0300	20.5400	39.1700
	Distributions (%) for the angular momentum of the proton at I = 16					
0.5	26.2500	11.4600	9.0800	38.7000	18.0800	6.0800
1.5	30.9000	12.9200	10.9900	32.0400	17.1300	5.7500
2.5	29.4800	14.0600	11.4700	15.9600	17.0400	9.7500
3.5	11.0700	15.9100	16.5900	10.3100	16.9200	12.2500
4.5	2.2600	19.4600	29.5000	2.9500	14.5700	21.6800
5.5	0.0400	26.1800	22.3700	0.0400	16.2600	44.4800
	Distributions (%) for the angular momentum of the proton at I = 20					
0.5	22.9100	9.6900	9.8700	29.9500	15.5200	8.9600
1.5	30.6800	11.7900	12.3200	27.1300	14.6700	8.1600
2.5	32.8400	13.3300	12.0300	19.3800	15.4200	12.3100
3.5	11.3000	15.7300	17.6700	18.1900	17.5900	16.3900
4.5	2.1900	20.7400	31.6600	5.2800	17.7200	21.9400
5.5	0.0500	28.7300	16.4600	0.0800	19.0900	32.2500

Table A.35

A ~ 130, non-restricted configuration						
Spin projection Ω ($\hbar$)	Distributions (%) for the angular momentum of the neutron at I = 8					
	yrast band			side band		
	$\gamma = 20^0$, long axis	$\gamma = -100^0$, intermediate axis	$\gamma = 40^0$, short axis	$\gamma = 20^0$, long axis	$\gamma = -100^0$, intermediate axis	$\gamma = 40^0$, short axis
0.5	0.0100	39.4400	45.1100	0.0700	35.2100	40.5500
1.5	0.0500	30.7900	32.2300	0.1900	29.2300	31.4900
2.5	0.2200	18.5000	16.1300	0.7100	19.8300	18.4100
3.5	2.0500	8.2700	5.3700	3.8400	10.5800	7.5000
4.5	6.9300	2.5400	1.0700	15.9100	4.1100	1.8400
5.5	90.7300	0.4600	0.1000	79.2800	1.0400	0.2000
	Distributions (%) for the angular momentum of the neutron at I = 16					
0.5	0.8600	24.2900	29.1900	0.9700	23.0200	27.8700
1.5	1.5800	23.5300	27.5200	1.9200	22.7900	26.9300
2.5	4.5800	21.1000	22.7300	4.8900	21.2300	23.2600
3.5	13.6800	16.3700	14.3500	15.0000	17.1000	15.1100
4.5	31.6800	9.9800	5.4600	33.3400	10.6800	6.0300
5.5	47.6200	4.7300	0.7500	43.8700	5.1800	0.8100
	Distributions (%) for the angular momentum of the neutron at I = 20					
0.5	1.6300	19.1600	24.0600	3.5400	16.6700	21.9600
1.5	2.8900	19.9800	24.6000	6.1800	17.6700	22.7500
2.5	8.0100	20.5300	23.8200	14.8100	18.4000	21.8100
3.5	20.8100	18.9200	18.2400	22.3200	18.5500	19.7800
4.5	34.9800	13.6900	8.1200	28.7100	16.2800	12.0200
5.5	31.6800	7.7300	1.1700	24.4400	12.4300	1.6800

Table A.36

A ~ 130, non-restricted configuration						
Spin projection Ω ($\hbar$)	Distributions (%) for the angular momentum of the proton at I = 8					
	yrast band			side band		
	$\gamma = 30^0$, long axis	$\gamma = -90^0$, intermediate axis	$\gamma = 30^0$, short axis	$\gamma = 30^0$, long axis	$\gamma = -90^0$, intermediate axis	$\gamma = 30^0$, short axis
0.5	50.2900	29.5800	0.8200	46.1300	26.7100	1.4000
1.5	32.7300	25.9100	1.1500	33.3400	24.1600	1.7100
2.5	13.3200	19.7800	2.1900	15.1700	19.7400	3.5400
3.5	3.2000	13.1300	5.7100	4.5100	14.3900	6.4000
4.5	0.4300	7.1600	11.9100	0.8300	8.7700	17.5400
5.5	0.0200	4.4400	78.2400	0.0300	6.2200	69.4100
	Distributions (%) for the angular momentum of the proton at I = 16					
0.5	25.6100	12.8900	7.7200	32.8900	18.0800	4.2100
1.5	26.1200	13.6900	9.7900	32.5600	18.4600	4.6600
2.5	28.8100	14.6000	10.4100	20.6800	18.7200	8.4900
3.5	15.5300	16.6400	21.5100	10.3400	17.6400	10.6700
4.5	3.7600	19.0900	28.6000	3.4200	14.2000	30.3800
5.5	0.1700	23.1000	21.9700	0.1000	12.9000	41.5800
	Distributions (%) for the angular momentum of the proton at I = 20					
0.5	22.4400	10.7700	9.2100	28.6100	15.3900	6.2000
1.5	23.4400	11.7600	11.8600	31.4700	16.1900	6.2800
2.5	31.7200	13.0100	11.4600	24.5600	17.6200	11.1400
3.5	17.9200	16.3500	25.7100	11.8300	18.3700	13.4900
4.5	4.2700	21.0800	27.8000	3.4100	16.4900	31.2900
5.5	0.2000	27.0300	13.9500	0.1200	15.9400	31.6000

Table A.37

A ~ 130, non-restricted configuration						
Spin projection Ω ($\hbar$)	Distributions (%) for the angular momentum of the neutron at I = 8					
	yrast band			side band		
	$\gamma = 30^0$, long axis	$\gamma = -90^0$, intermediate axis	$\gamma = 30^0$, short axis	$\gamma = 30^0$, long axis	$\gamma = -90^0$, intermediate axis	$\gamma = 30^0$, short axis
0.5	0.1000	36.5500	46.4100	0.1700	34.2100	43.7300
1.5	0.2400	29.6000	32.3900	0.4000	28.6600	32.3100
2.5	0.6900	19.2400	15.4800	1.1200	19.8600	16.9400
3.5	4.2400	9.8300	4.7900	4.7900	11.0800	5.7500
4.5	8.8500	3.7300	0.8600	13.9400	4.6700	1.1700
5.5	85.8700	1.0500	0.0700	79.5900	1.5200	0.0900
	Distributions (%) for the angular momentum of the neutron at I = 16					
0.5	1.9000	23.4600	31.8500	1.7000	23.4200	31.6700
1.5	2.6400	22.3600	28.8300	2.8700	22.7000	29.1400
2.5	5.5500	19.8700	22.2900	5.1500	20.4500	22.4200
3.5	13.7500	16.0700	12.7900	12.4200	16.2800	12.0300
4.5	28.2600	10.9900	3.8300	29.4300	10.6100	4.3800
5.5	47.9000	7.2400	0.4200	48.4200	6.5400	0.3700
	Distributions (%) for the angular momentum of the neutron at I = 20					
0.5	3.2500	18.6300	26.5700	3.5100	17.4200	25.1000
1.5	4.3800	19.0100	26.3500	4.3200	17.8400	25.2900
2.5	8.6300	19.0800	24.0000	9.2300	17.9600	22.7900
3.5	19.0300	18.0100	16.5900	20.1900	17.7100	18.5000
4.5	31.6300	14.3200	5.8600	31.6000	15.4800	7.5200
5.5	33.0700	10.9300	0.6300	31.1500	13.5800	0.8000

Table A.38

A ~ 190, non-restricted configuration						
Spin projection Ω ($\hbar$)	Distributions (%) for the angular momentum of the proton at I = 8					
	yrast band			side band		
	$\gamma = 36^0$, long axis	$\gamma = -84^0$, intermediate axis	$\gamma = 24^0$, short axis	$\gamma = 36^0$, long axis	$\gamma = -84^0$, intermediate axis	$\gamma = 40^0$, short axis
0.5	58.7300	37.1400	0.6300	54.1100	33.6400	1.2500
1.5	30.8500	29.9100	1.0900	32.6700	28.4900	2.8200
2.5	8.9300	19.5300	4.8700	10.7500	20.3000	5.2600
3.5	1.4100	9.3900	7.0300	2.3600	11.2200	17.3300
4.5	0.0800	3.9800	86.3500	0.1100	6.3000	73.2700
5.5	0.0000	0.0500	0.0300	0.0000	0.0500	0.0700
	Distributions (%) for the angular momentum of the proton at I = 16					
0.5	43.5900	25.1100	5.6000	45.0300	27.1400	3.4700
1.5	32.4800	23.7000	7.7900	32.9000	25.3500	7.4700
2.5	17.5200	19.8300	12.0300	14.7500	21.2900	8.5800
3.5	6.1200	15.0300	35.1500	7.1100	14.9900	32.7000
4.5	0.2800	16.2700	39.2800	0.2100	11.1500	47.6600
5.5	0.0000	0.0700	0.1400	0.0000	0.0800	0.1200
	Distributions (%) for the angular momentum of the proton at I = 20					
0.5	40.8300	22.8200	6.9500	40.6300	23.6800	6.0300
1.5	32.1300	22.3500	9.2000	30.8800	23.1500	10.3600
2.5	19.4000	19.5600	14.2300	17.6500	20.6800	13.1600
3.5	7.3100	15.9700	39.2200	10.5400	16.4900	36.4500
4.5	0.3300	19.2200	30.2400	0.2900	15.9200	33.8600
5.5	0.0000	0.0700	0.1600	0.0000	0.0900	0.1400

Table A.39

A ~ 190, non-restricted configuration						
Spin projection Ω ($\hbar$)	Distributions (%) for the angular momentum of the neutron at I = 8					
	yrast band			side band		
	$\gamma = 36^0$, long axis	$\gamma = -84^0$, intermediate axis	$\gamma = 24^0$, short axis	$\gamma = 36^0$, long axis	$\gamma = -84^0$, intermediate axis	$\gamma = 40^0$, short axis
0.5	0.5400	27.1000	37.9600	0.8400	21.2000	30.7800
1.5	0.8400	24.2500	30.3800	1.1400	20.8500	29.0100
2.5	1.4000	19.3100	19.0400	2.2700	19.3800	22.6000
3.5	3.3000	13.6000	9.2000	5.0100	16.1500	12.4700
4.5	9.2700	8.5000	2.8900	11.7600	11.6500	4.3600
5.5	18.2500	4.5700	0.4900	30.3200	6.7800	0.7200
6.5	66.3900	2.6700	0.0400	48.6600	3.9900	0.0600
	Distributions (%) for the angular momentum of the neutron at I = 16					
0.5	3.6900	13.7800	22.8200	2.0100	18.1100	27.0800
1.5	5.3800	14.5000	23.3600	2.0000	1.7990	26.1600
2.5	6.0700	15.0200	21.7500	4.2400	17.6500	23.3700
3.5	13.2000	14.9700	20.1000	7.0700	16.3900	15.0300
4.5	21.5200	15.1100	9.7600	16.4900	13.7300	7.1600
5.5	26.8100	13.5400	2.0000	30.8100	9.4100	1.0500
6.5	23.3300	13.0800	0.2200	37.3800	6.7200	0.1500
	Distributions (%) for the angular momentum of the neutron at I = 20					
0.5	5.0400	10.9300	19.7200	4.2800	13.8000	21.9900
1.5	7.2700	12.0600	21.2000	4.5200	14.3700	23.0200
2.5	7.6500	13.2400	21.0600	6.8100	15.1800	22.7100
3.5	16.8500	14.2600	23.0200	12.3100	15.6100	18.7800
4.5	24.8100	16.2800	12.1700	20.3700	15.5700	11.4500
5.5	24.7000	16.2500	2.5300	28.8900	13.2800	1.7500
6.5	13.6900	16.9800	0.2900	22.8300	12.1900	0.2900

Table A.40

A ~ 190, non-restricted configuration						
Spin projection Ω ($\hbar$)	Distributions (%) for the angular momentum of the proton at I = 8					
	yrast band			side band		
	$\gamma = 30^0$, long axis	$\gamma = -90^0$, intermediate axis	$\gamma = 30^0$, short axis	$\gamma = 30^0$, long axis	$\gamma = -90^0$, intermediate axis	$\gamma = 30^0$, short axis
0.5	61.5000	33.7700	1.4500	58.7100	31.9600	1.8900
1.5	29.8200	28.2300	2.1100	31.1100	27.4500	3.4200
2.5	7.5900	20.3500	7.2500	8.3800	20.5700	7.3500
3.5	1.0500	10.8500	8.8000	1.7500	11.8100	13.6700
4.5	0.0400	6.7300	80.3500	0.0500	8.1500	73.6000
5.5	0.0000	0.0600	0.0500	0.0000	0.0700	0.0700
	Distributions (%) for the angular momentum of the proton at I = 16					
0.5	42.3700	21.9000	8.0400	49.7500	26.4500	3.9200
1.5	33.8600	21.3500	9.5900	33.0300	24.8800	7.8200
2.5	19.1000	18.9600	13.5700	11.6800	21.0100	9.2200
3.5	4.4900	16.6000	33.9100	5.4400	14.8600	26.4300
4.5	0.1800	21.1300	34.7000	0.1000	12.7100	52.4700
5.5	0.0000	0.0600	0.2000	0.0000	0.0900	0.1400
	Distributions (%) for the angular momentum of the proton at I = 20					
0.5	39.1000	19.9700	9.5600	44.5300	23.5700	6.0900
1.5	33.8600	20.0200	10.7300	31.7200	23.0600	10.3100
2.5	21.7100	18.4200	15.3600	15.1700	20.6200	12.3000
3.5	5.1100	17.4900	37.0400	8.4300	16.5900	30.7600
4.5	0.2200	24.0400	27.0800	0.1400	16.0600	40.3600

Table A.40 continues

A ~ 190, non-restricted configuration						
Spin projection Ω ($\hbar$)	Distributions (%) for the angular momentum of the proton at I = 20					
	yrast band			side band		
	$\gamma = 30^0$, long axis	$\gamma = -90^0$, intermediate axis	$\gamma = 30^0$, short axis	$\gamma = 30^0$, long axis	$\gamma = -90^0$, intermediate axis	$\gamma = 30^0$, short axis
5.5	0.0000	0.0600	0.2200	0.0000	0.1100	0.1700

Table A.41

A ~ 190, non-restricted configuration						
Spin projection Ω ($\hbar$)	Distributions (%) for the angular momentum of the neutron at I = 8					
	yrast band			side band		
	$\gamma = 30^0$, long axis	$\gamma = -90^0$, intermediate axis	$\gamma = 30^0$, short axis	$\gamma = 30^0$, long axis	$\gamma = -90^0$, intermediate axis	$\gamma = 30^0$, short axis
0.5	0.1200	30.6700	38.8200	0.2000	25.2700	32.5800
1.5	0.2100	26.6000	30.7000	0.3300	23.8400	29.3000
2.5	0.5200	19.8600	18.7800	0.9200	20.4800	21.6500
3.5	1.6100	12.5800	8.5400	2.7000	15.2200	11.6200
4.5	6.2900	6.6100	2.6400	8.6300	9.2800	4.0300
5.5	15.9700	2.7300	0.4700	27.7500	4.3100	0.7600
6.5	75.2900	0.9500	0.0400	59.4700	1.6000	0.0700
	Distributions (%) for the angular momentum of the neutron at I = 16					
0.5	1.8800	15.6300	22.4400	1.2100	17.1700	23.8300
1.5	2.7000	16.4300	23.2500	1.6100	17.7300	24.1900
2.5	4.3000	17.0900	22.2700	3.3900	18.2600	23.3900
3.5	10.9600	16.6900	18.7600	7.4200	17.4300	17.6800
4.5	20.9600	15.0000	10.4400	19.4500	14.4100	8.7400
5.5	31.9300	11.2000	2.5000	34.5900	9.4100	1.9300
6.5	27.2700	7.9600	0.3300	32.3100	5.5900	0.2400
	Distributions (%) for the angular momentum of the neutron at I = 20					
0.5	2.8700	12.5700	19.3800	3.1900	13.5000	20.1300
1.5	3.9400	13.7000	20.8600	3.6300	14.3400	21.3300
2.5	6.0100	15.2100	21.5500	6.3500	15.5200	21.8800
3.5	15.0700	16.4100	21.1000	13.9400	16.2600	19.9100
4.5	25.5400	16.8000	13.3600	23.4400	16.1600	13.3000
5.5	29.9900	14.1300	3.2900	29.8300	13.4000	3.0300
6.5	16.5900	11.1700	0.4600	19.6200	10.8200	0.4900

Table A.42

A ~ 100, restricted configuration						
Spin projection Ω ($\hbar$)	Distributions (%) for the angular momentum of the proton at I = 8, 16, 20					
	yrast band			side band		
	$\gamma = 20^0$, long axis	$\gamma = -100^0$, intermediate axis	$\gamma = 40^0$, short axis	$\gamma = 20^0$, long axis	$\gamma = -100^0$, intermediate axis	$\gamma = 40^0$, short axis
0.5	0.0100	45.9200	53.0800	0.0100	45.9200	53.0800
1.5	0.0000	32.5700	32.5100	0.0000	32.5700	32.5100
2.5	1.2400	15.8900	11.8500	1.2400	15.8900	11.8500
3.5	0.0000	4.8900	2.3600	0.0000	4.8900	2.3600
4.5	98.7500	0.7400	0.2000	98.7500	0.7400	0.2000
	Distributions (%) for the angular momentum of the neutron at I = 8, 16, 20					
0.5	68.0500	30.2600	0.2100	68.0500	30.2600	0.2100
1.5	26.0200	26.9000	1.3300	26.0200	26.9000	1.3300
2.5	5.3800	19.6800	0.0500	5.3800	19.6800	0.0500
3.5	0.5300	13.5900	11.1100	0.5300	13.5900	11.1100

Table A.42 continues

A ~ 100, restricted configuration						
Spin projection Ω ($\hbar$)	Distributions (%) for the angular momentum of the neutron at I = 8, 16, 20					
	yrast band			side band		
	$\gamma = 20^0$, long axis	$\gamma = -100^0$, intermediate axis	$\gamma = 40^0$, short axis	$\gamma = 20^0$, long axis	$\gamma = -100^0$, intermediate axis	$\gamma = 40^0$, short axis
4.5	0.0300	6.2800	0.0200	0.0300	6.2800	0.0200
5.5	0.0000	3.3000	87.2900	0.0000	3.3000	87.2900
	Distributions (%) for the angular momentum of the proton at I = 8, 16, 20					
	$\gamma = 30^0$, long axis	$\gamma = -90^0$, intermediate axis	$\gamma = 30^0$, short axis	$\gamma = 30^0$, long axis	$\gamma = -90^0$, intermediate axis	$\gamma = 30^0$, short axis
0.5	0.0400	43.6800	56.1700	0.0400	43.6800	56.1700
1.5	0.0000	32.1500	31.8600	0.0000	32.1500	31.8600
2.5	2.8800	17.0200	10.1500	2.8800	17.0200	10.1500
3.5	0.0000	6.0000	1.7000	0.0000	6.0000	1.7000
4.5	97.0800	1.1400	0.1200	97.0800	1.1400	0.1200
	Distributions (%) for the angular momentum of the neutron at I = 8, 16, 20					
0.5	59.5200	34.5400	0.0300	59.5200	34.5400	0.0300
1.5	30.4300	28.9200	0.3700	30.4300	28.9200	0.3700
2.5	8.6100	19.7800	0.0000	8.6100	19.7800	0.0000
3.5	1.3300	11.0500	6.2600	1.3300	11.0500	6.2600
4.5	0.1100	4.4400	0.0000	0.1100	4.4400	0.0000
5.5	0.0000	1.2800	93.3400	0.0000	1.2800	93.3400

Table A.43

A ~ 130, restricted configuration						
Spin projection Ω ($\hbar$)	Distributions (%) for the angular momentum of the proton at I = 8, 16, 20					
	yrast band			side band		
	$\gamma = 20^0$, long axis	$\gamma = -100^0$, intermediate axis	$\gamma = 40^0$, short axis	$\gamma = 20^0$, long axis	$\gamma = -100^0$, intermediate axis	$\gamma = 40^0$, short axis
0.5	65.7600	31.0700	0.1200	65.7600	31.0700	0.1200
1.5	27.4300	27.2600	0.8900	27.4300	27.2600	0.8900
2.5	6.0900	19.8700	0.0300	6.0900	19.8700	0.0300
3.5	0.6700	13.0500	8.6000	0.6700	13.0500	8.6000
4.5	0.0400	6.0300	0.0100	0.0400	6.0300	0.0100
5.5	0.0000	2.7200	90.3500	0.0000	2.7200	90.3500
	Distributions (%) for the angular momentum of the neutron at I = 8, 16, 20					
0.5	0.0000	42.4000	48.3300	0.0000	42.4000	48.3300
1.5	0.0100	31.6800	32.4800	0.0100	31.6800	32.4800
2.5	0.0000	17.3800	14.4300	0.0000	17.3800	14.4300
3.5	1.5600	6.7000	4.0600	1.5600	6.7000	4.0600
4.5	0.0000	1.6500	0.6500	0.0000	1.6500	0.6500
5.5	98.4300	0.2000	0.0500	98.4300	0.2000	0.0500
	Distributions (%) for the angular momentum of the proton at I = 8, 16, 20					
	$\gamma = 30^0$, long axis	$\gamma = -90^0$, intermediate axis	$\gamma = 30^0$, short axis	$\gamma = 30^0$, long axis	$\gamma = -90^0$, intermediate axis	$\gamma = 30^0$, short axis
0.5	58.0600	35.2000	0.0100	58.0600	35.2000	0.0100
1.5	30.9900	29.2100	0.2200	30.9900	29.2100	0.2200
2.5	9.2800	19.7000	0.0000	9.2800	19.7000	0.0000
3.5	1.5300	10.6600	4.6000	1.5300	10.6600	4.6000
4.5	0.1300	4.1500	0.0000	0.1300	4.1500	0.0000
5.5	0.0000	1.0800	95.1600	0.0000	1.0800	95.1600

Table A.43 continues

A ~ 130, restricted configuration						
Spin projection Ω ($\hbar$)	Distributions (%) for the angular momentum of the neutron at I = 8, 16, 20					
	yrast band			side band		
	$\gamma = 30^0$, long axis	$\gamma = -90^0$, intermediate axis	$\gamma = 30^0$, short axis	$\gamma = 30^0$, long axis	$\gamma = -90^0$, intermediate axis	$\gamma = 30^0$, short axis
0.5	0.0000	40.5100	50.9600	0.0000	40.5100	50.9600
1.5	0.0600	31.1300	32.4100	0.0600	31.1300	32.4100
2.5	0.0000	18.1300	12.9900	0.0000	18.1300	12.9900
3.5	3.5000	7.7200	3.1700	3.5000	7.7200	3.1700
4.5	0.0000	2.1900	0.4300	0.0000	2.1900	0.4300
5.5	96.4400	0.3300	0.0300	96.4400	0.3300	0.0300

Table A.44

A ~ 190, restricted configuration						
Spin projection Ω ($\hbar$)	Distributions (%) for the angular momentum of the proton at I = 8, 16, 20					
	yrast band			side band		
	$\gamma = 36^0$, long axis	$\gamma = -84^0$, intermediate axis	$\gamma = 24^0$, short axis	$\gamma = 36^0$, long axis	$\gamma = -84^0$, intermediate axis	$\gamma = 24^0$, short axis
0.5	61.7200	39.4200	0.2200	61.7200	39.4200	0.2200
1.5	29.6700	30.8800	0.0200	29.6700	30.8800	0.0200
2.5	7.6000	19.0600	4.6100	7.6000	19.0600	4.6100
3.5	0.9500	8.1600	0.0000	0.9500	8.1600	0.0000
4.5	0.0500	2.4400	95.1500	0.0500	2.4400	95.1500
5.5	0.0000	0.0400	0.0000	0.0000	0.0400	0.0000
	Distributions (%) for the angular momentum of the neutron at I = 8, 16, 20					
0.5	0.0000	36.4000	49.1600	0.0000	36.4000	49.1600
1.5	0.0000	29.4800	32.3000	0.0000	29.4800	32.3000
2.5	0.1800	19.2100	13.9100	0.1800	19.2100	13.9100
3.5	0.0000	9.8800	3.8800	0.0000	9.8800	3.8800
3.5	5.8500	3.8500	0.6800	5.8500	3.8500	0.6800
5.5	0.0000	1.0400	0.0700	0.0000	1.0400	0.0700
6.5	93.9700	0.1500	0.0000	93.9700	0.1500	0.0000
	Distributions (%) for the angular momentum of the proton at I = 8, 16, 20					
	$\gamma = 30^0$, long axis	$\gamma = -90^0$, intermediate axis	$\gamma = 30^0$, short axis	$\gamma = 30^0$, long axis	$\gamma = -90^0$, intermediate axis	$\gamma = 30^0$, short axis
0.5	66.3600	37.0200	0.5600	66.3600	37.0200	0.5600
1.5	27.1300	29.7000	0.0700	27.1300	29.7000	0.0700
2.5	5.9100	20.1600	7.1300	5.9100	20.1600	7.1300
3.5	0.5800	9.2900	0.0200	0.5800	9.2900	0.0200
4.5	0.0300	3.7700	92.2100	0.0300	3.7700	92.2100
5.5	0.0000	0.0600	0.0000	0.0000	0.0600	0.0000
	Distributions (%) for the angular momentum of the neutron at I = 8, 16, 20					
0.5	0.0000	37.8100	47.0800	0.0000	37.8100	47.0800
1.5	0.0000	30.0700	32.2300	0.0000	30.0700	32.2300
2.5	0.0800	18.8600	15.0000	0.0800	18.8600	15.0000
3.5	0.0000	9.1300	4.6500	0.0000	9.1300	4.6500
4.5	4.0800	3.2500	0.9200	4.0800	3.2500	0.9200
5.5	0.0000	0.7800	0.1100	0.0000	0.7800	0.1100
6.5	95.8400	0.1000	0.0100	95.8400	0.1000	0.0100

Table A.45-68: *Calculated intra- and inter-band $B(M1)$ and $B(E2)$ reduced transition probabilities for the partner bands in A ~ 100, 130 and 190 mass regions. The calculations were performed with ε_2 = 0.15 and γ = 17^0, 20^0,24^0,27^0, 30^0,33^0, 36^0,40^0.*

Table A.45

A ~ 100, non-restricted configuration								
Spin I ($\hbar$)	$B(M1, I \to I-1)_{in}$ **(μ_N^2), yrast band**							
	$\gamma = 17^0$	$\gamma = 20^0$	$\gamma = 24^0$	$\gamma = 27^0$	$\gamma = 30^0$	$\gamma = 33^0$	$\gamma = 36^0$	$\gamma = 40^0$
9	1.5810	1.5873	1.6074	1.6265	1.6386	1.6370	1.6238	1.6014
10	1.3134	1.3081	1.3197	1.3461	1.3613	1.3428	1.3000	1.2574
11	1.1190	1.0937	1.0446	1.0518	1.1589	1.0782	0.9930	1.0149
12	0.9706	0.9376	0.8165	0.4917	0.8678	0.9895	0.7696	0.8470
13	0.8311	0.7580	0.4826	0.2574	0.9858	0.8515	0.0463	0.5616
14	0.8145	0.8181	0.8642	0.0906	0.9241	0.9357	0.8868	0.7890
15	0.6193	0.5881	0.5379	0.4328	0.2085	0.0060	0.0799	0.3027
16	0.7632	0.7962	0.8400	0.8707	0.9001	0.9093	0.8880	0.8344
17	0.4504	0.4458	0.3950	0.3001	0.1555	0.0272	0.0065	0.1142
18	0.7453	0.7751	0.8141	0.8457	0.8748	0.8894	0.8823	0.8472
19	0.3141	0.3188	0.2853	0.2205	0.1240	0.0350	0.0002	0.0345
20	0.7348	0.7615	0.7989	0.8294	0.8580	0.8762	0.8774	0.8532
21	0.2115	0.2204	0.2042	0.1630	0.0980	0.0350	0.0031	0.0093
22	0.7267	0.7525	0.7894	0.8188	0.8467	0.8662	0.8710	0.8502
	$B(M1, I \to I-1)_{in}$ **(μ_N^2), side band**							
9	1.4607	1.5478	1.7571	1.8353	1.8478	1.8160	1.7350	1.5845
10	1.1961	1.3568	1.6162	1.7021	1.7183	1.6594	1.5143	1.2247
11	0.9825	1.1452	1.2281	1.2840	1.4308	1.2779	1.0939	0.9537
12	0.9331	1.0043	0.8997	0.5431	0.9365	1.0460	0.7343	0.7723
13	0.7331	0.7323	0.4330	0.1993	0.8458	0.7467	0.0366	0.4564
14	0.6048	0.6967	0.7165	0.7805	0.8612	0.8829	0.7560	0.5607
15	0.4828	0.4921	0.4444	0.3613	0.1780	0.0078	0.0486	0.1926
16	0.2284	0.4320	0.4997	0.5358	0.5534	0.5232	0.4548	0.3521
17	0.2446	0.0000	0.3588	0.2838	0.1589	0.0402	0.0000	0.0422
18	0.0021	0.1404	0.2632	0.3048	0.3117	0.2783	0.2203	0.1473
19	0.0284	0.2174	0.2798	0.2372	0.1530	0.0650	0.0138	0.0005
20	0.0229	0.0003	0.1112	0.1674	0.1793	0.1569	0.1172	0.0679
21	0.0062	0.0131	0.1793	0.1940	0.1464	0.0852	0.0418	0.0143
22	0.0323	0.0186	0.0116	0.0824	0.1069	0.0958	0.0692	0.0354

Table A.46

A ~ 100, non-restricted configuration								
Spin I ($\hbar$)	$B(M1, I \to I-1)_{out}$ **(μ_N^2), yrast → side band**							
	$\gamma = 17^0$	$\gamma = 20^0$	$\gamma = 24^0$	$\gamma = 27^0$	$\gamma = 30^0$	$\gamma = 33^0$	$\gamma = 36^0$	$\gamma = 40^0$
11	···	···	···	0.1648	0.0062	0.1438	0.3055	
12	···	···	0.2872	0.6099	0.1723	0.0138	0.3132	0.3193
13	···	0.3755	0.6154	0.8007	0.0073	0.1098	0.9703	0.6081
14	···	0.1650	0.1099	0.0560	0.0228	0.0003	0.0551	0.1911
15	···	0.4461	0.4973	0.6506	0.9242	1.1340	1.0374	0.8461
16	···	0.1037	0.0695	0.0472	0.0168	0.0000	0.0174	0.0794
17	···	···	0.7080	0.8423	1.0214	1.1783	1.2169	1.1303
18	···	···	0.0633	0.0426	0.0176	0.0011	0.0049	0.0390
19	···	···	···	0.9717	1.0926	1.2132	1.2771	1.2673
20	···	···	···	0.0449	0.0215	0.0039	0.0008	0.0224
21	···	···	···	···	···	1.2417	1.2956	1.2974

Table A.46 continues

A ~ 100, non-restricted configuration								
Spin I ($\hbar$)	$B(M1, I \to I-1)_{out}$ **(μ_N^2), yrast → side band**							
	$\gamma = 17^0$	$\gamma = 20^0$	$\gamma = 24^0$	$\gamma = 27^0$	$\gamma = 30^0$	$\gamma = 33^0$	$\gamma = 36^0$	$\gamma = 40^0$
22	...	...	...	...	...	0.0074	0.0000	0.0129
	$B(M1, I \to I-1)_{out}$ **(μ_N^2), side → yrast band**							
9	0.0328	0.0301	0.0173	0.0073	0.0010	0.0006	0.0053	0.0121
10	0.0417	0.0401	0.0296	0.0122	0.0002	0.0075	0.0288	0.0461
11	0.0562	0.0694	0.1141	0.1125	0.0079	0.0779	0.1444	0.1056
12	0.0533	0.0730	0.1877	0.5127	0.1409	0.0267	0.2339	0.1381
13	0.0865	0.1454	0.4120	0.6389	0.0018	0.1080	0.7941	0.3150
14	0.0513	0.0632	0.0664	0.0446	0.0214	0.0001	0.0402	0.0950
15	0.1144	0.1606	0.2408	0.3455	0.5251	0.6643	0.5834	0.3812
16	0.0403	0.0352	0.0309	0.0252	0.0117	0.0004	0.0045	0.0219
17	0.1245	0.1635	0.2410	0.3332	0.4479	0.5285	0.5125	0.3872
18	0.0234	0.0270	0.0227	0.0176	0.0090	0.0015	0.0002	0.0036
19	0.1181	0.1543	0.2225	0.2933	0.3707	0.4185	0.4079	0.3281
20	0.0086	0.0168	0.0189	0.0141	0.0079	0.0024	0.0002	0.0001
21	0.1015	0.1336	0.1913	0.2462	0.3001	0.3273	0.3138	0.2559
22	0.0025	0.0061	0.0146	0.0124	0.0073	0.0030	0.0009	0.0003

Table A.47

A ~ 100, non-restricted configuration								
Spin I ($\hbar$)	$B(E2, I \to I-2)_{in}$ **(e^2b^2), yrast band**							
	$\gamma = 17^0$	$\gamma = 20^0$	$\gamma = 24^0$	$\gamma = 27^0$	$\gamma = 30^0$	$\gamma = 33^0$	$\gamma = 36^0$	$\gamma = 40^0$
10	0.0428	0.0350	0.0207	0.0094	0.0018	0.0002	0.0048	0.0159
11	0.0551	0.0485	0.0359	0.0220	0.0035	0.0038	0.0165	0.0296
12	0.0660	0.0607	0.0508	0.0429	0.0002	0.0002	0.0325	0.0441
13	0.0808	0.0774	0.0617	0.0329	0.0020	0.0149	0.0452	0.0633
14	0.0882	0.0862	0.0805	0.0796	0.0101	0.0084	0.0699	0.0735
15	0.1039	0.1040	0.1057	0.1031	0.0999	0.0992	0.1002	0.0950
16	0.1088	0.1107	0.1109	0.1089	0.1080	0.1071	0.1041	0.1002
17	0.1232	0.1254	0.1256	0.1247	0.1238	0.1227	0.1211	0.1168
18	0.1270	0.1286	0.1285	0.1278	0.1271	0.1261	0.1241	0.1191
19	0.1381	0.1398	0.1400	0.1394	0.1386	0.1375	0.1355	0.1304
20	0.1422	0.1428	0.1422	0.1412	0.1402	0.1390	0.1371	0.1325
21	0.1489	0.1503	0.1504	0.1498	0.1489	0.1476	0.1454	0.1396
22	0.1546	0.1546	0.1532	0.1517	0.1503	0.1488	0.1464	0.1408
	$B(E2, I \to I-2)_{in}$ **(e^2b^2), side band**							
10	0.0337	0.0201	0.0114	0.0058	0.0013	0.0001	0.0025	0.0095
11	0.0428	0.0285	0.0235	0.0167	0.0037	0.0015	0.0087	0.0173
12	0.0561	0.0450	0.0425	0.0405	0.0001	0.0013	0.0346	0.0369
13	0.0611	0.0525	0.0380	0.0190	0.0012	0.0082	0.0268	0.0444
14	0.0814	0.0686	0.0609	0.0607	0.0083	0.0102	0.0603	0.0640
15	0.0832	0.0710	0.0686	0.0734	0.0788	0.0750	0.0654	0.0624
16	0.1020	0.0940	0.0948	0.0979	0.0999	0.0978	0.0920	0.0892
17	0.1085	0.1028	0.1063	0.1074	0.1062	0.1045	0.1018	0.0954
18	0.1078	0.1151	0.1201	0.1206	0.1198	0.1182	0.1153	0.1107
19	0.1319	0.1307	0.1297	0.1279	0.1258	0.1235	0.1210	0.1168
20	0.1387	0.1108	0.1346	0.1353	0.1340	0.1322	0.1299	0.1256
21	0.1467	0.1462	0.1442	0.1418	0.1391	0.1364	0.1333	0.1286
22	0.1558	0.1446	0.1317	0.1450	0.1444	0.1426	0.1401	0.1348

Table A.48

A ~ 100, non-restricted configuration								
Spin I ($\hbar$)	$B(E2, I \to I-2)_{out}$ (e^2b^2), **yrast → side band**							
	$\gamma = 17^0$	$\gamma = 20^0$	$\gamma = 24^0$	$\gamma = 27^0$	$\gamma = 30^0$	$\gamma = 33^0$	$\gamma = 36^0$	$\gamma = 40^0$
11	...	...	0.0009	0.0041	0.0131	0.0125	0.0049	0.0005
12	0.0000	0.0001	0.0008	0.0024	0.0408	0.0369	0.0018	0.0000
13	0.0006	0.0032	0.0178	0.0430	0.0704	0.0563	0.0264	0.0044
14	0.0001	0.0018	0.0062	0.0050	0.0713	0.0693	0.0057	0.0005
15	0.0024	0.0030	0.0003	0.0005	0.0004	0.0000	0.0000	0.0032
16	0.0000	0.0000	0.0006	0.0014	0.0006	0.0003	0.0021	0.0010
17	0.0019	0.0006	0.0000	0.0000	0.0001	0.0002	0.0003	0.0009
18	0.0009	0.0004	0.0006	0.0005	0.0002	0.0000	0.0004	0.0012
19	0.0011	0.0005	0.0001	0.0000	0.0000	0.0001	0.0002	0.0006
20	0.0038	0.0013	0.0005	0.0003	0.0001	0.0000	0.0001	0.0006
21	0.0007	0.0004	0.0002	0.0001	0.0000	0.0000	0.0001	0.0003
22	0.0043	0.0033	0.0007	0.0002	0.0001	0.0000	0.0001	0.0003
	$B(E2, I \to I-2)_{out}$ (e^2b^2), **side → yrast band**							
10	0.0138	0.0182	0.0250	0.0315	0.0362	0.0367	0.0327	0.0232
11	0.0082	0.0094	0.0124	0.0198	0.0344	0.0334	0.0228	0.0146
12	0.0051	0.0040	0.0017	0.0000	0.0368	0.0367	0.0096	0.0069
13	0.0011	0.0000	0.0060	0.0229	0.0400	0.0306	0.0104	0.0000
14	0.0012	0.0000	0.0019	0.0024	0.0563	0.0538	0.0010	0.0008
15	0.0000	0.0020	0.0000	0.0003	0.0003	0.0000	0.0001	0.0007
16	0.0006	0.0001	0.0006	0.0010	0.0003	0.0005	0.0028	0.0025
17	0.0000	0.0000	0.0001	0.0002	0.0002	0.0003	0.0003	0.0004
18	0.0009	0.0005	0.0004	0.0002	0.0000	0.0001	0.0008	0.0018
19	0.0000	0.0000	0.0001	0.0001	0.0002	0.0003	0.0003	0.0003
20	0.0008	0.0007	0.0002	0.0001	0.0000	0.0001	0.0004	0.0009
21	0.0000	0.0000	0.0001	0.0001	0.0001	0.0002	0.0003	0.0003
22	0.0004	0.0005	0.0002	0.0000	0.0000	0.0001	0.0002	0.0005

Table A.49

A ~ 130, non-restricted configuration								
Spin I ($\hbar$)	$B(M1, I \to I-1)_{in}$ (μ_N^2), **yrast band**							
	$\gamma = 17^0$	$\gamma = 20^0$	$\gamma = 24^0$	$\gamma = 27^0$	$\gamma = 30^0$	$\gamma = 33^0$	$\gamma = 36^0$	$\gamma = 40^0$
9	2.3667	2.3727	2.3829	2.3895	2.3934	2.3938	2.3905	2.3796
10	1.9217	1.9277	1.9534	1.9835	2.0071	2.0141	2.0064	1.9868
11	1.5493	1.5450	1.5695	1.6258	1.6634	1.6627	1.6440	1.6250
12	1.2990	1.2660	1.1768	1.3335	1.2935	1.3322	1.3538	1.3708
13	1.1330	1.0746	0.6641	0.0651	1.2240	1.2798	1.2538	1.1208
14	1.0009	0.9425	0.8946	1.1370	1.0870	0.7560	0.0172	0.7067
15	0.9481	0.9566	1.0121	1.0246	0.9898	0.9925	1.1310	1.0238
16	0.8163	0.8146	0.8175	0.7627	0.6184	0.3578	0.0340	0.2339
17	0.8751	0.9176	0.9581	0.9799	1.0050	1.0369	1.0644	1.0480
18	0.6552	0.6510	0.6251	0.5602	0.4248	0.2144	0.0317	0.0533
19	0.8413	0.8816	0.9221	0.9515	0.9835	1.0170	1.0402	1.0373
20	0.5019	0.4916	0.4662	0.4119	0.3031	0.1526	0.0327	0.0101
21	0.8205	0.8583	0.9001	0.9315	0.9656	1.0000	1.0252	1.0283
22	0.3730	0.3609	0.3414	0.3003	0.2185	0.1112	0.0291	0.0013
	$B(M1, I \to I-1)_{in}$ (μ_N^2), **side band**							
9	2.4246	2.4325	2.3954	2.3959	2.4128	2.4053	2.3665	2.2889
10	1.8428	1.8774	2.1632	2.3344	2.3500	2.2979	2.1978	1.9901
11	1.3390	1.5424	2.0330	2.1700	2.1479	2.0437	1.9062	1.6706
12	1.1335	1.3813	1.4837	1.7365	1.5048	1.4349	1.3736	1.2486
13	1.0660	1.1335	0.6864	0.0657	1.1699	1.2261	1.1977	1.0715

Table A.49 continues

A ~ 130, non-restricted configuration								
Spin I ($\hbar$)	$B(M1, I \to I-1)_{in}$ (μ_N^2), **side band**							
	$\gamma = 17^0$	$\gamma = 20^0$	$\gamma = 24^0$	$\gamma = 27^0$	$\gamma = 30^0$	$\gamma = 33^0$	$\gamma = 36^0$	$\gamma = 40^0$
14	0.9154	0.8834	0.7453	0.9105	0.9149	0.6862	0.0228	0.5645
15	0.8382	0.8184	0.8230	0.8667	0.9045	0.9089	0.9696	0.7523
16	0.6959	0.6685	0.6565	0.6165	0.4916	0.2736	0.0288	0.1426
17	0.6220	0.6439	0.6661	0.6829	0.6892	0.6770	0.6416	0.5174
18	0.5375	0.5417	0.5389	0.4891	0.3757	0.1998	0.0417	0.0154
19	0.3649	0.3828	0.4165	0.4336	0.4224	0.3733	0.3015	0.2123
20	0.3923	0.4132	0.4243	0.3889	0.2993	0.1681	0.0550	0.0003
21	0.1606	0.1734	0.2205	0.2456	0.2401	0.2018	0.1506	0.0929
22	0.2346	0.2621	0.3046	0.2950	0.2341	0.1407	0.0609	0.0105

Table A.50

A ~ 130, non-restricted configuration								
Spin I ($\hbar$)	$B(M1, I \to I-1)_{out}$ (μ_N^2), **yrast → side band**							
	$\gamma = 17^0$	$\gamma = 20^0$	$\gamma = 24^0$	$\gamma = 27^0$	$\gamma = 30^0$	$\gamma = 33^0$	$\gamma = 36^0$	$\gamma = 40^0$
12	···	···	0.3197	0.0518	0.2392	0.2640	0.2861	···
13	···	0.3473	0.7473	1.3415	0.1011	0.0003	0.0380	0.2952
14	···	0.3818	0.3972	0.1138	0.1208	0.4868	1.3639	0.8202
15	···	0.2667	0.2017	0.2026	0.2614	0.2311	0.0216	0.1200
16	···	0.4232	0.4522	0.5735	0.7593	1.0077	1.3098	1.1873
17	···	···	0.2263	0.2157	0.1716	0.0937	0.0214	0.0118
18	···	···	0.7373	0.8338	0.9950	1.2287	1.4253	1.4318
19	···	···	0.2129	0.1845	0.1371	0.0739	0.0217	0.0006
20	···	···		1.0400	1.1684	1.3494	1.5013	1.5564
21	···	···		0.1673	0.1230	0.0698	0.0250	0.0001
22	···	···				1.4473	1.5627	1.6172
	$B(M1, I \to I-1)_{out}$ (μ_N^2), **side → yrast band**							
9	0.0125	0.0179	0.0086	0.0031	0.0002	0.0005	0.0030	0.0070
10	0.0272	0.0265	0.0140	0.0042	0.0000	0.0026	0.0095	0.0191
11	0.0445	0.0445	0.0321	0.0068	0.0023	0.0203	0.0399	0.0510
12	0.0605	0.0806	0.1707	0.0450	0.1362	0.1305	0.1172	0.0951
13	0.0641	0.1122	0.5173	1.1163	0.0588	0.0033	0.0142	0.1296
14	0.0794	0.1406	0.2483	0.0886	0.1096	0.3844	1.0188	0.4152
15	0.0630	0.0888	0.1001	0.1122	0.1489	0.1443	0.0130	0.0749
16	0.0907	0.1199	0.1647	0.2355	0.3608	0.5450	0.7463	0.5747
17	0.0468	0.0512	0.0606	0.0692	0.0657	0.0402	0.0085	0.0066
18	0.0991	0.1296	0.1887	0.2611	0.3687	0.5041	0.5968	0.5276
19	0.0295	0.0325	0.0392	0.0417	0.0359	0.0206	0.0058	0.0001
20	0.1027	0.1356	0.1951	0.2595	0.3446	0.4314	0.4731	0.4222
21	0.0153	0.0182	0.0241	0.0258	0.0217	0.0125	0.0044	0.0003
22	0.0991	0.1306	0.1855	0.2406	0.3050	0.3582	0.3716	0.3242

Table A.51

A ~ 130, non-restricted configuration								
Spin I ($\hbar$)	$B(E2, I \to I-2)_{in}$ (e^2b^2), **yrast band**							
	$\gamma = 17^0$	$\gamma = 20^0$	$\gamma = 24^0$	$\gamma = 27^0$	$\gamma = 30^0$	$\gamma = 33^0$	$\gamma = 36^0$	$\gamma = 40^0$
10	0.0620	0.0489	0.0260	0.0104	0.0015	0.0005	0.0065	0.0240
11	0.0869	0.0728	0.0423	0.0153	0.0008	0.0030	0.0156	0.0412
12	0.1170	0.1066	0.0830	0.0300	0.0038	0.0177	0.0367	0.0664
13	0.1471	0.1410	0.1187	0.0469	0.0105	0.0070	0.0343	0.0919
14	0.1781	0.1736	0.1380	0.0392	0.0185	0.0541	0.1012	0.1366
15	0.2019	0.2003	0.2022	0.1678	0.1289	0.1229	0.1351	0.1478
16	0.2293	0.2326	0.2329	0.2246	0.2191	0.2179	0.2161	0.1992
17	0.2461	0.2499	0.2467	0.2411	0.2356	0.2301	0.2270	0.2099
18	0.2692	0.2733	0.2727	0.2704	0.2672	0.2629	0.2580	0.2473
19	0.2801	0.2828	0.2817	0.2790	0.2750	0.2706	0.2655	0.2525
20	0.2978	0.3011	0.3012	0.2992	0.2959	0.2914	0.2852	0.2730
21	0.3058	0.3079	0.3069	0.3042	0.3003	0.2953	0.2889	0.2757
22	0.3179	0.3209	0.3210	0.3189	0.3152	0.3101	0.3031	0.2891
	$B(E2, I \to I-2)_{in}$ (e^2b^2), **side band**							
10	0.0373	0.0248	0.0088	0.0028	0.0001	0.0010	0.0052	0.0154
11	0.0664	0.0347	0.0187	0.0089	0.0009	0.0013	0.0088	0.0254
12	0.0894	0.0524	0.0494	0.0326	0.0002	0.0058	0.0216	0.0478
13	0.1121	0.0856	0.0680	0.0174	0.0040	0.0125	0.0578	0.0977
14	0.1363	0.1072	0.0755	0.0203	0.0124	0.0350	0.0736	0.1100
15	0.1691	0.1383	0.1320	0.1191	0.1137	0.1370	0.1670	0.1614
16	0.1845	0.1584	0.1616	0.1760	0.1836	0.1657	0.1449	0.1414
17	0.2201	0.2036	0.2136	0.2220	0.2213	0.2163	0.2150	0.2053
18	0.2295	0.2243	0.2378	0.2404	0.2367	0.2313	0.2217	0.2021
19	0.2661	0.2644	0.2710	0.2712	0.2685	0.2646	0.2577	0.2440
20	0.2757	0.2787	0.2813	0.2795	0.2756	0.2702	0.2632	0.2504
21	0.2968	0.2978	0.3028	0.3020	0.2987	0.2937	0.2861	0.2711
22	0.3034	0.3068	0.3074	0.3050	0.3007	0.2946	0.2866	0.2735

Table A.52

A ~ 130, non-restricted configuration								
Spin I ($\hbar$)	$B(E2, I \to I-2)_{out}$ (e^2b^2), **yrast → side band**							
	$\gamma = 17^0$	$\gamma = 20^0$	$\gamma = 24^0$	$\gamma = 27^0$	$\gamma = 30^0$	$\gamma = 33^0$	$\gamma = 36^0$	$\gamma = 40^0$
12	...	0.0000	0.0003	0.0143	0.0411	0.0318	0.0182	0.0056
13	0.0010	0.0027	0.0232	0.0818	0.0966	0.0849	0.0390	0.0023
14	0.0027	0.0094	0.0426	0.1326	0.1454	0.1050	0.0526	0.0062
15	0.0023	0.0058	0.0008	0.0288	0.0533	0.0337	0.0052	0.0002
16	0.0041	0.0032	0.0004	0.0030	0.0009	0.0000	0.0018	0.0117
17	0.0007	0.0000	0.0026	0.0045	0.0049	0.0051	0.0008	0.0020
18	0.0024	0.0040	0.0000	0.0001	0.0002	0.0002	0.0003	0.0019
19	0.0001	0.0020	0.0014	0.0016	0.0017	0.0010	0.0000	0.0012
20	0.0014	0.0005	0.0001	0.0000	0.0000	0.0000	0.0001	0.0007
21	0.0008	0.0022	0.0010	0.0009	0.0008	0.0004	0.0000	0.0004
22	0.0010	0.0006	0.0004	0.0002	0.0001	0.0000	0.0000	0.0003
	$B(E2, I \to I-2)_{out}$ (e^2b^2), **side → yrast band**							
10	0.0518	0.0643	0.0782	0.0856	0.0891	0.0874	0.0810	0.0651
11	0.0389	0.0102	0.0621	0.0153	0.0877	0.0836	0.0729	0.0545
12	0.0223	0.0219	0.0264	0.0654	0.0828	0.0673	0.0534	0.0375
13	0.0109	0.0048	0.0026	0.0511	0.0744	0.0803	0.0632	0.0241
14	0.0031	0.0001	0.0192	0.0775	0.0875	0.0597	0.0202	0.0002
15	0.0015	0.0001	0.0000	0.0199	0.0372	0.0270	0.0020	0.0061
16	0.0001	0.0002	0.0004	0.0017	0.0009	0.0002	0.0013	0.0029

Table A.52 continues

A ~ 130, non-restricted configuration								
Spin I ($\hbar$)	$B(E2, I \to I-2)_{out}$ (e^2b^2), side → yrast band							
	$\gamma = 17^0$	$\gamma = 20^0$	$\gamma = 24^0$	$\gamma = 27^0$	$\gamma = 30^0$	$\gamma = 33^0$	$\gamma = 36^0$	$\gamma = 40^0$
17	0.0009	0.0009	0.0030	0.0043	0.0047	0.0043	0.0002	0.0054
18	0.0000	0.0000	0.0002	0.0003	0.0003	0.0003	0.0003	0.0007
19	0.0018	0.0016	0.0021	0.0019	0.0016	0.0007	0.0000	0.0023
20	0.0000	0.0000	0.0000	0.0001	0.0001	0.0001	0.0002	0.0004
21	0.0023	0.0000	0.0016	0.0011	0.0007	0.0002	0.0000	0.0009
22	0.0000	0.0000	0.0000	0.0000	0.0000	0.0000	0.0001	0.0003

Table A.53

A ~ 190, non-restricted configuration								
Spin I ($\hbar$)	$B(M1, I \to I-1)_{in}$ (μ_N^2), yrast band							
	$\gamma = 17^0$	$\gamma = 20^0$	$\gamma = 24^0$	$\gamma = 27^0$	$\gamma = 30^0$	$\gamma = 33^0$	$\gamma = 36^0$	$\gamma = 40^0$
9	1.3415	1.3735	1.4105	1.4289	1.4392	1.4429	1.4423	1.4381
10	1.1323	1.1666	1.2029	1.2152	1.2113	1.1933	1.1689	1.1409
11	1.0089	1.0147	1.0256	1.0359	1.0061	0.9614	0.9293	0.9159
12	0.9314	0.9137	0.8259	0.9106	0.6502	0.7094	0.7240	0.7359
13	0.8658	0.8213	0.5008	0.0384	0.7971	0.7754	0.6881	0.6182
14	0.8221	0.7772	0.7470	0.8164	0.7349	0.4374	0.0091	0.3841
15	0.7906	0.7795	0.7776	0.7555	0.7209	0.7286	0.7112	0.5726
16	0.7468	0.7213	0.6739	0.5977	0.4522	0.2041	0.0012	0.1458
17	0.7613	0.7796	0.7898	0.7881	0.7795	0.7565	0.7094	0.6178
18	0.6777	0.6318	0.5390	0.4341	0.2808	0.1019	0.0040	0.0464
19	0.7488	0.7768	0.7980	0.8009	0.7890	0.7560	0.7034	0.6238
20	0.6087	0.5408	0.4273	0.3221	0.1934	0.0694	0.0056	0.0161
21	0.7423	0.7761	0.8019	0.8043	0.7887	0.7511	0.6964	0.6170
22	0.5469	0.4646	0.3445	0.2472	0.1419	0.0508	0.0055	0.0069
	$B(M1, I \to I-1)_{in}$ (μ_N^2), side band							
8	1.4774	1.4881	1.4727	...	...	...	...	...
9	1.2600	1.2017	0.9194	1.4132	1.4202	1.4382	1.4537	1.4683
10	1.0306	0.9214	1.1075	1.3617	1.3825	1.3260	1.2284	1.0971
11	0.8783	0.8844	1.1605	1.2774	1.2742	1.2025	1.1129	0.9801
12	0.7834	0.8440	0.8326	1.0462	0.7808	0.8057	0.7784	0.6862
13	0.7684	0.7395	0.4260	0.0609	0.8403	0.7863	0.7018	0.6426
14	0.7084	0.6566	0.6112	0.6940	0.6267	0.3622	0.0121	0.3474
15	0.6828	0.6566	0.6814	0.7183	0.7131	0.6756	0.6005	0.4284
16	0.6356	0.5976	0.5417	0.4691	0.3396	0.1436	0.0005	0.1069
17	0.6389	0.6490	0.6456	0.6217	0.5852	0.5185	0.4232	0.2986
18	0.5805	0.5312	0.4495	0.3591	0.2292	0.0835	0.0047	0.0232
19	0.6066	0.5738	0.4886	0.4283	0.3599	0.2727	0.1868	0.1146
20	0.5369	0.4801	0.3860	0.2920	0.1763	0.0664	0.0088	0.0035
21	0.5459	0.4670	0.3539	0.2846	0.2174	0.1475	0.0887	0.0441
22	0.5102	0.4484	0.3442	0.2495	0.1463	0.0579	0.0121	0.0000

Table A.54

A ~ 190, non-restricted configuration								
Spin I ($\hbar$)	$B(M1, I \rightarrow I-1)_{out}$ (μ_N^2), **yrast → side band**							
	$\gamma = 17^0$	$\gamma = 20^0$	$\gamma = 24^0$	$\gamma = 27^0$	$\gamma = 30^0$	$\gamma = 33^0$	$\gamma = 36^0$	$\gamma = 40^0$
12	···	···	0.2181	0.0333	0.3021	0.2536	0.2532	···
13	···	···	0.4449	0.8267	0.0092	0.0004	0.0918	···
14	···	0.1762	0.1561	0.0330	0.0701	0.3778	0.8477	0.5198
15	···	0.1086	0.0723	0.0726	0.0855	0.0321	0.0246	0.1688
16	···	···	0.2278	0.3269	0.4725	0.6851	0.8517	0.7220
17	···	···	···	0.0308	0.0093	0.0007	0.0254	0.1009
18	···	···	···	0.5279	0.6845	0.8530	0.9249	0.8549
19	···	···	···	···	0.0000	0.0096	0.0387	0.0000
20	···	···	···	···	0.8065	0.9273	0.9723	0.9180
21	···	···	···	···	0.0013	0.0168	0.0475	···
22	···	···	···	···	0.8853	0.9738	0.9952	···
	$B(M1, I \rightarrow I-1)_{out}$ (μ_N^2), **side → yrast band**							
8	0.0371	0.0323	0.0288	0.0183	···	···	···	···
9	0.0023	0.0028	0.0026	0.0031	0.0060	0.0097	0.0117	0.0115
10	0.0078	0.0060	0.0003	0.0022	0.0126	0.0272	0.0394	0.0450
11	0.0265	0.0257	0.0115	0.0002	0.0262	0.0593	0.0737	0.0660
12	0.0398	0.0519	0.1206	0.0130	0.2564	0.1820	0.1450	0.1047
13	0.0497	0.0860	0.3919	0.7939	0.0025	0.0042	0.0609	0.1036
14	0.0565	0.1021	0.1384	0.0403	0.0712	0.3047	0.6152	0.2410
15	0.0578	0.0776	0.0746	0.0756	0.0836	0.0423	0.0066	0.0642
16	0.0632	0.0830	0.1139	0.1676	0.2618	0.4029	0.4862	0.3190
17	0.0506	0.0465	0.0393	0.0341	0.0211	0.0044	0.0008	0.0141
18	0.0652	0.0878	0.1422	0.2096	0.3015	0.3903	0.4048	0.3083
19	0.0407	0.0318	0.0216	0.0148	0.0068	0.0008	0.0004	0.0025
20	0.0683	0.0945	0.1514	0.2140	0.2860	0.3360	0.3298	0.2581
21	0.0337	0.0229	0.0119	0.0066	0.0023	0.0001	0.0002	0.0003
22	0.0701	0.0960	0.1483	0.2017	0.2558	0.2841	0.2691	0.2103

Table A.55

A ~ 190, non-restricted configuration								
Spin I ($\hbar$)	$B(E2, I \rightarrow I-2)_{in}$ (e^2b^2), **yrast band**							
	$\gamma = 17^0$	$\gamma = 20^0$	$\gamma = 24^0$	$\gamma = 27^0$	$\gamma = 30^0$	$\gamma = 33^0$	$\gamma = 36^0$	$\gamma = 40^0$
9	0.0385	0.0249	0.0057	0.0000	···	···	···	···
10	0.1295	0.0896	0.0321	0.0043	0.0027	0.0267	0.0711	0.1531
11	0.2531	0.1999	0.0983	0.0200	0.0031	0.0444	0.1085	0.2045
12	0.3744	0.3297	0.2548	0.0718	0.0668	0.1203	0.1874	0.2832
13	0.4846	0.4513	0.3581	0.1340	0.0322	0.0331	0.1948	0.3464
14	0.5847	0.5594	0.4594	0.1221	0.1489	0.2616	0.3943	0.4749
15	0.6638	0.6483	0.6411	0.5070	0.4049	0.3879	0.4531	0.5009
16	0.7443	0.7519	0.7458	0.7222	0.7111	0.7117	0.6978	0.6519
17	0.8039	0.8107	0.7865	0.7616	0.7416	0.7347	0.7359	0.6840
18	0.8658	0.8768	0.8710	0.8645	0.8558	0.8446	0.8307	0.7934
19	0.9095	0.9154	0.9054	0.8949	0.8838	0.8746	0.8595	0.8171
20	0.9494	0.9576	0.9569	0.9523	0.9436	0.9309	0.9121	0.8724
21	0.9832	0.9904	0.9869	0.9790	0.9676	0.9534	0.9333	0.8907
22	1.0067	1.0146	1.0161	1.0120	1.0028	0.9879	0.9647	0.9118
	$B(E2, I \rightarrow I-2)_{in}$ (e^2b^2), **side band**							
9	0.0085	0.0012	0.0068	0.0172	···	···	···	···
10	0.0809	0.0202	0.0000	0.0003	0.0027	0.0126	0.0323	0.0863
11	0.2025	0.0584	0.0234	0.0064	0.0008	0.0161	0.0427	0.1073
12	0.2476	0.1406	0.1209	0.0630	0.0115	0.0504	0.1014	0.1831

Table A.55 continues

A ~ 190, non-restricted configuration								
Spin I ($\hbar$)	$B(E2, I \to I-2)_{in}$ (e^2b^2), **side band**							
	$\gamma = 17^0$	$\gamma = 20^0$	$\gamma = 24^0$	$\gamma = 27^0$	$\gamma = 30^0$	$\gamma = 33^0$	$\gamma = 36^0$	$\gamma = 40^0$
13	0.3213	0.2699	0.1918	0.0535	0.0249	0.0767	0.2682	0.3298
14	0.4098	0.3396	0.2415	0.0579	0.0978	0.1693	0.2782	0.3569
15	0.5189	0.4453	0.4231	0.3824	0.3977	0.4691	0.5441	0.5173
16	0.5716	0.5156	0.5185	0.5590	0.5622	0.4902	0.4382	0.4524
17	0.6719	0.6538	0.6943	0.7139	0.7045	0.6925	0.6816	0.6497
18	0.7140	0.7103	0.7501	0.7528	0.7377	0.7177	0.6780	0.6155
19	0.8230	0.8406	0.8627	0.8611	0.8515	0.8361	0.8079	0.7655
20	0.8568	0.8777	0.8887	0.8814	0.8685	0.8516	0.8300	0.7901
21	0.9351	0.9502	0.9574	0.9521	0.9405	0.9223	0.8956	0.8511
22	0.9620	0.9747	0.9720	0.9628	0.9486	0.9296	0.9062	0.8696

Table A.56

A ~ 190, non-restricted configuration								
Spin I ($\hbar$)	$B(E2, I \to I-2)_{out}$ (e^2b^2), **yrast → side band**							
	$\gamma = 17^0$	$\gamma = 20^0$	$\gamma = 24^0$	$\gamma = 27^0$	$\gamma = 30^0$	$\gamma = 33^0$	$\gamma = 36^0$	$\gamma = 40^0$
9	...	...	0.2174	...	...	...	...	...
10	...	...	0.2551	...	...	...	...	...
11	...	...	0.2051	...	...	...	...	...
12	...	0.0029	0.0745	0.0487	0.0916	0.0573	0.0264	0.0057
13	0.0005	0.0061	0.0161	0.2514	0.2954	0.2432	0.0527	0.0020
14	0.0020	0.0258	0.0534	0.4228	0.3796	0.2604	0.1157	0.0170
15	0.0048	0.0155	0.0013	0.1088	0.1563	0.0956	0.0072	0.0003
16	0.0086	0.0075	0.0009	0.0064	0.0006	0.0000	0.0011	0.0306
17	0.0020	0.0002	0.0116	0.0232	0.0271	0.0206	0.0001	0.0052
18	0.0030	0.0001	0.0006	0.0000	0.0000	0.0000	0.0000	0.0037
19	0.0001	0.0034	0.0059	0.0081	0.0068	0.0021	0.0002	0.0048
20	0.0005	0.0001	0.0002	0.0002	0.0003	0.0002	0.0001	0.0003
21	0.0011	0.0028	0.0027	0.0031	0.0021	0.0005	0.0001	0.0024
22	0.0002	0.0002	0.0001	0.0005	0.0005	0.0004	0.0001	0.0001
	$B(E2, I \to I-2)_{out}$ (e^2b^2), **side → yrast band**							
9	0.1339	0.1483	...	0.2552	...	...	...	...
10	0.1439	0.2040	...	0.2747	0.2767	0.2622	0.2354	0.1838
11	0.0982	0.1395	...	0.2648	0.2751	0.2412	0.1980	0.1418
12	0.0568	0.0601	0.0020	0.2197	0.2071	0.1627	0.1273	0.0931
13	0.0246	0.0108	0.0820	0.1609	0.2289	0.2547	0.1413	0.0611
14	0.0061	0.0006	0.1104	0.2475	0.2124	0.1261	0.0277	0.0026
15	0.0016	0.0007	0.0003	0.0736	0.1146	0.0801	0.0000	0.0206
16	0.0000	0.0010	0.0020	0.0027	0.0006	0.0001	0.0032	0.0031
17	0.0005	0.0019	0.0145	0.0180	0.0211	0.0129	0.0011	0.0180
18	0.0000	0.0002	0.0002	0.0003	0.0001	0.0000	0.0000	0.0003
19	0.0015	0.0037	0.0073	0.0059	0.0041	0.0050	0.0015	0.0097
20	0.0002	0.0003	0.0002	0.0001	0.0000	0.0000	0.0000	0.0000
21	0.0018	0.0027	0.0033	0.0021	0.0009	0.0000	0.0010	0.0047
22	0.0003	0.0003	0.0005	0.0000	0.0000	0.0000	0.0000	0.0000

Table A.57

A ~ 100, restricted configuration								
Spin I ($\hbar$)	$B(M1, I \to I-1)_{in}$ **(μ_N^2), yrast band**							
	$\gamma = 17^0$	$\gamma = 20^0$	$\gamma = 24^0$	$\gamma = 27^0$	$\gamma = 30^0$	$\gamma = 33^0$	$\gamma = 36^0$	$\gamma = 40^0$
9	1.5785	1.6442	1.7270	1.7855	1.8304	1.8480	1.8333	1.7799
10	1.5455	1.6087	1.7004	1.7781	1.8458	1.8685	1.8423	1.7810
11	1.5090	1.5683	1.6619	1.7527	1.8406	1.8625	1.8239	1.7623
12	1.4709	1.5236	1.6075	1.6946	1.7923	1.8077	1.7688	1.7265
13	1.4317	1.4736	1.5327	1.6068	1.7399	1.7308	1.6797	1.6738
14	1.3908	1.4158	1.4494	1.5668	1.7410	1.6889	1.6082	1.6047
15	1.3468	1.3464	1.4129	1.5797	1.4119	1.5890	1.6136	1.5252
16	1.2974	1.2578	1.6206	1.3552	0.3631	0.4592	1.7342	1.4430
17	1.2386	1.1196	0.0013	1.2211	1.6917	1.5764	1.7237	1.3408
18	1.1645	0.7870	1.3812	0.9240	0.3490	0.4228	1.3379	0.9743
19	1.0678	0.3614	1.1595	1.1333	1.5532	1.7496	1.3779	1.8937
20	0.9526	0.6905	1.0483	0.9294	0.5112	0.4150	1.0962	1.0082
21	0.8666	0.9413	1.0474	1.0701	1.3651	1.7312	1.3117	1.2175
22	0.8644	1.0002	1.0080	0.9511	0.7342	0.5327	1.0821	1.2159
	$B(M1, I \to I-1)_{in}$ **(μ_N^2), side band**							
9	1.3466	1.4440	1.5780	1.6674	1.7242	1.7267	1.6697	1.5306
10	1.3382	1.4242	1.5617	1.6766	1.7647	1.7698	1.6906	1.5465
11	1.3231	1.3984	1.5335	1.6697	1.7932	1.7930	1.6872	1.5457
12	1.3037	1.3684	1.4962	1.6479	1.8087	1.7946	1.6641	1.5321
13	1.2815	1.3348	1.4526	1.6161	1.8124	1.7748	1.6290	1.5087
14	1.2568	1.2970	1.4112	1.5981	1.7830	1.7208	1.6007	1.4778
15	1.2291	1.2520	1.4048	1.5970	1.4193	1.5966	1.6190	1.4402
16	1.1967	1.1897	1.6287	1.3605	0.3641	0.4588	1.7415	1.3925
17	1.1561	1.0743	0.0011	1.2229	1.6926	1.5768	1.7285	1.3120
18	1.1008	0.7604	1.3472	0.9250	0.3492	0.4229	1.3402	0.9580
19	1.0226	0.3531	1.1555	1.1346	1.5525	1.7504	1.3795	1.8845
20	0.9248	0.6916	1.0454	0.9304	0.5114	0.4154	1.0972	1.0050
21	0.8535	0.9466	1.0448	1.0711	1.3656	1.7319	1.3127	1.2142
22	0.8621	1.0062	1.0057	0.9522	0.7346	0.5330	1.0833	1.2132

Table A.58

A ~ 100, restricted configuration								
Spin I ($\hbar$)	$B(M1, I \to I-1)_{out}$ **(μ_N^2), yrast → side band**							
	$\gamma = 17^0$	$\gamma = 20^0$	$\gamma = 24^0$	$\gamma = 27^0$	$\gamma = 30^0$	$\gamma = 33^0$	$\gamma = 36^0$	$\gamma = 40^0$
11	...	...	0.1065	0.0570	0.0051	0.0195	0.0829	...
12	...	...	0.1509	0.0956	0.0090	0.0375	0.1269	0.1754
13	...	0.2121	0.2170	0.1536	0.0155	0.0700	0.1885	0.2208
14	0.2342	0.2659	0.2978	0.1988	0.0534	0.1345	0.2449	0.2808
15	0.2718	0.3397	0.3461	0.2213	0.4303	0.2707	0.2483	0.3532
16	0.3214	0.4411	0.1551	0.4758	1.5006	1.4215	0.1419	0.4344
17	0.3870	0.5977	1.8082	0.6290	0.1886	0.3162	0.1671	0.5413
18	0.4736	0.9472	0.4450	0.9403	1.5410	1.4802	0.5652	0.9143
19	0.5864	1.3830	0.6807	0.7424	0.3468	0.1618	0.5346	0.0008
20	0.7178	1.0735	0.8038	0.9563	1.3965	1.5042	0.8242	0.8957
21	0.8225	0.8425	0.8148	0.8238	0.5492	0.1940	0.6150	0.6937
22	0.8436	0.8000	0.8628	0.9502	1.1866	1.3986	0.8505	0.7017
	$B(M1, I \to I-1)_{out}$ **(μ_N^2), side → yrast band**							
9	0.1945	0.1510	0.0896	0.0438	0.0095	0.0007	0.0215	0.0772
10	0.2099	0.1718	0.1106	0.0554	0.0093	0.0043	0.0420	0.1079
11	0.2238	0.1920	0.1347	0.0714	0.0095	0.0117	0.0683	0.1372
12	0.2386	0.2184	0.1661	0.0963	0.0107	0.0259	0.1040	0.1686

Table A.58 continues

A ~ 100, restricted configuration								
Spin I ($\hbar$)	$B(M1, I \to I-1)_{out}$ (μ_N^2), side → yrast band							
	$\gamma = 17^0$	$\gamma = 20^0$	$\gamma = 24^0$	$\gamma = 27^0$	$\gamma = 30^0$	$\gamma = 33^0$	$\gamma = 36^0$	$\gamma = 40^0$
13	0.2561	0.2437	0.2108	0.1369	0.0150	0.0555	0.1549	0.2070
14	0.2784	0.2836	0.2717	0.1811	0.0521	0.1238	0.2132	0.2572
15	0.3080	0.3415	0.3189	0.2139	0.4272	0.2657	0.2317	0.3232
16	0.3485	0.4300	0.1449	0.4730	1.5009	1.4195	0.1372	0.4066
17	0.4049	0.5830	1.7939	0.6284	0.1867	0.3162	0.1657	0.5223
18	0.4841	0.9415	0.4449	0.9403	1.5412	1.4804	0.5644	0.9143
19	0.5934	1.3946	0.6810	0.7424	0.3469	0.1617	0.5338	0.0010
20	0.7263	1.0822	0.8048	0.9558	1.3962	1.5036	0.8232	0.8930
21	0.8309	0.8440	0.8164	0.8233	0.5492	0.1937	0.6142	0.6941
22	0.8491	0.7976	0.8651	0.9491	1.1858	1.3976	0.8492	0.7034

Table A.59

A ~ 100, restricted configuration								
Spin I ($\hbar$)	$B(E2, I \to I-2)_{in}$ (e^2b^2), yrast band							
	$\gamma = 17^0$	$\gamma = 20^0$	$\gamma = 24^0$	$\gamma = 27^0$	$\gamma = 30^0$	$\gamma = 33^0$	$\gamma = 36^0$	$\gamma = 40^0$
10	0.0396	0.0305	0.0179	0.0086	0.0016	0.0003	0.0048	0.0146
11	0.0468	0.0373	0.0232	0.0115	0.0017	0.0012	0.0091	0.0214
12	0.0533	0.0437	0.0291	0.0152	0.0018	0.0031	0.0148	0.0285
13	0.0591	0.0499	0.0355	0.0197	0.0019	0.0066	0.0220	0.0358
14	0.0644	0.0561	0.0425	0.0253	0.0038	0.0144	0.0309	0.0434
15	0.0695	0.0625	0.0502	0.0324	0.0249	0.0314	0.0401	0.0516
16	0.0746	0.0698	0.0470	0.0518	0.0282	0.0771	0.0412	0.0607
17	0.0797	0.0784	0.0720	0.0765	0.0487	0.0866	0.0403	0.0711
18	0.0852	0.0850	0.0652	0.0944	0.0929	0.0937	0.0689	0.0812
19	0.0908	0.0681	0.0907	0.1016	0.1014	0.0991	0.0900	0.0651
20	0.0957	0.0721	0.1046	0.1065	0.1038	0.1041	0.0998	0.0666
21	0.0995	0.1054	0.1105	0.1115	0.1109	0.1088	0.1049	0.0989
22	0.1044	0.1145	0.1147	0.1149	0.1114	0.1111	0.1087	0.1033
	$B(E2, I \to I-2)_{in}$ (e^2b^2), side band							
10	0.0493	0.0405	0.0249	0.0118	0.0019	0.0009	0.0091	0.0234
11	0.0580	0.0491	0.0326	0.0163	0.0020	0.0027	0.0161	0.0327
12	0.0655	0.0570	0.0405	0.0216	0.0022	0.0059	0.0243	0.0415
13	0.0720	0.0642	0.0485	0.0277	0.0024	0.0108	0.0333	0.0498
14	0.0779	0.0710	0.0563	0.0334	0.0046	0.0191	0.0421	0.0576
15	0.0831	0.0775	0.0626	0.0375	0.0269	0.0348	0.0482	0.0651
16	0.0880	0.0841	0.0542	0.0541	0.0286	0.0787	0.0446	0.0723
17	0.0925	0.0907	0.0761	0.0771	0.0486	0.0868	0.0413	0.0797
18	0.0967	0.0930	0.0672	0.0944	0.0928	0.0936	0.0692	0.0862
19	0.1002	0.0697	0.0914	0.1013	0.1012	0.0990	0.0900	0.0680
20	0.1020	0.0707	0.1052	0.1062	0.1038	0.1041	0.0997	0.0680
21	0.1022	0.1026	0.1111	0.1112	0.1107	0.1086	0.1048	0.1000
22	0.1042	0.1121	0.1153	0.1147	0.1113	0.1111	0.1086	0.1040

Table A.60

A ~ 100, restricted configuration								
Spin I ($\hbar$)	$B(E2, I \to I-2)_{out}$ (e^2b^2), yrast → side band							
	$\gamma = 17^0$	$\gamma = 20^0$	$\gamma = 24^0$	$\gamma = 27^0$	$\gamma = 30^0$	$\gamma = 33^0$	$\gamma = 36^0$	$\gamma = 40^0$
10	...	...	...	0.0063	0.0091	0.0089	0.0058	...
11	...	0.0011	0.0043	0.0098	0.0161	0.0150	0.0080	0.0021
12	0.0003	0.0013	0.0057	0.0155	0.0291	0.0251	0.0111	0.0024

Table A.60 continues

A ~ 100, restricted configuration								
Spin I ($\hbar$)	$B(E2, I \to I-2)_{out}$ (e^2b^2), **yrast → side band**							
	$\gamma = 17^0$	$\gamma = 20^0$	$\gamma = 24^0$	$\gamma = 27^0$	$\gamma = 30^0$	$\gamma = 33^0$	$\gamma = 36^0$	$\gamma = 40^0$
13	0.0004	0.0014	0.0076	0.0228	0.0454	0.0361	0.0144	0.0028
14	0.0004	0.0015	0.0095	0.0294	0.0561	0.0405	0.0170	0.0031
15	0.0003	0.0015	0.0122	0.0352	0.0441	0.0349	0.0205	0.0032
16	0.0002	0.0011	0.0286	0.0273	0.0518	0.0000	0.0323	0.0028
17	0.0001	0.0002	0.0139	0.0123	0.0400	0.0000	0.0431	0.0016
18	0.0000	0.0031	0.0293	0.0020	0.0029	0.0002	0.0217	0.0006
19	0.0003	0.0311	0.0106	0.0011	0.0004	0.0007	0.0066	0.0238
20	0.0019	0.0338	0.0023	0.0013	0.0030	0.0006	0.0018	0.0281
21	0.0048	0.0052	0.0010	0.0007	0.0003	0.0002	0.0009	0.0006
22	0.0056	0.0001	0.0008	0.0011	0.0035	0.0015	0.0008	0.0002
	$B(E2, I \to I-2)_{out}$ (e^2b^2), **side → yrast band**							
10	0.0081	0.0118	0.0188	0.0250	0.0299	0.0297	0.0242	0.0152
11	0.0061	0.0091	0.0155	0.0229	0.0296	0.0286	0.0209	0.0117
12	0.0046	0.0071	0.0131	0.0216	0.0310	0.0285	0.0182	0.0091
13	0.0036	0.0056	0.0114	0.0217	0.0359	0.0303	0.0165	0.0073
14	0.0028	0.0044	0.0106	0.0247	0.0457	0.0340	0.0162	0.0059
15	0.0021	0.0033	0.0117	0.0314	0.0409	0.0325	0.0190	0.0047
16	0.0015	0.0022	0.0264	0.0262	0.0508	0.0000	0.0308	0.0036
17	0.0009	0.0006	0.0129	0.0121	0.0398	0.0000	0.0421	0.0020
18	0.0003	0.0019	0.0291	0.0020	0.0029	0.0002	0.0214	0.0004
19	0.0000	0.0271	0.0110	0.0010	0.0004	0.0007	0.0065	0.0239
20	0.0009	0.0312	0.0024	0.0013	0.0029	0.0006	0.0018	0.0286
21	0.0032	0.0049	0.0010	0.0007	0.0003	0.0002	0.0009	0.0006
22	0.0042	0.0001	0.0008	0.0011	0.0034	0.0015	0.0008	0.0002

Table A.61

A ~ 130, restricted configuration								
Spin I ($\hbar$)	$B(M1, I \to I-1)_{in}$ (μ_N^2), **yrast band**							
	$\gamma = 17^0$	$\gamma = 20^0$	$\gamma = 24^0$	$\gamma = 27^0$	$\gamma = 30^0$	$\gamma = 33^0$	$\gamma = 36^0$	$\gamma = 40^0$
9	2.0697	2.1665	2.2703	2.3276	2.3634	2.3726	2.3597	2.3144
10	2.0283	2.1232	2.2466	2.3309	2.3882	2.4042	2.3856	2.3347
11	1.9776	2.0692	2.2063	2.3187	2.4029	2.4214	2.3921	2.3345
12	1.9225	2.0077	2.1469	2.2801	2.3934	2.4141	2.3769	2.3187
13	1.8650	1.9391	2.0613	2.1935	2.3335	2.3611	2.3325	2.2895
14	1.8056	1.8620	1.9453	2.0695	2.2684	2.2722	2.2522	2.2471
15	1.7435	1.7737	1.8324	1.9738	2.3106	2.2372	2.1562	2.1904
16	1.6768	1.6735	1.8104	1.7325	2.3393	2.2304	2.0870	2.1209
17	1.6024	1.5633	1.9581	1.0179	2.2144	0.5758	2.0659	2.0466
18	1.5152	1.4291	1.9531	0.9628	1.2593	2.4167	2.0369	1.9799
19	1.4056	1.0185	1.5647	1.1604	1.0985	0.3634	2.1958	1.9249
20	1.2533	2.2008	1.3245	1.2087	1.2684	1.8110	2.2968	1.8770
21	1.0385	1.0076	1.2315	1.1637	1.0314	0.3785	1.4282	1.8348
22	0.8500	1.2038	1.1971	1.1803	1.2576	1.8558	2.3620	1.6642
	$B(M1, I \to I-1)_{in}$ (μ_N^2), **side band**							
9	1.7106	1.8797	2.0695	2.1659	2.2136	2.2107	2.1604	2.0321
10	1.6963	1.8476	2.0566	2.1909	2.2683	2.2687	2.2059	2.0741
11	1.6740	1.8082	2.0240	2.1967	2.3109	2.3089	2.2271	2.0931
12	1.6452	1.7629	1.9758	2.1827	2.3406	2.3303	2.2275	2.0952
13	1.6121	1.7133	1.9156	2.1482	2.3558	2.3313	2.2100	2.0850
14	1.5758	1.6601	1.8495	2.0944	2.3590	2.3129	2.1777	2.0655
15	1.5369	1.6037	1.7955	2.0096	2.3684	2.2861	2.1356	2.0394

Table A.61 continues

A ~ 130, restricted configuration								
Spin I ($\hbar$)	$B(M1, I \to I-1)_{in}$ (μ_N^2), **side band**							
	$\gamma = 17^0$	$\gamma = 20^0$	$\gamma = 24^0$	$\gamma = 27^0$	$\gamma = 30^0$	$\gamma = 33^0$	$\gamma = 36^0$	$\gamma = 40^0$
16	1.4946	1.5431	1.8084	1.7432	2.3558	2.2496	2.0906	2.0087
17	1.4467	1.4737	1.9689	1.0173	2.2180	0.5791	2.0706	1.9749
18	1.3883	1.3721	1.9638	0.9634	1.2605	2.4158	2.0393	1.9401
19	1.3082	0.9847	1.5706	1.1615	1.0991	0.3633	2.1969	1.9044
20	1.1847	2.1754	1.3281	1.2100	1.2681	1.8082	2.2985	1.8664
21	0.9972	0.9984	1.2344	1.1647	1.0323	0.3789	1.4279	1.8294
22	0.8322	1.1946	1.1997	1.1815	1.2578	1.8560	2.3621	1.6596

Table A.62

A ~ 130, restricted configuration								
Spin I ($\hbar$)	$B(M1, I \to I-1)_{out}$ (μ_N^2), **yrast → side band**							
	$\gamma = 17^0$	$\gamma = 20^0$	$\gamma = 24^0$	$\gamma = 27^0$	$\gamma = 30^0$	$\gamma = 33^0$	$\gamma = 36^0$	$\gamma = 40^0$
12	...	...	0.1535	0.0729	0.0035	0.0243	0.0824	...
13	...	0.2591	0.2223	0.1252	0.0064	0.0429	0.1188	0.1612
14	...	0.3203	0.3217	0.2067	0.0107	0.0748	0.1736	0.1963
15	0.3486	0.4032	0.4288	0.3183	0.0080	0.1126	0.2437	0.2437
16	0.4064	0.5097	0.4657	0.6062	0.0342	0.1611	0.3139	0.3040
17	0.4815	0.6366	0.3416	1.3512	0.1886	1.8456	0.3527	0.3726
18	0.5785	0.7939	0.3729	1.4241	1.1617	0.0214	0.3988	0.4407
19	0.7052	1.2265	0.7851	1.2424	1.3362	2.0876	0.2530	0.5032
20	0.8776	0.0675	1.0437	1.2073	1.1772	0.6504	0.1626	0.5610
21	1.1115	1.2828	1.1518	1.2635	1.4227	2.0890	1.0416	0.6131
22	1.3188	1.1042	1.1988	1.2564	1.2049	0.6194	0.1151	0.7931
	$B(M1, I \to I-1)_{out}$ (μ_N^2), **side → yrast band**							
9	0.2376	0.1668	0.0832	0.0351	0.0065	0.0007	0.0161	0.0609
10	0.2681	0.2032	0.1113	0.0468	0.0062	0.0035	0.0316	0.0881
11	0.2919	0.2350	0.1420	0.0618	0.0061	0.0087	0.0503	0.1126
12	0.3138	0.2666	0.1786	0.0834	0.0064	0.0172	0.0731	0.1363
13	0.3372	0.3026	0.2273	0.1185	0.0076	0.0319	0.1033	0.1617
14	0.3649	0.3481	0.2966	0.1810	0.0103	0.0593	0.1469	0.1917
15	0.3998	0.4094	0.3841	0.2942	0.0076	0.1001	0.2100	0.2299
16	0.4456	0.4935	0.4309	0.5932	0.0340	0.1553	0.2876	0.2798
17	0.5074	0.6065	0.3275	1.3473	0.1889	1.8422	0.3394	0.3423
18	0.5920	0.7643	0.3680	1.4248	1.1616	0.0210	0.3936	0.4127
19	0.7108	1.2099	0.7831	1.2429	1.3355	2.0854	0.2522	0.4830
20	0.8832	0.0643	1.0427	1.2072	1.1770	0.6503	0.1626	0.5490
21	1.1249	1.2735	1.1506	1.2632	1.4227	2.0905	1.0412	0.6065
22	1.3397	1.1030	1.1973	1.2558	1.2044	0.6203	0.1153	0.7910

Table A.63

A ~ 130, restricted configuration								
Spin I ($\hbar$)	$B(E2, I \to I-2)_{in}$ (e^2b^2), **yrast band**							
	$\gamma = 17^0$	$\gamma = 20^0$	$\gamma = 24^0$	$\gamma = 27^0$	$\gamma = 30^0$	$\gamma = 33^0$	$\gamma = 36^0$	$\gamma = 40^0$
10	0.0686	0.0485	0.0232	0.0081	0.0004	0.0022	0.0118	0.0308
11	0.0908	0.0673	0.0348	0.0124	0.0004	0.0048	0.0203	0.0452
12	0.1113	0.0861	0.0483	0.0183	0.0004	0.0089	0.0309	0.0600
13	0.1302	0.1046	0.0640	0.0261	0.0003	0.0155	0.0441	0.0750
14	0.1476	0.1230	0.0818	0.0370	0.0002	0.0259	0.0606	0.0904
15	0.1640	0.1417	0.1018	0.0560	0.0000	0.0426	0.0813	0.1065
16	0.1798	0.1613	0.1220	0.1036	0.0064	0.0689	0.1085	0.1239

Table A.63 continues

A ~ 130, restricted configuration								
Spin I ($\hbar$)	$B(E2, I \to I-2)_{in}$ (e^2b^2), **yrast band**							
	$\gamma = 17^0$	$\gamma = 20^0$	$\gamma = 24^0$	$\gamma = 27^0$	$\gamma = 30^0$	$\gamma = 33^0$	$\gamma = 36^0$	$\gamma = 40^0$
17	0.1956	0.1830	0.1252	0.1984	0.0001	0.0570	0.1396	0.1433
18	0.2119	0.2085	0.1225	0.2364	0.1421	0.1433	0.1688	0.1652
19	0.2291	0.2380	0.1829	0.2592	0.2501	0.1832	0.1736	0.1891
20	0.2468	0.2038	0.2555	0.2735	0.2660	0.2614	0.1486	0.2125
21	0.2601	0.2131	0.2855	0.2872	0.2818	0.2751	0.2394	0.2331
22	0.2620	0.2944	0.3013	0.2998	0.2941	0.2864	0.2421	0.2535
	$B(E2, I \to I-2)_{in}$ (e^2b^2), **side band**							
10	0.0920	0.0686	0.0332	0.0109	0.0003	0.0050	0.0223	0.0533
11	0.1192	0.0942	0.0508	0.0176	0.0003	0.0099	0.0365	0.0741
12	0.1437	0.1184	0.0707	0.0267	0.0002	0.0171	0.0533	0.0941
13	0.1656	0.1412	0.0921	0.0383	0.0002	0.0272	0.0720	0.1130
14	0.1852	0.1625	0.1143	0.0529	0.0002	0.0409	0.0924	0.1310
15	0.2028	0.1827	0.1356	0.0731	0.0000	0.0582	0.1142	0.1483
16	0.2190	0.2022	0.1500	0.1171	0.0069	0.0797	0.1369	0.1650
17	0.2340	0.2213	0.1402	0.2052	0.0001	0.0585	0.1577	0.1813
18	0.2483	0.2409	0.1277	0.2376	0.1422	0.1442	0.1774	0.1971
19	0.2617	0.2602	0.1844	0.2589	0.2500	0.1830	0.1767	0.2125
20	0.2732	0.2188	0.2553	0.2730	0.2659	0.2615	0.1494	0.2274
21	0.2770	0.2214	0.2847	0.2867	0.2816	0.2753	0.2397	0.2416
22	0.2681	0.3013	0.3004	0.2993	0.2938	0.2865	0.2422	0.2580

Table A.64

A ~ 130, restricted configuration								
Spin I ($\hbar$)	$B(E2, I \to I-2)_{out}$ (e^2b^2), **yrast → side band**							
	$\gamma = 17^0$	$\gamma = 20^0$	$\gamma = 24^0$	$\gamma = 27^0$	$\gamma = 30^0$	$\gamma = 33^0$	$\gamma = 36^0$	$\gamma = 40^0$
11	...	...	0.0120	0.0211	0.0263	0.0221	0.0136	...
12	0.0013	0.0044	0.0161	0.0334	0.0453	0.0346	0.0178	0.0058
13	0.0014	0.0051	0.0219	0.0537	0.0799	0.0550	0.0237	0.0065
14	0.0015	0.0059	0.0294	0.0780	0.1236	0.0793	0.0309	0.0074
15	0.0016	0.0067	0.0374	0.0921	0.1591	0.0959	0.0369	0.0085
16	0.0016	0.0072	0.0488	0.0756	0.1802	0.1016	0.0391	0.0094
17	0.0014	0.0067	0.0815	0.0120	0.2126	0.1470	0.0401	0.0100
18	0.0009	0.0043	0.1144	0.0018	0.0931	0.0832	0.0403	0.0100
19	0.0002	0.0008	0.0760	0.0000	0.0048	0.0633	0.0592	0.0092
20	0.0005	0.0567	0.0212	0.0027	0.0055	0.0019	0.1025	0.0079
21	0.0073	0.0663	0.0062	0.0034	0.0039	0.0023	0.0264	0.0063
22	0.0258	0.0009	0.0032	0.0031	0.0039	0.0033	0.0362	0.0015
	$B(E2, I \to I-2)_{out}$ (e^2b^2), **side → yrast band**							
10	0.0333	0.0464	0.0656	0.0776	0.0824	0.0777	0.0658	0.0461
11	0.0252	0.0362	0.0562	0.0722	0.0798	0.0726	0.0568	0.0364
12	0.0193	0.0285	0.0483	0.0683	0.0799	0.0690	0.0492	0.0290
13	0.0151	0.0228	0.0422	0.0669	0.0844	0.0678	0.0433	0.0236
14	0.0119	0.0185	0.0383	0.0698	0.0984	0.0706	0.0392	0.0195
15	0.0094	0.0152	0.0378	0.0772	0.1294	0.0800	0.0371	0.0165
16	0.0073	0.0125	0.0452	0.0691	0.1661	0.0922	0.0367	0.0143
17	0.0055	0.0098	0.0758	0.0119	0.2085	0.1411	0.0383	0.0126
18	0.0036	0.0061	0.1098	0.0017	0.0926	0.0824	0.0395	0.0112
19	0.0014	0.0003	0.0741	0.0000	0.0048	0.0637	0.0586	0.0098
20	0.0000	0.0572	0.0207	0.0027	0.0055	0.0019	0.1021	0.0082
21	0.0041	0.0686	0.0061	0.0033	0.0039	0.0023	0.0263	0.0065
22	0.0199	0.0008	0.0031	0.0031	0.0039	0.0033	0.0362	0.0015

Table A.65

A ~ 190, restricted configuration								
Spin I ($\hbar$)	$B(M1, I \to I-1)_{in}$ (μ_N^2), **yrast band**							
	$\gamma = 17^0$	$\gamma = 20^0$	$\gamma = 24^0$	$\gamma = 27^0$	$\gamma = 30^0$	$\gamma = 33^0$	$\gamma = 36^0$	$\gamma = 40^0$
8	1.1473	1.2317	...	...	...	...	...	1.3319
9	1.3442	1.3862	1.4011	1.3914	1.3709	1.3437	1.3128	1.2675
10	1.4698	1.4954	1.4842	1.4432	1.3843	1.3227	1.2677	1.2066
11	1.5512	1.5712	1.5500	1.4892	1.3944	1.2979	1.2217	1.1500
12	1.6007	1.6186	1.5891	1.5198	1.3950	1.2633	1.1725	1.0791
13	1.6238	1.6410	1.5906	1.5223	1.3648	1.2080	1.1196	1.0476
14	1.6184	1.6453	1.5761	1.4979	1.2460	1.1429	1.0610	0.9998
15	1.5675	1.6882	1.5736	0.7521	1.3377	1.0969	0.9818	0.9524
16	1.4214	0.9895	1.4996	1.1147	1.4100	0.6786	0.9213	0.9049
17	1.2226	1.6437	1.4377	1.3613	1.1997	0.0715	0.8627	0.8526
18	1.2787	1.5537	1.4289	1.3822	1.3185	1.0774	0.6567	0.8067
19	1.4093	1.5276	1.4351	1.3932	1.3402	1.2585	1.4395	0.7490
20	1.4699	1.5164	1.4425	1.4039	1.3557	1.3012	0.2886	0.7228
21	1.4957	1.5115	1.4490	1.4135	1.3697	1.3104	1.4473	0.6749
22	1.5080	1.5096	1.4548	1.4219	1.3818	1.3311	1.2120	0.6215
	$B(M1, I \to I-1)_{in}$ (μ_N^2), **side band**							
8	0.8894	...	...	...	...	...	...	...
9	1.0718	1.1652	1.2473	1.2736	1.2714	1.2437	1.1945	1.1026
10	1.1636	1.2588	1.3567	1.3643	1.3179	1.2431	1.1614	1.0557
11	1.2761	1.3589	1.4562	1.4440	1.3454	1.2228	1.1180	1.0093
12	1.3564	1.4312	1.5321	1.5039	1.3554	1.1914	1.0734	0.9666
13	1.4057	1.4792	1.5900	1.5478	1.3645	1.1604	1.0310	0.9265
14	1.4247	1.5171	1.6352	1.5357	1.2996	1.1244	0.9817	0.8874
15	1.4012	1.6165	1.6311	0.7410	1.3816	1.1013	0.9302	0.8523
16	1.2953	0.9357	1.5274	1.1078	1.4237	0.6823	0.8965	0.8167
17	1.1562	1.5788	1.4582	1.3649	1.1997	0.0757	0.8514	0.7834
18	1.2672	1.5129	1.4393	1.3868	1.3194	1.0755	0.6552	0.7556
19	1.4276	1.4980	1.4445	1.3975	1.3415	1.2595	1.4404	0.7168
20	1.4972	1.4934	1.4511	1.4079	1.3570	1.3013	0.2886	0.7047
21	1.5237	1.4927	1.4567	1.4172	1.3709	1.3105	1.4465	0.6642
22	1.5338	1.4938	1.4616	1.4252	1.3830	1.3311	1.2117	0.6172

Table A.66

A ~ 190, restricted configuration								
Spin I ($\hbar$)	$B(M1, I \to I-1)_{out}$ (μ_N^2), **yrast → side band**							
	$\gamma = 17^0$	$\gamma = 20^0$	$\gamma = 24^0$	$\gamma = 27^0$	$\gamma = 30^0$	$\gamma = 33^0$	$\gamma = 36^0$	$\gamma = 40^0$
8	...	...	...	...	...	...	...	0.2360
9	...	...	...	...	...	...	...	0.2522
10	...	...	...	...	...	...	...	0.2640
11	...	...	0.0086	...	...	...	...	0.2746
12	...	0.0582	0.0122	0.0019	0.0465	0.1039	...	0.2868
13	0.0932	0.0719	0.0132	0.0001	0.0838	0.1677	0.1866	0.3019
14	0.1222	0.0824	0.0112	0.0415	0.2102	0.2580	0.2586	0.3230
15	0.1820	0.0257	0.0409	0.8605	0.1781	0.3499	0.3706	0.3522
16	0.3180	0.7576	0.1597	0.5250	0.1697	0.8356	0.4838	0.3926
17	0.4886	0.1032	0.2525	0.3063	0.4276	1.4891	0.6014	0.4517
18	0.4202	0.1991	0.2832	0.3105	0.3395	0.5272	0.8597	0.5209
19	0.2968	0.2327	0.2947	0.3206	0.3434	0.3785	0.1178	0.6203
20	0.2495	0.2513	0.3025	0.3278	0.3496	0.3638	1.3063	0.6976
21	0.2374	0.2632	0.3095	0.3335	0.3541	0.3775	0.1784	0.7993
22	0.2376	0.2713	0.3154	0.3386	0.3579	0.3765	0.4396	0.8977

Table A.66 continues

A ~ 190, restricted configuration								
Spin I ($\hbar$)	$B(M1, I \to I-1)_{out}$ (μ_N^2), side → yrast band							
	$\gamma = 17^0$	$\gamma = 20^0$	$\gamma = 24^0$	$\gamma = 27^0$	$\gamma = 30^0$	$\gamma = 33^0$	$\gamma = 36^0$	$\gamma = 40^0$
8	0.0006	0.0061	...	...	...	...	...	...
9	0.0080	0.0002	0.0214	0.0547	0.0965	0.1425	0.1897	...
10	0.0222	0.0035	0.0075	0.0407	0.0928	0.1498	0.2026	...
11	0.0384	0.0140	0.0009	0.0277	0.0895	0.1592	0.2166	...
12	0.0565	0.0276	0.0003	0.0158	0.0894	0.1776	0.2364	...
13	0.0796	0.0425	0.0021	0.0027	0.1046	0.2138	0.2637	...
14	0.1154	0.0538	0.0043	0.0336	0.2086	0.2594	0.3037	...
15	0.1851	0.0114	0.0362	0.8448	0.1676	0.3260	0.3783	0.2818
16	0.3412	0.6966	0.1605	0.5351	0.1730	0.8120	0.4593	0.3466
17	0.5396	0.0919	0.2575	0.3136	0.4317	1.4817	0.5749	0.4323
18	0.4677	0.1875	0.2890	0.3164	0.3441	0.5247	0.8423	0.5266
19	0.3249	0.2251	0.2998	0.3255	0.3475	0.3757	0.1140	0.6386
20	0.2646	0.2471	0.3065	0.3317	0.3531	0.3610	1.3060	0.7189
21	0.2443	0.2617	0.3120	0.3366	0.3570	0.3751	0.1799	0.8142
22	0.2389	0.2721	0.3167	0.3408	0.3603	0.3743	0.4412	0.9075

Table A.67

A ~ 190, restricted configuration								
Spin I ($\hbar$)	$B(E2, I \to I-2)_{in}$ (e^2b^2), yrast band							
	$\gamma = 17^0$	$\gamma = 20^0$	$\gamma = 24^0$	$\gamma = 27^0$	$\gamma = 30^0$	$\gamma = 33^0$	$\gamma = 36^0$	$\gamma = 40^0$
9	0.0468	0.0161	...	0.0063	...	0.0529	...	0.1418
10	0.1089	0.0513	0.0046	0.0029	0.0273	0.0678	0.1157	0.1832
11	0.1807	0.1020	0.0191	0.0004	0.0295	0.0847	0.1448	0.2220
12	0.2556	0.1626	0.0453	0.0005	0.0315	0.1050	0.1758	0.2583
13	0.3313	0.2289	0.0816	0.0088	0.0351	0.1323	0.2098	0.2927
14	0.4085	0.2962	0.1231	0.0672	0.0580	0.1641	0.2473	0.3261
15	0.4885	0.3222	0.2082	0.3920	0.0697	0.1985	0.2929	0.3599
16	0.5609	0.5084	0.4040	0.4883	0.0596	0.3611	0.3458	0.3950
17	0.5846	0.5770	0.6017	0.6498	0.5615	0.2893	0.4126	0.4337
18	0.6355	0.6314	0.7124	0.7014	0.6829	0.3479	0.5340	0.4765
19	0.7716	0.7331	0.7819	0.7634	0.7344	0.7128	0.3599	0.5274
20	0.8575	0.7993	0.8355	0.8170	0.7888	0.7463	0.6190	0.5844
21	0.9004	0.8510	0.8802	0.8623	0.8354	0.7942	0.7157	0.6441
22	0.9331	0.8934	0.9186	0.9013	0.8753	0.8369	0.7454	0.7061
	$B(E2, I \to I-2)_{in}$ (e^2b^2), side band							
9	0.0460	0.0166	...	...	...	...	...	...
10	0.1058	0.0611	0.0076	0.0029	0.0363	0.0958	0.1667	0.2618
11	0.1995	0.1543	0.0459	0.0001	0.0373	0.1214	0.2099	0.3134
12	0.2960	0.2521	0.1008	0.0037	0.0440	0.1557	0.2561	0.3607
13	0.3863	0.3463	0.1498	0.0166	0.0504	0.1928	0.3017	0.4039
14	0.4682	0.4319	0.2252	0.0951	0.0758	0.2339	0.3501	0.4447
15	0.5384	0.4649	0.2659	0.4656	0.0855	0.2738	0.4020	0.4832
16	0.5762	0.6293	0.4367	0.4973	0.0622	0.4361	0.4518	0.5206
17	0.5445	0.6930	0.6051	0.6297	0.5679	0.3131	0.5033	0.5576
18	0.5512	0.6991	0.6997	0.6870	0.6769	0.3624	0.5939	0.5935
19	0.6608	0.7895	0.7636	0.7511	0.7272	0.7124	0.3794	0.6309
20	0.7514	0.8446	0.8163	0.8052	0.7821	0.7508	0.6272	0.6658
21	0.8113	0.8896	0.8615	0.8509	0.8288	0.7976	0.7163	0.7017
22	0.8598	0.9278	0.9006	0.8903	0.8689	0.8404	0.7434	0.7410

Table A.68

A ~ 190, restricted configuration								
Spin I ($\hbar$)	$B(E2, I \to I-2)_{out}$ (e^2b^2), **yrast → side band**							
	$\gamma = 17^0$	$\gamma = 20^0$	$\gamma = 24^0$	$\gamma = 27^0$	$\gamma = 30^0$	$\gamma = 33^0$	$\gamma = 36^0$	$\gamma = 40^0$
11	0.0036	0.0185	0.0589	0.0766	0.0642	0.0401	···	···
12	0.0026	0.0206	0.0927	0.1382	0.1111	0.0581	0.0265	···
13	0.0016	0.0249	0.1498	0.2372	0.1930	0.0854	0.0000	0.0097
14	0.0002	0.0330	0.2252	0.2838	0.2831	0.1287	0.0000	0.0109
15	0.0015	0.0869	0.2500	0.0109	0.3795	0.1787	0.0535	0.0124
16	0.0250	0.0016	0.1536	0.0606	0.4871	0.0906	0.0653	0.0142
17	0.1052	0.0126	0.0514	0.0003	0.0522	0.2831	0.0734	0.0158
18	0.1296	0.0424	0.0201	0.0200	0.0100	0.2976	0.0359	0.0178
19	0.0466	0.0145	0.0133	0.0170	0.0204	0.0034	0.3027	0.0177
20	0.0046	0.0087	0.0109	0.0137	0.0169	0.0202	0.1022	0.0183
21	0.0000	0.0060	0.0092	0.0113	0.0138	0.0176	0.0552	0.0174
22	0.0013	0.0046	0.0077	0.0094	0.0115	0.0135	0.0673	0.0106
	$B(E2, I \to I-2)_{out}$ (e^2b^2), **side → yrast band**							
9	0.1513	0.1995	···	···	···	···	···	0.1255
10	0.1287	0.1805	0.2284	0.2335	0.2130	0.1786	0.1413	0.0964
11	0.0980	0.1452	0.2106	0.2300	0.2058	0.1605	0.1179	0.0753
12	0.0716	0.1135	0.1914	0.2308	0.2057	0.1468	0.0996	0.0599
13	0.0497	0.0899	0.1831	0.2401	0.2166	0.1369	0.0000	0.0485
14	0.0296	0.0767	0.1972	0.2325	0.2311	0.1358	0.0000	0.0401
15	0.0095	0.1144	0.2037	0.0123	0.3006	0.1544	0.0681	0.0337
16	0.0014	0.0004	0.1303	0.0503	0.4352	0.0817	0.0662	0.0291
17	0.0498	0.0075	0.0449	0.0004	0.0491	0.2615	0.0697	0.0254
18	0.0843	0.0598	0.0175	0.0184	0.0097	0.2964	0.0355	0.0232
19	0.0334	0.0214	0.0114	0.0154	0.0194	0.0035	0.2904	0.0205
20	0.0037	0.0128	0.0091	0.0123	0.0159	0.0207	0.0981	0.0195
21	0.0000	0.0089	0.0075	0.0100	0.0129	0.0182	0.0543	0.0180
22	0.0006	0.0068	0.0062	0.0083	0.0107	0.0140	0.0662	0.0110

Table A.69-72: *Calculated relative intra- and inter-band $B(M1)$ and $B(E2)$ reduced transition probabilities for the partner bands in A ~ 100, 130 and 190 mass regions at ε_2 = 0.15 and γ = 20^0, 30^0,36^0.*

Table A.69

Spin I ($\hbar$)	**Non-restricted configuration**					
	$\Delta B(M1)_{in} = B(M1)_{yrast} - B(M1)_{side}$ (μ_N^2)					
	A ~ 100		**A ~ 130**		**A ~ 190**	
	$\gamma = 20^0$	$\gamma = 30^0$	$\gamma = 20^0$	$\gamma = 30^0$	$\gamma = 36^0$	$\gamma = 30^0$
9	0.0395	-0.2092	-0.0598	-0.0194	-0.0114	0.0190
10	-0.0487	-0.3570	0.0503	-0.3429	-0.0595	-0.1712
11	-0.0515	-0.2719	0.0026	-0.4845	-0.1836	-0.2681
12	-0.0667	-0.0687	-0.1153	-0.2113	-0.0544	-0.1306
13	0.0257	0.1400	-0.0589	0.0541	-0.0137	-0.0432
14	0.1214	0.0629	0.0591	0.1721	-0.0030	0.1082
15	0.0960	0.0305	0.1382	0.0853	0.1107	0.0078
16	0.3642	0.3467	0.1461	0.1268	0.0007	0.1126
17	0.4458	-0.0034	0.2737	0.3158	0.2862	0.1943
18	0.6347	0.5631	0.1093	0.0491	-0.0007	0.0516
19	0.1014	-0.0290	0.4988	0.5611	0.5166	0.4291

Table A.69 continues

Spin I ($\hbar$)	Non-restricted configuration					
	$\Delta B(M1)_{in} = B(M1)_{yrast} - B(M1)_{side}$ (μ_N^2)					
	A ~ 100		A ~ 130		A ~ 190	
	$\gamma = 20^0$	$\gamma = 30^0$	$\gamma = 20^0$	$\gamma = 30^0$	$\gamma = 36^0$	$\gamma = 30^0$
20	0.7612	0.6787	0.0784	0.0038	-0.0032	0.0171
21	0.2073	-0.0484	0.6849	0.7255	0.6077	0.5713
22	0.7339	0.7398	0.0988	-0.0156	-0.0066	-0.0044
	Restricted configuration					
9	0.2002	0.1062	0.2868	0.1498	0.1183	0.0995
10	0.1845	0.0811	0.2756	0.1199	0.1063	0.0664
11	0.1699	0.0474	0.2610	0.0920	0.1037	0.0490
12	0.1552	-0.0164	0.2448	0.0528	0.0991	0.0396
13	0.1388	-0.0725	0.2258	-0.0223	0.0886	0.0003
14	0.1188	-0.0420	0.2019	-0.0906	0.0793	-0.0536
15	0.0944	-0.0074	0.1700	-0.0578	0.0516	-0.0439
16	0.0681	-0.0010	0.1304	-0.0165	0.0248	-0.0137
17	0.0453	-0.0009	0.0896	-0.0036	0.0113	0.0000
18	0.0266	-0.0002	0.0570	-0.0012	0.0015	-0.0009
19	0.0083	0.0007	0.0338	-0.0006	-0.0009	-0.0013
20	-0.0011	-0.0002	0.0254	0.0003	0.0000	-0.0013
21	-0.0053	-0.0005	0.0092	-0.0009	0.0008	-0.0012
22	-0.0060	-0.0004	0.0092	-0.0002	0.0003	-0.0012

Table A.70

Spin I ($\hbar$)	Non-restricted configuration					
	$\Delta B(M1)_{out} = B(M1)_{side \to yrast} - B(M1)_{yrast \to side}$ (μ_N^2)					
	A ~ 100		A ~ 130		A ~ 190	
	$\gamma = 20^0$	$\gamma = 30^0$	$\gamma = 20^0$	$\gamma = 30^0$	$\gamma = 36^0$	$\gamma = 30^0$
11	...	0.0017	...	...	...	...
12	...	-0.0314	...	-0.1030	-0.1082	-0.0457
13	-0.2301	-0.0055	-0.2351	-0.0423	-0.0309	-0.0067
14	-0.1018	-0.0014	-0.2412	-0.0112	-0.2325	0.0011
15	-0.2855	-0.3991	-0.1779	-0.1125	-0.0180	-0.0019
16	-0.0685	-0.0051	-0.3033	-0.3985	-0.3655	-0.2107
17	...	-0.5735	...	-0.1059	-0.0246	0.0118
18	...	-0.0086	...	-0.6263	-0.5201	-0.3830
19	...	-0.7219	...	-0.1012	-0.0383	0.0068
20	...	-0.0136	...	-0.8238	-0.6425	-0.5205
21	...	...	...	-0.1013	-0.0473	0.0010
22	...	-0.0189	...	...	-0.7261	-0.6295
	Restricted configuration					
11	...	0.0044	...	...	...	...
12	...	0.0017	...	0.0029	...	0.0429
13	0.0316	-0.0005	0.0435	0.0012	0.0771	0.0208
14	0.0177	-0.0013	0.0278	-0.0004	0.0451	-0.0016
15	0.0018	-0.0031	0.0062	-0.0004	0.0077	-0.0105
16	-0.0111	0.0003	-0.0162	-0.0002	-0.0245	0.0033
17	-0.0147	-0.0019	-0.0301	0.0003	-0.0265	0.0041
18	-0.0057	0.0002	-0.0296	-0.0001	-0.0174	0.0046
19	0.0116	0.0001	-0.0166	-0.0007	-0.0038	0.0041
20	0.0087	-0.0003	-0.0032	-0.0002	-0.0003	0.0035
21	0.0015	0.0000	-0.0093	0.0000	0.0015	0.0029
22	-0.0024	-0.0008	-0.0012	-0.0005	0.0016	0.0024

Table A.71

Spin I ($\hbar$)	Non-restricted configuration					
	$\Delta B(E2)_{in} = B(E2)_{yrast} - B(E2)_{side}$ (e^2b^2)					
	A ~ 100		A ~ 130		A ~ 190	
	$\gamma = 20^0$	$\gamma = 30^0$	$\gamma = 20^0$	$\gamma = 30^0$	$\gamma = 36^0$	$\gamma = 30^0$
10	0.0149	0.0005	0.0241	0.0014	0.0388	0.0000
11	0.0200	-0.0002	0.0381	-0.0001	0.0658	0.0023
12	0.0157	0.0001	0.0542	0.0036	0.0860	0.0553
13	0.0249	0.0008	0.0554	0.0065	-0.0734	0.0073
14	0.0176	0.0018	0.0664	0.0061	0.1161	0.0511
15	0.0330	0.0211	0.0620	0.0152	-0.0910	0.0072
16	0.0167	0.0081	0.0742	0.0355	0.2596	0.1489
17	0.0226	0.0176	0.0463	0.0143	0.0543	0.0371
18	0.0135	0.0073	0.0490	0.0305	0.1527	0.1181
19	0.0091	0.0128	0.0184	0.0065	0.0516	0.0323
20	0.0320	0.0062	0.0224	0.0203	0.0821	0.0751
21	0.0041	0.0098	0.0101	0.0016	0.0377	0.0271
22	0.0100	0.0059	0.0141	0.0145	0.0585	0.0542
	Restricted configuration					
10	-0.0100	-0.0003	-0.0201	0.0001	-0.0510	-0.0090
11	-0.0118	-0.0003	-0.0269	0.0001	-0.0651	-0.0078
12	-0.0133	-0.0004	-0.0323	0.0002	-0.0803	-0.0125
13	-0.0143	-0.0005	-0.0366	0.0001	-0.0919	-0.0153
14	-0.0149	-0.0008	-0.0395	0.0000	-0.1028	-0.0178
15	-0.0150	-0.0020	-0.0410	0.0000	-0.1091	-0.0158
16	-0.0143	-0.0004	-0.0409	-0.0005	-0.1060	-0.0026
17	-0.0123	0.0001	-0.0383	0.0000	-0.0907	-0.0064
18	-0.0080	0.0001	-0.0324	-0.0001	-0.0599	0.0060
19	-0.0016	0.0002	-0.0222	0.0001	-0.0195	0.0072
20	0.0014	0.0000	-0.0150	0.0001	-0.0082	0.0067
21	0.0028	0.0002	-0.0083	0.0002	-0.0006	0.0066
22	0.0024	0.0001	-0.0069	0.0003	0.0020	0.0064

Table A.72

Spin I ($\hbar$)	Non-restricted configuration					
	$\Delta B(E2)_{out} = B(E2)_{side \to yrast} - B(E2)_{yrast \to side}$ (e^2b^2)					
	A ~ 100		A ~ 130		A ~ 190	
	$\gamma = 20^0$	$\gamma = 30^0$	$\gamma = 20^0$	$\gamma = 30^0$	$\gamma = 36^0$	$\gamma = 30^0$
11	...	0.0213	...	...	...	...
12	0.0039	-0.0040	0.0219	0.0417	0.1009	0.1155
13	-0.0032	-0.0304	0.0021	-0.0222	0.0886	-0.0665
14	-0.0018	-0.0150	-0.0093	-0.0579	-0.0880	-0.1672
15	-0.0010	-0.0001	-0.0057	-0.0161	-0.0072	-0.0417
16	0.0001	-0.0003	-0.0030	0.0000	0.0021	0.0000
17	-0.0006	0.0001	0.0009	-0.0002	0.0010	-0.0060
18	0.0001	-0.0002	-0.0040	0.0001	0.0000	0.0001
19	-0.0005	0.0002	-0.0004	-0.0001	0.0013	-0.0027
20	-0.0006	-0.0001	-0.0005	0.0001	-0.0001	-0.0003
21	-0.0004	0.0001	-0.0022	-0.0001	0.0009	-0.0012
22	-0.0028	-0.0001	-0.0006	-0.0001	-0.0001	-0.0005
	Restricted configuration					
10	...	0.0208	...	...	...	...
11	0.0080	0.0135	...	0.0535	...	0.1416
12	0.0058	0.0019	0.0241	0.0346	0.0731	0.0946
13	0.0042	-0.0095	0.0177	0.0045	0.0000	0.0236
14	0.0029	-0.0104	0.0126	-0.0252	0.0000	-0.0520

Table A.72 continues

Spin I ($\hbar$)	Restricted configuration					
	$\Delta B(E2)_{out} = B(E2)_{side\to yrast} - B(E2)_{yrast\to side}$ (e^2b^2)					
	A ~ 100		A ~ 130		A ~ 190	
	$\gamma = 20^0$	$\gamma = 30^0$	$\gamma = 20^0$	$\gamma = 30^0$	$\gamma = 36^0$	$\gamma = 30^0$
15	0.0018	-0.0032	0.0085	-0.0297	0.0146	-0.0789
16	0.0011	-0.0010	0.0053	-0.0141	0.0009	-0.0519
17	0.0004	-0.0002	0.0031	-0.0041	-0.0037	-0.0031
18	-0.0012	0.0000	0.0018	-0.0005	-0.0004	-0.0003
19	-0.0040	0.0000	-0.0005	0.0000	-0.0123	-0.0010
20	-0.0026	-0.0001	0.0005	0.0000	-0.0041	-0.0010
21	-0.0003	0.0000	0.0023	0.0000	-0.0009	-0.0009
22	0.0000	-0.0001	-0.0001	0.0000	-0.0011	-0.0008

Table A.73: *Calculated relative excitation energy (ΔE) for the partner bands in A ~ 130 mass region at $\varepsilon_2 = 0.25$ and $\gamma = 20^0, 30^0$.*

A ~ 130				
Spin I ($\hbar$)	$\Delta E = E_{side} - E_{yrast}$ (keV)			
	Non-restricted configuration		Restricted configuration	
	$\gamma = 20^0$	$\gamma = 30^0$	$\gamma = 20^0$	$\gamma = 30^0$
8	853.000	668.000	566.000	410.000
9	877.000	598.000	524.000	348.000
10	826.000	452.000	479.000	280.000
11	700.000	272.000	427.000	205.000
12	588.000	125.000	368.000	127.000
13	544.000	164.000	303.000	58.000
14	603.000	263.000	233.000	18.000
15	715.000	312.000	163.000	3.000
16	869.000	443.000	101.000	1.000
17	997.000	505.000	51.000	3.000
18	1124.000	619.000	18.000	2.000
19	1248.000	703.000	22.000	3.000
20	1314.000	772.000	38.000	4.000
21	1473.000	898.000	51.000	5.000
22	1461.000	902.000	62.000	5.000

Table A.74: *Calculated energy staggering parameter $S(I)$ for the partner bands in A ~ 130 mass region at $\varepsilon_2 = 0.25$ and $\gamma = 20^0, 30^0$.*

A ~ 130								
Spin I ($\hbar$)	$S(I) = [E(I) - E(I-1)]/2I$ ($keV/\hbar$)							
	Non-restricted configuration				Restricted configuration			
	Yrast band		Side band		Yrast band		Side band	
	$\gamma = 20^0$	$\gamma = 30^0$	$\gamma = 20^0$	$\gamma = 30^0$	$\gamma = 20^0$	$\gamma = 30^0$	$\gamma = 20^0$	$\gamma = 30^0$
9	6.667	6.611	8.000	2.722	7.500	6.056	5.167	2.611
10	13.300	13.150	10.750	5.850	11.150	10.050	8.900	6.650
11	18.364	18.591	12.636	10.409	13.727	13.091	11.364	9.682
12	21.542	22.167	16.875	16.042	15.625	15.125	13.167	11.875

Table A.74 continues

A ~ 130								
Spin I ($\hbar$)	$S(I) = [E(I) - E(I-1)]/2I$ ($keV/\hbar$)							
	Non-restricted configuration				Restricted configuration			
	Yrast band		Side band		Yrast band		Side band	
	$\gamma = 20^0$	$\gamma = 30^0$	$\gamma = 20^0$	$\gamma = 30^0$	$\gamma = 20^0$	$\gamma = 30^0$	$\gamma = 20^0$	$\gamma = 30^0$
13	23.154	21.346	21.462	22.846	16.923	15.923	14.423	13.269
14	23.214	20.143	25.321	23.679	17.786	15.393	15.286	13.964
15	23.600	20.567	27.333	22.200	18.200	14.633	15.867	14.133
16	23.563	19.438	28.375	23.531	18.219	14.156	16.281	14.094
17	24.235	20.618	28.000	22.441	17.971	13.912	16.500	13.971
18	24.389	19.972	27.917	23.139	17.556	13.806	16.639	13.778
19	24.842	20.868	28.105	23.079	16.868	13.684	16.974	13.711
20	25.350	20.675	27.000	22.400	16.575	13.600	16.975	13.625
21	25.167	21.119	28.952	24.119	16.476	13.524	16.786	13.548
22	26.386	21.432	26.114	21.523	16.432	13.477	16.682	13.477

Table A.75-76: *Calculate intra- and inter-band $B(M1)$ and $B(E2)$ reduced transition probabilities for the partner bands in A ~ 130 mass region at ε_2 = 0.25 and γ = 20^0, 30^0.*

Table A.75

A ~ 130								
Spin I ($\hbar$)	$B(M1, I \to I-1)_{in}$ (μ_N^2)							
	Non-restricted configuration				Restricted configuration			
	Yrast band		Side band		Yrast band		Side band	
	$\gamma = 20^0$	$\gamma = 30^0$	$\gamma = 20^0$	$\gamma = 30^0$	$\gamma = 20^0$	$\gamma = 30^0$	$\gamma = 20^0$	$\gamma = 30^0$
9	2.1881	2.2508	2.0352	2.2134	2.0733	2.3006	1.8035	2.1577
10	1.8148	1.9520	1.6098	2.1905	2.0253	2.3252	1.7614	2.2106
11	1.5220	1.7009	1.6195	2.0395	1.9671	2.3374	1.7152	2.2513
12	1.2968	1.4258	1.4580	1.5887	1.9015	2.3213	1.6684	2.2789
13	1.1319	1.2369	1.1981	1.2114	1.8281	2.2530	1.6103	2.2917
14	1.0441	1.2092	1.0058	1.0750	1.7442	2.2018	1.5509	2.2906
15	1.0256	1.0422	0.9179	0.9271	1.6448	2.2687	1.4838	2.3140
16	0.9773	0.9518	0.8363	0.7875	1.5211	1.9999	1.3985	2.0112
17	0.9687	1.0151	0.8025	0.8281	1.3307	1.7104	1.2456	1.7141
18	0.8810	0.8433	0.7564	0.7178	0.6954	1.2244	0.6514	1.2250
19	0.9009	0.9614	0.7017	0.7161	0.0797	0.9491	0.0761	0.9502
20	0.7801	0.7474	0.7096	0.6733	0.8931	1.2612	0.9066	1.2621
21	0.8443	0.9103	0.5981	0.6067	1.0959	0.8541	1.1117	0.8549
22	0.6855	0.6618	0.6671	0.6348	1.1212	1.2616	1.1355	1.2629
	$B(M1, I \to I-1)_{out}$ (μ_N^2)							
	Yrast → side band		Side → yrast band		Yrast → side band		Side → yrast band	
9	...	...	0.0250	0.0025	...	...	0.1792	0.0102
10	...	...	0.0410	0.0013	...	...	0.2156	0.0098
11	...	...	0.0543	0.0002	...	0.0035	0.2484	0.0097
12	...	0.1441	0.0844	0.0806	...	0.0061	0.2822	0.0103
13	0.3111	0.1847	0.1185	0.1217	0.2775	0.0113	0.3224	0.0127
14	0.3138	0.1038	0.1260	0.1134	0.3478	0.0208	0.3757	0.0200
15	0.2662	0.3498	0.0966	0.2277	0.4452	0.0064	0.4514	0.0061
16	0.2887	0.4731	0.0866	0.2485	0.5789	0.3261	0.5656	0.3244
17	...	0.3414	0.0657	0.1515	0.7878	0.6405	0.7679	0.6413
18	...	0.5590	0.0765	0.2120	1.4324	1.1448	1.4347	1.1448
19	...	0.3433	0.0546	0.1087	2.0459	1.4326	2.0898	1.4332

Table A.75 continues

A ~ 130								
Spin I ($\hbar$)	$B(M1, I \to I-1)_{out}$ (μ_N^2)							
	Non-restricted configuration				Restricted configuration			
	Yrast → side band		Side → yrast band		Yrast → side band		Side → yrast band	
	$\gamma = 20^0$	$\gamma = 30^0$	$\gamma = 20^0$	$\gamma = 30^0$	$\gamma = 20^0$	$\gamma = 30^0$	$\gamma = 20^0$	$\gamma = 30^0$
20	···	0.6303	0.0738	0.1857	1.2698	1.1319	1.2861	1.1316
21	···	0.3458	0.0465	0.0826	1.0984	1.5480	1.1003	1.5482
22	···	0.6932	0.0712	0.1669	1.0976	1.1489	1.0923	1.1478

Table A.76

A ~ 130								
Spin I ($\hbar$)	$B(E2, I \to I-2)_{in}$ (e^2b^2)							
	Non-restricted configuration				Restricted configuration			
	Yrast band		Side band		Yrast band		Side band	
	$\gamma = 20^0$	$\gamma = 30^0$	$\gamma = 20^0$	$\gamma = 30^0$	$\gamma = 20^0$	$\gamma = 30^0$	$\gamma = 20^0$	$\gamma = 30^0$
10	0.1916	0.0155	0.0852	0.0034	0.1834	0.0079	0.2287	0.0050
11	0.2723	0.0132	0.1065	0.0093	0.2458	0.0075	0.3095	0.0049
12	0.3724	0.0000	0.1935	0.0105	0.3068	0.0067	0.3860	0.0044
13	0.4712	0.0180	0.2821	0.0035	0.3660	0.0052	0.4570	0.0038
14	0.5563	0.0440	0.3451	0.0340	0.4239	0.0041	0.5232	0.0039
15	0.6398	0.4362	0.4231	0.3689	0.4818	0.0007	0.5858	0.0007
16	0.7223	0.6265	0.5043	0.5419	0.5431	0.1065	0.6468	0.1132
17	0.7831	0.7037	0.6026	0.6242	0.6148	0.0000	0.7089	0.0000
18	0.8368	0.7706	0.6857	0.6894	0.6545	0.5652	0.7110	0.5645
19	0.8766	0.8125	0.7772	0.7537	0.3124	0.7318	0.3077	0.7308
20	0.9171	0.8564	0.8374	0.7961	0.4657	0.7734	0.4440	0.7721
21	0.9461	0.8840	0.8943	0.8429	0.8820	0.8181	0.8501	0.8168
22	0.9773	0.9162	0.9276	0.8706	0.9243	0.8510	0.9014	0.8494
	$B(E2, I \to I-2)_{out}$ (e^2b^2)							
	Yrast → side band		Side → yrast band		Yrast → side band		Side → yrast band	
10	···	···	0.1604	0.2407	···	···	0.1231	0.2359
11	···	0.0653	0.1014	0.2394	0.0083	0.0821	0.0949	0.2293
12	0.0014	0.1408	0.0427	0.2514	0.0094	0.1439	0.0737	0.2307
13	0.0137	0.3143	0.0055	0.2392	0.0109	0.2516	0.0577	0.2468
14	0.0292	0.4305	0.0012	0.2687	0.0124	0.3748	0.0453	0.2934
15	0.0210	0.1057	0.0029	0.0619	0.0130	0.4729	0.0349	0.3942
16	0.0074	0.0090	0.0009	0.0068	0.0108	0.4384	0.0239	0.4115
17	0.0006	0.0094	0.0002	0.0081	0.0027	0.6235	0.0083	0.6140
18	0.0001	0.0040	0.0004	0.0033	0.0494	0.1210	0.0325	0.1198
19	0.0002	0.0042	0.0015	0.0037	0.4955	0.0085	0.4433	0.0084
20	0.0000	0.0016	0.0006	0.0016	0.3879	0.0128	0.3639	0.0126
21	0.0002	0.0018	0.0016	0.0019	0.0093	0.0070	0.0093	0.0069
22	0.0001	0.0004	0.0004	0.0007	0.0005	0.0078	0.0004	0.0077

Table A.77: *Calculated relative excitation energy (ΔE) for the partner bands in A ~ 130 mass region at ε_2 = 0.15, ξ = 0.8 and γ = 20^0, 30^0.*

A ~ 130				
Spin I ($\hbar$)	$\Delta E = E_{side} - E_{yrast}$ (keV)			
	Non-restricted configuration		Restricted configuration	
	$\gamma = 20^0$	$\gamma = 30^0$	$\gamma = 20^0$	$\gamma = 30^0$
8	959.000	766.000	581.000	424.000
9	904.000	671.000	541.000	363.000
10	845.000	521.000	499.000	295.000
11	737.000	337.000	450.000	221.000
12	600.000	175.000	393.000	142.000
13	507.000	151.000	331.000	70.000
14	522.000	221.000	262.000	23.000
15	588.000	215.000	192.000	5.000
16	743.000	396.000	127.000	1.000
17	829.000	384.000	74.000	1.000
18	969.000	553.000	35.000	1.000
19	1064.000	579.000	10.000	1.000
20	1124.000	665.000	-10.000	2.000
21	1257.000	786.000	-20.000	2.000
22	1226.000	742.000	-28.000	2.000

Table A.78: *Calculated energy staggering parameter $S(I)$ for the partner bands in A ~ 130 mass region at ε_2 = 0.15, ξ = 0.8 and γ = 20^0, 30^0.*

A ~ 130								
Spin I ($\hbar$)	$S(I) = [E(I) - E(I-1)]/2I$ ($keV/\hbar$)							
	Non-restricted configuration				Restricted configuration			
	Yrast band		Side band		Yrast band		Side band	
	$\gamma = 20^0$	$\gamma = 30^0$	$\gamma = 20^0$	$\gamma = 30^0$	$\gamma = 20^0$	$\gamma = 30^0$	$\gamma = 20^0$	$\gamma = 30^0$
9	8.556	7.278	5.500	2.000	6.722	5.389	4.500	2.000
10	15.850	14.600	12.900	7.100	10.500	9.500	8.400	6.100
11	21.455	20.727	16.545	12.364	13.182	12.636	10.955	9.273
12	24.917	24.708	19.208	17.958	15.167	14.833	12.792	11.542
13	26.923	24.923	23.346	24.000	16.538	15.846	14.154	13.077
14	26.536	22.643	27.071	25.143	17.536	15.536	15.071	13.857
15	26.733	23.200	28.933	23.000	18.067	14.733	15.733	14.133
16	25.688	20.438	30.531	26.094	18.219	14.188	16.188	14.063
17	26.647	22.853	29.176	22.500	18.000	13.971	16.441	13.971
18	26.111	20.722	30.000	25.417	17.667	13.806	16.583	13.806
19	26.711	22.579	29.211	23.263	17.289	13.711	16.632	13.711
20	27.025	21.600	28.525	23.750	17.050	13.600	16.550	13.625
21	26.405	22.119	29.571	25.000	16.786	13.548	16.548	13.548
22	28.364	22.795	27.659	21.795	16.659	13.477	16.477	13.477

Table A.79-80: *Calculated intra- and inter-band $B(M1)$ and $B(E2)$ reduced transition probabilities for the partner bands in A ~ 130 mass region at ε_2 = 0.15, ξ = 0.8 and γ = 20^0, 30^0.*

Table A.79

A ~ 130								
Spin I ($\hbar$)	$B(M1, I \to I-1)_{in}$ (μ_N^2)							
	Non-restricted configuration				Restricted configuration			
	Yrast band		Side band		Yrast band		Side band	
	$\gamma = 20^0$	$\gamma = 30^0$	$\gamma = 20^0$	$\gamma = 30^0$	$\gamma = 20^0$	$\gamma = 30^0$	$\gamma = 20^0$	$\gamma = 30^0$
9	2.2964	2.3614	2.1182	2.3996	2.1665	2.3624	1.8798	2.2136
10	1.9544	2.0870	1.5123	2.3007	2.1232	2.3882	1.8477	2.2683
11	1.6614	1.8551	1.2250	2.1143	2.0692	2.4029	1.8082	2.3109
12	1.4258	1.6451	1.5240	1.7611	2.0076	2.3934	1.7629	2.3406
13	1.2083	1.4668	1.3613	1.4443	1.9391	2.3335	1.7133	2.3558
14	1.0405	1.2810	1.1479	1.1888	1.8619	2.2684	1.6601	2.3590
15	1.0049	1.0123	1.0687	0.9827	1.7736	2.3106	1.6037	2.3684
16	0.9449	0.8497	0.9202	0.6929	1.6733	2.3393	1.5430	2.3558
17	0.9856	1.0584	0.8661	0.8516	1.5628	2.2144	1.4732	2.2180
18	0.8350	0.6399	0.7256	0.5491	1.4276	1.2593	1.3706	1.2605
19	0.9409	1.0351	0.5102	0.5305	1.0115	1.0985	0.9777	1.0991
20	0.6931	0.4918	0.5498	0.4601	2.2082	1.2684	2.1828	1.2681
21	0.8993	1.0048	0.1003	0.2311	1.0027	1.0314	0.9935	1.0323
22	0.5497	0.3752	0.2555	0.3673	1.2024	1.2576	1.1932	1.2578
	$B(M1, I \to I-1)_{out}$ (μ_N^2)							
	Yrast → side band		Side → yrast band		Yrast → side band		Side → yrast band	
9	...	...	0.0444	0.0005	...	...	0.1668	0.0065
10	...	...	0.0614	0.0001	...	...	0.2032	0.0062
11	...	...	0.0778	0.0060	...	...	0.2350	0.0061
12	...	0.0603	0.1139	0.0305	...	0.0035	0.2666	0.0064
13	0.2990	0.0468	0.1739	0.0323	0.2591	0.0064	0.3026	0.0076
14	0.3742	0.1385	0.2195	0.1246	0.3204	0.0107	0.3481	0.0103
15	0.3418	0.4448	0.1702	0.3043	0.4033	0.0080	0.4095	0.0076
16	0.4094	0.6717	0.1481	0.3638	0.5099	0.0342	0.4937	0.0340
17	0.3166	0.2940	0.0890	0.1418	0.6371	0.1886	0.6070	0.1889
18	0.5497	0.8775	0.1241	0.3590	0.7955	1.1617	0.7659	1.1616
19	0.2961	0.2202	0.0577	0.0757	1.2334	1.3362	1.2170	1.3355
20	0.7680	1.0390	0.1246	0.3418	0.0599	1.1772	0.0569	1.1770
21	...	0.1774	0.0262	0.0415	1.2877	1.4227	1.2784	1.4227
22	...	1.2016	0.1249	0.3159	1.1056	1.2049	1.1044	1.2044

Table A.80

A ~ 130								
Spin I ($\hbar$)	$B(E2, I \to I-2)_{in}$ (e^2b^2)							
	Non-restricted configuration				Restricted configuration			
	Yrast band		Side band		Yrast band		Side band	
	$\gamma = 20^0$	$\gamma = 30^0$	$\gamma = 20^0$	$\gamma = 30^0$	$\gamma = 20^0$	$\gamma = 30^0$	$\gamma = 20^0$	$\gamma = 30^0$
10	0.0492	0.0008	0.0228	0.0002	0.0485	0.0004	0.0686	0.0003
11	0.0730	0.0004	0.0264	0.0004	0.0673	0.0004	0.0942	0.0003
12	0.1031	0.0003	0.0463	0.0002	0.0861	0.0004	0.1184	0.0002
13	0.1351	0.0020	0.0992	0.0011	0.1046	0.0003	0.1412	0.0002
14	0.1631	0.0136	0.1232	0.0115	0.1230	0.0002	0.1625	0.0002
15	0.1890	0.1222	0.1449	0.1221	0.1417	0.0000	0.1827	0.0000
16	0.2216	0.2063	0.1652	0.1850	0.1613	0.0064	0.2022	0.0069
17	0.2449	0.2258	0.2021	0.2163	0.1830	0.0001	0.2213	0.0001

Table A.80 continues

A ~ 130								
Spin I ($\hbar$)	$B(E2, I \to I-2)_{in}$ (e^2b^2)							
	Non-restricted configuration				**Restricted configuration**			
	Yrast band		**Side band**		**Yrast band**		**Side band**	
	$\gamma = 20^0$	$\gamma = 30^0$	$\gamma = 20^0$	$\gamma = 30^0$	$\gamma = 20^0$	$\gamma = 30^0$	$\gamma = 20^0$	$\gamma = 30^0$
18	0.2665	0.2571	0.2188	0.2313	0.2086	0.1421	0.2409	0.1422
19	0.2788	0.2674	0.2554	0.2630	0.2379	0.2501	0.2601	0.2500
20	0.2949	0.2871	0.2666	0.2679	0.2023	0.2660	0.2172	0.2659
21	0.3030	0.2939	0.2569	0.2918	0.2112	0.2818	0.2195	0.2816
22	0.3154	0.3076	0.2983	0.2961	0.2943	0.2941	0.3012	0.2938
	$B(E2, I \to I-2)_{out}$ (e^2b^2)							
	Yrast → side band		**Side → yrast band**		**Yrast → side band**		**Side → yrast band**	
10	...	...	0.0511	0.0853	...	...	0.0464	0.0824
11	...	0.0250	0.0407	0.0827	...	0.0263	0.0362	0.0798
12	0.0004	0.0480	0.0199	0.0806	0.0044	0.0453	0.0285	0.0799
13	0.0011	0.1008	0.0046	0.0828	0.0051	0.0799	0.0228	0.0844
14	0.0088	0.1387	0.0001	0.0930	0.0059	0.1236	0.0185	0.0984
15	0.0105	0.0450	0.0010	0.0349	0.0067	0.1591	0.0152	0.1294
16	0.0058	0.0015	0.0006	0.0019	0.0072	0.1802	0.0125	0.1661
17	0.0005	0.0066	0.0002	0.0068	0.0067	0.2126	0.0098	0.2085
18	0.0003	0.0007	0.0001	0.0009	0.0043	0.0931	0.0060	0.0926
19	0.0003	0.0027	0.0016	0.0026	0.0009	0.0048	0.0003	0.0048
20	0.0001	0.0001	0.0001	0.0004	0.0582	0.0055	0.0587	0.0055
21	0.0011	0.0015	0.0030	0.0013	0.0682	0.0039	0.0705	0.0039
22	0.0003	0.0000	0.0000	0.0001	0.0010	0.0039	0.0009	0.0039

Table A.81: *Calculated relative excitation energy (ΔE) for the partner bands in A ~ 130 mass region at ε_2 = 0.15 and γ =17^0, 20^0, 24^0, 27^0, 30^0, 33^0, 36^0, 40^0 with a change in the Fermi surface of either one of the odd particles or both of them.*

A ~ 130, restricted configuration								
Spin I ($\hbar$)	**Fermi surface of the proton**							
	$\Delta E = E_{side} - E_{yrast}$ (keV)							
	$\gamma = 17^0$	$\gamma = 20^0$	$\gamma = 24^0$	$\gamma = 27^0$	$\gamma = 30^0$	$\gamma = 33^0$	$\gamma = 36^0$	$\gamma = 40^0$
8	329.000	315.000	321.000	321.000	331.000	363.000	422.000	544.000
9	355.000	329.000	292.000	266.000	270.000	306.000	373.000	512.000
10	374.000	327.000	231.000	182.000	188.000	235.000	315.000	472.000
11	402.000	324.000	160.000	89.000	109.000	167.000	254.000	424.000
12	447.000	332.000	112.000	7.000	58.000	102.000	185.000	368.000
13	512.000	355.000	120.000	48.000	37.000	35.000	117.000	307.000
14	590.000	393.000	157.000	78.000	34.000	21.000	69.000	241.000
15	675.000	445.000	199.000	103.000	48.000	23.000	22.000	176.000
16	763.000	505.000	241.000	127.000	61.000	26.000	19.000	119.000
17	853.000	570.000	284.000	152.000	76.000	35.000	14.000	71.000
18	943.000	638.000	325.000	178.000	91.000	43.000	18.000	45.000
19	1035.000	708.000	368.000	205.000	106.000	51.000	22.000	17.000
20	1128.000	779.000	410.000	231.000	122.000	61.000	27.000	17.000
21	1222.000	849.000	453.000	258.000	138.000	70.000	32.000	5.000
22	1317.000	920.000	496.000	285.000	155.000	80.000	38.000	13.000
	Fermi surface of the neutron							
8	679.000	540.000	423.000	370.000	310.000	350.000	377.000	440.000
9	661.000	507.000	372.000	311.000	281.000	284.000	320.000	409.000

Table A.81 continues

A ~ 130, restricted configuration								
Spin I ($\hbar$)	**Fermi surface of the neutron**							
	$\Delta E = E_{side} - E_{yrast}$ **(keV)**							
	$\gamma = 17^0$	$\gamma = 20^0$	$\gamma = 24^0$	$\gamma = 27^0$	$\gamma = 30^0$	$\gamma = 33^0$	$\gamma = 36^0$	$\gamma = 40^0$
10	634.000	466.000	315.000	244.000	209.000	212.000	255.000	366.000
11	600.000	416.000	252.000	173.000	132.000	136.000	185.000	314.000
12	556.000	359.000	184.000	102.000	64.000	65.000	117.000	257.000
13	506.000	296.000	117.000	46.000	22.000	20.000	61.000	200.000
14	448.000	230.000	62.000	15.000	5.000	4.000	28.000	151.000
15	385.000	164.000	26.000	6.000	2.000	7.000	17.000	116.000
16	319.000	106.000	9.000	2.000	3.000	9.000	21.000	98.000
17	255.000	61.000	-4.000	3.000	5.000	11.000	25.000	93.000
18	195.000	31.000	-5.000	4.000	6.000	13.000	30.000	97.000
19	144.000	17.000	-7.000	3.000	7.000	16.000	36.000	104.000
20	106.000	18.000	-10.000	7.000	9.000	19.000	41.000	115.000
21	82.000	24.000	-9.000	4.000	8.000	20.000	45.000	126.000
22	74.000	30.000	-14.000	10.000	12.000	24.000	51.000	139.000
	Fermi surface of both the proton and neutron							
8	277.000	271.000	264.000	236.000	242.000	262.000	309.000	398.000
9	289.000	265.000	225.000	184.000	171.000	195.000	251.000	362.000
10	309.000	260.000	179.000	111.000	92.000	124.000	189.000	315.000
11	347.000	272.000	142.000	49.000	27.000	67.000	128.000	261.000
12	408.000	303.000	132.000	41.000	24.000	27.000	72.000	204.000
13	487.000	349.000	150.000	66.000	34.000	10.000	43.000	151.000
14	578.000	403.000	182.000	91.000	44.000	20.000	27.000	109.000
15	674.000	463.000	220.000	114.000	54.000	23.000	22.000	88.000
16	771.000	527.000	260.000	140.000	72.000	40.000	33.000	82.000
17	867.000	593.000	300.000	161.000	79.000	30.000	19.000	84.000
18	962.000	661.000	342.000	192.000	104.000	61.000	51.000	98.000
19	1057.000	731.000	382.000	212.000	106.000	40.000	15.000	100.000
20	1152.000	800.000	426.000	244.000	137.000	84.000	72.000	124.000
21	1245.000	869.000	465.000	263.000	135.000	53.000	12.000	120.000
22	1340.000	940.000	511.000	299.000	171.000	107.000	92.000	153.000

Table A.82-84: *Calculated energy staggering parameter $S(I)$ for the partner bands in A ~ 130 mass region at ε_2 = 0.15 and γ =17^0, 20^0, 24^0, 27^0, 30^0, 33^0, 36^0, 40^0 with a change in the Fermi surface of either one of the odd particles or both of them.*

Table A.82

A ~ 130, restricted configuration								
Spin I ($\hbar$)	**Fermi surface of the proton**							
	$S(I) = [E(I) - E(I-1)]/2I$ **($keV/\hbar$), yrast band**							
	$\gamma = 17^0$	$\gamma = 20^0$	$\gamma = 24^0$	$\gamma = 27^0$	$\gamma = 30^0$	$\gamma = 33^0$	$\gamma = 36^0$	$\gamma = 40^0$
9	14.167	13.111	11.667	10.556	9.667	9.222	9.111	9.222
10	15.950	15.500	14.800	14.000	13.150	12.550	12.250	12.150
11	16.773	16.591	16.455	16.136	15.273	14.727	14.500	14.273
12	17.042	16.750	16.583	16.792	15.875	16.000	16.042	15.875
13	17.000	16.462	15.538	14.308	15.154	16.308	16.808	17.000
14	16.929	16.143	14.857	14.179	14.429	15.179	16.714	17.750
15	16.833	15.867	14.600	14.000	13.900	14.600	16.467	18.133
16	16.781	15.719	14.500	13.875	13.750	14.344	15.531	18.125
17	16.706	15.647	14.382	13.765	13.588	14.088	15.353	17.882

Table A.82 continues

A ~ 130, restricted configuration								
Spin I ($\hbar$)	Fermi surface of the proton							
	$S(I)=[E(I)-E(I-1)]/2I$ ($keV/\hbar$), yrast band							
	$\gamma=17^0$	$\gamma=20^0$	$\gamma=24^0$	$\gamma=27^0$	$\gamma=30^0$	$\gamma=33^0$	$\gamma=36^0$	$\gamma=40^0$
18	16.694	15.611	14.333	13.667	13.500	14.000	15.083	17.444
19	16.684	15.553	14.263	13.579	13.421	13.921	14.947	17.263
20	16.675	15.525	14.225	13.550	13.350	13.800	14.825	16.750
21	16.643	15.524	14.190	13.476	13.286	13.762	14.762	16.786
22	16.659	15.500	14.159	13.455	13.227	13.682	14.682	16.455
	$S(I)=[E(I)-E(I-1)]/2I$ ($keV/\hbar$), side band							
9	15.611	13.889	10.056	7.500	6.278	6.056	6.389	7.444
10	16.900	15.400	11.750	9.800	9.050	9.000	9.350	10.150
11	18.045	16.455	13.227	11.909	11.682	11.636	11.727	12.091
12	18.917	17.083	14.583	13.375	13.750	13.292	13.167	13.542
13	19.500	17.346	15.846	15.885	14.346	13.731	14.192	14.654
14	19.714	17.500	16.179	15.250	14.321	14.679	15.000	15.393
15	19.667	17.600	16.000	14.833	14.367	14.667	14.900	15.967
16	19.531	17.594	15.813	14.625	14.156	14.438	15.438	16.344
17	19.353	17.559	15.647	14.500	14.029	14.353	15.206	16.471
18	19.194	17.500	15.472	14.389	13.917	14.222	15.194	16.722
19	19.105	17.395	15.395	14.289	13.816	14.132	15.053	16.526
20	19.000	17.300	15.275	14.200	13.750	14.050	14.950	16.750
21	18.881	17.190	15.214	14.119	13.667	13.976	14.881	16.500
22	18.818	17.114	15.136	14.068	13.614	13.909	14.818	16.636

Table A.83

A ~ 130, restricted configuration								
Spin I ($\hbar$)	Fermi surface of the neutron							
	$S(I)=[E(I)-E(I-1)]/2I$ ($keV/\hbar$), yrast band							
	$\gamma=17^0$	$\gamma=20^0$	$\gamma=24^0$	$\gamma=27^0$	$\gamma=30^0$	$\gamma=33^0$	$\gamma=36^0$	$\gamma=40^0$
9	9.722	9.333	9.000	8.889	9.056	9.500	10.111	11.056
10	12.450	12.250	12.200	12.300	12.550	13.050	13.600	14.200
11	14.409	14.455	14.500	14.636	14.955	15.409	15.864	16.273
12	15.958	16.000	16.042	16.000	16.000	16.458	17.000	17.542
13	17.077	17.115	16.808	16.154	15.654	16.038	17.077	18.192
14	18.000	17.857	16.821	15.500	14.786	15.179	16.464	18.286
15	18.633	18.167	16.333	14.800	14.267	14.533	15.800	18.000
16	19.031	18.156	15.750	14.500	14.000	14.344	15.313	17.531
17	19.235	17.853	15.471	14.235	13.824	14.206	15.147	17.147
18	19.250	17.472	15.139	14.111	13.750	14.083	15.000	16.833
19	19.105	17.079	15.026	14.053	13.632	13.974	14.895	16.658
20	18.825	16.750	14.950	13.900	13.550	13.900	14.800	16.525
21	18.548	16.548	14.810	13.905	13.524	13.857	14.762	16.429
22	18.227	16.477	14.818	13.750	13.409	13.750	14.659	16.341
	$S(I)=[E(I)-E(I-1)]/2I$ ($keV/\hbar$), side band							
9	8.722	7.500	6.167	5.611	7.444	5.833	6.944	9.333
10	11.100	10.200	9.350	8.950	8.950	9.450	10.350	12.050
11	12.864	12.182	11.636	11.409	11.455	11.955	12.682	13.909
12	14.125	13.625	13.208	13.042	13.167	13.500	14.167	15.167
13	15.154	14.692	14.231	14.000	14.038	14.308	14.923	16.000
14	15.929	15.500	14.857	14.393	14.179	14.607	15.286	16.536
15	16.533	15.967	15.133	14.500	14.167	14.633	15.433	16.833
16	16.969	16.344	15.219	14.375	14.031	14.406	15.438	16.969
17	17.353	16.529	15.088	14.265	13.882	14.265	15.265	17.000
18	17.583	16.639	15.111	14.139	13.778	14.139	15.139	16.944

Table A.83 continues

A ~ 130, restricted configuration								
Spin I ($\hbar$)	**Fermi surface of the neutron**							
	$S(I)=[E(I)-E(I-1)]/2I$ **($keV/\hbar$), side band**							
	$\gamma=17^0$	$\gamma=20^0$	$\gamma=24^0$	$\gamma=27^0$	$\gamma=30^0$	$\gamma=33^0$	$\gamma=36^0$	$\gamma=40^0$
19	17.763	16.711	14.974	14.026	13.658	14.053	15.053	16.842
20	17.875	16.775	14.875	14.000	13.600	13.975	14.925	16.800
21	17.976	16.690	14.833	13.833	13.500	13.881	14.857	16.690
22	18.045	16.614	14.705	13.886	13.500	13.841	14.795	16.636

Table A.84

A ~ 130, restricted configuration								
Spin I ($\hbar$)	**Fermi surface of both the proton and neutron**							
	$S(I)=[E(I)-E(I-1)]/2I$ **($keV/\hbar$), yrast band**							
	$\gamma=17^0$	$\gamma=20^0$	$\gamma=24^0$	$\gamma=27^0$	$\gamma=30^0$	$\gamma=33^0$	$\gamma=36^0$	$\gamma=40^0$
9	15.556	15.056	14.389	13.833	13.444	13.278	13.333	13.556
10	16.450	16.350	16.150	16.000	15.800	15.600	15.650	15.800
11	16.864	16.682	16.545	16.500	16.409	16.455	16.909	17.227
12	16.875	16.500	15.917	15.250	14.958	16.083	17.167	18.083
13	16.846	16.192	15.154	14.308	14.269	15.231	16.538	18.385
14	16.750	15.929	14.786	14.071	14.000	14.464	16.000	18.214
15	16.733	15.767	14.533	13.933	13.833	14.367	15.533	17.733
16	16.688	15.656	14.438	13.750	13.563	14.000	15.094	17.281
17	16.676	15.618	14.382	13.765	13.647	14.294	15.353	16.971
18	16.667	15.583	14.278	13.556	13.306	13.611	14.556	16.667
19	16.658	15.526	14.263	13.632	13.553	14.237	15.395	16.684
20	16.650	15.525	14.200	13.450	13.125	13.350	14.125	16.325
21	16.667	15.524	14.190	13.548	13.452	14.167	15.452	16.571
22	16.636	15.477	14.114	13.341	13.023	13.182	13.841	16.091
	$S(I)=[E(I)-E(I-1)]/2I$ **($keV/\hbar$), side band**							
9	16.222	14.722	12.222	10.944	9.500	9.556	10.111	11.556
10	17.450	16.100	13.850	12.350	11.850	12.050	12.550	13.450
11	18.591	17.227	14.864	13.682	13.455	13.864	14.136	14.773
12	19.417	17.792	15.500	14.917	14.833	14.417	14.833	15.708
13	19.885	17.962	15.846	15.269	14.654	14.577	15.423	16.346
14	20.000	17.857	15.929	14.964	14.357	14.821	15.429	16.714
15	19.933	17.767	15.800	14.700	14.167	14.467	15.367	17.033
16	19.719	17.656	15.688	14.563	14.125	14.531	15.438	17.094
17	19.500	17.559	15.559	14.382	13.853	14.000	14.941	17.029
18	19.306	17.472	15.444	14.417	14.000	14.472	15.444	17.056
19	19.158	17.368	15.316	14.158	13.605	13.684	14.447	16.737
20	19.025	17.250	15.300	14.250	13.900	14.450	15.550	16.925
21	18.881	17.167	15.119	14.000	13.405	13.429	14.024	16.476
22	18.795	17.091	15.159	14.159	13.841	14.409	15.659	16.841

Table A.85-96: *Calculated intra- and inter-band $B(M1)$ and $B(E2)$ reduced transition probabilities for the partner bands in A ~ 130 mass region at ε_2 = 0.15 and γ =17^0, 20^0, 24^0, 27^0, 30^0, 33^0, 36^0, 40^0 with a change in the Fermi surface of either one of the odd particles or both of them.*

Table A.85

A ~ 130, restricted configuration								
Spin I ($\hbar$)	**Fermi surface of the proton**							
	$B(M1, I \to I-1)_{in}$ **(μ_N^2), yrast band**							
	$\gamma = 17^0$	$\gamma = 20^0$	$\gamma = 24^0$	$\gamma = 27^0$	$\gamma = 30^0$	$\gamma = 33^0$	$\gamma = 36^0$	$\gamma = 40^0$
9	1.0814	1.3201	1.5577	1.7174	1.7174	1.7250	1.7124	1.6834
10	1.1463	1.3289	1.5471	1.7310	1.7310	1.7151	1.6882	1.6537
11	1.1633	1.2917	1.4484	1.7100	1.7100	1.6838	1.6554	1.6199
12	1.1577	1.2265	1.1590	1.6009	1.6009	1.6456	1.6127	1.5814
13	1.1440	1.1629	0.9200	1.5956	1.5956	1.5935	1.5260	1.5382
14	1.1301	1.1206	1.0041	0.9741	0.9741	0.8619	1.4759	1.4930
15	1.1189	1.0985	1.0558	0.9683	0.9683	1.5876	1.4522	1.4304
16	1.1109	1.0879	1.0625	1.0346	1.0346	0.8906	0.8535	1.3884
17	1.1055	1.0823	1.0590	1.0241	1.0241	0.9799	1.5414	1.2996
18	1.1017	1.0789	1.0545	1.0206	1.0206	0.9994	0.6453	1.2805
19	1.0990	1.0765	1.0507	1.0154	1.0154	0.9829	0.9904	1.2649
20	1.0969	1.0746	1.0478	1.0133	1.0133	0.9922	0.9649	0.9172
21	1.0951	1.0729	1.0455	1.0107	1.0107	0.9855	0.9327	1.6204
22	1.0934	1.0715	1.0436	1.0086	1.0086	0.9881	0.9719	0.2943
	$B(M1, I \to I-1)_{in}$ **(μ_N^2), side band**							
9	1.2484	1.2458	1.4331	1.6064	1.6064	1.6029	1.5635	1.4818
10	1.2995	1.3129	1.4546	1.6375	1.6375	1.6111	1.5545	1.4710
11	1.3290	1.3395	1.3640	1.6656	1.6656	1.6191	1.5406	1.4534
12	1.3366	1.3109	1.0895	1.6572	1.6572	1.6034	1.4997	1.4268
13	1.3174	1.2498	0.9038	1.6927	1.6927	1.5869	1.4558	1.4043
14	1.2773	1.2041	1.0436	0.9997	0.9997	0.8827	1.4464	1.3725
15	1.2345	1.1796	1.1147	0.9786	0.9786	1.6103	1.4367	1.3400
16	1.2022	1.1647	1.1199	1.0502	1.0502	0.8974	0.8568	1.3226
17	1.1812	1.1524	1.1098	1.0392	1.0392	0.9835	1.5483	1.2588
18	1.1671	1.1411	1.0984	1.0345	1.0345	1.0045	0.6458	1.2615
19	1.1567	1.1305	1.0883	1.0279	1.0279	0.9874	0.9901	1.2506
20	1.1481	1.1209	1.0796	1.0245	1.0245	0.9966	0.9659	0.9136
21	1.1405	1.1124	1.0722	1.0205	1.0205	0.9893	0.9330	1.6198
22	1.1337	1.1047	1.0657	1.0170	1.0170	0.9916	0.9724	0.2938

Table A.86

A ~ 130, restricted configuration								
Spin I ($\hbar$)	**Fermi surface of the proton**							
	$B(M1, I \to I-1)_{out}$ **(μ_N^2), yrast → side band**							
	$\gamma = 17^0$	$\gamma = 20^0$	$\gamma = 24^0$	$\gamma = 27^0$	$\gamma = 30^0$	$\gamma = 33^0$	$\gamma = 36^0$	$\gamma = 40^0$
10	···	···	0.0781	···	···	···	···	···
11	···	0.1042	0.1743	0.0140	0.0140	0.0601	0.0961	···
12	0.0456	0.1419	0.4243	0.0538	0.0538	0.0790	0.1308	···
13	···	0.1969	0.6081	0.0212	0.0212	0.1126	0.2073	0.1856
14	···	0.2421	0.5083	0.7113	0.7113	0.8548	0.2507	0.2258
15	···	0.2684	0.4679	0.7428	0.7428	0.1356	0.2897	0.2894
16	···	0.2854	0.4793	0.6913	0.6913	0.8686	0.9092	0.3407

Table A.86 continues

A ~ 130, restricted configuration								
Spin I ($\hbar$)	**Fermi surface of the proton**							
	$B(M1, I \rightarrow I-1)_{out}$ **(μ_N^2), yrast → side band**							
	$\gamma = 17^0$	$\gamma = 20^0$	$\gamma = 24^0$	$\gamma = 27^0$	$\gamma = 30^0$	$\gamma = 33^0$	$\gamma = 36^0$	$\gamma = 40^0$
17	...	0.2998	0.5002	0.7174	0.7174	0.7969	0.2294	0.4446
18	...	...	0.5202	0.7339	0.7339	0.7912	1.1521	0.4813
19	...	...	0.5380	0.7508	0.7508	0.8202	0.8205	0.5172
20	...	...	0.5536	0.7631	0.7631	0.8213	0.8587	0.8807
21	...	...	0.5676	0.7753	0.7753	0.8377	0.9021	0.1878
22	...	...	0.5803	0.7861	0.7861	0.8433	0.8721	1.5309
	$B(M1.I \rightarrow I-1)_{out}$ **(μ_N^2), side → yrast band**							
9	0.0040	0.0137	0.0150	0.0092	0.0092	0.0406	0.0805	0.1334
10	0.0059	0.0297	0.0582	0.0100	0.0100	0.0550	0.1013	0.1526
11	0.0092	0.0581	0.1681	0.0231	0.0231	0.0759	0.1218	0.1697
12	0.0180	0.1156	0.4488	0.0605	0.0605	0.0767	0.1443	0.1892
13	0.0365	0.1880	0.6699	0.0270	0.0270	0.0984	0.2057	0.2131
14	0.0635	0.2386	0.5554	0.7229	0.7229	0.8297	0.2271	0.2404
15	0.0912	0.2623	0.4897	0.7617	0.7617	0.1475	0.2662	0.2901
16	0.1127	0.2721	0.4814	0.7052	0.7052	0.8779	0.8896	0.3256
17	0.1269	0.2770	0.4863	0.7239	0.7239	0.8059	0.2377	0.4250
18	0.1355	0.2805	0.4923	0.7334	0.7334	0.7965	1.1547	0.4616
19	0.1408	0.2835	0.4974	0.7433	0.7433	0.8216	0.8253	0.5051
20	0.1442	0.2862	0.5014	0.7849	0.7849	0.8188	0.8608	0.8723
21	0.1466	0.2886	0.5046	0.7545	0.7545	0.8312	0.9023	0.1906
22	0.1483	0.2908	0.5073	0.7589	0.7589	0.8330	0.8706	1.5294

Table A.87

A ~ 130, restricted configuration								
Spin I ($\hbar$)	**Fermi surface of the proton**							
	$B(E2, I \rightarrow I-2)_{in}$ **(e^2b^2), yrast band**							
	$\gamma = 17^0$	$\gamma = 20^0$	$\gamma = 24^0$	$\gamma = 27^0$	$\gamma = 30^0$	$\gamma = 33^0$	$\gamma = 36^0$	$\gamma = 40^0$
10	0.0634	0.0479	0.0209	0.0022	0.0022	0.0154	0.0323	0.0550
11	0.0980	0.0796	0.0471	0.0039	0.0039	0.0229	0.0434	0.0683
12	0.1328	0.1144	0.0919	0.0094	0.0094	0.0303	0.0554	0.0811
13	0.1674	0.1523	0.1360	0.0008	0.0008	0.0378	0.0715	0.0939
14	0.2000	0.1903	0.1791	0.0744	0.0744	0.1041	0.0882	0.1068
15	0.2282	0.2230	0.2162	0.1769	0.1769	0.0505	0.1038	0.1212
16	0.2510	0.2481	0.2387	0.2087	0.2087	0.1350	0.1617	0.1363
17	0.2691	0.2672	0.2570	0.2288	0.2288	0.2149	0.0611	0.1547
18	0.2837	0.2822	0.2727	0.2475	0.2475	0.2322	0.1845	0.1753
19	0.2957	0.2944	0.2859	0.2629	0.2629	0.2482	0.2368	0.1934
20	0.3057	0.3047	0.2971	0.2759	0.2759	0.2623	0.2438	0.2201
21	0.3142	0.3135	0.3068	0.2870	0.2870	0.2738	0.2586	0.0835
22	0.3216	0.3212	0.3151	0.2965	0.2965	0.2840	0.2695	0.2328
	$B(E2, I \rightarrow I-2)_{in}$ **(e^2b^2), side band**							
10	0.1590	0.1259	0.0262	0.0063	0.0063	0.0276	0.0532	0.0851
11	0.1737	0.1362	0.0410	0.0064	0.0064	0.0361	0.0685	0.1024
12	0.1838	0.1438	0.0897	0.0096	0.0096	0.0475	0.0864	0.1189
13	0.1932	0.1588	0.1274	0.0013	0.0013	0.0605	0.1058	0.1338
14	0.2030	0.1796	0.1491	0.0798	0.0798	0.1317	0.1219	0.1480
15	0.2136	0.1986	0.1781	0.1765	0.1765	0.0560	0.1357	0.1622
16	0.2255	0.2154	0.2048	0.1977	0.1977	0.1327	0.1839	0.1748
17	0.2377	0.2312	0.2273	0.2182	0.2182	0.2117	0.0648	0.1893
18	0.2493	0.2459	0.2457	0.2372	0.2372	0.2263	0.1851	0.2018

Table A.87 continues

A ~ 130, restricted configuration								
Spin I ($\hbar$)	Fermi surface of the proton							
	$B(E2, I \to I-2)_{in}$ (e^2b^2), side band							
	$\gamma = 17^0$	$\gamma = 20^0$	$\gamma = 24^0$	$\gamma = 27^0$	$\gamma = 30^0$	$\gamma = 33^0$	$\gamma = 36^0$	$\gamma = 40^0$
19	0.2600	0.2594	0.2609	0.2529	0.2529	0.2429	0.2349	0.2125
20	0.2699	0.2714	0.2738	0.2662	0.2662	0.2569	0.2408	0.2305
21	0.2790	0.2820	0.2849	0.2777	0.2777	0.2686	0.2563	0.0861
22	0.2874	0.2915	0.2946	0.2876	0.2876	0.2788	0.2667	0.2342

Table A.88

A ~ 130, restricted configuration								
Spin I ($\hbar$)	Fermi surface of the proton							
	$B(E2, I \to I-2)_{out}$ (e^2b^2), yrast → side band							
	$\gamma = 17^0$	$\gamma = 20^0$	$\gamma = 24^0$	$\gamma = 27^0$	$\gamma = 30^0$	$\gamma = 33^0$	$\gamma = 36^0$	$\gamma = 40^0$
10	0.0167	0.0193	0.0255	0.0253	0.0253	0.0165	...	...
11	0.0238	0.0272	0.0290	0.0424	0.0424	0.0245	0.0117	0.0038
12	0.0278	0.0300	0.0095	0.0755	0.0755	0.0416	0.0157	0.0043
13	0.0264	0.0234	0.0008	0.1312	0.1312	0.0627	0.0184	0.0048
14	0.0209	0.0131	0.0022	0.0801	0.0801	0.0172	0.0247	0.0055
15	0.0145	0.0068	0.0005	0.0035	0.0035	0.1197	0.0339	0.0058
16	0.0094	0.0043	0.0031	0.0043	0.0043	0.0632	0.0031	0.0069
17	0.0061	0.0033	0.0037	0.0061	0.0061	0.0032	0.1413	0.0061
18	0.0041	0.0028	0.0034	0.0049	0.0049	0.0059	0.0362	0.0056
19	0.0029	0.0024	0.0029	0.0041	0.0041	0.0051	0.0001	0.0074
20	0.0023	0.0021	0.0025	0.0033	0.0033	0.0040	0.0076	0.0000
21	0.0018	0.0018	0.0021	0.0028	0.0028	0.0034	0.0039	0.1553
22	0.0015	0.0016	0.0018	0.0024	0.0024	0.0028	0.0033	0.0162
	$B(E2, I \to I-2)_{out}$ (e^2b^2), side → yrast band							
10	0.0054	0.0200	0.0572	0.0739	0.0739	0.0607	0.0458	0.0296
11	0.0059	0.0180	0.0425	0.0735	0.0735	0.0550	0.0382	0.0230
12	0.0062	0.0147	0.0149	0.0730	0.0730	0.0531	0.0328	0.0183
13	0.0054	0.0089	0.0001	0.0963	0.0963	0.0582	0.0277	0.0148
14	0.0037	0.0041	0.0006	0.0597	0.0597	0.0163	0.0263	0.0124
15	0.0021	0.0017	0.0003	0.0029	0.0029	0.1029	0.0320	0.0102
16	0.0010	0.0009	0.0013	0.0036	0.0036	0.0558	0.0037	0.0093
17	0.0005	0.0005	0.0014	0.0047	0.0047	0.0028	0.1317	0.0075
18	0.0003	0.0004	0.0011	0.0036	0.0036	0.0052	0.0333	0.0063
19	0.0001	0.0003	0.0009	0.0028	0.0028	0.0043	0.0001	0.0077
20	0.0001	0.0002	0.0007	0.0023	0.0023	0.0033	0.0070	0.0000
21	0.0001	0.0002	0.0006	0.0018	0.0018	0.0028	0.0036	0.1515
22	0.0000	0.0001	0.0005	0.0015	0.0015	0.0022	0.0030	0.0154

Table A.89

A ~ 130, restricted configuration								
Spin I ($\hbar$)	Fermi surface of the neutron							
	$B(M1, I \to I-1)_{in}$ (μ_N^2), yrast band							
	$\gamma = 17^0$	$\gamma = 20^0$	$\gamma = 24^0$	$\gamma = 27^0$	$\gamma = 30^0$	$\gamma = 33^0$	$\gamma = 36^0$	$\gamma = 40^0$
9	1.5657	1.6416	1.7427	1.8207	1.8914	1.9372	1.9457	1.9057
10	1.5032	1.5767	1.6902	1.7962	1.9074	1.9812	1.9935	1.9550
11	1.4434	1.5121	1.6284	1.7526	1.9014	1.9986	2.0076	1.9753
12	1.3866	1.4475	1.5536	1.6772	1.8467	1.9664	1.9733	1.9701
13	1.3322	1.3810	1.4581	1.5742	1.7921	1.9280	1.8751	1.9417
14	1.2791	1.3102	1.3524	1.4645	1.9192	1.7181	1.6502	1.8961

Table A.89 continues

A ~ 130, restricted configuration								
Spin I ($\hbar$)	**Fermi surface of the neutron**							
	$B(M1, I \to I-1)_{in}$ **(μ_N^2), yrast band**							
	$\gamma = 17^0$	$\gamma = 20^0$	$\gamma = 24^0$	$\gamma = 27^0$	$\gamma = 30^0$	$\gamma = 33^0$	$\gamma = 36^0$	$\gamma = 40^0$
15	1.2257	1.2307	1.2856	1.5415	0.6028	2.0093	1.1754	1.8444
16	1.1698	1.1404	1.2852	1.8636	1.6118	1.7101	1.2902	1.7902
17	1.1082	1.0234	0.0137	0.0625	1.1969	1.5303	1.5194	1.7337
18	1.0374	0.8246	1.7686	1.9402	1.7819	1.6066	1.5916	1.6879
19	0.9503	0.3935	0.7148	0.0123	1.1434	1.4996	1.5864	1.6590
20	0.8433	0.2848	1.1792	1.9612	1.7871	1.6074	1.6018	1.6443
21	0.7260	0.5936	0.6083	0.0031	1.2139	1.5056	1.5836	1.6348
22	0.6573	0.7928	1.0444	1.9261	1.7333	1.5960	1.5967	1.6301
	$B(M1, I \to I-1)_{in}$ **(μ_N^2), side band**							
9	1.5657	1.4211	1.5821	1.6959	1.7822	1.8178	1.7908	1.6685
10	1.5032	1.3726	1.5379	1.6850	1.8219	1.8864	1.8580	1.7488
11	1.4434	1.3238	1.4860	1.6600	1.8518	1.9361	1.8915	1.7944
12	1.3866	1.2749	1.4265	1.6185	1.8663	1.9641	1.8911	1.8197
13	1.3322	1.2265	1.3626	1.5699	1.8704	1.9822	1.8372	1.8332
14	1.2791	1.1770	1.3008	1.4868	1.9655	1.7689	1.6283	1.8386
15	1.2257	1.1242	1.2666	1.5569	0.6045	2.0293	1.1563	1.8314
16	1.1698	1.0631	1.2818	1.8705	1.6111	1.7164	1.2845	1.8010
17	1.1082	0.9725	0.0152	0.0631	1.1975	1.5340	1.5232	1.7516
18	1.0374	0.7941	1.7612	1.9417	1.7835	1.6099	1.5982	1.7066
19	0.9503	0.3805	0.7120	0.0122	1.1440	1.5024	1.5931	1.6770
20	0.8433	0.2822	1.1764	1.9627	1.7884	1.6102	1.6082	1.6613
21	0.7260	0.5962	0.6068	0.0030	1.2147	1.5081	1.5894	1.6504
22	0.6573	0.7973	1.0422	1.9270	1.7341	1.5983	1.6021	1.6443

Table A.90

A ~ 130, restricted configuration								
Spin I ($\hbar$)	**Fermi surface of the neutron**							
	$B(M1, I \to I-1)_{out}$ **(μ_N^2), yrast → side band**							
	$\gamma = 17^0$	$\gamma = 20^0$	$\gamma = 24^0$	$\gamma = 27^0$	$\gamma = 30^0$	$\gamma = 33^0$	$\gamma = 36^0$	$\gamma = 40^0$
11	···	···	0.1592	0.1023	0.0254	0.0042	0.0530	
12	···	···	0.2250	0.1700	0.0488	0.0101	0.0891	0.1245
13	···	0.2958	0.3255	0.2684	0.0765	0.0137	0.1692	0.1509
14	···	0.3687	0.4535	0.4081	0.0057	0.2483	0.3982	0.1830
15	0.3719	0.4668	0.5586	0.3809	1.3912	0.0115	0.8872	0.2220
16	0.4353	0.5905	0.6009	0.0999	0.4103	0.3412	0.7804	0.2750
17	0.5161	0.7489	1.9097	1.9344	0.8473	0.5414	0.5639	0.3390
18	0.6161	0.9884	0.1888	0.0804	0.2807	0.4808	0.5047	0.3948
19	0.7390	1.4504	1.2677	2.0283	0.9351	0.6009	0.5217	0.4338
20	0.8835	1.5889	0.8247	0.0953	0.3041	0.5041	0.5165	0.4579
21	1.0366	1.3123	1.4134	2.0687	0.8892	0.6159	0.5438	0.4764
22	1.1391	1.1408	0.9930	0.1568	0.3792	0.5338	0.5385	0.4894
	$B(M1, I \to I-1)_{out}$ **(μ_N^2), side → yrast band**							
9	0.3105	0.2541	0.1727	0.1067	0.0463	0.0078	0.0012	0.0254
10	0.3256	0.2771	0.1989	0.1234	0.0451	0.0020	0.0106	0.0480
11	0.3398	0.2999	0.2297	0.1479	0.0474	0.0000	0.0286	0.0698
12	0.3557	0.3268	0.2712	0.1863	0.0579	0.0031	0.0616	0.0921
13	0.3755	0.3623	0.3350	0.2487	0.0733	0.0075	0.1371	0.1172
14	0.4016	0.4116	0.4266	0.3794	0.0052	0.2549	0.3673	0.1485
15	0.4366	0.4827	0.5221	0.3679	1.3851	0.0108	0.8759	0.1915
16	0.4837	0.5829	0.5782	0.0985	0.4116	0.3436	0.7847	0.2526

Table A.90 continues

A ~ 130, restricted configuration								
Spin I ($\hbar$)	Fermi surface of the neutron							
	$B(M1, I \rightarrow I-1)_{out}$ (μ_N^2), side → yrast band							
	$\gamma = 17^0$	$\gamma = 20^0$	$\gamma = 24^0$	$\gamma = 27^0$	$\gamma = 30^0$	$\gamma = 33^0$	$\gamma = 36^0$	$\gamma = 40^0$
17	0.5476	0.7308	1.8996	1.9342	0.8492	0.5432	0.5672	0.3249
18	0.6328	0.9744	0.1894	0.0800	0.2814	0.4817	0.5058	0.3857
19	0.7460	1.4526	1.2678	2.0287	0.9356	0.6012	0.5211	0.4262
20	0.8876	1.5997	0.8261	0.0949	0.3044	0.5038	0.5145	0.4497
21	1.0425	1.3167	1.4150	2.0675	0.8886	0.6146	0.5404	0.4665
22	1.1455	1.1394	0.9953	0.1563	0.3791	0.5321	0.5339	0.4773

Table A.91

A ~ 130, restricted configuration								
Spin I ($\hbar$)	Fermi surface of the neutron							
	$B(E2, I \rightarrow I-2)_{in}$ (e^2b^2), yrast band							
	$\gamma = 17^0$	$\gamma = 20^0$	$\gamma = 24^0$	$\gamma = 27^0$	$\gamma = 30^0$	$\gamma = 33^0$	$\gamma = 36^0$	$\gamma = 40^0$
10	0.1133	0.0899	0.0566	0.0308	0.0088	0.0000	0.0074	0.0283
11	0.1336	0.1088	0.0718	0.0395	0.0090	0.0010	0.0178	0.0458
12	0.1515	0.1266	0.0880	0.0498	0.0093	0.0051	0.0340	0.0647
13	0.1676	0.1436	0.1055	0.0615	0.0092	0.0129	0.0599	0.0848
14	0.1822	0.1604	0.1247	0.0812	0.0013	0.0000	0.1067	0.1065
15	0.1961	0.1776	0.1465	0.0991	0.1530	0.0028	0.1657	0.1309
16	0.2096	0.1963	0.1694	0.0549	0.2167	0.0855	0.1930	0.1598
17	0.2234	0.2182	0.1651	0.2410	0.2425	0.2236	0.2306	0.1917
18	0.2378	0.2429	0.2457	0.2569	0.2555	0.2516	0.2491	0.2208
19	0.2531	0.2398	0.2159	0.2846	0.2757	0.2701	0.2633	0.2435
20	0.2684	0.1946	0.2906	0.2992	0.2914	0.2848	0.2768	0.2605
21	0.2808	0.2478	0.3067	0.3105	0.3012	0.2967	0.2888	0.2737
22	0.2903	0.3140	0.3204	0.3216	0.3154	0.3079	0.2992	0.2845
	$B(E2, I \rightarrow I-2)_{in}$ (e^2b^2), side band							
10	0.1418	0.1172	0.0753	0.0393	0.0090	0.0007	0.0193	0.0648
11	0.1657	0.1411	0.0965	0.0522	0.0096	0.0039	0.0362	0.0876
12	0.1864	0.1627	0.1183	0.0673	0.0102	0.0117	0.0589	0.1089
13	0.2045	0.1825	0.1402	0.0841	0.0111	0.0233	0.0903	0.1287
14	0.2205	0.2009	0.1620	0.1053	0.0016	0.0001	0.1389	0.1470
15	0.2349	0.2184	0.1813	0.1142	0.1641	0.0025	0.1847	0.1646
16	0.2482	0.2356	0.1939	0.0581	0.2188	0.0846	0.1951	0.1836
17	0.2606	0.2531	0.1739	0.2433	0.2411	0.2218	0.2259	0.2043
18	0.2723	0.2693	0.2520	0.2565	0.2544	0.2497	0.2442	0.2240
19	0.2831	0.2521	0.2165	0.2845	0.2751	0.2684	0.2591	0.2407
20	0.2917	0.1954	0.2922	0.2981	0.2902	0.2828	0.2730	0.2546
21	0.2955	0.2439	0.3075	0.3106	0.3008	0.2951	0.2852	0.2666
22	0.2963	0.3090	0.3217	0.3206	0.3142	0.3061	0.2958	0.2771

Table A.92

A ~ 130, restricted configuration								
Spin I ($\hbar$)	Fermi surface of the neutron							
	$B(E2, I \rightarrow I-2)_{out}$ (e^2b^2), yrast → side band							
	$\gamma = 17^0$	$\gamma = 20^0$	$\gamma = 24^0$	$\gamma = 27^0$	$\gamma = 30^0$	$\gamma = 33^0$	$\gamma = 36^0$	$\gamma = 40^0$
10	...	...	...	0.0164	...	0.0269	0.0198	0.0089
11	...	0.0028	0.0108	0.0253	0.0443	0.0452	0.0273	0.0105
12	0.0009	0.0032	0.0144	0.0400	0.0796	0.0743	0.0357	0.0126
13	0.0010	0.0037	0.0190	0.0595	0.1240	0.1066	0.0384	0.0153

Table A.92 continues

A ~ 130, restricted configuration								
Spin I ($\hbar$)	**Fermi surface of the neutron**							
	$B(E2, I \to I-2)_{out}$ **(e^2b^2), yrast → side band**							
	$\gamma = 17^0$	$\gamma = 20^0$	$\gamma = 24^0$	$\gamma = 27^0$	$\gamma = 30^0$	$\gamma = 33^0$	$\gamma = 36^0$	$\gamma = 40^0$
14	0.0010	0.0041	0.0236	0.0711	0.1687	0.1649	0.0205	0.0183
15	0.0010	0.0043	0.0287	0.0892	0.0336	0.1911	0.0003	0.0200
16	0.0010	0.0038	0.0377	0.1694	0.0040	0.1330	0.0119	0.0183
17	0.0007	0.0019	0.0774	0.0056	0.0040	0.0171	0.0009	0.0132
18	0.0003	0.0002	0.0174	0.0114	0.0104	0.0082	0.0020	0.0080
19	0.0000	0.0306	0.0670	0.0002	0.0061	0.0056	0.0037	0.0048
20	0.0012	0.0991	0.0072	0.0002	0.0044	0.0046	0.0036	0.0032
21	0.0065	0.0601	0.0041	0.0003	0.0059	0.0040	0.0031	0.0025
22	0.0139	0.0051	0.0010	0.0001	0.0023	0.0029	0.0026	0.0020
	$B(E2, I \to I-2)_{out}$ **(e^2b^2), side → yrast band**							
10	0.0222	0.0318	0.0499	0.0669	0.0816	0.0837	0.0702	0.0437
11	0.0166	0.0244	0.0412	0.0608	0.0809	0.0814	0.0613	0.0342
12	0.0127	0.0190	0.0346	0.0571	0.0844	0.0817	0.0530	0.0278
13	0.0098	0.0150	0.0299	0.0575	0.0977	0.0891	0.0434	0.0236
14	0.0077	0.0120	0.0272	0.0606	0.1375	0.1344	0.0228	0.0211
15	0.0060	0.0094	0.0282	0.0797	0.0311	0.1743	0.0000	0.0194
16	0.0045	0.0069	0.0359	0.1622	0.0038	0.1283	0.0093	0.0165
17	0.0031	0.0035	0.0718	0.0055	0.0040	0.0166	0.0007	0.0118
18	0.0017	0.0000	0.0169	0.0112	0.0102	0.0080	0.0020	0.0071
19	0.0003	0.0254	0.0683	0.0002	0.0060	0.0054	0.0035	0.0042
20	0.0003	0.0915	0.0074	0.0002	0.0043	0.0044	0.0034	0.0028
21	0.0039	0.0571	0.0042	0.0003	0.0058	0.0039	0.0029	0.0021
22	0.0105	0.0049	0.0011	0.0001	0.0022	0.0028	0.0024	0.0017

Table A.93

A ~ 130, restricted configuration								
Spin I ($\hbar$)	**Fermi surface of both the proton and neutron**							
	$B(M1, I \to I-1)_{in}$ **(μ_N^2), yrast band**							
	$\gamma = 17^0$	$\gamma = 20^0$	$\gamma = 24^0$	$\gamma = 27^0$	$\gamma = 30^0$	$\gamma = 33^0$	$\gamma = 36^0$	$\gamma = 40^0$
9	0.9149	1.0800	1.2476	1.3644	1.4486	1.4713	1.4577	1.4234
10	0.9105	1.0403	1.1725	1.3010	1.4391	1.4540	1.4384	1.4120
11	0.8903	0.9810	1.0287	1.0224	1.3717	1.3833	1.3993	1.3917
12	0.8650	0.9148	0.8581	0.3454	1.1970	1.3912	1.3329	1.3627
13	0.8410	0.8576	0.7788	0.6580	0.9732	0.0001	1.1970	1.3367
14	0.8214	0.8185	0.7738	0.7901	0.8452	1.2784	1.3314	1.3189
15	0.8065	0.7945	0.7657	0.7525	0.6643	0.3090	0.5495	1.2977
16	0.7955	0.7804	0.7619	0.7643	0.8077	1.0913	1.4304	1.2946
17	0.7874	0.7711	0.7509	0.7324	0.6725	0.3933	0.3373	1.1542
18	0.7812	0.7647	0.7462	0.7396	0.7572	0.9427	1.4560	1.1813
19	0.7764	0.7598	0.7396	0.7244	0.6936	0.5664	0.4783	1.0444
20	0.7723	0.7556	0.7345	0.7207	0.7103	0.7518	1.3619	1.1058
21	0.7690	0.7526	0.7325	0.7217	0.7166	0.7255	1.0604	1.0307
22	0.7659	0.7491	0.7258	0.7060	0.6718	0.5903	0.8323	1.0553
	$B(M1, I \to I-1)_{in}$ **(μ_N^2), side band**							
9	0.9546	0.9562	1.1401	1.2910	1.3782	1.3805	1.3305	1.2328
10	0.9748	0.9894	1.1330	1.2648	1.4018	1.3949	1.3353	1.2451
11	0.9835	1.0106	1.0394	0.9990	1.3892	1.3788	1.3237	1.2459
12	0.9753	0.9909	0.8844	0.3278	1.2650	1.4239	1.2973	1.2480
13	0.9501	0.9352	0.8150	0.6715	1.0064	0.0004	1.2003	1.2607
14	0.9157	0.8854	0.8179	0.8186	0.8616	1.2784	1.3389	1.2873

Table A.93 continues

A ~ 130, restricted configuration								
Spin I ($\hbar$)	**Fermi surface of both the proton and neutron**							
	$B(M1, I \rightarrow I-1)_{in}$ **(μ_N^2), side band**							
	$\gamma = 17^0$	$\gamma = 20^0$	$\gamma = 24^0$	$\gamma = 27^0$	$\gamma = 30^0$	$\gamma = 33^0$	$\gamma = 36^0$	$\gamma = 40^0$
15	0.8826	0.8535	0.8094	0.7795	0.6757	0.3117	0.5506	1.3057
16	0.8566	0.8332	0.8013	0.7888	0.8206	1.0985	1.4369	1.3161
17	0.8382	0.8183	0.7855	0.7541	0.6833	0.3960	0.3383	1.1751
18	0.8249	0.8059	0.7753	0.7579	0.7667	0.9462	1.4602	1.1985
19	0.8150	0.7959	0.7652	0.7415	0.7036	0.5714	0.4809	1.0575
20	0.8065	0.7862	0.7549	0.7335	0.7162	0.7518	1.3596	1.1167
21	0.7996	0.7791	0.7510	0.7349	0.7257	0.7327	1.0702	1.0410
22	0.7928	0.7709	0.7395	0.7144	0.6750	0.5885	0.8272	1.0621

Table A.94

A ~ 130, restricted configuration								
Spin I ($\hbar$)	**Fermi surface of both the proton and neutron**							
	$B(M1, I \rightarrow I-1)_{out}$ **(μ_N^2), yrast → side band**							
	$\gamma = 17^0$	$\gamma = 20^0$	$\gamma = 24^0$	$\gamma = 27^0$	$\gamma = 30^0$	$\gamma = 33^0$	$\gamma = 36^0$	$\gamma = 40^0$
10	0.0375	0.0757	0.1232	0.0806	0.0013	0.0298	0.0698	···
11	0.0378	0.0893	0.2362	0.3356	0.0185	0.0650	0.0984	0.1161
12	0.0466	0.1255	0.3895	0.9865	0.1594	0.0248	0.1468	0.1381
13	0.0626	0.1810	0.4603	0.6662	0.4162	1.4570	0.2727	0.1535
14	···	0.2327	0.4652	0.5506	0.5758	0.1872	0.1457	0.1601
15	···	0.2688	0.4815	0.6048	0.7711	1.1674	0.9466	0.1745
16	···	0.2924	0.4964	0.6055	0.6369	0.3951	0.0719	0.1829
17	···	0.3104	0.5193	0.6492	0.7839	1.1063	1.1788	0.3374
18	···	···	0.5348	0.6508	0.7053	0.5603	0.0631	0.3212
19	···	···	0.5521	0.6762	0.7790	0.9476	1.0535	0.4707
20	···	···	0.5665	0.6874	0.7677	0.7655	0.1715	0.4164
21	···	···	0.5778	0.6952	0.7692	0.7986	0.4772	0.5009
22	···	···	0.5927	0.7177	0.8198	0.9397	0.7137	0.4817
	$B(M1, I \rightarrow I-1)_{out}$ **(μ_N^2), side → yrast band**							
9	0.0059	0.0260	0.0594	0.0327	0.0014	0.0111	0.0421	0.0768
10	0.0068	0.0310	0.1119	0.0829	0.0019	0.0256	0.0641	0.0939
11	0.0113	0.0479	0.2265	0.3322	0.0206	0.0555	0.0853	0.1084
12	0.0232	0.0940	0.3873	1.0085	0.1537	0.0167	0.1250	0.1237
13	0.0435	0.1601	0.4657	0.6973	0.4310	1.4440	0.2498	0.1308
14	0.0679	0.2125	0.4644	0.5612	0.5820	0.1914	0.1345	0.1342
15	0.0910	0.2429	0.4690	0.6031	0.7749	1.1754	0.9419	0.1523
16	0.1090	0.2583	0.4704	0.5922	0.6340	0.3964	0.0704	0.1674
17	0.1218	0.2675	0.4814	0.6265	0.7743	1.1032	1.1762	0.3255
18	0.1302	0.2729	0.4844	0.6180	0.6902	0.5573	0.0622	0.3111
19	0.1359	0.2775	0.4917	0.6351	0.7570	0.9370	1.0457	0.4602
20	0.1397	0.2807	0.4950	0.6365	0.7394	0.7547	0.1694	0.4045
21	0.1425	0.2837	0.4981	0.6378	0.7364	0.7831	0.4713	0.4871
22	0.1445	0.2861	0.5026	0.6504	0.7785	0.9185	0.7049	0.4655

Table A.95

A ~ 130, restricted configuration								
Spin I ($\hbar$)	**Fermi surface of both the proton and neutron**							
	$B(E2, I \to I-2)_{in}$ **(e^2b^2), yrast band**							
	$\gamma = 17^0$	$\gamma = 20^0$	$\gamma = 24^0$	$\gamma = 27^0$	$\gamma = 30^0$	$\gamma = 33^0$	$\gamma = 36^0$	$\gamma = 40^0$
10	0.1083	0.0887	0.0590	0.0263	0.0005	0.0104	0.0310	0.0557
11	0.1424	0.1189	0.0923	0.0649	0.0009	0.0223	0.0467	0.0721
12	0.1775	0.1543	0.1357	0.1258	0.0261	0.0261	0.0660	0.0885
13	0.2119	0.1947	0.1824	0.1552	0.0049	0.1233	0.0994	0.1043
14	0.2416	0.2316	0.2228	0.2175	0.1722	0.1744	0.1197	0.1186
15	0.2651	0.2596	0.2508	0.2382	0.2220	0.1971	0.1905	0.1346
16	0.2831	0.2798	0.2706	0.2585	0.2458	0.2334	0.2135	0.1530
17	0.2971	0.2949	0.2858	0.2745	0.2610	0.2439	0.2371	0.1894
18	0.3084	0.3068	0.2986	0.2888	0.2778	0.2674	0.2550	0.2201
19	0.3176	0.3164	0.3090	0.2996	0.2877	0.2690	0.2583	0.2407
20	0.3254	0.3246	0.3180	0.3097	0.2999	0.2896	0.2781	0.2569
21	0.3320	0.3316	0.3256	0.3176	0.3070	0.2908	0.2388	0.2659
22	0.3378	0.3377	0.3323	0.3251	0.3159	0.3057	0.2944	0.2763
	$B(E2, I \to I-2)_{in}$ **(e^2b^2), side band**							
10	0.1956	0.1704	0.0806	0.0251	0.0000	0.0215	0.0577	0.1013
11	0.2019	0.1761	0.1059	0.0706	0.0012	0.0357	0.0778	0.1208
12	0.2084	0.1825	0.1479	0.1399	0.0305	0.0416	0.1007	0.1378
13	0.2172	0.1961	0.1800	0.1446	0.0047	0.1432	0.1312	0.1507
14	0.2271	0.2142	0.2019	0.1917	0.1659	0.1829	0.1410	0.1587
15	0.2374	0.2318	0.2228	0.2179	0.2143	0.1903	0.2016	0.1632
16	0.2483	0.2468	0.2420	0.2397	0.2348	0.2264	0.2130	0.1682
17	0.2594	0.2600	0.2589	0.2575	0.2522	0.2416	0.2374	0.1951
18	0.2700	0.2719	0.2730	0.2716	0.2668	0.2596	0.2485	0.2170
19	0.2797	0.2827	0.2852	0.2841	0.2792	0.2667	0.2592	0.2364
20	0.2885	0.2923	0.2954	0.2942	0.2897	0.2824	0.2716	0.2490
21	0.2964	0.3011	0.3046	0.3035	0.2988	0.2875	0.2390	0.2597
22	0.3036	0.3087	0.3123	0.3111	0.3067	0.2995	0.2889	0.2681

Table A.96

A ~ 130, restricted configuration								
Spin I ($\hbar$)	**Fermi surface of both the proton and neutron**							
	$B(E2, I \to I-2)_{out}$ **(e^2b^2), yrast → side band**							
	$\gamma = 17^0$	$\gamma = 20^0$	$\gamma = 24^0$	$\gamma = 27^0$	$\gamma = 30^0$	$\gamma = 33^0$	$\gamma = 36^0$	$\gamma = 40^0$
10	0.0251	0.0271	0.0303	0.0437	0.0545	0.0376	0.0192	0.0068
11	0.0322	0.0384	0.0301	0.0354	0.0939	0.0584	0.0266	0.0086
12	0.0321	0.0399	0.0130	0.0035	0.1112	0.0942	0.0336	0.0112
13	0.0255	0.0289	0.0021	0.0251	0.1730	0.0211	0.0279	0.0162
14	0.0174	0.0157	0.0011	0.0003	0.0302	0.0049	0.0416	0.0250
15	0.0110	0.0078	0.0021	0.0042	0.0053	0.0180	0.0004	0.0346
16	0.0069	0.0043	0.0026	0.0038	0.0038	0.0033	0.0060	0.0423
17	0.0044	0.0028	0.0025	0.0033	0.0044	0.0078	0.0001	0.0263
18	0.0029	0.0021	0.0022	0.0025	0.0024	0.0010	0.0004	0.0143
19	0.0021	0.0017	0.0019	0.0023	0.0033	0.0092	0.0060	0.0067
20	0.0016	0.0014	0.0016	0.0017	0.0016	0.0007	0.0001	0.0029
21	0.0012	0.0012	0.0014	0.0017	0.0024	0.0069	0.0460	0.0027
22	0.0010	0.0010	0.0011	0.0012	0.0011	0.0005	0.0000	0.0011
	$B(E2, I \to I-2)_{out}$ **(e^2b^2), side → yrast band**							
10	0.0085	0.0201	0.0437	0.0671	0.0850	0.0708	0.0495	0.0281
11	0.0092	0.0200	0.0284	0.0386	0.0906	0.0653	0.0420	0.0222
12	0.0081	0.0168	0.0105	0.0011	0.0837	0.0775	0.0375	0.0190

Table A.96 continues

A ~ 130, restricted configuration								
Spin I ($\hbar$)	**Fermi surface of both the proton and neutron**							
	$B(E2, I \rightarrow I-2)_{out}$ (e^2b^2), **side → yrast band**							
	$\gamma = 17^0$	$\gamma = 20^0$	$\gamma = 24^0$	$\gamma = 27^0$	$\gamma = 30^0$	$\gamma = 33^0$	$\gamma = 36^0$	$\gamma = 40^0$
13	0.0056	0.0098	0.0019	0.0164	0.1412	0.0138	0.0272	0.0187
14	0.0031	0.0043	0.0007	0.0002	0.0245	0.0047	0.0375	0.0223
15	0.0016	0.0017	0.0009	0.0027	0.0043	0.0168	0.0006	0.0277
16	0.0007	0.0008	0.0010	0.0022	0.0029	0.0027	0.0058	0.0333
17	0.0004	0.0004	0.0009	0.0018	0.0033	0.0071	0.0001	0.0211
18	0.0002	0.0003	0.0007	0.0013	0.0016	0.0008	0.0004	0.0116
19	0.0001	0.0002	0.0006	0.0012	0.0023	0.0082	0.0057	0.0056
20	0.0001	0.0001	0.0004	0.0008	0.0010	0.0005	0.0001	0.0025
21	0.0000	0.0001	0.0004	0.0008	0.0016	0.0060	0.0445	0.0022
22	0.0000	0.0001	0.0003	0.0005	0.0006	0.0004	0.0000	0.0010